Agrociencia

eISSN: 2521-9766

VOLUME 59, NUMBER 4 | May 16 - June 30, 2025 | MEXICO

AGRICULTURA
SECRETARÍA DE AGRICULTURA Y DESARROLLO RURAL

COPYRIGHT AND RELATED RIGHTS, **Volume 59, Number 4, May 16 - June 30, 2025**, Agrociencia is a semi-monthly publication edited by Colegio de Postgraduados. Carretera Mexico-Texcoco, Km 36.5, Montecillo, Texcoco, State of Mexico. C. P. 56264. Phone: 5959284427. www.colpos.mx. Editor in chief: Dr. Fernando Carlos Gómez Merino. Reservations of Rights to Exclusive Use 04-2021-031913431800-203. eISSN: 2521-9766, granted by the National Copyright Institute. Last modification date, **June 30, 2025**.

All correspondence (subscription information, sales, advertising, author contributions, etc.) should be addressed to:

Central Office:

Agrociencia
Guerrero No. 9, Esquina con Avenida Hidalgo,
San Luis Huexotla, Texcoco 56220,
State of Mexico. MEXICO
Tel.: +52-595 92 84427

https://agrociencia-colpos.org/index.php/agrociencia

Cover: Rabbit
Photography and credits: Designed by Freepik
www.freepik.es

AGRICULTURA
SECRETARÍA DE AGRICULTURAY DESARROLLO RURAL

Contents

Volume 59, Number 4 | May 16 - June 30, 2025

Animal Science

Applied Mathematics-Statistics-Computer Science

Agrociencia

EFFECT OF TWO STUNNING METHODS ON WELFARE INDICATORS AND CARCASS LESIONS IN CALIFORNIA RABBITS

Yamileth **Jerónimo-Romero**[1,2], José Guadalupe **Herrera-Haro**[1*], María Esther **Ortega-Cerrilla**[1], María Concepción **Méndez Gómez-Humarán**[3], Aleida Selene **Hernández-Cázares**[4]

[1]Colegio de Postgraduados Campus Montecillo. Carretera México-Texcoco km 36.5, Montecillo, Texcoco, State of Mexico, Mexico. C. P. 56264.
[2]Consejo Mexiquense de Ciencia y Tecnología. Paseo Cristóbal Colón 112A, Residencial Colón, Colonia Ciprés, Toluca de Lerdo, State of Mexico, Mexico. C. P. 50120.
[3]Universidad Autónoma de Querétaro. Avenida de las Ciencias s/n, Juriquilla, Querétaro, Mexico. C. P. 76230.
[4]Colegio de Postgraduados Campus Córdoba. Carretera Córdoba-Veracruz km 348, Amatlán de los Reyes, Veracruz, Mexico. C. P. 94953.
* Author for correspondence: haro@colpos.mx

Citation: Jerónimo-Romero Y, Herrera-Haro JG, Ortega-Cerrilla ME, Méndez Gómez-Humarán MC, Hernández-Cázares AS. 2025. Effect of two stunning methods on welfare indicators and carcass lesions in California rabbits. **Agrociencia** 59(4): 443-456. https://doi.org/ 10.47163/agrociencia.v59i4.2687

Editor in Chief:
Dr. Fernando C. Gómez Merino

Received: September 26, 2024.
Approved: June 02, 2025.
Published in Agrociencia: June 19, 2025.

ABSTRACT

Consumers have legitimate concerns about the application of animal welfare procedures during the slaughter of rabbits. However, there is insufficient evaluation of such practices, particularly in small-scale rabbit-breeding operations in Mexico. This study aimed to assess animal welfare indicators during slaughter under different stunning methods. A total of 120 California rabbits (*Oryctolagus cuniculus* L.) were used, each one of which weighed 2 kg, and were distributed into four treatments in a 2^2 factorial arrangement to relate two methods of stunning (a_1 = concussion, a_2 = electronarcosis) and the sex of the animal (b_1 = male, b_2 = female) with the behaviors observed during slaughtering and the lesions in the carcass as factors that affect the animal's welfare. Management indicators (number and precision of the application), behavioral indicators (attempts at escaping, kicking, vocalization, gaping, and arching of the back), and lesions in the carcass were registered. Descriptive statistics were obtained, and the behaviors were compared using nonparametric tests. Additionally, risk factors were identified in the carcass related to the slaughter methods, weight, and sex. During stunning, precision and kicking were different ($p < 0.05$), unlike vocalization ($p = 0.7$). During the slitting of the throat, time ($p = 0.4$), vocalization ($p = 0.6$), blinking ($p = 0.7$), corneal reflex ($p = 0.8$), and dilated pupils ($p = 0.2$) presented no differences between methods. However, there were differences in kicking ($p < 0.01$), gaping ($p < 0.01$), and arching of the back ($p < 0.01$). In the *post-mortem* evaluation of lesions, the carcasses that displayed the lowest number of lesions, with the smallest size and located on the legs, were from rabbits on which the method of electronarcosis ($p < 0.001$) was applied. The slaughtering method was a risk factor in the appearance of bruises ($p > 0.0003$). The method of electronarcosis was concluded to be more effective than concussion to induce the animal to lose consciousness during the slaughtering of rabbits.

Keywords: *Oryctolagus cuniculus* L., animal welfare, desensitization, electronarcosis, concussion, contusions.

INTRODUCTION

In recent years, consumer demand has increasingly emphasized the importance of ensuring that animal-derived products are obtained in accordance with animal welfare standards (Stoier *et al.*, 2016). This has promoted the development of slaughter systems that consider the well-being of animals, enhancing meat quality and creating new economic opportunities. In the case of the rabbits, pre-slaughter stunning induces unconsciousness, minimizing stress during exsanguination. The assessment of unconsciousness in rabbits prior to slaughter is typically based on behavioral indicators, including the presence or absence of ocular reflexes, blinking, pupil dilation, limb movements such as kicking, loss of body posture, head lifting, back arching, vocalizations, and monitoring of the respiratory rate (Verhoeven *et al.*, 2015). According to the Mexican Official Standard NOM-033-SAG/ZOO-2014 (DOF, 2014), animals must not exhibit signs of pain, stress, or distress at the time of slaughter, as such conditions compromise their welfare, physical integrity, health status, biochemical profile, and ultimately the quality and yield of the meat. Similarly, in the European Union, compliance with higher animal welfare standards has been associated with improved carcass quality and a reduction in lesions (European Commission, 2017). The primary objective of stunning is to rapidly induce unconsciousness, which is the inability to perceive and respond to external stimuli due to profound brain depression. This procedure is intended to prevent the animal from experiencing pain and stress during neck cutting and subsequent bleeding (DOF, 2014).

In countries such as Italy and Hungary, stunning by electronarcosis is a common practice before slaughtering rabbits in slaughterhouses (European Commission, 2017). In Mexico, the most widely used stunning methods are cervical dislocation and mechanical concussion stunning. Some countries, along with stunning by concussion, use electronarcosis and penetrating and non-penetrating captive bolt stunning. Stunning by electronarcosis consists of running an electric current through the animal's head at a magnitude that can induce tonic-clonic epileptiform activity, resulting in a state of insensitivity (McKinstry and Anil, 2004). Meanwhile, the concussion method involves delivering a forceful impact to the occipital region at the base of the head using a long, blunt, non-sharp solid object or the hand.

Electronarcosis induces immediate unconsciousness in pigs, poultry, and rabbits, thereby contributing positively to animal welfare. To ensure effective stunning, electrodes must be positioned correctly, as improper placement may fail to induce unconsciousness and can exacerbate fear, anxiety, pain, stress, or even result in death (Stoier *et al*., 2016). According to Anil *et al*. (1998), electrical stunning can produce a sufficiently long duration of insensibility, making it a suitable method for the humane slaughter of rabbits.

Several indicators are recommended to assess and determine unconsciousness before slaughtering, exsanguination, and skinning. If the animal is not considered unconscious after evaluating the indicators, the stunning procedure must be repeated (Verhoeven *et al.*, 2015). Animal welfare must also be evaluated in the *ante-mortem* handling, along with its repercussions on the physical quality of the carcass. Bruises are indicators of improper handling of the carcass prior to slaughter, which may include insufficient grasping of the animal, inadequate transportation, and extended waiting periods before slaughter. (Grandin, 2017).

The interaction of the sex of the rabbits with the stunning method before slaughtering has been scarcely studied. Studies performed during stunning and slaughtering do not distinguish between females and males and focus only on the method of stunning, as observed in the work carried out by Anil *et al.* (1998), Petracci *et al.* (2010), and Valkova *et al.* (2021b).

The hypothesis in this study was that electronarcosis, as a stunning method used for slaughtering rabbits, has a lesser impact on animal welfare compared to the mechanical concussion method. Therefore, the aims were to compare the effectiveness of electronarcosis and concussion as stunning techniques in California rabbits, as well as to evaluate the animal welfare conditions with both methods and to assess the interaction between the sex of the rabbits and the stunning method used.

MATERIALS AND METHODS

The study was carried out at the Rabbit Breeding Unit of the Livestock Program of the Postgraduate College, Campus Montecillo, Mexico, located at 19° 27′ 48.4′′ N and 98° 54′ 30.8″ W, at an altitude of 2250 m. The stunning and slaughter procedures were carried out following the regulations for the use and care of animals destined for research at the Postgraduate College. The experiment was conducted between January and May 2021.

A total of 120 California breed rabbits were utilized in this study, comprising 60 males and 60 females, each aged 65 ± 5 days and weighing 2.2 ± 0.2 kg. The animals were not subjected to prior fasting. They were randomly distributed into four treatment groups in a completely randomized design with a 2 × 2 factorial arrangement. The main factors considered were the type of stunning (mechanical stunning by concussion (a_1) and electronarcosis (a_2)) and sex (male (b_1) and female (b_2)). Each treatment combination included 30 replicates, with each rabbit representing one experimental unit. The animals were organized into five groups of five rabbits each and transported to the fattening area located adjacent to the slaughterhouse. Stunning and slaughter procedures commenced immediately; however, the rabbits were held for a waiting period of 10 min prior to processing.

The mechanical stunning was performed by striking the base of the heads in the occipital region with our hands. A manual electric stunning machine (model VS200, Midwest Processing Systems, Minneapolis, MN, USA) with 120 V and 1 A was used for

electronarcosis stunning. The rabbits received an electric discharge of 600 V and 1 A in the occipital region for 2 s. After the application of the stunning method, the rabbit was hung by its hind legs, upside down, and its neck was slit. The time elapsed between stunning and slaughtering was measured using a stopwatch, and the assessment of bruises was carried out using a millimeter ruler.

Evaluation of the method of stunning

Management and behavioral indicators

The evaluation of handling indicators and rabbit behavior commenced at the moment the animal was removed from its cage, located in the facility adjacent to the slaughterhouse, and concluded upon slaughter. A single trained observer conducted the assessments, independently reviewing each indicator, while a designated operator administered the stunning procedure according to the assigned treatment (either concussion or electronarcosis).

For both stunning methods, the following variables were recorded: the precision of the application (i.e., whether the anatomical target site was correct, specifically the occipital region, or incorrect, involving any other area), the number of applications (one or more than one), and the time elapsed between stunning and slaughter (<30 or >30 s). Additionally, the presence or absence of behavioral indicators was documented at three critical stages: during restraint (escape attempts and kicking), stunning (vocalization and kicking), and slaughter (vocalization, kicking, blinking, corneal reflex, pupil dilation, gaping, head lifting, and arching of the back), in accordance with established criteria (Grandin, 2017) (Table 1).

Table 1. Ethogram of the behavioral indicators evaluated during the stunning of California rabbits (*Oryctolagus cuniculus* L.).

Indicator	Definition
Attempt to escape	The animal performs movements to find a way out and avoid being held.
Kicking	Violent movement of hind legs; when this takes place after stunning, it refers to the clonic phase.
Vocalization	Voluntary sounds are produced by the vibration of the vocal cords. Short and high-pitched squeals.
Blinking	Opening and closing of the eyelids.
Corneal reflex	Reaction when touching the eyeball with the tip of the finger after stunning.
Dilated pupils	Increase in the diameter of the pupils.
Gaping	Deep, non-rhythmical breaths through the open mouth.
Lifting head	Lifting or attempting to lift its head.
Arching of the back	Any reflex that tends to take the body to its normal position.

Evaluation of carcass lesions

The carcass was divided into two regions: limbs (front and hind legs) and torso (neck, thorax, and back). The traumatic lesions with blood vessel ruptures, leading to blood accumulation without skin discontinuity, were considered as bruises. All observed injuries were recorded, including their location and size. The extent was determined based on the approximate diameter of the affected area and classified into three levels: ≤ 0.5 cm, between 0.6 and 1 cm, and > 1 cm. In carcasses with more than one bruise of different extents, the criterion of the largest size was used for classification (Knock and Carroll, 2019).

Statistical analysis

Descriptive statistics were obtained for the handling indicators (precision of application, number of applications, and time between stunning and slaughtering) and behavioral indicators (attempt to escape, kicking, vocalization, blinking, corneal reflex, dilated pupils, gaping, lifting of the head, and arched back). These data were transformed into ranges and analyzed using the Mann-Whitney U test and analysis of variance via the Kruskal–Wallis test. To evaluate the association between the presence of carcass lesions and variables such as the stunning method, sex, animal weight, and time between stunning and slaughtering, a logistic regression analysis was conducted. This analysis enabled the estimation of risk or opportunity factors (odds ratios, OR). All statistical analyses were performed using SAS software, version 9.4 (SAS Institute Inc., Cary, NC, USA). The general model used was as follows:

$$P\left(Y=\frac{1}{X}\right)=\frac{e^{(\beta_0+\beta_1X_1+\beta_2X_2+\cdots\beta_4X_4)}}{1+e^{(\beta_0+\beta_1X_1+\beta_2X_2+\cdots\beta_4X_4)}}$$

where P is the probability that variable Y_i takes the value of $Y = 1$ if lesions appear and $Y = 0$ otherwise; β_0, β_1, …, β_4 are unknown parameters, and X_1, …, X_4 are independent variables (method of stunning, sex of the rabbit, size of the animal, and time between stunning and slaughtering).

RESULTS AND DISCUSSION

Rabbit behavior and handling during restraint and stunning

During restraint, when animals were removed from their cages and held in the area adjacent to the slaughterhouse, 28 % of rabbits attempted to escape, while 43 % exhibited kicking behavior. These responses were interpreted as indicators of stress, potentially reflecting a reduction in animal welfare. The precision of the operator in applying the stunning method varied significantly ($p < 0.009$), resulting in an overall failure rate of 17.5 %, with 13.3 % of these failures occurring during the use of the

concussion method. According to established standards, the maximum acceptable failure rate is 1 %; rates exceeding 4 % are indicative of serious deficiencies in handling during the slaughter process. Furthermore, 5 % of the animals required a second application of the stunning method ($p < 0.095$), which represents the upper limit of acceptability (Grandin, 2013).

Rabbit behavior during slaughter

To avoid rabbits regaining consciousness, slaughter must be performed within 30 s after stunning (Anil *et al*., 1998). The interval between stunning and slaughtering is determined by the operator's ability rather than by the stunning method used, thereby impeding direct comparison between methods. Nonetheless, 10.8 % of the rabbits were slaughtered beyond the time threshold. Behavioral indicators such as kicking, gaping, head lifting, and back arching exhibited significant differences between stunning techniques ($p < 0.02$), with electronarcosis identified as the most benign method (Table 2).

Table 2. Indicators evaluated during the stunning and slaughtering process of California rabbits (*Oryctolagus cuniculus* L.).

Indicators	Total			Concussion			Electronarcosis			*p*-value
	%	±	SEM	%	±	SEM	%	±	SEM	
				Stunning						
Precision	17.5		7.7	13.3		8.2	4.2		9.8	0.009
Applications	5.0		9.5	4.2		9.8	0.8		----	0.095
Vocalization	5.8		9.3	2.5		10.9	3.3		10.2	0.698
Kicking	43.3		5.2	35.8		5.9	7.5		9.0	<.001
				Slaughtering						
Vocalization	2.5		10.9	1.7		12.7	0.8		----	0.560
Kicking	49.2		4.7	35.8		5.9	13.3		8.2	<.001
Blinking	26.7		6.8	12.5		8.3	14.2		8.1	0.681
Corneal reflex	14.2		8.1	7.5		9.0	6.7		9.1	0.794
Dilated pupils	26.7		6.8	10.8		8.5	15.8		7.9	0.217
Gaping	30.0		6.8	10.0		9.3	20.0		8.0	0.017
Straightened head	15.8		7.9	13.3		8.2	2.5		10.9	0.0012
Arched back	11.7		8.4	9.2		8.7	2.5		10.9	0.023

SEM: standard error of the mean. Statistical differences are presented between rows.

The behaviors that indicate unconsciousness differ between physical and electrical stunning methods. In the case of physical stunning, the most important indicators are the righting and ocular reflexes, whereas for the methods that do not physically destroy the brain, such as electric stunning, the most important indicators are the righting reflex and vocalization (Verhoeven *et al.*, 2015). The European Food Safety Authority considers an indicator to be 100 % sensitive if it correctly identifies all conscious animals (EFSA, 2020).

Vocalization before and during stunning

No differences were found between methods for vocalization before (p = 0.698) or during stunning (p = 0.56). In a rabbit-specific slaughterhouse, Rota-Nodari *et al*. (2009) reported vocalization rates ranging from 0.1 to 0.3 % prior to and during the application of electric stunning. In the present study, the percentage of vocalization for each method remained below 5 %. For bovines and pigs, acceptable vocalization thresholds during handling and stunning have been established at ≤3 and ≤5 %, respectively (Grandin, 2013). However, standardized acceptable vocalization levels for rabbits have yet to be defined.

Vocalization is considered a behavioral indicator, as rabbits infrequently vocalize, and they typically do so only when conscious and experiencing significant pain or stress (Mayer, 2007). Nevertheless, not all conscious animals vocalize; thus, the absence of vocalization cannot be taken as definitive evidence of unconsciousness. Vocalizations occurring immediately prior to stunning may indicate handling issues, whereas vocalizations during the stunning process suggest inadequate application of the stunning method. Following effective stunning, no vocalization should be observed (Grandin, 2013). Vocalization is a readily measurable indicator, with a sensitivity of approximately 71 % for physical methods and 57 % for electrical methods (EFSA, 2020).

Clonic phase (post-stunning kicking)

A significant difference was observed in the clonic phase between both stunning methods ($p < 0.001$). This variation can be attributed to the neural circuits responsible for reciprocal leg movements, which are located in the spinal cord. These circuits require a functional spinal cord but do not depend on cerebral coordination. Spinal reflexes, such as kicking, tend to manifest more vigorously following physical stunning methods. In contrast, electrical stunning more frequently results in a mild tonic-clonic phase (Grandin, 2013), which facilitates its identification and recording when the concussion method is used.

Adequate stunning causes the tonic (rigid) and clonic (repeated muscular contractions) phases, during which an individual is unconscious. An error in evaluating this behavior is mistaking the clonic phase for a return to sensitivity, despite the fact that kicking reflexes can be present after effective desensitization, and the absence of these phases is due to the animal not becoming desensitized (Grandin, 2013). The appearance of the tonic-clonic phase is a medium-difficulty indicator with 89–93 % sensitivity for a physical and electric method, respectively (EFSA, 2020).

Corneal reflex, blinking, and dilated pupils

No statistically significant differences were observed between treatments compared to the presence of corneal reflex, blinking, or dilated pupils ($p > 0.05$). In cases of physical stunning, the absence of corneal reflexes and blinking is expected due to the cerebral trauma inflicted. However, these indicators may still be observed following effective

electrical stunning as a consequence of residual brainstem activity (Gregory and Shaw, 2000). For instance, Vogel *et al*. (2011) reported the occurrence of corneal reflex and blinking in 93.8 and 40.8 % of electrically stunned pigs, respectively. In contrast, the present study recorded these responses in only 6.7 and 14.2 % of cases, respectively. This discrepancy may be attributed to the timing of the evaluations. In the current study, corneal reflex was measured approximately 6 s after stunning, or about 30 s after the start of slaughter. It is possible that the blood loss caused by this point was enough to impair brainstem function, preventing the detection of these reflexes during examination (Vogel *et al*., 2011).

Conversely, Rota-Nodari *et al*. (2009) reported even lower frequencies of corneal reflex (1.8 %) and blinking (2.6 %) than those found in the current study. This variation may be due to procedural differences, as data in the aforementioned study were collected in a specialized commercial slaughterhouse where longer delays prior to observation could have further diminished the visibility of these indicators. Although the unconsciousness of the animal can be assured when the behaviors are absent, their presence does not necessarily imply that the animal is conscious (Verhoeven *et al.*, 2015). The corneal reflex is an indicator with a medium difficulty in measurement, with a sensitivity of 96 and 94 % for the concussion and electric methods, respectively, whereas blinking has a sensitivity of 69 %, regardless of the method of stunning. The dilated pupils (midriasis) are good indicators of death and have a sensitivity of 98 %, regardless of the stunning method, although measuring them is difficult (EFSA, 2020).

Gaping

The gaping showed significant differences between concussion and electronarcosis methods ($p < 0.02$). The last respiratory pattern in a dying animal is gaping or agonal breathing, which always results in terminal apnea and can appear after adequate electric stunning and is considered a positive sign (Pluta and Romaniuk, 1990).

Righting reflex

There was a significant difference between the methods for this indicator ($p < 0.05$). Vogel *et al*. (2011) discovered a 14.3 % righting reflex in electrically stunned pigs, while this study found only 2.5 %. The reflex of righting refers to any movement that causes the body to return to its normal position, such as lifting the head or arching the back. A conscious animal can exhibit this reflex following a failed stunning (EFSA, 2020). The recovery movements are oriented but can be difficult to distinguish from others (Terlouw *et al*., 2016). The righting reflex is a medium-difficulty indicator with a 77 % sensitivity (EFSA, 2020).

Evaluation of the lesions in the carcass

The *post-mortem* evaluation of lesions has been studied in cows, pigs, sheep, goats, poultry, and rabbits, mainly related to the transportation from the farms to the slaughterhouses (considering factors including the type and time of transportation

and load density) and, to a lesser extent, with the method of stunning (Mendonça *et al.*, 2016; Valkova *et al.*, 2021a, 2021b).

Location of the lesions

The post-mortem lesions found in carcasses during slaughterhouse inspections reflect animal management prior to slaughter. Inspecting the carcasses for evaluation helps value the lesions individually, highlighting any bruises that would otherwise go unnoticed. These lesions can be evaluated based on where they are located in the body (torso or limbs) (Huneau-Salaün *et al.*, 2015).

Of all the rabbits evaluated, 93 % displayed at least one lesion in the carcass (Table 3). Differences were found ($p < 0.01$) in the location of the lesions, with 24 % on the torso alone, 20 % on the limbs, and 48 % on the torso and limbs. Valkova *et al.*(2021b), in their study comparing the position of *post-mortem* traumatic lesions in rabbits, found an incidence of traumatic lesions of 1.52 %, out of which 0.83 % were on the limbs and 0.69 % on the torso, finding differences between both ($p < 0.01$ In another study, Petracci *et al*. (2010) discovered that 2 % of carcasses had lesions, though they only looked at hematomas larger than 1 cm^2, with the majority of hematomas on the limbs, thorax muscles, and inner back.

The concussion and electronarcosis methods showed differences in terms of the location of the lesions ($p < 0.01$). The concussion method produced 16.7 % of lesions on the torso and 0.8 % on the limbs, whereas electronarcosis produced 7.5 % on the torso

Table 3. Evaluation of the lesions in carcasses of California rabbits (*Oryctolagus cuniculus* L.) after using two stunning methods.

	Total			Concussion			Electronarcosis			
	%	±	SEM	%	±	SEM	%	±	SEM	*p*-value
Carcasses with lesions	93.3		0.61	50.0		4.51	43.3		5.27	0.004
Anatomic location										
Torso	24.2		7.05	16.7		7.80	7.5		8.96	0.019
Limbs	20.8		7.38	0.8		----	20.0		7.46	<.001
Both	48.3		4.76	32.5		6.24	15.8		7.89	<.001
None	6.7		9.91	0.0		----	6.7		9.91	0.004
Number of lesions										
Low (0–3)	54.2		4.22	18.3		8.17	35.8		6.12	<.001
High (4–14)	45.8		4.99	31.7		6.60	14.2		8.70	<.001
Size of lesions										
Small (≤0.5 cm)	18.3		8.17	0.0		----	18.3		8.17	<.001
Medium (0.6–1 cm)	10.0		9.30	4.2		10.67	5.8		10.11	0.545
Large (>1 cm)	65.0		2.79	45.8		4.98	19.2		8.07	<.001
None	6.7		9.91	0.0		----	6.7		9.91	0.004

SEM: standard error of the mean. Statistical differences are presented between rows.

and 20 % on the limbs. The electronarcosis method produces more lesions on the limbs than on the torso, as opposed to the concussion method, which affects the torso more, most likely due to a lesion caused by the stunning method in the occipital region. As a result, the concussion method can explain 32.5 % of lesions in both carcass regions, compared to 15.8 % for electronarcosis.

The location of the lesions may be related to the handling prior to slaughter, which damages the animals' limbs more than their torsos because the limbs are also a central part of the body through which rabbits are captured during catching, loading and unloading, and hanging in the slaughterhouse (Petracci *et al*., 2010). Data on hematoma percentages between studies and slaughterhouses are difficult to compare due to differences in veterinary inspection and carcass classification methods (Petracci *et al*., 2010).

Number and size of lesions

The concussion method displayed a more significant number of lesions, between 4 and 14 (31.7 ± 6.6), unlike the electronarcosis method, between 0 and 3 (35.8 ± 6.12) ($p < 0.01$). Regarding the size of the lesion, when the lesions were medium, there were no differences ($p = 0.54$); when they were large, the highest frequency was presented in the concussion method (45.8 ± 4.98). Therefore, applying the concussion method causes a higher number and more extensive lesions than the method of electronarcosis ($p < 0.01$).

Small lesions (18.3 ± 8.17, $p < 0.01$) were more commonly associated with electronarcosis in limbs (20 ± 7.46, $p < 0.01$). However, there was no significant difference in kicking behavior between stunning and the concussion method ($p < 0.001$). Such lesions could be caused by the passage of electric currents, which can cause muscle contractions, resulting in muscle fiber damage and hemorrhage. The hemorrhage is due to a substantial increase in the intravascular pressure, and as a result, blood capillaries can break and lead to bleeding (Kranen *et al*., 2000). Studies on cows displayed more significant small and medium lesions (74.9 and 19.1 %, respectively) (Knock and Carroll, 2019). On sheep, a prevalence of small lesions has been found (Teiga-Teixeira *et al*., 2021).

Lesion comparison based on the treatment used

The comparison of ranges (Kruskal-Wallis) expressed as categorical values displayed differences between treatments ($ChiSq < 0.01$) (Figure 1), with treatments 1 and 2 being different from treatments 3 and 4; that is, the frequency of lesions had more significant scores when the concussion method was used ($ChiSq < 0.05$), without differences between sexes ($ChiSq > 0.05$).

There was an average of 3.76 lesions per carcass, ranging from 0 to 14, across the 120 carcasses. The average number of lesions per method was 4.81 for concussion and 2.7 for electronarcosis ($p < 0.01$). The treatment means were T1 = 4.77, T2 = 4.87, T3 = 2.9, and T4 = 2.5, with a standard error of 0.49 ($p < 0.0005$). Small species, such as rabbits,

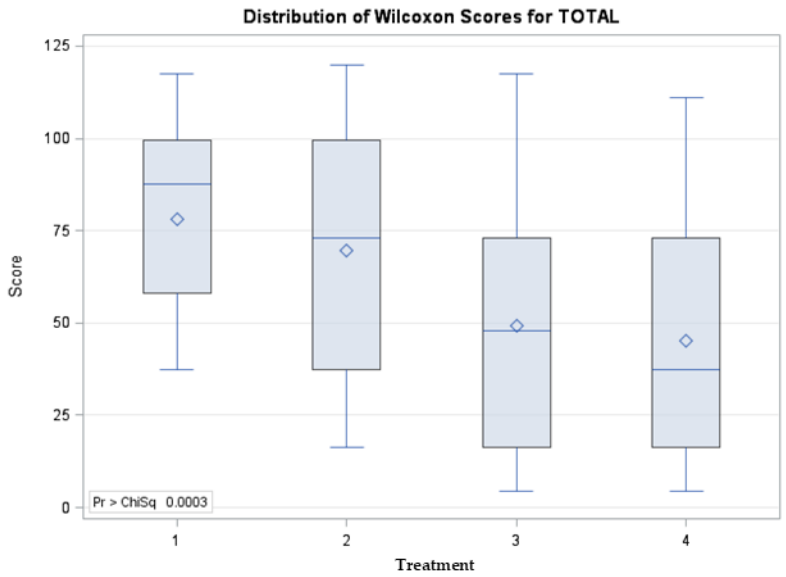

Figure 1. Kruskal-Wallis test comparing the total frequency of lesions in California rabbits (*Oryctolagus cuniculus* L.), depending on the treatment applied. T1: concussion, males; T2: concussion, females; T3: electronarcosis, males; T4: electronarcosis, females. Categories are presented in ranges.

are easier to handle and restrain, allowing for better control of external factors that can cause lesions prior to slaughter. As a result, the lesions discovered during the post-mortem carcass evaluation are associated with the stunning method.

Risk factors for the overall presentation of lesions in the carcass

The logistic regression analysis revealed that the sex and weight of the rabbits, as well as the time between stunning and slaughtering, had no relationship with the total number of lesions found in the carcass (*ChiSq* > 0.05). The concussion method was found to be 4.6 times more likely to cause lesions compared to the electronarcosis method (Table 4; *ChiSq* < 0.01). In other studies, the risk factors associated with the lesions found in the *post-mortem* evaluation of the carcass were sex, race, bodily condition, live weight, zootechnical objective, transportation distance and time, lodging type during transportation, load density, handling conditions, type of truck, loading and unloading conditions, season of the year, farm of origin, and resting time prior to slaughter (Petracci *et al.*, 2010; Tarumán *et al.*, 2018; Bethancourt-Garcia *et al.*, 2019; Knock y Carroll, 2019; Teiga-Teixeira *et al.*, 2021).

Table 4. Probability of lesions in California rabbits (*Oryctolagus cuniculus* L.) for each variable based on the logistical regression analysis.

Variable	Category		Parameter	SEM (b_i)	OR	IC 95 %	*p* > *ChiSq*
Method	Concussion Electronarcosis	(0) (1)	1.53	0.42	4.60	2.01–10.49	0.0003
Sex	Male Female	(0) (1)	0.40	0.41	1.49	0.66–3.35	0.34
Weight	2.0–2.2 Kg 2.2–2.4 Kg	(0) (1)	-0.19	0.46	0.82	0.33–2.04	0.68
Time	<30 s >30 s	(0) (1)	0.16	0.66	1.17	0.32–4.24	0.81

SEM: standard error of the mean; OR: risk factor; IC: trust interval at 95 %.

CONCLUSIONS

Electronarcosis is an effective method for stunning rabbits before slaughtering, as it causes fewer negative behaviors related to kicking, gaping, lifting of the head, and arching of the back in comparison to the method of concussion, without being influenced by the weight and sex of the animal. The concussion method hurts the welfare of rabbits during slaughter and is not affected by the sex and weight of the animal, either. However, it is affected by the evaluated handling categories.

REFERENCES

Anil MH, Raj ABM, McKinstry JL. 1998. Electrical stunning in commercial rabbits: Effective currents, spontaneous physical activity, and reflex behavior. Meat Science 48 (1–2): 21–28. https://doi.org/10.1016/s0309-1740(97)00071-5

Bethancourt-Garcia JA, Vaz RZ, Vaz FN, Silva WB, Pascoal LL, Mendonça FS, da-Vara CC Nuñez AJC, Restle J. 2019. Pre-slaughter factors affecting the incidence of severe bruising in cattle carcasses. Livestock Science 222: 41–48. https://doi.org/10.1016/j.livsci.2019.02.009

DOF (Diario Oficial de la Federación). 2014. NORMA Oficial Mexicana NOM-033-SAG/ZOO-2014. Métodos para dar muerte a los animales domésticos y silvestres. Gobierno de México. Secretaría de Agricultura, Ganadería, Desarrollo Rural, Pesca y Alimentación. Ciudad de México, México. www.dof.gob.mx/nota_detalle.php?codigo=5405210 (Retrieved: August 2021).

EFSA (European Food Safety Authority). 2020. Stunning methods and slaughter of rabbits for human consumption. EFSA Journal 18 (1): 106. https://doi.org/10.2903/j.efsa.2020.5927

European Commission. 2017. Preparation of best practices on the protection of animals at the time of killing. Publications Office of the European Union: Brussels, Belgium. https://doi.org/10.2875/15243

Grandin T. 2013. Making slaughterhouses more humane for cattle, pigs, and sheep. Annual Review of Animal Biosciences 1 (1): 491–512.

Grandin T. 2017. Recommended animal handling guidelines and audit guide: A systematic approach to animal welfare. North American Meat Institute: Washington, DC, USA. https://www.grandin.com/RecAnimalHandlingGuidelines.html (Retrieved: December 2021).

Gregory N, Shaw F. 2000. Penetrating captive bolt stunning and exsanguination of cattle in abattoirs. Journal of Applied Animal Welfare Science 3 (3): 215–230. https://doi.org/10.1207/s15327604jaws0303_3

Huneau-Salaün A, Stärk KDC, Mateus A, Lupo C, Lindberg A, Bouquin-Leneveu LS. 2015. Contribution of meat inspection to the surveillance of poultry health and welfare in the European Union. Epidemiology and Infection 143 (11): 2459–2472. https://doi.org/10.1017/s0950268814003379

Knock M, Carroll GA. 2019. The potential of *post-mortem* carcass assessments in reflecting the welfare of beef and dairy cattle. Animals 9 (11): 959. https://doi.org/10.3390/ani9110959

Kranen RW, Lambooy E, Veerkamp CH, van-Kuppevelt TH, Veerkamp JH. 2000. Histological characterization of hemorrhages in muscles of broiler chickens. Poultry science 79 (1): 110–116. https://doi.org/10.1093/ps/79.1.110

Mayer J. 2007. Use of behavior analysis to recognize pain in small mammals. Lab Animal 36 (6): 43–48. https://doi.org/10.1038/laban0607-43

McKinstry JL, Anil MH. 2004. The effect of repeat application of electrical stunning on the welfare of pigs. Meat Science 67 (1): 121–128. https://doi.org/10.1016/j.meatsci.2003.10.002

Mendonça FS, Vaz RZ, Cardoso FF, Restle J, Vaz FN, Pascoal LL, Reimann FA, Boligon AA. 2016. Pre-slaughtering factors related to bruises on cattle carcasses. Animal Production Science 58 (2): 385–392. https://doi.org/10.1071/an16177

Petracci M, Bianchi M, Biguzzi G, Cavani C. 2010. Preslaughter risk factors associated with mortality and bruising in rabbits. World Rabbit Science 18 (4): 219–228. https://doi.org/10.4995/wrs.2010.781

Pluta R, Romaniuk JR. 1990. Recovery of breathing pattern after 15 min of cerebral ischemia in rabbits. Journal of Applied Physiology 69 (5): 1676–1681. https://doi.org/10.1152/jappl.1990.69.5.1676

Rota-Nodari S, Lavazza A, Candotti P. 2009. Technical note: Rabbit welfare during electrical stunning and slaughter at a commercial abattoir. World Rabbit Science 17 (3): 163–167. https://doi.org/10.4995/wrs.2009.656

Stoier S, Larsen HD, Aaslyng MD, Lykke L. 2016. Improved animal welfare, the right technology and increased business. Meat Science 120: 71–77. https://doi.org/10.1016/j.meatsci.2016.04.010

Tarumán JA, Smulders JP, Gallo CB. 2018. Risk factors for bruises and high muscle pH in lamb carcasses of Tierra del Fuego, Chilean Patagonia. Open Access Library Journal 5 (1): 1–11. https://doi.org/10.4236/oalib.1104291

Teiga-Teixeira P, Moura D, García-Díez J, Esteves A. 2021. Characterization of carcass bruises in cattle in Northern Portugal, a preliminary study. Italian Journal of Animal Science 20 (1): 1168–1174. https://doi.org/10.1080/1828051x.2021.1957030

Terlouw C, Bourguet C, Deiss V. 2016. Consciousness, unconsciousness and death in the context of slaughter. Part II. Evaluation methods. Meat Science 118: 147–156. https://doi.org/10.1016/j.meatsci.2016.03.010

Valkova L, Vecerek V, Voslarova E, Kaluza M, Takacova D. 2021a. The welfare of cattle, sheep, goats and pigs from the perspective of traumatic injuries detected at slaughterhouse postmortem inspection. Animals 11 (5): 1406–1420. https://doi.org/10.3390/ani11051406

Valkova L, Vecerek V, Voslarova E, Kaluza M, Takacova D. 2021b. Traumatic injuries detected during *post-mortem* slaughterhouse inspection as welfare indicators in poultry and rabbits. Animals 11 (9): 2610–2621. https://doi.org/10.3390/ani11092610

Verhoeven MTW, Gerritzen MA, Hellebrekers LJ, Kemp B. 2015. Indicators used in livestock to assess unconsciousness after stunning: A review. Animal 9 (2): 320–330. https://doi.org/10.1017/s1751731114002596

Vogel KD, Badtram G, Claus JR, Grandin T, Turpin S, Weyker RE, Voogd E. 2011. Head-only followed by cardiac arrest electrical stunning is an effective alternative to head-only electrical stunning in pigs. Journal of Animal Science 89 (5): 1412–1418. https://doi.org/10.2527/jas.2010-2920

Agrociencia

CARCASS AND PARTS YIELD OF MEXICAN CRIOLLO AND SASSO CHICKENS RAISED IN CONFINEMENT OR GRAZING

Lisbeth **Avendaño-López**[1], Fernando **González-Cerón**[1*], Berenice **Hernández-Blancas**[2], Arturo **Pro-Martínez**[2], Sergio Iban **Mendoza-Pedroza**[2], Diego **Zárate-Contreras**[2]

[1]Universidad Autónoma Chapingo. Departamento de Zootecnia. Carretera México-Texcoco km 38.5, Texcoco, State of Mexico, Mexico. C. P. 56230.
[2]Colegio de Postgraduados Campus Montecillo, Programa en Recursos Genéticos y Productividad-Ganadería. Carretera México-Texcoco km 36.5, Montecillo, Texcoco, State of Mexico, Mexico. C. P. 56264.
* Author for correspondence: fgceron@colpos.mx

Citation: Avendaño-López L, González-Cerón F, Hernández-Blancas B, Pro-Martínez A, Mendoza-Pedroza SI, Zárate-Contreras DI. 2025. Carcass and parts yield of Mexican Criollo and Sasso chickens raised in confinement or grazing. **Agrociencia** 59(4): 457-466. https://doi.org/ 10.47163/agrociencia.v59i4.3244

Editor in Chief:
Dr. Fernando C. Gómez Merino

Received: August 03, 2024.
Approved: June 11, 2025.
Published in Agrociencia: June 25, 2025.

ABSTRACT

The consumption of chicken meat (*Gallus gallus domesticus* L.) has gradually increased. Changes in economic and social development have changed consumer perceptions of the quality and safety of food in terms of animal welfare, resulting in the implementation of new alternative farming systems. This research was conducted at the poultry farm "El Horno" within the Valley of Mexico Experimental Field of the National Institute of Forestry, Agriculture, and Livestock Research (CEVAMEX-INIFAP) in 2022. The objective was to determine the carcass and parts yield of Mexican Criollo (CM) and Sasso (S) chickens raised in confinement or grazing conditions. Ninety-two birds (44 CM and 48 S), randomly distributed in both production systems, were used to obtain four replicates of the following combinations of bird genotype and production system: CM grazing, CM confinement, S grazing, and S confinement, with feed and water *ad libitum*. At 84 days of age, the birds were weighed individually per treatment and sacrificed by desensitizing them by cervical dislocation. The weight of the legs, thigh, breast, skin, muscle, and bone was evaluated separately for each piece. A completely randomized experimental design with a 2 × 2 factorial arrangement was used, with genotype and production system as main factors. Data were analyzed using PROC MIXED of SAS. Cold and hot carcass yield was higher in S birds compared to CM birds. The live weight recorded in S birds was 946 g higher compared to CM birds. It is concluded that S birds perform better in the main pieces (breast, leg, and thigh), as well as in their variables (skin, muscle, and bone), regardless of the production system to which they are subjected (grazing or confinement).

Keywords: *Gallus gallus domesticus* L. skin, muscle, bone, poultry, animal welfare.

INTRODUCTION

Poultry farming represents the most dynamic sector within the Mexican livestock industry, positioning the country as the fifth largest producer of poultry meat globally. Three primary poultry production systems are used nationwide: technified, semi-

technified, and backyard or family-based systems. Among these, the backyard system remains the most traditional and widely distributed across the country; however, its contribution to overall production is minimal (around 10 %) as it primarily serves subsistence purposes (SAGARPA, 2012).

In Mexico, chicken meat has become a staple dietary component due to its affordability and widespread acceptance as a nutritious and safe food source. Its culinary versatility further enhances its importance in daily household meals (Iruegas-Evaristo, 2011). Compared to meat from other species, chicken meat contains lower intramuscular fat, making it more easily digestible. Moreover, it possesses significant nutritional value, providing, on average, 20 % protein, comparable to beef, and approximately 9 % fat. It also contains essential minerals, including iron, zinc, phosphorus, and potassium, which are vital for human health (Moreiras *et al*., 2005).

The growth and performance of birds are determined by genotype, age, sex, diet, and environment. These factors help improve performance within production (Gordon and Charles, 2002). However, it is necessary to investigate the specific conditions that guarantee the optimal productive performance of the Mexican Criollo chicken compared to the breeds used in non-conventional production systems, such as the Sasso chicken. Matus-Aragón *et al*. (2021) evaluated the performance of Mexican Criollo chickens at 12 weeks of age and reported a higher carcass yield in males (1548.53 g) compared to females (872.72 g). In general, males showed higher weight and performance in most of the variables evaluated, except for breast, thigh, and wing. Dzungwe *et al*. (2022) reported that Sasso chickens yielded 1929 g at the same age, which was higher than Creole birds.

Although the general conditions of broiler production are known, the yield of the parts most valued by consumers (breast, legs, and thighs) is unknown, which is required to effectively utilize the poultry genetic resources in Mexico and commercialize them. Therefore, the current study assessed the carcass yield, its components, and the skin-muscle-bone relationship in Mexican Criollo and Sasso poultry, as well as how the rearing system affects these variables.

MATERIALS AND METHODS

Study site

The study was conducted at the facilities of the poultry farm "El Horno," located in the Valley of Mexico Experimental Field under the National Institute of Forestry, Agriculture, and Livestock Research (CEVAMEX-INIFAP), at 19° 48′ 95′′ N, 98° 89′ 42′′ W, and an altitude of 2250 m (Sangerman-Jarquín *et al*., 2009).

Animal management

A total of 92 birds were used, including 44 Mexican Criollo (CM) and 48 Sasso (S) chickens, which were randomly distributed in grazing (P) or confinement (C)

production systems, with four replicates each. A factorial arrangement of treatments (CMP, CMC, SP, and SC) was used. Birds in confinement were kept permanently in pens inside a natural environment poultry house with movable side curtains. Birds in the grazing system had access to a white clover (*Trifolium repens* L.) grazing for 8 h a day (9:00 am to 5:00 pm), and spent the rest of their time inside the house.

The chickens were housed in pens inside the house with dimensions of 1.1 × 1.4 m, and the floor was covered with 5 cm of shavings litter. Each pen was equipped with a hopper feeder (10 kg) and a 5 L drinker. From 35 to 56 days of age, the birds were fed a diet of 2550 kcal of metabolizable energy per kilogram and 17 % crude protein (PC); from 56 to 84 days of age, they were offered commercial balanced feed (minimum PC of 17.5 %, crude fat 4 %, minimum crude fiber of 4.5 %, maximum ash of 5.5 %, maximum moisture of 12 %, and nitrogen-free extract by difference of 55.5 %). Food and water were offered *ad libitum*.

Poultry processing

At 84 days of age, birds were weighed individually according to treatment on a digital scale (Ohaus Ranger® 3000 Counting Scale, Mexico) with a capacity of 15 kg. Subsequently, they were slaughtered in accordance with the Official Mexican Standard NOM-O33-ZOO-1995 (DOF, 1995) by dislocation at the level of the first cervical vertebra and the occipital condyle, followed by decapitation and exsanguination. Birds were scalded by being immersed in a container with hot water (45 s) at a temperature of 62 to 65 °C (González-Cortés *et al*., 2019).

Each bird was identified with a plastic tag attached to their tibia. To obtain the hot carcass (HC), the viscera were removed, and the legs were cut between the tibia and the metatarsus. Subsequently, the carcasses were placed in 200-L containers with cold water (<4 °C) for 16 h (Carciofi and Laurindo, 2007). Subsequently, the carcasses were removed from the water and placed on a table, where the excess water was removed by gravity (2 h); they were then weighed, and the cold carcass weight (CF) was determined.

Quartering and fleshing

The quartering process consisted of separating the main pieces (legs, thighs, and breast) and the minor pieces (wings, neck, shoulder, and breast bone) to obtain their weight separately. Once the weight was recorded, the skin was separated from the muscle and the bone from the muscle with the help of a knife, taking great care not to damage the material, in order to weigh the skin, bone, and muscle individually.

Variables evaluated

Live weight (LW), hot carcass weight (HCW), cold carcass weight (CCW), total muscle weight (TMuscW), total bone weight (TBoneW), and total skin weight (TSkinW) were evaluated in all chickens.

In relation to the leg, total leg weight (TLgW), leg bone weight (LgBoneW), leg skin weight (LgSkinW), and leg muscle weight (LgMuscW) were recorded, and the yield of

total leg weight to live weight (TLgW-LW), to hot carcass (TLgW-HCW), and to cold carcass (TLgW-CCW) was calculated.

In relation to the thigh, total thigh weight (TThW), thigh bone weight (ThBoneW), thigh skin weight (ThSkinW), and thigh muscle weight (ThMuscW) were recorded, and the yield of total thigh weight to live weight (TThW-LW), to hot carcass (TThW-HCW), and to cold carcass (TThW-CCW) was calculated.

For breast, total breast weight (TBrW), breast weight of the minor breast (BrWminor), and breast weight of the major breast (BrWmajor) were recorded, while breast bone weight (BrBoneW) and breast skin weight (BrSkinW), and the yield of total breast weight to live weight (TBrW-LW), to hot carcass (TBrW-HCW), and to cold carcass (TBrW-CCW) were calculated.

Statistical analysis

The data for the variables studied were analyzed with the SAS MIXED procedure (SAS version 9.3; SAS Institute, Cary, NC, USA) under a completely randomized experimental design with a 2 × 2 factorial arrangement, with bird genotype and production system as main factors. The effect of each factor was considered significant at a value of $p \leq 0.05$. The adjusted means obtained were compared using Tukey's test.

RESULTS AND DISCUSSION

Carcass yield

Live weight (LW), hot carcass weight (HCW), and cold carcass weight (CCW) (Table 1) were higher in birds of the S commercial line compared to CM birds at 84 days of age. For LW, S birds had 946 g more compared to CM birds (2150 and 1204 g, respectively), the latter being higher than the 1158.46 g reported by Matus-Aragón *et al*. (2020) for CM birds at the same age. For HCW, the same trend continues in favor of the S line (68 %) in relation to CM birds (60 %).

Lower yields were recorded than those reported by Lorenzo *et al*. (2011), with S chickens (T-44) and CM birds exhibiting yields of 79.63 and 66 %, respectively, in comparison to other Creole birds. Similarly, lower values were observed for CCW (62 % for CM and 71 % for S), with higher percentages compared to HCW, which can be attributed to the cooling method used. It could be said that cooling by immersion in cold water causes a carcass weight gain (water absorption) of up to 6 %. Generally, the appearance of the carcass after chilling is better (Demirok *et al*., 2013).

Production system yield

Regarding the production system, no significant differences were observed ($p > 0.05$), with yields of 68.7 and 67.7 % in confinement and grazing, respectively. Similar results were reported by Paredes and Vásquez (2020), who obtained 68.4 % in confined Criollo birds, while Santos *et al.* (2014) obtained a carcass yield of 75 % with bare-necked birds in grazing.

Table 1. Adjusted means (± standard error) of variables associated with carcass yield of Mexican Criollo and Sasso chickens (*Gallus gallus domesticus* L.) raised in confinement or grazing conditions.

Factor	Level	LW (g)	HCW (g)	CCW (g)
GEN	CM	1204 ± 42[b]	722 ± 29[b]	755 ± 32[b]
	S	2150 ± 41[a]	1477 ± 29[a]	1530 ± 32[a]
SYST	CONF	1682 ± 41	1121 ± 28	1157 ± 31
	GRAZ	1671 ± 42	1078 ± 30	1129 ± 33
GEN × SYST	CM × CONF	1258 ± 56	773 ± 39	791 ± 43
	CM × GRAZ	1149 ± 61	671 ± 43	719 ± 47
	S × CONF	2106 ± 59	1469 ± 41	1522 ± 45
	S × GRAZ	2194 ± 59	1485 ± 41	539 ± 45
p-value	GEN	<0.0001	<0.0001	<0.0001
	SYST	0.8494	0.2959	0.5420
	GEN × SYST	0.0972	0.1565	0.3310

LW: live weight; HCW: hot carcass weight; CCW: cold carcass weight; GEN: genotype; SYST: production system; CM: Mexican Creole chicken; S: Sasso chicken; CONF: confinement raising; GRAZ: grazing-raised. [abc] Mean values per column with different letters between factors are statistically different ($p \leq 0.05$).

Leg yield

For leg yield, significant differences ($p \leq 0.05$) were observed among the bird genotypes (Table 2), with values of 9.8 and 10.2 % in relation to live weight for CM and S, respectively. The values reported exceed those documented by Lorenzo *et al*. (2011), who recorded a leg yield of 4.07 % in Sasso T-44 birds, compared to 4.22 % for the native Moss bird. Their components (skin, muscle, and bone) followed the superior trend in the S strain, with 6.7, 66.7, and 26.2 %, respectively, compared to CM with 5.9, 61.8, and 32.2 %. On the contrary, the results of this research are lower than those obtained by Ángeles-Coronado *et al*. (2013) for creole birds, who obtained leg yields of 13.5 to 16.6 %.

Thigh yields

In CM birds, the thigh yield was 10.8 % in relation to live weight, whereas in S birds it was 10.5 %, indicating a statistically significant difference ($p \leq 0.05$). Consequently, the skin, muscle, and bone components followed the trend in favor of the S line (Table 3), obtaining lower values for thigh yield compared to those reported by Lorenzo *et al*. (2011), who found a thigh yield of 15.9 % in Sasso T-44 birds, while for the native Moss bird, a value of 13.5 % was obtained. Similarly, the values found in this study are lower than those obtained by Sanka *et al*. (2021), who reported a thigh yield of 17 % in Sasso chickens, below the Kuroiler hybrid with 17.4 %.

Table 2. Adjusted means (± standard error) of variables associated with leg performance of Mexican Criollo and Sasso chickens (*Gallus gallus domesticus* L.) raised in confinement or grazing conditions.

Factor	Level	TLgW (g)	LgBoneW (g)	LgMuscW (g)	LgSkinW (g)	TLgW-LW (%)	TLgW-HCW (%)	TLgW-CCW (%)
GEN	CM	118 ± 6^{b}	38 ± 2^{b}	73 ± 4^{b}	7 ± 1^{b}	0.097 ± 0.003	0.164 ± 0.004	0.158 ± 0.005
	S	221 ± 6^{a}	58 ± 2^{a}	148 ± 4^{a}	15 ± 1^{a}	0.103 ± 0.003	0.151 ± 0.004	0.145 ± 0.005
SYST	CONF	172 ± 5	49 ± 2	112 ± 4	11 ± 1	0.100 ± 0.003	0.155 ± 0.004	0.153 ± 0.005
	GRAZ	167 ± 6	47 ± 2	109 ± 4	11 ± 1	0.100 ± 0.003	0.159 ± 0.004	0.151 ± 0.005
GEN × SYST	CM × CONF	123 ± 8	40 ± 3	76 ± 5	7 ± 1	0.097 ± 0.004	0.160 ± 0.006	0.161 ± 0.007
	CM × GRAZ	113 ± 8	37 ± 3	69 ± 6	7 ± 1	0.097 ± 0.004	0.167 ± 0.006	0.156 ± 0.007
	S × CONF	221 ± 8	59 ± 3	147 ± 5	15 ± 1	0.104 ± 0.004	0.150 ± 0.006	0.145 ± 0.007
	S × GRAZ	221 ± 8	57 ± 3	149 ± 5	15 ± 1	0.102 ± 0.004	0.151 ± 0.006	0.146 ± 0.007
p-value	GEN	<0.0001	<0.0001	<0.0001	<0.0001	0.0854	0.034	0.077
	SYST	0.5217	0.3925	0.6530	0.8282	0.7898	0.473	0.234
	GEN × SYST	0.5163	0.8899	0.4275	0.6854	0.6920	0.587	0.309

TLgW: total leg weight; LgBoneW: leg bone weight; LgMuscW: leg muscle weight; LgSkinW: leg skin weight; TLgW-LW: total leg weight yield to live weight; TLgW-HCW: total leg weight yield to hot carcass; TLgW-CCW: total leg weight yield to cold carcass; GEN: genotype; SYST: production system; CM: Mexican Creole chicken; S: Sasso chicken; CONF: confinement rearing; GRAZ: graze rearing. ^{abc} Mean values per column with different letters between factors are statistically different ($p \leq 0.05$).

Table 3. Adjusted means (± standard error) of variables associated with thigh performance of Mexican Criollo and Sasso chickens (*Gallus gallus domesticus* L.) raised in confinement or grazing conditions.

Factor	Level	TThW (g)	ThBoneW (g)	ThMuscW (g)	ThSkinW (g)	TThW-LW (%)	TThW-HCW (%)	TThW-CCW (%)
GEN	CM	130 ± 7^{b}	27 ± 1.374^{b}	88 ± 5^{b}	14 ± 1^{b}	0.111 ± 0.005	0.191 ± 0.010	0.184 ± 0.010
	S	225 ± 7^{a}	41 ± 1.368^{a}	169 ± 5^{a}	25 ± 1^{a}	0.105 ± 0.005	0.152 ± 0.009	0.146 ± 0.010
SYST	CONF	180 ± 7	34 ± 1.340	130 ± 5	19 ± 1	0.110 ± 0.005	0.170 ± 0.009	0.167 ± 0.009
	GRAZ	175 ± 7	34 ± 1.4	127 ± 5	19 ± 1	0.106 ± 0.005	0.172 ± 0.010	0.163 ± 0.010
GEN × SYST	CM × CONF	135 ± 10	27 ± 2.0	90 ± 7	14 ± 1	0.112 ± 0.007	0.187 ± 0.013	0.186 ± 0.013
	CM × GRAZ	126 ± 11	26 ± 2.0	87 ± 8	13 ± 1	0.111 ± 0.007	0.195 ± 0.014	0.182 ± 0.014
	S × CONF	225 ± 10	41 ± 2.0	170 ± 7	24 ± 1	0.108 ± 0.007	0.154 ± 0.014	0.150 ± 0.013
	S × GRAZ	224 ± 10	41 ± 2.0	167 ± 7	26 ± 1	0.102 ± 0.007	0.150 ± 0.013	0.145 ± 0.013
p-value	GEN	<0.0001	<0.0001	<0.0001	<0.0001	0.355	0.005	0.006
	SYST	0.6096	0.990	0.6677	0.745	0.647	0.894	0.756
	GEN × SYST	0.6957	0.728	0.9840	0.487	0.720	0.646	0.986

TThW: total thigh weight; ThBoneW: thigh bone weight; ThMuscW: thigh muscle weight; ThSkinW: thigh skin weight; TThW-LW: total thigh weight yield to live weight; TThW-HCW: total thigh weight yield to hot carcass; TThW-CCW: total thigh weight yield to cold carcass; GEN: genotype; SYST: production system; CM: Mexican Creole chicken; S: Sasso chicken; CONF: confinement rearing; GRAZ: graze rearing. ^{abc} Mean values per column with different letters between factors are statistically different ($p \leq 0.05$).

Breast yield

The breast muscle was divided into two sections: pectoralis major (BrWmajor) and pectoralis minor (Table 4). A yield of 15.2 % was obtained in CM birds, while S birds yielded 17.9 %, showing a difference between genotypes in favor of the commercial S strain, which can be attributed to the genetic improvement of slow-growing strains for this type of production, improving their carcass yield and meat-to-bone ratio (Brackenbury and Williamson, 1989) compared to CM birds.

The results are higher than those reported by Pavlovski *et al*. (2009), who observed a yield of 13.5 to 13 % in native Naked Neck birds at 98 days of fattening age, and Miguel *et al*. (2008), who reported a yield of 18.6 to 16 % in Sasso strain birds at 105 days of age.

Total skin and muscle yield

Total skin and muscle yield values in relation to live weight were found for CM birds to be 2.9 and 23.8 %, respectively (Table 5), whereas S birds yielded 3.4 and 27.7 %. A small difference was found in both variables in favor of the S strain. The data presented

Table 4. Adjusted means (± standard error) of variables associated with breast performance of Mexican Criollo and Sasso chickens (*Gallus gallus domesticus* L.) raised in confinement or grazing condition.

Factor	Level	TBrW (g)	BrBoneW (g)	BrWminor (g)	BrWmajor (g)	BrSkinW (g)	TBrW-LW (%)	TBrW-HCW (%)	TBrW-CCW (%)
GEN	CM	184 ± 10^{b}	44 ± 3^{b}	33 ± 2^{b}	93 ± 6^{b}	14 ± 1^{b}	0.152 ± 0.006	0.256 ± 0.009	0.247 ± 0.009
	S	385 ± 10^{a}	74 ± 3^{a}	71 ± 2^{a}	209 ± 6^{a}	32 ± 1^{a}	0.181 ± 0.006	0.263 ± 0.009	0.254 ± 0.009
SYST	CONF	294 ± 10	61 ± 3	54 ± 2	157 ± 6	21 ± 1	0.170 ± 0.006	0.261 ± 0.009	0.256 ± 0.009
	GRAZ	275 ± 10	56 ± 3	49 ± 2	144 ± 6	25 ± 1	0.163 ± 0.006	0.258 ± 0.009	0.245 ± 0.009
GEN × SYST	CM × CONF	195 ± 14	49 ± 4	34 ± 3	98 ± 8	13 ± 2	0.153 ± 0.008	0.253 ± 0.012	0.252 ± 0.013
	CM × GRAZ	173 ± 15	39 ± 4	32 ± 3	87 ± 9	15 ± 2	0.150 ± 0.008	0.260 ± 0.013	0.241 ± 0.014
	S × CONF	393 ± 14	74 ± 4	75 ± 3	215 ± 8	30 ± 2	0.187 ± 0.008	0.269 ± 0.013	0.260 ± 0.013
	S × GRAZ	377 ± 14	73 ± 4	66 ± 3	202 ± 8	35 ± 2	0.175 ± 0.008	0.258 ± 0.013	0.250 ± 0.013
p-value	GEN	<0.0001	<0.0001	<0.0001	<0.0001	<0.0001	0.0005	0.557	0.558
	SYST	0.181	0.167	0.085	0.145	0.061	0.373	0.871	0.443
	GEN × SYST	0.867	0.206	0.336	0.877	0.292	0.562	0.511	0.985

TBrW: total breast weight; BrBoneW: breast bone weight; BrWminor: minor breast weight; BrWmajor: major breast weight; BrSkinW: breast skin weight; TBrW-LW: total breast weight yield to live weight; TBrW-HCW: total breast weight yield to hot carcass; TBrW-HCW: total breast weight yield to live weight; TBrW-HCW: total breast weight yield to cold carcass; SYST: production system; GEN: genotype; SYST: production system; CM: Mexican Criollo chicken; S: Sasso chicken; CONF: confinement rearing; GRAZ: graze rearing. ^{abc} Mean values per column with different letters between factors are statistically different ($p \leq 0.05$).

Table 5. Adjusted means (± standard error) of variables associated with carcass yield of Mexican Criollo chicken and Sasso chickens (*Gallus gallus domesticus* L.) raised in confinement or grazing conditions.

Factor	Level	TMuscW (g)	TBoneW (g)	TSkinW (g)
GEN	CM	287 ± 14[b]	109 ± 5[b]	35 ± 2[b]
	S	596 ± 14[a]	172 ± 5[a]	73 ± 2[a]
SYST	CONF	453 ± 14	144 ± 5	52 ± 2
	GRAZ	430 ± 15	137 ± 5	55 ± 2
GEN × SYST	CM × CONF	298 ± 19	116 ± 7	34 ± 3
	CM × GRAZ	275 ± 21	102 ± 7	35 ± 3
	S × CONF	607 ± 20	173 ± 7	69 ± 3
	S × GRAZ	584 ± 20	172 ± 7	76 ± 3
p-value	GEN	<0.0001	<0.0001	<0.0001
	SYST	0.258	0.296	0.238
	GEN × SYST	0.999	0.425	0.293

TMuscW: total muscle weight; TBoneW: total bone weight; TSkinW: total skin weight; GEN: genotype; SYST: production system; CM: Mexican Creole chicken; S: Sasso chicken; CONF: confinement rearing; GRAZ: graze rearing. [abc] Mean values per column with different letters between factors are different ($p \leq 0.05$).

is consistent with what was stated by Franco *et al*. (2012) regarding the yield for skin that was obtained (0.96 and 1.34 %) in favor of Sasso birds, contrary to meat (11.42 and 9.6 %; $p < 0.001$), which was higher in samples of Moss hens.

On the other hand, according to the production system to which they were subjected, no significant difference was observed. Skin yield was 3 % in both grazing and confinement, while muscle yield was 27 % in grazing and 25 % in confinement, with results that are very similar and statistically insignificant.

Total bone yield

Regarding the production system, values of 8.6 % were obtained for the confinement system and 8.1 % for the grazing system, with no significant differences. Regarding the bone variable (Table 5), independently of the main pieces, values were obtained for the CM birds of 9 % and for S of 8 % in relation to the total weight. There was no significant difference between genotypes, which can be attributed to the fact that CM birds are an unimproved line and nutrients are used by them for survival, in this case, having a more resistant bone system, a product of genetic selection that has been carried out for many years in the commercial Sasso line (Aman *et al*., 2017). Similarly, the results agree with those obtained by Muriel-Durán *et al*. (1997), who evaluated Spanish birds and crosses of specialized lines for meat at 89 days of age, raised in a grazing system, where a bone yield of 5.8 % was obtained.

CONCLUSIONS

Birds of the Sasso commercial line showed better productive performance compared to the Mexican Criollo in terms of live weight and overall carcass yield and its main parts (leg, thigh, and breast) at 84 days of age. Mexican Criollo and Sasso birds performed similarly, regardless of the production system they were subjected to (grazing or confinement). Furthermore, they showed no significant difference in bone weight, regardless of the production system.

REFERENCES

Aman G, Bangu B, Bereket Z, Desta G, Abiti T, Edget A, Hamid J. 2017. Production performance of Sasso (distributed by ethio-chicken private poultry farms) and Bovans brown chickens breed under village production system in three agro-ecologies of Southern Nations, Nationalities, and Peoples Regional State (SNNPR), Ethiopia. International Journal of Livestock 8 (9): 145–157. https://doi.org/10.5897/ijlp2017.0391

Ángeles-Coronado IA, Jerez-Salas MP, Pérez-León MI, Villegas-Aparicio Y. 2013. Efecto de *Portulaca oleracea* y *Lolium perenne* en la carne de gallina criolla. Revista Mexicana de Ciencias Agrícolas 6: 1221–1229. https://doi.org/10.29312/remexca.v0i6.1285

Brackenbury JH, Willianson ADB. 1989. Treadmill exercise training increases the oxidative capacity of chicken iliotibialis muscle. Poultry Science 68 (4): 577–581. https://doi.org/10.3382/ps.0680577

Carciofi BAM, Laurindo JB. 2007. Water uptake by poultry carcasses during cooling by water immersion. Chemical Engineering and Processing: Process Intensification 46 (5): 444–450. https://doi.org/10.1016/j.cep.2006.05.020

Demirok E, Veluz G, Stuyvenberg WV, Castañeda MP, Byrd A, Alvarado CZ. 2013. Quality and safety of broiler meat in various chilling systems. Poultry Science 92 (4): 1117–1126. https://doi.org/10.3382/ps.2012-02493

DOF (Diario Oficial de la Federación). NORMA Oficial Mexicana NOM-033-ZOO-1995, sacrificio humanitario de los animales domésticos y silvestres. Gobierno de México. Secretaría de Agricultura, Ganadería, Desarrollo Rural, Pesca y Alimentación. Ciudad de México, México.

Dzungwe JT, Tozo K, Chrysostome C. 2022. Growth performance, mortality and carcass yield evaluation of pure and reciprocal crosses between Sasso and Wassache chickens. Tropical Animal Health and Production 54 (5). https://doi.org/10.1007/s11250-022-03272-x

Franco D, Rois D, Vázquez JA, Lorenzo JM. 2012. Comparison of growth performance, carcass components, and meat quality between Mos rooster (Galician indigenous breed) and Sasso T-44 line slaughtered at 10 months. Poultry Science 91 (5): 1227–1239. https://doi.org/10.3382/ps.2011-01942

González-Cortés N, Reyes-Pérez R, Jiménez-Vera R, Guzmán-Ceferino J, Estrada-Lievano JM. 2019. Rendimiento de la canal de pollos (*Gallus gallus domesticus* L.) sometidos a pastoreo con *Canavalia ensiformis* L. Agro Productividad 12 (4). https://doi.org/10.32854/agrop.v0i0.1195

Gordon SH, Charles DR. 2002. Niche and organic chicken products: Their technology and scientific principles. Nottingham University Press: Nottingham, UK. 320 p.

Iruegas-Evaristo LF. 2011. El pollo en México. El Economista, 12 de abril de 2011. https://www.eleconomista.com.mx/opinion/El-pollo-en-Mexico-20110411-0006.html (Retrieved: February 2025).

Lorenzo JM, Rois D, Purriños L, Rivero J, Fernández M, Franco D. 2011. Efecto de la raza (Mos vs. Sasso T-44) sobre las características de la canal de gallos criados en libertad. Actas Iberoamericanas de Conservación Animal 1: 218–221.

Matus-Aragón MÁ, González-Cerón F, Salinas-Ruiz J, Sosa-Montes E, Pro-Martínez A, Hernández-Mendo O, Cuca-García JM, Chan-Díaz DJ. 2021. Productive performance of Mexican Creole chickens from hatching to 12 weeks of age fed diets with different concentrations of metabolizable energy and crude protein. Animal Bioscience 34 (11): 1794–1801. https://doi.org/10.5713/ab.20.0682

Miguel A, Ciria J, Asenjo B, Calvo L, Gómara A, Francesh A. 2008. Comparación del crecimiento y la canal de diferentes tipos genéticos de pollos criados en régimen semiextensivo en la provincia de Soria. Información Técnica Económica Agraria 104 (3): 381–398.

Moreiras O, Carbajal A, Cabrera L, Cuadrado M. 2005. Tablas de composición de alimentos. Editorial Pirámide: Madrid, España.

Muriel-Durán A, Solana-Ramos J, Cancho-Alfonso M. 1997. Resultados productivos, Rendimiento y composición de la canal de dos cruces de pollos de carne criados en libertad. Archivos de Zootecnia 175 (46): 240.

Paredes M, Vásquez B. 2020 Crecimiento, características de carcasa, peso de órganos internos y composición proximal de carne de seis genotipos de pollos criados en la región Andina del norte peruano. Scientia Agropecuaria 11 (3): 365–374. https://doi.org/10.17268/sci.agropecu.2020.03.08

Pavlovski ZŠ, Lukić M, Vitorović D, Petričević V, Milošević N. 2009. Naked neck chicken of Serbian and foreign origin: Carcass characteristic. Biotechnology in Animal Husbandry 25 (5–6): 1023–1032.

SAGARPA (Secretaría de Agricultura, Ganadería, Desarrollo Rural, Pesca y Alimentación). 2012. Situación actual y perspectiva de la producción de carne de pollo en México. 2000. Ciudad de México, México. 25 p.

Sangerman-Jarquín DMJ, Espitia-Rangel E, Villaseñor-Mir HE, Ramírez-Valverde B, Alberti-Manzanares P. 2009. Estudio de caso del impacto de la transferencia de tecnología en trigo del INIFAP. Agricultura Técnica en México 35 (1): 25–37.

Sanka YD, Mbaga SH, Mutayoba SK, Katule AM, Goromela SH. 2021. Evaluation of growth performance of Sasso and Kuroiler chickens fed three diets at varying levels of supplementation under semi-intensive system of production in Tanzania. Tropical Animal Health and Production 52 (6): 3315–3322. https://doi.org/10.1007/s11250-020-02363-x

Santos M, Lon-Wo E, Savón L, Herrera M. 2014. Comportamiento productivo de pollos cuello desnudo heterocigotos en pastoreo, con diferentes espacios vitales y harina de hojas de *Morus alba* en la ración. Revista Cubana de Ciencia Agrícola 3 (48): 265–269.

Agrociencia

PRODUCTIVE EVALUATION AND FEEDING POTENTIAL OF TSIRI PUMA AND TLAOLI PUMA MAIZE INCLUDED IN THE DIETS OF GESTATING GOATS

Laura **Castillo-Hernández**[1], Joob **Zaragoza-Esparza**[1], Axel J. **Castillo-Hernández**[1], Margarita **Tadeo-Robledo**[1], Alejandro **Espinosa-Calderón**[2], Jesús **Ramírez-Espinosa**[1], José de Jesús **Macedo-González**[1], Paolo **Cano-Suárez**[1], Angélica **Terrazas-García**[1*]

[1]Universidad Nacional Autónoma de México. Facultad de Estudios Superiores Cuautitlán. Carretera Cuautitlán-Teoloyucan km 2.5, San Sebastián Xhala, Cuautitlán Izcalli, Estado de México, México. C. P. 54714.
[2]Instituto Nacional de Investigaciones Forestales, Agrícolas y Pecuarias. Campo Experimental Valle de México. Carretera Texcoco-Los Reyes km 13.5, Coatlinchán, Texcoco, Estado de México, México. C. P. 56250.
* Author for correspondence: garciate@unam.mx

Citation: Castillo-Hernández L, Zaragoza-Esparza J, Castillo-Hernández AJ, Tadeo-Robledo M, Espinosa-Calderón A, Ramírez-Espinosa J, Macedo-González J de J, Cano-Suárez P, Terrazas-García A. 2025. Productive evaluation and feeding potential of Tsiri Puma and Tlaoli Puma maize included in the diets of gestating goats. **Agrociencia** 59(4): 467-482. https://doi.org/ 10.47163/agrociencia.v59i4.3320

Editor in Chief:
Dr. Fernando C. Gómez Merino

Received: October 08, 2024.
Approved: May 07, 2025.
Published in Agrociencia: June 06, 2025.

ABSTRACT

Feeding silage to goats (*Capra aegagrus hircus* L.) is a strategy used in regions with scarce fodder availability; however, the maize tested for this purpose was of commercial varieties. The goal was to assess the amount of fodder produced, the silage made, and the effects on pregnant goats and their young from two maize hybrids, Tsiri Puma and Tlaoli Puma, compared to a commercial hybrid (H-50). The yields of green matter (GM), dry matter (DM), and percentage of DM were determined. The material was chopped to 2 cm, taken to a bunker-style silo, and placed in three separate spaces for each hybrid. Once this was ready, 38 multiparous goats were distributed at random in three treatments with a diet including 50 % maize silage, and it was provided from day 64 of gestation to one weeks postpartum. Intake, weight, body condition scoring (BCS), and glucose levels were measured during gestation and up to two weeks postpartum. Kids were weighed at birth and 15 days after birth, and internal and external temperatures were measured. GM and DM yield, as well as the percentage of DM, were not different among the three maize hybrids ($p > 0.05$). In the goats, food intake was greater in the Tlaoli Puma group, followed by Tsiri Puma ($p < 0.0001$). Weight was greater in the Tsiri Puma and Tlaoli Puma groups ($p = 0.0001$), whereas BCS and glucose concentrations were not affected by the treatments ($p > 0.05$). Finally, body weight and the external temperature of the kids were greater in the Tlaoli Puma group ($p < 0.05$). Maize hybrids Tsiri Puma and Tlaoli Puma had an adequate fodder yield that helps produce quality silage that favors the productive estimators in goats and their offspring.

Keywords: *Capra aegagrus hircus* L., *Zea mays* L., kids, silage, productivity, animal nutrition.

INTRODUCTION

Goat production is predominantly carried out under extensive systems; consequently, most of the animal feed comes from either native herbs, grasses or crop leftovers (Boudalia *et al.,* 2024). Occasionally, they may not provide enough nutrients to satisfy the needs of animals, and stages such as gestation and lactation can be affected (Teixeira *et al*., 2024). In Mexico, reproductive stages coincide with the seasons of fall and winter, which are characterized by a low availability of forage and contribution of nutrients (Salinas-González *et al.,* 2016).

Nutrient restriction in goats leads to a deficient development of the fetus, which causes low birth weight, reduces offspring survival rate, affects milk production, and deteriorates the mother-offspring relationship (Terrazas *et al.,* 2009; Ramírez-Vera *et al*., 2012; Laporte-Broux *et al.,* 2012; Castagnino *et al.,* 2015; Goetsch, 2019; Rahmani *et al.,* 2019). Likewise, it leads to a loss in live weight and body condition of the female (Castagnino *et al.,* 2015), induces birth complications (Baxter *et al.,* 2016), and causes the mobilization of fat reserves for lactation (Li *et al.,* 2020). In the case of the kids, it causes a lack of reserve fat to maintain homeothermy and reduces vitality for suckling (Terrazas *et al*., 2009; Baxter *et al.,* 2016). This underscores the importance of providing adequate nutrition to gestating females, particularly in the final third of the gestation. During gestation and lactation, females must be provided with adequate levels of crude protein (CP) and metabolizable energy (ME). Likewise, the nutritional state of the animals must be monitored with the metabolic profile, since both the product and the placenta demand high energy levels from the maternal system when inducing changes in the metabolites in the blood. The carbohydrates derived from the circulation of the mother are the most important energy source for the developing fetus. In late gestation, the demand for this nutrient increases exponentially, so gestating goats must be provided with diets containing high levels of energy and easy availability (Nogueira *et al.,* 2017).

For the production of small ruminants, residues from crops, silage, pasture, hay, bushes, agro-industrial byproducts, poultry manure, and other alternative feed sources are frequently used (Boudalia *et al.,* 2024). The most commonly used process to preserve fodder is silage (Kumar *et al.,* 2024), which is also used as an alternative source of feed in small ruminants, particularly when there is a scarcity of forage (Boudalia *et al.,* 2024; Castillo-Hernández *et al.,* 2024). In gestating and lactating goats fed with maize silage, this allows for a better use of nutrients due to its good digestibility (Tarverdi *et al.,* 2021). However, these studies have been mostly carried out with commercial maize varieties that are not adapted to the particular conditions of each region, which may generate higher production costs.

In the High Valleys of Mexico, maize hybrids have been developed for grain production, such as Tlaoli Puma and Tsiri Puma, which contain adequate *in vitro* digestibility and high forage yields compared to commercial varieties. Likewise, they are resistant to lodging and some diseases, which suggests their potential to be used as fodder (Tadeo-Robledo *et al.,* 2016, 2021). Both hybrids have been tested for silage production

and supplied in the diets of gestating sheep, displaying a good response in productive and metabolic estimators both in mothers and in lambs (Castillo-Hernández *et al.*, 2024). However, the use of these maize hybrids has not yet been tested in goats' diets. This study proposes the hypothesis that the Tlaoli Puma and Tsiri Puma maize hybrids will produce adequate fodder yields while also promoting silage quality. Since they are supplied in the feed of gestating goats, they will allow for improved productive and metabolic parameters, as well as benefitting the viability of their offspring. The aim of this work was to evaluate the fodder yield and the productive and metabolic impacts on gestating goats and their offspring of two maize hybrids (Tsiri Puma and Tlaoli Puma) in comparison with a commercial hybrid (H-50).

MATERIALS AND METHODS

Site of study

This study was conducted in the caprine unit of the Agricultural Teaching Center of the Cuautitlán Faculty of Higher Studies of the National Autonomous University of Mexico (UNAM), located in the country's central highlands (19° 31′ 35′′ N, 99° 11′ 42′′ W) at an altitude of 2256 m. The weather is moderate, with rains in the summer, small temperature fluctuations, an average yearly rainfall of 600 mm, an average low temperature of 8.7 °C, an average high of 34 °C, and an annual mean of 15.7 °C (INEGI, 2020).

Establishing crops for the silage

The hybrids were evaluated using a randomized complete block experimental design with six repetitions, with a total of 18 experimental units. Every unit corresponded to a 5 m long furrow with a distance of 0.8 m between furrows, obtaining a 4 m^2 useful plot. The crops were established in the spring-summer cycle of 2021. Two androsterile maize hybrids (Tsiri Puma and Tlaoli Puma) were used, along with commercial hybrid H-50 (Semillas El Trébol, Mexico). The soil was prepared by plowing, followed by two passes with a harrow, as well as furrowing and fertilization.

Sowing was carried out using the "a tapa pie" method, in which three seeds were placed per hole at a distance of approximately 15 cm. On the following day, flood irrigation was carried out to ensure seed germination. The crop was maintained under rainfed conditions. Thirty days after germination, thinning was performed to leave 32 plants per every 5 m row (corresponding to each experimental unit) to establish a density of 80 000 plants per hectare. Weed control was carried out 10 days after irrigation using a selective herbicide (Lumax Gold ZC® s-metolachlor, atrazine, and mesotron). At the same time, the crop was sown for silage for each of the hybrids on a 2000 m^2 area using a pre-calibrated MP-25 (John Deere, Mexico), establishing an approximate population of 80 000 plants per hectare. Fertilization was applied at the time of sowing with a dose of 80-60-00 of N-P-K.

Measuring of the vegetative material

Green matter yield

The yield of green matter (GM) was determined per hectare from the harvest of all the plants in the row belonging to each experimental unit. The cut was carried out 10 cm above the ground level, and the fresh weight per plant was measured according to Zaragoza-Esparza *et al.* (2019).

Percentage of dry matter

Ten plants were chosen at random from every experimental unit and were chopped into pieces measuring 3 to 5 cm and manually homogenized. One kilogram of pieces was taken and placed in a paper bag labelled with the experiment number and initial weight, becoming a representative subsample as follows: the material was divided into four equal parts, and two opposite quarters were separated. The remaining quarters were mixed again, and the procedure was repeated until approximately 1 kg was gathered. The subsamples were dried at 55 °C in a forced-air oven for 48 h until a constant weight was reached and were then weighed to determine the percentage of dry matter (DM).

Yield of dry matter

The yield of dry matter (DM) was calculated from the yield of GM and the percentage of DM per surface unit.

Harvest and preparation of the silage

The harvest was performed on October 15 and 16, 2021, approximately 124 days after planting. The harvest was carried out when the state of optimum maturity appeared, which was determined visually after taking five plants at random and observing the state of the grain (1/4 to 1/3 progression of the milk line) for each of the hybrids of the three maize varieties (Zaragoza-Esparza *et al*., 2019).

To cut and chop the plants, a forage harvester with a two-row header and an F-28 harvester (New Holland, Italy) were used. The plant material was chopped into 2 cm pieces and deposited into an agricultural forage dump trailer, which had been previously weighed. Once filled with the chopped fodder, it was taken to a scale for vehicles located on campus, where the trailer was weighed with each load. The fodder was later placed in a bunker-type silo, where the material of each hybrid was placed in a space of its own. Then, it was compacted with a tractor between layers, each approximately 60 cm thick. The compacted material was covered with black plastic and held in place with heavy objects to avoid air entering. This process lasted approximately 30 days. The nutritional composition of the silage prepared with the maize hybrids (Table 1) was determined by proximal chemical analysis in a private laboratory (Servicios GAQ S.A. de C.V., Mexico). These determinations were based on the description according to Shimada (2003).

Table 1. Nutritional composition of dry matter (DM) of maize silage (*Zea mays* L.) of the Tlaoli Puma, Tsiri Puma, and H-50 hybrids used in the diet of each group of gestating goats (*Capra aegagrus hircus* L.).

Components	Tlaoli Puma silage	Tsiri Puma silage	H-50 silage
Crude protein (% DM)	8.1	9.0	7.1
Neutral detergent fiber (% DM)	47.0	46.2	43.2
Acid detergent fiber (% DM)	29.5	29.9	27.0
Total digestible nutrients (% DM)	65.1	63.1	67.5
Net energy in DM (kcal kg^{-1})	1.56	1.48	1.65

Animals and maintenance conditions

The protocol was approved by the Institutional Subcommittee for the Care and Use of Experimental Animals of the Animal Production and Health Science Postgraduate Department of UNAM, project number SICUAE.DC-2021/2-4. A herd of 38 multiparous goats was used (with more than two and up to five previous births, with 45.5 ± 2.27 kg live weight and a body condition score (BCS) of 2.53 ± 0.12) under a stabled system. The flock was made up of females from a cross between the Alpina and Toggenburg races, with an aptitude for dairy. For estrus synchronization, the goats underwent a protocol with the use of SINCRO-GEST®, intravaginal polyurethane sponges impregnated with 60 mg of medroxyprogesterone acetate (MA) for 11 days. On day 10 after the placement of the sponge, an intramuscular injection of Lutalyse® (5 mg of dinoprost tromethamine) was given; the sponges were removed 24 h later. Marker males were fitted with harnesses immediately after the sponges were removed and were kept in mating for 7 days.

During the entire experimental phase, the flock was kept stabled in three 15 × 15 m pens for each experimental group. Each pen was fitted with a roof for shade, an area exposed to sunlight, cement floors, a 15 m linear cement trough, and water dispensers. At 69 days post-mating, a pregnancy diagnosis was performed using a portable device, model 9618, B Mode Ultrasonic Diagnostic Equipment (Welld 9618®, Shenzhen, China) with a convex probe operating at a frequency of 3–5 MHz.

A total of 38 gestating goats were recorded, which were distributed according to their weight and body condition in the following treatments: Tsiri Puma: n = 14, with an average weight of 45.5 ± 2.27 kg and a BCS of 2.5 ± 0.12; Tlaoli Puma: n = 9, with an average weight of 45.24 ± 2.26 kg and a BCS of 2.5 ± 0.12; and H-50: n = 15, with an average weight of 45.81 ± 2.29 kg and a BCS of 2.6 ± 0.13. The weight of the goats was measured using a PLABA-12 (Rhino Maquinaria S.A. de C.V., Mexico) digital platform scale, with a capacity of 3 t and 500 g of precision. Their body condition was registered with the palpation of the lumbar region, based on a scale from 1 to 5, in which 1 is considered emaciated and 5, obese (Mendizabal *et al.*, 2011).

Feeding

During mating and before gestation diagnosis, the goats had a maintenance diet (9.3 % CP and 2 Mcal ME kg^{-1} DM) composed of 73 % oat, 24 % cracked maize, and 3 % concentrate, as well as water *ad libitum*. Experimental feeding began on day 64 of gestation and continued up to one week postpartum. The animals were accommodated in groups in three different pens. The ingredients and percentage of inclusion that made up their diet were: 25.48 % alfalfa hay, 24.52 % commercial concentrate, and 50 % silage. The nutritional content of the diet provided to the goats from each experimental group (Table 2) was determined in a particular laboratory (Servicios GAQ S.A. de C.V., Mexico) using a proximal chemical analysis such as described by Shimada (2003).

Table 2. Nutritional composition of dry matter (DM) in the diet of gestating goats (*Capra aegagrus hircus* L.) based on the feeding potential of maize (*Zea mays* L.) hybrids Tsiri Puma, Tlaoli Puma, and H-50.

Components	Tlaoli Puma diet	Tsiri Puma diet	H-50 diet
Crude protein (% DM)	17.5	16.0	16.6
Neutral detergent fiber (% DM)	34.4	38.1	32.5
Acid detergent fiber (% DM)	25.7	27.5	23.0
Total digestible nutrients (% DM)	67.5	66.7	70.8
Net energy in DM (kcal kg^{-1})	1.65	1.67	1.78

Measurement of weight and body condition

The weight and BCS of the goats were measured on days 67, 128, and 134 of gestation, at 2 h postpartum, and 15 days postpartum. To take these measurements, the goats were managed in each group's pen. Using three 2 × 1 m portable panels, a smaller pen was built to contain the animals. Weights were taken using a digital PLABA-12 platform scale. The BCS was measured by palpating the sternal triangle using a scale from 1 to 5, where 1 is considered an emaciated goat and 5, an obese goat (Mendizabal *et al*., 2011).

Measuring food intake

Every day, after providing the experimental diets, the alfalfa and concentrate were weighed with a portable Trip2 (Wei Hang, China) digital scale with a capacity of 40 kg and an accuracy of 10 g. To weigh the silage, a digital hook scale (Crane Scane SF-915, China) was used, with a capacity of 300 kg and an accuracy of 50 g. To determine the apparent daily intake of the goats, the components of the diet were provided once a day and sequentially: first, the maize silage, followed by the concentrate, and finally alfalfa. The uneaten food in each group was gathered and weighed with a digital scale the next day early in the morning.

Measurement of blood glucose

In each goat, blood samples were taken 67, 128, and 134 days after gestation and 2 h postpartum. The sampling was performed with fasting animals, except for the postpartum sampling. The blood sample (3 mL) was taken by puncturing the jugular vein with 21G × 25 mm Vacutainer® needles in tubes with EDTA (3 mL). The samples were refrigerated until centrifuged in the laboratory on campus premises on the same day the blood was drawn. A Hettich Universal 16 R (Andreas Hettich GmbH and Co., Germany) centrifuge was used at 4 °C and 3000 rpm (2147 × g) for 20 min to separate the plasma from the cell package. The plasma of the centrifuged samples was gathered and placed in 2mL Eppendorf tubes using Pasteur pipettes. To preserve it, the plasma obtained was frozen at -20 °C until the moment of analysis. The plasma samples were taken to a commercial laboratory (Centro de Diagnóstico Veterinario, Mexico) to determine glucose levels by spectrophotometry according to the technique described by Briseño-Castellanos *et al*. (2021).

Measurements on kids

After birth, the goat and kids were placed in small individual pens for the first 2 h postpartum in order to ensure that the mother-offspring bond was established, as well as to verify that the kid consumed colostrum. After this period, the following measurements were taken on the kid:

Rectal temperature: The kid was held in place, and only the mercury bulb of a digital thermometer (Hergom®, Mexico) was introduced into the kid's rectum and maintained there until the alarm sounded. The temperature was noted, and the thermometer was cleaned for the next reading.

External temperature: with the kid still held down in place, its temperature was taken in the scapular area using an infrared thermometer gun with a range of -20 to 50 °C and ±2.5 °C (Steren® HER-424, Mexico), which was placed 5 cm away from the animal. Two repeated readings were taken, and an average reading was recorded.

Body weight after birth and at 15 days postpartum: every kid was weighed after taking their temperatures. A rope was used as a harness to secure the kid and place it on the metal hook of the Trip2 portable digital scale (Wei Hang, China) with a capacity of 40 kg and an accuracy of 10 g.

Sex and delivery type: The sex and size of the litter were registered.

Statistical analysis

All variables of the experiment underwent a Kolmogorov-Smirnov test with Lilliefors probability to determine data normality. An analysis of variance (ANOVA) was conducted for repeated measurements over time using the Proc GLIMMIX procedure in SAS OnDemand for Academics (v. 3.1.0, SAS Institute Inc., Cary, NC, USA). Depending on the variable in the model, the fixed effects considered were the feeding group, litter size, and measurement time. Mean comparisons were performed using Tukey's test with a significance level of 0.05 for each variable. Data are presented as means and standard errors.

RESULTS AND DISCUSSION

Vegetative material

The GM, DM yield values, and percentage of DM were not affected by the hybrid ($p > 0.05$). The average of these three variables was similar in the three groups (Table 3). These results may indicate that there was no variation in the planting and environmental conditions. However, they also point out that the growth of the three varieties was similar in the evaluated parameters. The DM and GM values are mainly related to the moment of harvest.

Table 3. Yield (mean ± standard error) of green matter (GM), dry matter (DM), and percentage of DM of the maize (*Zea mays* L.) hybrids Tlaoli Puma, Tsiri Puma, and H-50.

Maize hybrid	Yield (Mg ha^{-1})		DM (%)
	GM	DM	
Tlaoli Puma	70.0 ± 3.3	17.9 ± 0.95	25.6 ± 0.6
Tsiri Puma	65.9 ± 2.2	17.9 ± 0.83	27.0 ± 0.7
H-50	66.8 ± 2.9	16.9 ± 0.69	25.0 ± 0.4
Variation coefficient	16.44	14.84	8.67
Value of *p*	0.57	0.54	0.10

The DM composition of the forage may affect its intake by the animals. Goats are known to be a species with a more selective trophic behavior than cows and sheep (Berthel *et al*., 2022). Goats have a considerable ability to select different plants and plant parts, and the botanical composition of the diet better reflects the variety of chosen species (Goetsch, 2019; Ackermans *et al.,* 2019; Silva and Filho, 2021). However, other factors, such as the reproductive stage, can affect the intake of DM. In Creole goats, a higher DM intake was found when they were in early lactation compared to when they were not pregnant (Egea *et al.,* 2019). This may imply that the goats were able to adequately use the diets with silages from the hybrids tested here, as appropriate productive indicators were observed according to their reproductive stages.

Feed intake

An effect on intake was found in favor of the experimental group Tlaoli Puma ($p < 0.0001$) in comparison with Tsiri Puma and H-50 (Figure 1), whereas the intake of the Tsiri Puma group was only higher than H-50 ($p < 0.0001$). Additionally, an effect of time was found (week of gestation), in which all groups increase their intake of feed as gestation progresses ($p < 0.0001$). Finally, an interaction was found between the type of silage provided and time of gestation ($p = 0.045$), implying that the intake of their diet increased as gestation progressed, although this increase magnified depending on the silage of the hybrids offered.

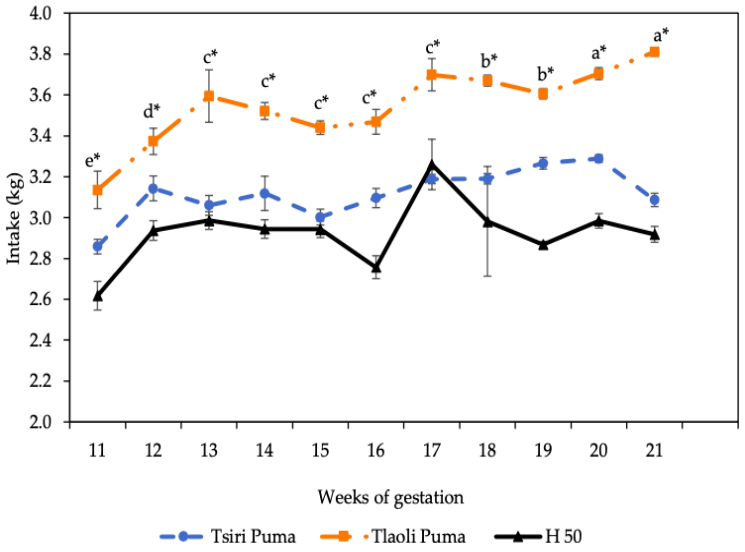

Figure 1. Individual intake (mean ± standard error) of goats (*Capra aegagrus hircus* L.) fed with silage made of three maize (*Zea mays* L.) hybrids during gestation. Different letters indicate time differences ($p < 0.05$), asterisks indicate differences between groups ($p < 0.0001$).

These results differ from reports by Tarverdi *et al.* (2021) on gestating and lactating Mahabadi goats, where the intake of diets that included different percentages of maize silages did not differ in both stages. However, Fedele *et al.* (2002) reported that the goats that were stabled and fed *ad libitum* or with hay and concentrate increased their intake of dry matter from 12 to 62 % in the final third of their gestation in relation to the dry period. This is consistent with this investigation, since the intake in the three hybrids increased as gestation progressed, which also responds to the increase in the nutritional need in this stage; hence, giving them a diet with a higher energy value would reinforce the intake of the animals.

Goat body weight

Differences were observed ($p = 0.0001$), since goats from the Tsiri Puma and Tlaoli Puma groups had higher weights in comparison with the H-50 group (Figure 2). Likewise, differences were found for time ($p < 0.0001$), in which the goats from the three groups were found to increase in weight from day 67 to day 134 and decline after giving birth (Figure 2). These results correspond with the data observed for weight and greater intake in the treatments with the hybrids Tlaoli Puma and Tsiri Puma, unlike the lower intake and goats with lower weights from group H-50.

These results may be related to the nutritional characteristics of the hybrids used and the final composition of the diet, as mentioned earlier. In this sense, Berthel *et al.* (2024) reported that goats select what they eat depending on its nutritional content, which shows a lower preference for protein components. This may not be consistent with

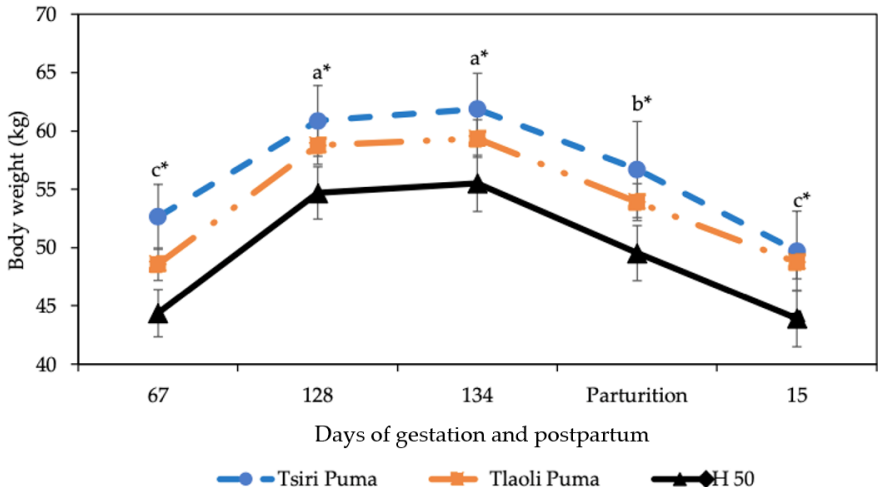

Figure 2. Body weight (mean ± standard error) of goats (*Capra aegagrus hircus* L.) fed with silage made of three maize (*Zea mays* L.) hybrids. Different words indicate differences in time ($p < 0.05$), asterisks indicate differences between groups ($p < 0.0001$).

our results, since the diet composed of the hybrid H-50 contained a lower amount of protein and higher energy in comparison to the diets with Tsiri Puma and Tlaoli Puma silages. However, this assertion is hypothetical, as it is based on nutritional values obtained from a single analyzed diet sample. Therefore, it would be interesting to evaluate whether variations in the intake of goats with the fodders of the hybrids examined can be attributed to the nutritional content, particularly of protein.

Body conditions of goats

No differences were found between groups or whether there was any interaction between group and time ($p > 0.05$) (Figure 3). However, there were differences ($p < 0.0001$) observed for time. The BCS was higher from day 128 to day 134, with a decrease at birth. The BCS in all groups was adequate in relation to the ideal interval for the physiological stage of the goats (Ghosh *et al.*, 2019).

Glucose

No significant differences were found in the plasmatic concentrations of glucose between groups, nor was there any interaction observed between group and time ($p > 0.05$) (Figure 4). However, for time, differences were observed at the moment of birth ($p < 0.0001$). The results of the concentrations of glucose are similar to those reported by Faisal *et al.* (2022) and Abou-Elkhair *et al*. (2020) in gestating and maintenance goats fed with cornstarch and molasses or molasses meal.

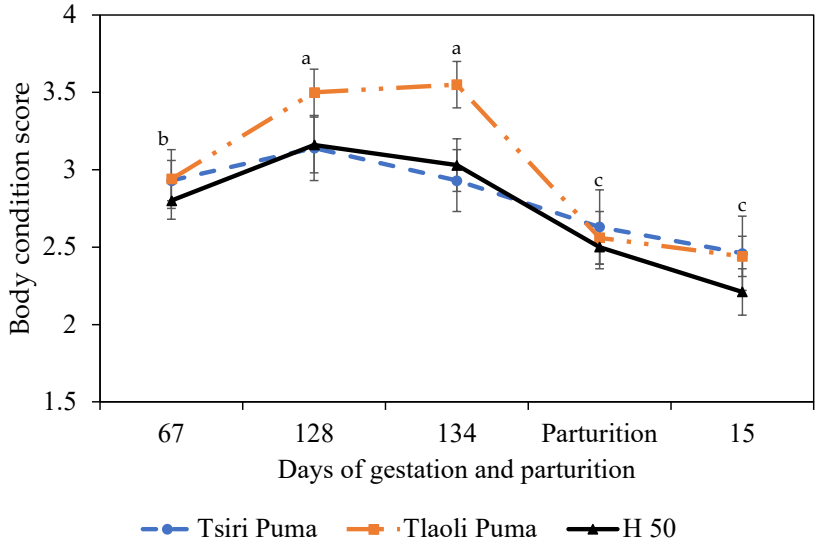

Figure 3. Body condition (mean ± standard error) of goats (*Capra aegagrus hircus* L.) fed with silage made of three maize (*Zea mays* L.) hybrids. Different letters indicate time differences ($p < 0.05$). A tendency ($p = 0.073$) is observed for days 67 and 134.

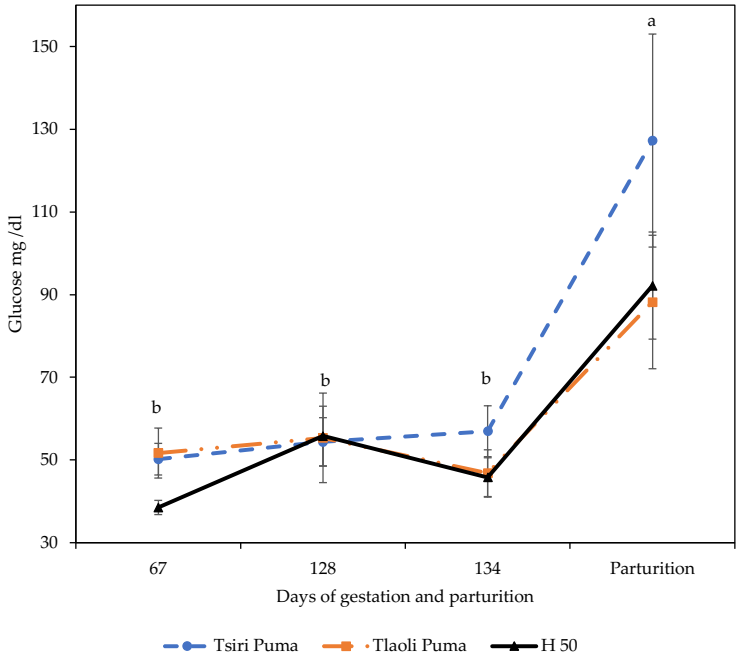

Figure 4. Glucose concentration in plasma (mean ± standard error) goats (*Capra aegagrus hircus* L.) fed with silage made with three maize (*Zea mays* L.) hybrids. Different letters indicate time differences ($p < 0.05$).

Weight of the kids

Kids in the Tlaoli Puma group presented a higher weight at birth in comparison to the two other groups (p = 0.005) (Figure 5), and this difference was maintained until they were aged 15 days (p < 0.0001). Throughout time, a significant effect was observed (p < 0.0001). Finally, there was a tendency (p = 0.068) towards the group and time interaction, which indicates that the weight of the goats increased as their age advanced, although this effect was mostly significant in the Tlaoli Puma group. This is consistent with the goats in this group having been the ones that presented the highest intake and weight gain. Abou-Elkhair *et al*. (2020) reported similar findings, stating that the kids with the highest weights were born to mothers who were fed a more nutritionally balanced diet.

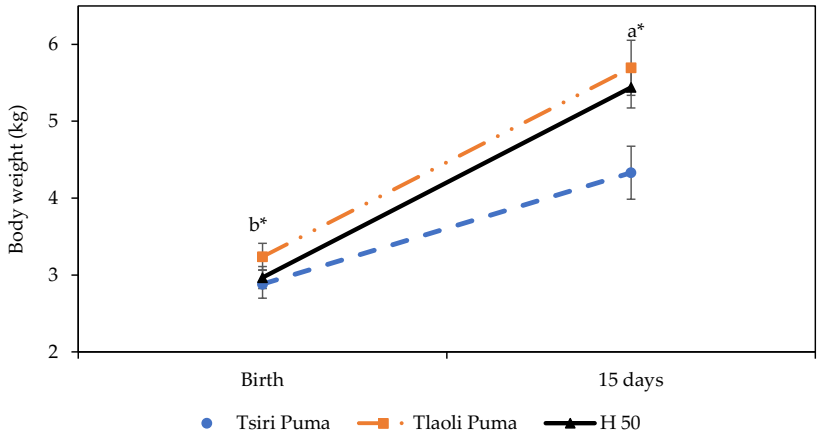

Figure 5. Weights of kids (*Capra aegagrus hircus* L.) (mean ± standard error) born from goats fed with silage made with three maize (*Zea mays* L.) hybrids at the moment of delivery and 15 days afterwards. Different letters indicate time differences (p < 0.05). Asterisks indicate differences between groups (p < 0.005).

In the case of the effect of the litter, it was found that the weight of single kids was higher than that of twin or triplet kids. In turn, twin kids had a higher weight than triplet kids (p < 0.0001). In the case of the sex of the kid, no differences were found (p = 0.555). The results observed for both characteristics contrast with Vázquez-García *et al*. (2021), as these authors did not observe differences due to the type of birth, but they did for sex, since the males weighed more than the females.

Temperature of the kids

The rectal temperature of the kids was similar in all groups (p > 0.05) (Figure 6). However, for the external temperature, kids of the Tsiri Puma and Tlaoli Puma groups displayed values higher than those of the H-50 group (p < 0.05). These results are similar to those observed by Vázquez-García *et al*. (2021), in which the rectal temperature displayed no significant differences between the diets used.

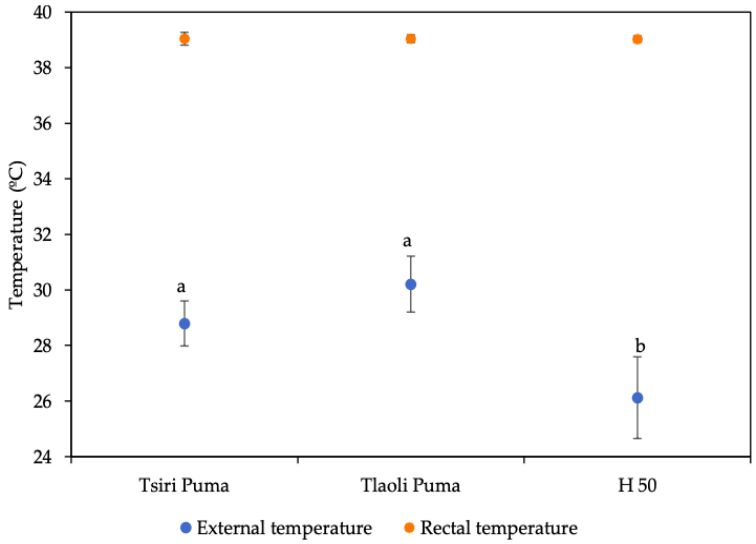

Figure 6. Comparison of the external and rectal temperatures (T) (means ± standard error) of kids born from goats (*Capra aegagrus hircus* L.) fed with silage made with three maize (*Zea mays* L.) hybrids. Different letters indicate differences between groups for external temperature ($p < 0.05$).

CONCLUSIONS

The evaluated maize hybrids adapted to the particular production conditions of the High Valleys of Mexico provide a better plant yield and an optimum nutritional balance for the feeding of gestating goats, in comparison with the commercial hybrid. The Tlaoli Puma and Tsiri Puma hybrids had better forage yields in green matter, dry matter, and percentage of dry matter that favors their use as silages for gestating goat fodder. Feeding these diets during gestation and postpartum allowed goats to consume an adequate amount of feed, which resulted in an increase in weight during gestation, a body condition of more than 2.5, and the maintenance of adequate glucose levels. Likewise, the fodder provided helped the kids maintain an adequate homeothermy and weight increase in their first 15 days of life.

ACKNOWLEDGEMENTS

This investigation was carried out thanks to the funds granted by UNAM-DGAPA-PAPIIT IN224220, IT200122 and IT201618; department of investigation FESC-UNAM-CI2245; and the State of Mexico Council of Science and Technology (COMECYT), Women Researchers fund FICDTEM-2021-068. Laura Castillo was granted a scholarship from CONAHCyT

Thanks also go to M.C. Rosario Arvizu of FES Cuautitlán, UNAM, for her invaluable support in her laboratory with the determination of the metabolite. To Ing. Israel Arteaga Escamilla and Magdalena Franco Oviedo, as well as to social service students and volunteers for their

great support in the handling of animals and collection of data during the experimental phase. Thanks to Martín Arana and Jaime Sánchez for their support in the care and handling of the animals.

REFERENCES

Abou-Elkhair R, Mahboub H, Sadek K, Ketkal S. 2020. Effect of prepartum dietary energy source on goat maternal metabolic profile, neonatal performance, and economic profitability. Journal of Advanced Veterinary and Animal Research 7 (3): 566–574. https://doi.org/10.5455/javar.2020.g454

Ackermans NL, Martin LF, Hummel J, Müller DWH, Clauss M, Hatt JM. 2019. Feeding selectivity for diet abrasiveness in sheep and goats. Small Ruminant Research 175: 160–164. https://doi.org/10.1016/j.smallrumres.2019.05.002

Baxter EM, Mulligan J, Hall SA, Donbavand JE, Palme R, Aldujaili E, Zanella AJ, Dwyer CM. 2016. Positive and negative gestational handling influences placental traits and mother-offspring behavior in dairy goats. Physiology and Behavior 157: 129–138. https://doi.org/10.1016/j.physbeh.2016.02.001

Berthel R, Dohme-Meier F, Keil N. 2024. Dairy sheep and goats sort particle size and protein in mixed rations. Applied Animal Behaviour Science 271: 106144. https://doi.org/10.1016/j.applanim.2023.106144

Berthel R, Simmler M, Dohme-Meier F, Keil N. 2022. Dairy sheep and goats prefer the single components over the mixed ration. Frontiers in Veterinary Science 9: 1017669. https://doi.org/10.3389/fvets.2022.1017669

Boudalia S, Smeti S, Dawit M, Senbeta EK, Gueroui Y, Dotas V, Bousbia A, Symeon GK. 2024. Alternative approaches to feeding small ruminants and their potential benefits. Animals 14 (6): 904. https://doi.org/10.3390/ani14060904

Briseño-Castellanos M, Hernández-Gonzalez MA, Ramos-Moreno JM, Cisneros-Carrasco JM, Jiménez-Ruvalcaba J. 2021. Determinación niveles de glucosa por medio de espectroscopía como método no invasivo. Revista Médica del Instituto Mexicano del Seguro Social 59 (6): 517–527.

Castagnino DS, Härter CJ, Rivera AR, Lima LDD, Silva HGO, Biagioli B, Resende KT, Teixeira IAMA. 2015. Changes in maternal body composition and metabolism of dairy goats during pregnancy. Revista Brasileira de Zootecnia 44 (3): 92–102. https://doi.org/10.1590/S1806-92902015000300003

Castillo-Hernández L, Zaragoza-Esparza J, Tadeo-Robledo M, Espinosa-Calderón A, Ramírez-Espinosa J, Macedo-González J, Castillo-Hernández A, Cano-Suárez P, Terrazas-García A. 2024. Potencial alimenticio de ensilados híbridos de maíz Puma incluidos en la dieta de ovejas gestantes. Revista MVZ Córdoba 29 (1): 3262–3262. https://doi.org/10.21897/rmvz.3262

Egea ÁV, Bakker ML, Allegretti LI, Paez SA, Grilli DJ, Guevara JC, Villalba JJ. 2019. Seasonal changes in feed intake, diet digestibility and diet composition by lactating and non-lactating goats browsing in a semi-arid rangeland of Argentina. Grass and Forage Science 74 (1): 115–128. https://doi.org/10.1111/gfs.12393

Faisal HT, Abid MK, Abed A. 2022. Study of some biochemical parameters in dose during pregnancy in goats. Journal of Advanced Zoology 43 (1): 1–6. https://doi.org/10.17762/jaz.v43i1.109

Fedele V, Claps S, Rubino R, Calandrelli M, Pilla AM. 2002. Effect of free-choice and traditional feeding systems on goat feeding behaviour and intake. Livestock Production Science 74 (1): 19–31. https://doi.org/10.1016/S0301-6226(01)00285-8

Ghosh CP, Datta S, Mandal D, Das AK, Roy DC, Roy A, Tudu NK. 2019. Body condition scoring in goat: Impact and significance. Journal of Entomology and Zoology Studies 7 (2): 554–560.

Goetsch AL. 2019. Recent research of feeding practices and the nutrition of lactating dairy goats. Journal of Applied Animal Research 47 (1): 103–114, https://doi.org/10.1080/09712119.2019.1580585

INEGI (Instituto Nacional de Estadística y Geografía). 2020. Climatología. Ciudad de México, México. https://www.inegi.org.mx/temas/climatologia/#descargas (Retrieved: February 2025).

Kumar R, Arif M, Kumar A. 2024. Silage based feeding system for goats. Indian Farming 74 (1): 28–30.

Laporte-Broux B, Roussel S, Ponter AA, Giger-Reverdin S, Camous S, Chavatte-Palmer P, Duvaux-Ponter C. 2012. Long-term consequences of feed restriction during late pregnancy in goats on feeding behavior and emotional reactivity of female offspring. Physiology and Behavior 106 (2): 178–184. https://doi.org/10.1016/j.physbeh.2012.02.001

Li X, Li H, He Z, Tan Z, Yan Q. 2020. Effects of maternal intake restriction during early pregnancy on fetal growth and bone metabolism in goats. Small Ruminant Research 183: 106027. https://doi.org/10.1016/j.smallrumres.2019.106027

Mendizabal JA, Delfa R, Arana A, Purroy A. 2011. Body condition score and fat mobilization as management tools for goats on native pastures. Small Ruminant Research 98 (1–3): 121–127. https://doi.org/10.1016/j.smallrumres.2011.03.029

Nogueira DM, Eshtaeba A, Cavalieri J, Fitzpatrick LA, Gummow B, Blache D, Parker AJ. 2017. Short-term supplementation with maize increases ovulation rate in goats when dietary metabolizable energy provides requirements for both maintenance and 1.5 times maintenance. Theriogenology 89: 97–105. https://doi.org/10.1016/j.theriogenology.2016.10.014

Rahmani Firozi R, Teimouri Yansari A, Dirandeh E. 2019. Effect of different of levels energy and protein on performance, microbial protein, Some of metabolites and ruminal parameters in late pregnancy of Sistani goat. Iranian Journal of Animal Science Research 11 (1): 27–43. https://doi.org/10.22067/ijasr.v1397i1.66307

Ramírez-Vera S, Terrazas A, Delgadillo JA, Serafín N, Flores JA, Elizundia JM, Hernández H. 2012. Feeding corn during the last 12 days of gestation improved colostrum production and neonatal activity in goats grazing subtropical semi-arid rangeland. Journal of Animal Science 90 (7): 2362–2370. https://doi.org/10.2527/jas.2011-4306

Salinas-González H, Moysen EDV, de Santiago MDLA, Deras FGV, Jáquez JAM, Monroy LIV, Torres DH, Requejo LMI, Viramontes UF. 2016. Análisis descriptivo de unidades caprinas en el suroeste de la región lagunera, Coahuila, México. Interciencia 41 (11): 763–768.

Shimada A. 2003. Nutrición animal. Editorial Trillas: Ciudad de México, México. 194 p.

Silva TPD, Filho ALA. 2021. Sheep and goat behavior profile in grazing systems. Acta Scientiarum. Animal Sciences 43 (1): e51265. https://doi.org/10.4025/actascianimsci.v43i1.51265

Tadeo-Robledo M, Espinosa-Calderón A, García-Zavala JJ, Lobato-Ortiz R, Gómez-Montiel N, Sierra-Macías M, Valdivia-Bernal R, Zamudio-González B, Martínez-Yáñez B, López-López C, *et al*. 2016. Tsiri Puma, híbrido de maíz para Valles Altos con esquema de androesterilidad para producción de semillas. Revista Fitotecnia Mexicana 39 (3): 331–333. https://doi.org/10.35196/rfm.2016.3.331-333

Tadeo-Robledo M, Espinosa-Calderón A, Zaragoza-Esparza J, López-López C, Canales-Islas I, Zamudio-González B, Turrent-Fernández A, Virgen-Vargas J, Sierra-Macías M, Gómez-Montiel N, *et al*. 2021. Tlaoli Puma, híbrido de maíz para grano y forraje con androesterilidad y restauración de la fertilidad masculina. Revista Fitotecnia 44 (2): 265–267. https://doi.org/10.35196/rfm.2021.2.265

Tarverdi S, Fattah A, Papi N, Ebrahimi-Mahmoudabad SR. 2021. The effects of dietary substitution of dry forage with corn silage on dry matter intake, production and reproductive performance, and nutrient digestibility of Mahabadi lactating goats. Animal Sciences Journal 34 (131): 187–198. https://doi.org/10.22092/ASJ.2020.343140.2071

Teixeira IAMA, Härter CJ, Vargas JAC, Souza AP, Fernandes MHMR. 2024. Update of nutritional requirements of goats for growth and pregnancy in hot environments. Animal 18 (S2): 101219. https://doi.org/10.1016/j.animal.2024.101219

Terrazas A, Robledo V, Serafin N, Soto R, Hernandez H, Poindron P. 2009. Differential effects of undernutrition during pregnancy on the behaviour of does and their kids at parturition and on the establishment of mutual recognition. Animal 3 (2): 294–306. https://doi.org/10.1017/S1751731108003558

Vázquez-García JM, Álvarez-Fuentes G, Orozco-Gregorio HO, García-López JC, González-Hernández M, Rosales-Nieto CA. 2021. Energy supplementation during the last third of gestation improves mother–young bonding in goats. Animals 11 (2): 287. https://doi.org/10.3390/ani11020287

Zaragoza-Esparza J, Tadeo-Robledo M, Espinosa-Calderón A, López-López C, García-Espinosa JC, Zamudio-González B, Turrente-Fernández A, Rosado-Núñez F. 2019. Rendimiento y calidad de forraje de híbridos de maíz en Valles Altos de México. Revista Mexicana de Ciencias Agrícolas 10 (1): 101–111. https://doi.org/10.29312/remexca.v10i1.1403

Agrociencia

COMPUTATIONAL ANALYSIS OF THE EFFECT OF AN EXTERNAL BARRIER ON THE VENTILATION AND THERMAL PERFORMANCE OF A GREENHOUSE

Mirka Maily **Acevedo-Romero**[1], Cruz Ernesto **Aguilar-Rodríguez**[2], Constantin Alberto **Hernández-Bocanegra**[1*], José Ángel **Ramos-Banderas**[1], Gildardo **Solorio-Díaz**[3]

[1]Instituto Tecnológico de Morelia. Doctorado en Ingeniería. Avenida Tecnológico 1500, Morelia, Michoacán, Mexico. C. P. 58120.
[2]Instituto Tecnológico Superior de los Reyes. Carretera Jacona-Los Reyes, Libertad, Los Reyes de Salgado, Michoacán, Mexico. C. P. 60300.
[3]Universidad Michoacana de San Nicolás de Hidalgo. Posgrado en Ingeniería Mecánica. C. de Santiago Tapia 403, Centro, Morelia, Michoacán, Mexico. C. P. 58030.
* Author for correspondence: constantin.hb@morelia.tecnm.mx

Citation: Acevedo-Romero MM, Aguilar-Rodríguez CE, Hernández-Bocanegra CA, Ramos-Banderas JA, Solorio-Díaz G. 2025. Computational analysis of the effect of an external barrier on the ventilation and thermal performance of a greenhouse. **Agrociencia** 59(4): 483-499. https://doi.org/ 10.47163/agrociencia.v59i4.3296

Editor in Chief:
Dr. Fernando C. Gómez Merino

Received: September 04, 2024.
Approved: May 12, 2025.
Published in Agrociencia: June 12, 2025.

ABSTRACT

The construction of greenhouses in semi-urban areas implies the presence of neighboring buildings that can be an obstacle to natural ventilation, modifying the intensity and direction of air currents. However, they could also function as protective barriers against these currents at off-peak hours. The objective of this work was to analyze the effect of an external physical barrier on the thermal behavior and air currents inside a Gothic type greenhouse for tomato (*Solanum lycopersicum* L.) production. A 3D steady-state simulation was performed and validated using 15-day experimental temperature data with typical climatic conditions for the month of July 2023. The effect of the 3 m high external barrier was analyzed, which was placed at 5, 10, and 15 m distance from the greenhouse, located in the direction of the prevailing winds, on the fluid dynamic and thermal behavior inside the greenhouse. The results showed differences in the behavior of air currents inside the greenhouse with the presence of the external barrier, which affected the velocity and direction of the air inlet, accentuated by the proximity between the obstacle and the greenhouse. Under the studied conditions, placing the barrier 5 m away represents an advantage when there are low temperatures at dawn, managing to preserve the temperature inside the greenhouse up to 4 °C above the temperatures recorded in the barrier-free scenario or with the barrier 10 and 15 m away. The simulated data at 14:00 h showed differences of less than 0.4 °C between the cases with different barrier distances, so the influence of the barrier at the above-mentioned time is not significant.

Keywords: computational fluid dynamics, turbulence, external physical barrier.

INTRODUCTION

The use of greenhouses for food production is currently a viable option to meet food demand in many countries. These structures allow partial control of variables such

as temperature, humidity, CO_2 concentration, and radiation, which allow optimal plant development (Flores-Velázquez and Ojeda-Bustamante, 2015) and improve the standard of living of the population with fresh food all year round (El-Alaoui *et al*., 2023). In Mexico, most greenhouses in the country operate through empirical knowledge (Aguilar-Rodríguez *et al*., 2020a). The use of computational fluid dynamics in protected agriculture stems from the need for a detailed understanding of the physicochemical processes that take place in these systems (Flores-Velázquez and Ojeda-Bustamante, 2015; Aguilar-Rodríguez *et al*., 2021; Bournet and Rojano, 2022). In passively ventilated greenhouses, air intake and its velocity are determinant in the management of the indoor climate; this type of ventilation is currently the most widely used in tropical and subtropical countries due to its low or no maintenance cost (Villagrán *et al*., 2019; Ortiz-Rocha *et al*., 2021).

The importance and influence of wind velocity and direction on temperature control have been reported inside the greenhouse through different combinations of window opening and closing (Espinoza *et al*., 2017; He *et al*., 2018; Li *et al*., 2020). On the other hand, studies on the behavior of wind currents and temperature in greenhouses with three (Espinoza *et al*., 2017) or more bays (Ruiz-García *et al*., 2015; Aguilar-Rodríguez *et al*., 2021) have been conducted to determine the thermal behavior under natural ventilation, highlighting the combination of window opening, wind direction, and comparisons between structures such as saw, hood, and arched types.

In greenhouses with ridge vents, ventilation rates are best when they are open and perpendicular to the wind direction (Chu and Lan, 2019). Wind direction and temperature are affected by the zenith window; however, this effect is negligible at the plant level, and humidity is lower below the windward window (Akrami *et al*., 2020). Similarly, ventilation in living spaces and how the proximity of these assemblies can affect air currents and temperature have been studied (Carpentieri and Robins, 2015; Castro *et al*., 2017; King *et al*., 2017).

Greenhouse construction is aimed at production intensification with the greatest possible cost reduction. To this end, different environmental factors are taken into consideration during their construction, such as the direction of prevailing winds, latitude and altitude of the site, geometry of the building, window configuration, and radiation (Flores-Velázquez and Ojeda-Bustamante, 2015; Villagrán *et al*., 2020a; Choab *et al*., 2019). Currently, the use of space for greenhouse construction is a factor to be considered due to the interaction of contiguous built-up areas. The growth of protected agriculture in recent years has taken place in semi-urbanized areas with the presence of buildings or natural barriers.

Simulations in the study by Ghoulem *et al*. (2020) showed that greenhouses with wind traps provided higher ventilation rates than side windows when nearby structures are present. Villagrán and Bojacá (2019), on the other hand, studied the effect of natural obstacles on the thermal performance of passively ventilated greenhouses, finding that the presence of surrounding objects can deteriorate ventilation inside the greenhouse. Gómez-Mataix *et al*. (2012) and Fatnassi *et al*. (2017) studied the spacing

between double-ridge greenhouses at different distances and determined that the best ventilation rates coincide with the largest spacing spans provided by the opening of the double ridge, with the first bay being the best ventilated. The minimum distance between the greenhouse and the obstacle depends on the height of the latter (López *et al*., 2011). Evaluations by He *et al*. (2018) indicate that, in summer, the side window and roof combination provide a better performance for cooling, while in winter, the roof opening is better for dehumidifying the environment.

This study analyzes the effect of a physical barrier on wind trajectory, wind velocity, and temperatures in a passively ventilated gothic-type greenhouse with a tomato crop in the productive stage, installed in a semi-arid environment using numerical simulation techniques.

MATERIALS AND METHODS

Experimental site

The study was carried out in a 14.5 m wide and 80 m long Gothic-type greenhouse covered with translucent polyethylene. The structure has an anti-aphid mesh on the windows, a natural ventilation system, two 3 m high lateral windows, and a 1.4 m zenithal window. It is located at coordinates 23° 59′ 28.87′′ N and 104° 32′ 34.98′′ W, at an altitude of 1868 m. The region has a semi-warm temperate climate with summer rains and an average annual rainfall of around 500 mm, 85 % of which occurs from June to October. The topography is flat, and the soil is alluvial with a loamy texture.

Temperature and relative humidity data were recorded using two Vantage Pro2 Plus stations (Davis Instruments, Hayward, CA, USA), equipped with sensors for ambient temperature (measurement range of 40–65 °C, error ±0.5 °C), relative humidity (measurement range of 1 to 100 %, error ±3 and ±4 % over 90 %), wind velocity (measurement range of 1 to 80 m s^{-1}, error ±5 m s^{-1}), and wind direction (measurement range of 16 compass points, error ±5). The data obtained were stored in the Vantage Pro2 Plus console assigned to each piece of equipment. The stations were placed on the central bed of the crop 40 m from the greenhouse entrance (S3) and outside (in the -z direction, considering the length of the greenhouse), separated 1 m from the air inlet (S6) (Figure 1A).

Four HOBO UX100-003 storage units (Onset Company, Bourne, MA, USA) were also used, with temperature and relative humidity sensors with a measurement range of -40 to 70 °C and 0 to 100 %, and an accuracy of ±0.2 °C and ±2.5 %. Sensors were placed in the central growing bed at 20 and 60 m (S1 and S5, respectively). Sensor S2 was placed 0.5 m from the air inlet and S4 0.5 m from the left window (Figure 1A), both 40 m from the inlet in the -z direction. Data from these sensors were downloaded via Bluetooth using the free HOBOmobile app (Onset Computer Corporation, MA, USA). All variables were measured at canopy height (2 m), including soil temperature (at 0.15 m depth). Data recording was carried out at 10-minute intervals. All windows

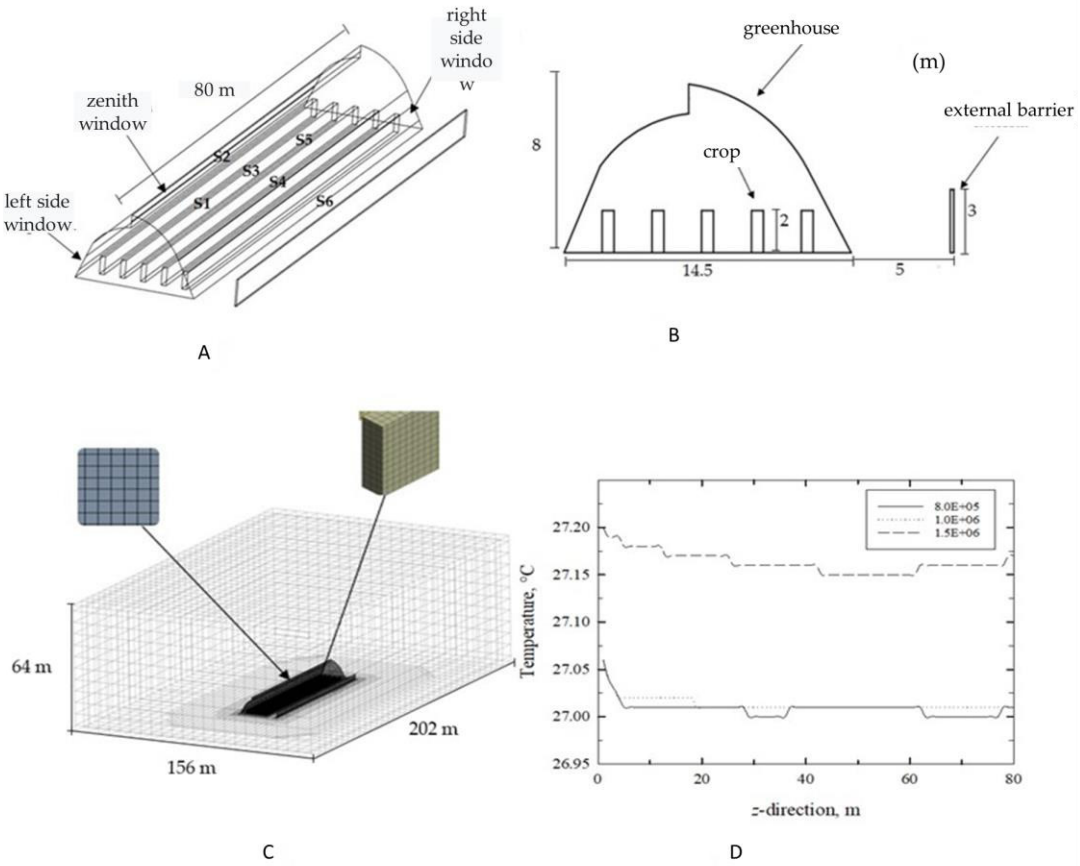

Figure 1. A: geometry isometric view; B: geometry front view; C: meshing, domain dimensions; D: mesh sensitivity analysis.

remained 50 % open during data collection. The study was carried out with an established tomato (*Solanum lycopersicum* L.) crop at the productive stage, 2 m high, distributed in five beds planted in double rows, with mulch.

Development of the computational model

The geometry of the environment is composed of a greenhouse and a barrier placed parallel to the length of the long face of the vessel at a 5 m distance (Figure 1B). The computational domain and total volume dimensions, including the greenhouse, are 156 m wide × 202 m long × 64 m high (Figure 1C). This excess volume guarantees a reliable model according to the recommendations of different authors (Fatnassi *et al*., 2017; Piscia *et al*., 2015). Similarly, a structured type mesh (Figure 1C) consisting of 835 491 elements was considered, with a distortion value of 0.02 and an orthogonal quality of 0.97 on average, indicative of a good fit (Román-Roldán *et al*., 2019; Villagrán

et al., 2020a). The sensitivity analysis of the mesh to calculate the independence of the results on the number of elements (Figure 1D) showed that the numerical model reached a point where the solution does not change significantly by making the mesh more refined, implying that the solution is sufficiently accurate.

Mesh sensitivity analysis was performed by recording 80 temperature points at 2 m from the ground longitudinally in the center of the greenhouse. Three scenarios were analyzed by varying the number of elements in the mesh (He *et al*., 2018; Villagrán *et al*., 2019; Villagrán *et al*., 2020b). The results showed independence in the behavior of temperature in relation to the number of elements; a variation of 0.2 °C is appreciated in the 1 500 000-element mesh compared to the 1 000 000- and 8 000 000-element meshes.

Equations defining fluid dynamics

To solve the fluid dynamic behavior, the Navier-Stokes equations were solved through a matter and energy balance:

$$\frac{\partial \Phi}{\partial t} + \frac{\partial (U\Phi)}{\partial x} + \frac{\partial (V\Phi)}{\partial y} + \frac{\partial (W\Phi)}{\partial z} = -\Gamma \Delta \Phi^2 + S_\Phi$$

where Φ represents the concentration of the dimensionless term, which refers to the amount of motion, mass, or energy; U, V, and W are the components of the velocity vector in three dimensions (m s^{-1}); Γ is the diffusivity coefficient (kg m s^{-1}); and S_Φ is the source term.

The turbulence model used is the two-equation *k-ε*, which has been used in greenhouse simulation (Piscia *et al*., 2015). The Boussinesq hypothesis is considered valid for natural ventilation studies in greenhouses where thermal gradients are below 20 °C. Thus, an inclusion of gravity forces originating from changes in air density due to changes in temperature is performed when solving the momentum equation. The Boussinesq model is represented as follows (Baeza *et al*., 2009; Villagrán *et al*., 2020a):

$$(\rho - \rho_0) g = -\rho_0 \beta (T - T_0) g$$

where β is the coefficient of thermal expansion, g is the force of gravity, and ρ and T are the density and temperature of the air, with the subscript representing a reference state.

Anti-aphid meshes are considered in CFD models as porous jumps due to the pressure drop of the airflowing through them. Bartzanas *et al*. (2004) indicate that meshes can decrease ventilation rates between 33 and 50 % depending on the type, and therefore affect temperature gradients. Darcy's law states that the flow velocity in a porous medium is proportional to the pressure loss due to viscosity effects, but it is violated

in high-velocity flows, which are frequently encountered in the natural environment. To calculate the pressure drop caused by the mesh, the following equation was used (Romero-Gómez *et al*., 2010):

$$\Delta p = -\left(\frac{\mu}{\alpha}v + C_2\frac{1}{2}\rho v^2\right)\Delta J$$

where Δp is the pressure drop (kg m^{-1} s^{-2}), μ is the dynamic flow viscosity (kg m^{-1} s^{-1}), α is the face permeability (m^2), C^2 is the pressure jump coefficient (m^{-1}), and ΔJ is the thickness of the porous jump (m).

Boundary conditions

A symmetry condition was assigned to the front, back, and upper walls of the domain. The air inlet was set at the right wall, according to the predominant wind direction in the region and considering hourly averaged velocity values (Table 1). A pressure outlet was set at the left wall of the domain P = 101.3 kPa (atmospheric pressure). The lower part with soil properties for domain, greenhouse, and cultivation was established as a wall condition. The greenhouse canopy was defined as wall condition v = 0 m s^{-1}. The insect screens on the windows were set as a porous jump, the crop as a porous medium, and the external barrier as a solid wall without slippage, with defined values of the characteristics of the materials considered (Table 2).

Table 1. Hourly averaged climatic variables of the study site for July 5, 2023.

Time	T (°C)	RH (%)	v (m s^{-1})	Time	T (°C)	RH (%)	v (m s^{-1})
06:00	15.13	95	0.2	12:00	27.03	50	0.4
07:00	15.80	96	0.0	13:00	28.95	40	0.0
08:00	17.60	96	0.2	14:00	29.58	34	0.0
09:00	20.35	84	0.0	15:00	31.05	34	0.3
10:00	23.35	69	0.4	16:00	30.20	40	0.6
11:00	25.15	59	0.0	17:00	20.00	79	2.4

Table 2. Physical properties of the materials (Villagrán *et al*., 2020a) used in the mathematical model.

Material	Density (kg m^{-3})	Specific heat (J kg^{-1} K^{-1})	Thermal conductivity (W m^{-1} K^{-1})
Plastic	925.5	1600	0.33
Crop	1000	4180	0.6
Soil	1400	1738	1.5
Air	1.225	1006.46	0.0242
Brick	1700	800	1.31

Case studies

The greenhouse is built on a plot of land with a perimeter fence on the right side, 5 m away. This configuration was used to validate the numerical simulation. Once validated, four scenarios were analyzed, feeding the same environmental conditions at three different times of the day (6:00, 14:00, and 17:00 h) to study the variations in thermal and wind behavior.

To generate a solution, a pressure-based algorithm was used, where a convergence value of 1×10^{-6} was established and the following considerations, demonstrated by various authors, were taken into account (Flores-Velázquez *et al*., 2014; Piscia *et al*., 2015; Aguilar-Rodríguez *et al*., 2020b; Si *et al*., 2023): a) the energy equation is solved, b) the temperature and wind velocity profiles are constant, c) there is a pressure jump in the windows caused by the antiaphid meshes (Table 3), d) the crop behaves as a porous medium, and e) the air density is affected by the Boussinesq effect.

For each scenario, a 50 % window opening was considered as this was the greenhouse's operating conditions at the time of data collection. The crop (tomato) in production stage was considered as a barrier. Crop transpiration was not considered in the simulation, since the trajectory of wind currents and their influence on the thermal field was evaluated. The case studies and an illustration of the computational domain are shown (Table 4). The numerical models were solved using the commercial software Ansys Fluent®.

Table 3. Physical characteristics of the antiaphid netting used in the mathematical model.

Property	Measure
Face permeability	2.86×10^{-9} m^2
Thickness of porous medium	3.72×10^{-4} m
Pressure drop coefficient	11 131.45 m^{-1}
Thermal resistance	0

Table 4. Study cases varying the barrier position. A: no barrier; B: barrier at 5 m; C: barrier at 10 m; D: barrier at 15 m.

Case	Barrier position	Geometry
A	No barrier	
B	5 m (validation)	
C	10 m	
D	15 m	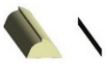

RESULTS AND DISCUSSION

Model validation

The data used were those obtained by the sensors on July 5, 2023. The model was evaluated during the diurnal period between 6:00 and 18:00 h, recording the climatic conditions of the study site on an hourly average (Table 1). Mean absolute error (MAE), root mean square error (RSME), and R^2 were calculated as measures of data goodness-of-fit, as they adequately allow determining the reliability of the model:

$$MAE = \frac{1}{n}\sum_{i=1}^{n}|real_i - simulated_i|$$

$$RSME = \sqrt{\frac{\sum_{i=1}^{n}|real_i - simulated_i|^2}{n}}$$

$$R^2 = 1 - \frac{\sum_{i=1}^{n}|real_i - simulated_i|^2}{\sum_{i=1}^{n}\left|real_i - \overline{real}\right|^2}$$

Values of MAE = 1.5, RSME = 2.5, and R^2 = 0.869 were obtained, indicating that the model has a good fit with the experimental data (Villagrán *et al*., 2019; Román-Roldán *et al*., 2019; Villagrán *et al*., 2020b). The average error was ±1.5 °C, suggesting that the simulated values are not far away from the real values. A higher RMSE value compared to MAE indicates that the model presents a lower predictive capacity at some points. This is demonstrated by the correlation between the computed and measured data at various times of the day (Figure 2). In addition, the regression curve is shown, where it can be observed that the dispersion is 14 %.

Velocity fields

This analysis was performed indirectly in the absence of wind sensors inside the greenhouse, but based on temperature measurements, as reported by Villagrán and Bojacá (2019). The observed behaviors for wind velocities lower than 1 m s^{-1} presented similar behavior among themselves, so the analysis was performed on the simulated case with v = 2.4 m s^{-1} and T = 20 °C outside the greenhouse in the transverse profile obtained at 40 m (-z axis), where the most notorious temperature and velocity gradients are concentrated. The vectors described a behavior that agrees with the wind trajectory diagrams reported by Kacira *et al*. (2004) and Baeza *et al*. (2009).

The comparison between the four case studies shows that, in the absence of the barrier, vectors with constant velocity and trajectory are observed until they reach the greenhouse window, where the velocity is reduced by the presence of the insect

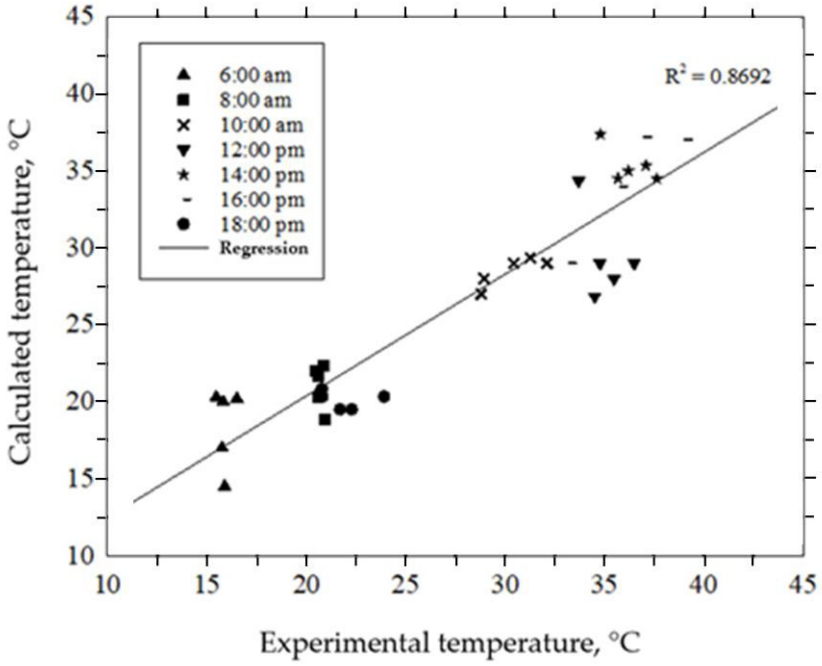

Figure 2. Validation of the computational model, recording hourly averaged measurements from each sensor.

screen (Figure 3A, point 1). Inside the greenhouse, the airflow rises and crosses the greenhouse, exiting through the left and zenith windows; this flow creates a recirculation at point 2 as it comes into contact with the air moving through the crop driven by the temperature difference.

With the presence of the external barrier at 5, 10, and 15 m, at points 3, 6, and 7 (Figure 3B-D), the recirculation formed between the greenhouse and the barrier decreases the airflow at the entrance. Regardless of the position of the external barrier, the airflow inside the greenhouse at the entrance of the right window is between 0 and 0.5 m s^{-1}, in contrast to the case without the barrier, where the velocity is up to 1.2 m s^{-1}. Although the velocity with which the air reaches the right greenhouse window decreases with increasing distance between the vessel and the barrier (1.6, 1, and 0.85 m s^{-1} for 5, 10, and 15 m, respectively), no changes in the velocity inside the vessel are observed.

By reducing the air entry in the right window, airflow through the left and zenith windows is promoted, and the formation of recirculation within the greenhouse at points 4, 6, and 8 is favored (Figure 3B–D). This affects the trajectory of the vectors through the crop and forces the flow of hot air to remain in these areas. The velocity of 0–0.2 m s^{-1} inside the shed in all cases with the external barrier indicates that the air current movement is due to the temperature difference (Kacira *et al*., 2004). In cases with data obtained at 2 and 4 m height and 40 m in the -*z* direction (Figure 4), the best

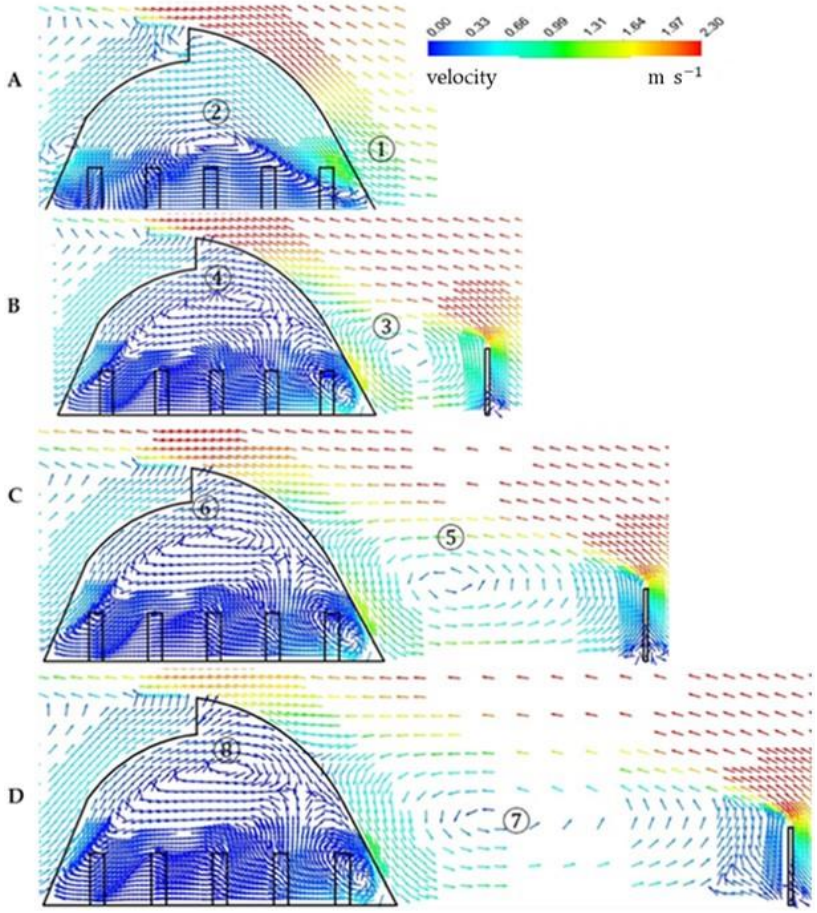

Figure 3. Wind velocity and trajectory profile projected at 18:00 h. A: no barrier; B: barrier at 5 m; C: barrier at 10 m; D: barrier at 15 m.

ventilation conditions correspond to the scenario without the presence of the external barrier, which agrees with Fatnassi *et al*. (2017). It is also observed that it does not cause a total obstruction in ventilation due to the height of the barrier (3 m) (López *et al*., 2011).

On the other hand, all scenarios with barriers had lower values of velocity at crop height (0.1–0.2 m s^{-1}) (Figure 4). The simulation results showed higher wind velocity at 4 m from the ground, where the recirculation formed by the flows between the left and zenith windows was generated. This promoted velocities at the center of the greenhouse of 0.3–0.2 m s^{-1} for the cases with the barrier at 5 and 15 m, respectively. The barrier at 10 m maintained uniform velocity values of less than 0.1 m s^{-1}. The recirculation does not affect the crop level, but it does influence the movement of the airflow through it (Akrami *et al*., 2020).

The highest velocity was reached in the case without a barrier (1.4 m s^{-1} at the entrance, which decreased to 0.35 m s^{-1} in the center of the greenhouse to increase again at the

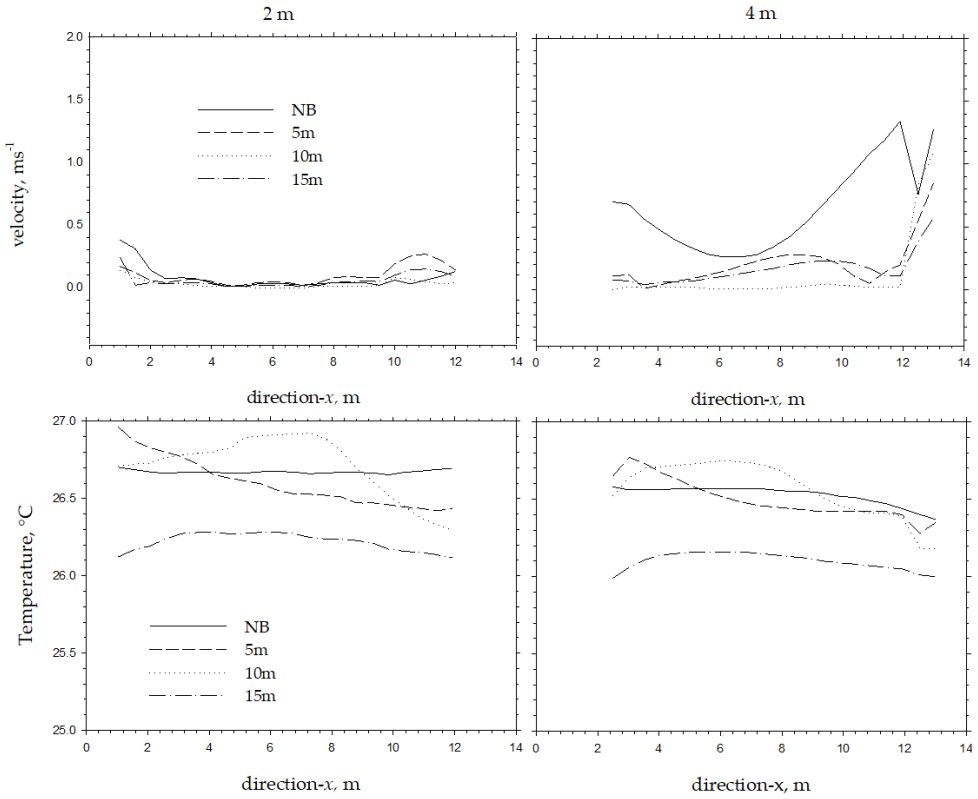

Figure 4. Wind and temperature behavior at 2 and 4 m height for the cases without barrier, with barrier at 5 m, barrier at 10 m, and barrier at 15 m in the -*x* and -*z* directions.

exit through the left window), where no recirculation was formed at that height, but a flow from the right window to the left and zenith window was observed. On the other hand, for the wind velocity that was simulated, the changes in temperature were not caused by the airflow but by convective phenomena. The scenario that presented the lowest temperature was the barrier at 10 m (Figure 4), with variations of about 1 °C when compared to the other scenarios, which indicates that with the simulated conditions at 18:00 h, the presence or placement of the barrier does not represent a significant temperature change for the crop.

Temperature contours

To analyze the thermal behavior inside the greenhouse, three planes were analyzed in the transverse profile, located at 20, 40, and 60 m (-*z*-axis) and a plane 2 m above the ground, which corresponds to the height of the canopy. The thermal distribution at 6:00 and 14:00 h was analyzed to identify the times of lowest and highest temperature in the study region for a common day in July (Figure 5). At 6:00 h, with an external temperature of 15.13 °C and wind velocity of 0.2 m s^{-1}, the temperature profile is the

most homogeneous in the no-barrier scenario (Figure 5, A–A'), where a temperature of ~19 °C predominates at the center of the greenhouse at crop height due to the heat emanating from the ground and its distance from the windows, where the temperature is ~18 °C.

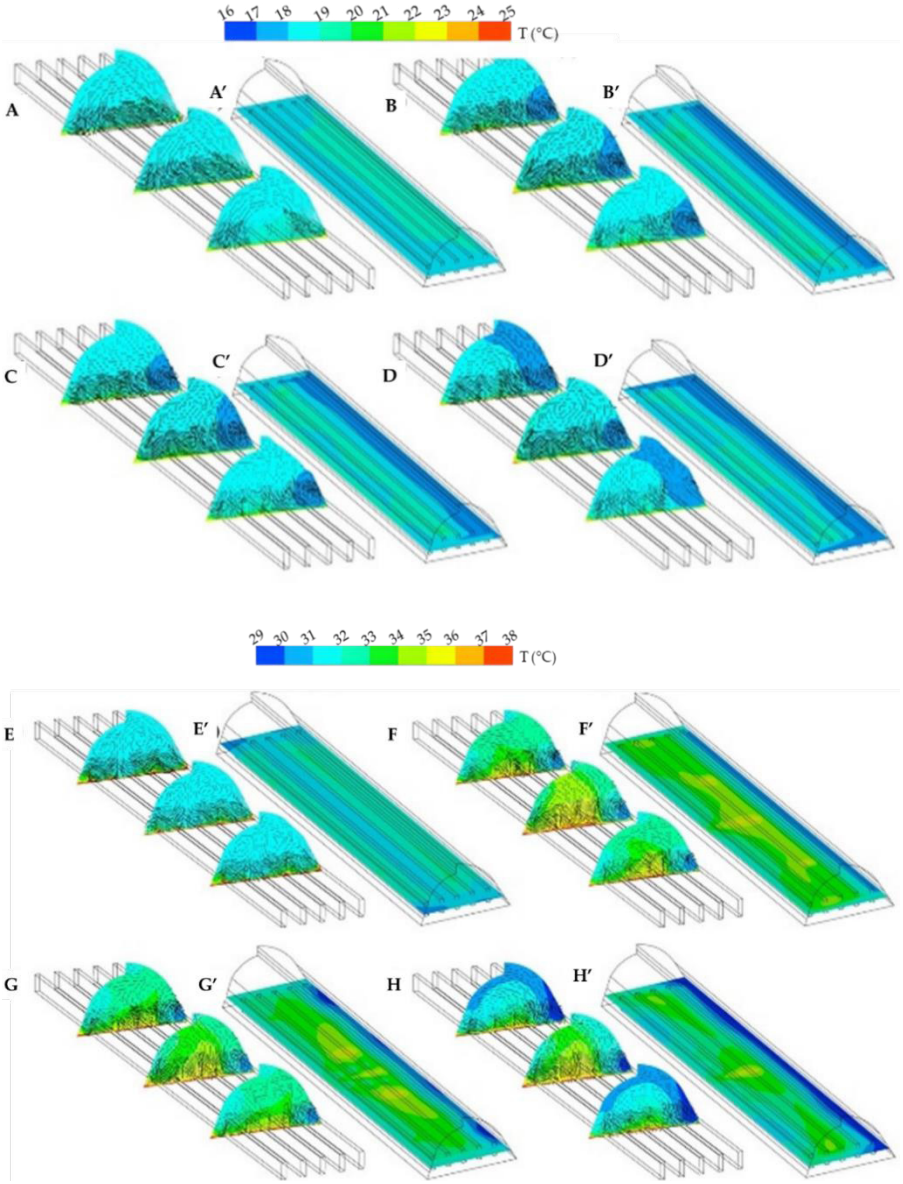

Figure 5. Greenhouse temperature profiles at 6:00 am: A: no barrier; B: barrier at 5 m; C: barrier at 10 m; D: barrier at 15 m. Temperature profiles at 14:00 h: E: no barrier; F: barrier at 5 m; G: barrier at 10 m; H: barrier at 15 m. A'–H': thermal contours in the transverse planes for the case without barrier and at 5, 10, and 15 m, at 6:00 and 14:00 h, respectively.

In the cases with a barrier at 5 and 10 m, a deflection is observed in the inflow current that forms a vortex next to the right window and maintains the temperature at ∼17 °C in this area (Figure 5, B–B′ and C–C′), which caused an increase of up to 4 °C compared to the case without a barrier, obtaining temperatures of 23 °C at the center of the vessel and decreasing to 21 °C at the left window for the case with a barrier at 5 m.

For the case with the barrier at 10 m, the temperature was 20 °C in the left window and 22 °C in the center; this is due to the limitation that the barrier offers to the entry of cold air, which allows temperatures of 20–23 °C to cover approximately 85 % of the building at canopy height. Since this increase in temperature is proportional to the proximity of the barrier, in the case where the barrier is located at 15 m (Figure 5, D–D′), the low temperature containment next to the window mentioned in the cases at 5 and 10 m was not generated. For this case (at 15 m), the lower temperature (18 °C) was not only located at the entrance of the right window but extended to the upper part of the greenhouse, adjacent to the right wall of the greenhouse and up to the zenith window.

Also, a lower temperature was observed at the front and rear ends of the greenhouse, so that the values of 22 °C were concentrated from the middle zone of the greenhouse towards the left window, where a decrease of 1 °C was observed. Despite a very low wind velocity (0.2 m s^{-1}), the change in internal temperature with the presence of the barrier was observed. According to the simulation, the optimum temperatures were obtained when the barrier was 5 m away, showing a homogeneous behavior and a greater positive temperature gradient with respect to the outside temperature (5–6 °C).

In the profiles corresponding to 14:00 h, where the external temperature is ∼29 °C and the wind velocity is ∼1.8 m s^{-1} with no barrier (Figure 5, E–E′), a uniform temperature profile was shown due to the behavior of the air currents (Figure 3A). In this case, wind velocities barely reach 0.2 m s^{-1} in most of the greenhouse, so it is not a determining factor in the temperature change, which remains at 31 °C, but the direction of the currents formed by the difference in densities is. In the cases with barriers at 5 and 10 m (Figure 5, F–F′ and G–G′), their presence caused lower temperatures at the air inlet (30 °C), the center, and the left window (31–32 °C), keeping the temperature distribution uniform in all cases in the -*z* direction. At canopy height, a variation of only 0.5 °C was observed between the exposed scenarios.

Contrary to the plans described above, in the case of the presence of the barrier at 15 m (Figure 5, H–H′), there was a more noticeable temperature decrease towards the top on the right wall, which caused a difference of 1 °C compared to the center of the greenhouse. However, it only reached the first row of crops, while in the rest of the greenhouse a homogeneous temperature of 30–31 °C was obtained.

The four study cases were analyzed by plotting the temperature of each of them at a height of 2 m in the central part of the greenhouse in the -x and -z directions. At 6:00 h, the case without a barrier showed the lowest temperature (Figure 6), which remained uniform in the -*z* direction (18.5 °C) and showed a variation of approximately 1 °C

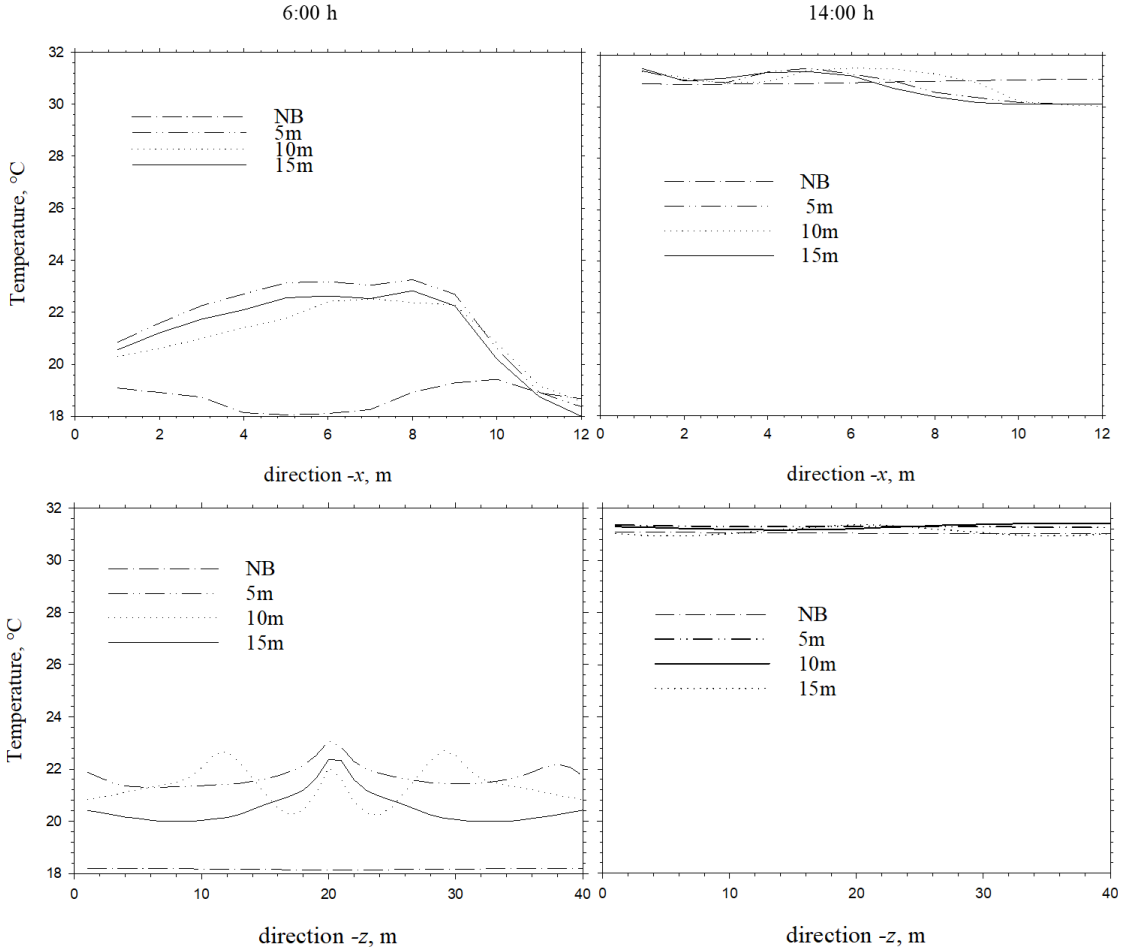

Figure 6. Temperature behavior at 6:00 and 14:00 hours on July 5, 2023, for the cases without a barrier, barrier at 5 m, barrier at 10 m, and barrier at 15 m in the *-x* and *-z* directions.

along the -x direction. The case with a barrier at 5 m showed the highest temperature on the *-x* axis (23 °C) compared to the cases with a barrier at 10 and 15 m; this temperature was reached at the center of the vessel, decreasing to 22 °C as the line approaches the right and left ends of the greenhouse.

These 22 °C coincide along the *-z* axis, indicating that the presence of the barrier placed at 5 m allows maintaining the temperature 4 to 5 °C higher during the coldest hours than in the case without a barrier. This phenomenon was not observed at 14:00 h, where the presence of the barrier did not show changes in the thermal behavior of the greenhouse, with differences of only 0.5 °C in the *-z* direction and 1 °C in the *-x* direction, where the average temperature for the four cases remained at 31 °C.

CONCLUSIONS

The presence of the external physical barrier, regardless of its distance, decreased ventilation inside the greenhouse by up to 60 %, modifying the trajectory of the air current outside and inside the greenhouse. Inside, the flow path was affected in the same way, regardless of the distance from the barrier; however, the temperature at canopy height increased between 2 and 4 °C depending on its placement. The barrier located at 5 m was useful in the summer climate to slow the temperature drop at dawn, maintaining up to 4 °C above the external temperature. The most homogeneous ventilation and temperature distribution were obtained in the absence of the barrier. It is suggested that the results of this study be taken into account in the design of greenhouses located in urban areas.

ACKNOWLEDGEMENTS

The authors wish to thank the TecNM-ITM, SNI, TecNM-ITVG for the scholarship granted for the DCI graduate studies, FIM-UMSNH, and Dr. José de Jesús Muñoz Ramos, research professor of the TecNM-ITVG, for the support provided to carry out this study.

REFERENCES

Aguilar-Rodríguez CE, Flores-Velázquez J, Ojeda-Bustamante W, Rojano F, Iñiguez-Covarrubias M. 2020a. Valuation of the energy performance of a greenhouse with an electric heater using numerical simulations. Processes 8 (5): 600. https://doi.org/10.3390/pr8050600

Aguilar-Rodríguez CE, Flores-Velázquez J, Rojano F, Flores-Magdaleno H, Rubiños-Panta E. 2021. Simulation of water vapor and near infrared radiation to predict vapor pressure deficit in a greenhouse using CFD. Processes 9 (9): 1587. https://doi.org/10.3390/pr9091587

Aguilar-Rodríguez CE, Flores-Velázquez J, Rojano-Aguilar F, Ojeda-Bustamante W, Iñiguez-Covarrubias M. 2020b. Tomato (*Solanum lycopersicum* L.) crop cycle estimation in greenhouse, based on degree day heat (GDC) simulated in CFD. Tecnología y Ciencias del Agua 11 (4): 27–59. https://doi.org/10.24850/j-tyca-2020-04-02

Akrami M, Javadi AA, Hassanein MJ, Farmani R, Dibaj M, Tabor GR, Negm A. 2020. Study of the effects of vent configuration on mono-span greenhouse ventilation using computational fluid dynamics. Sustainability 12 (3): 986. https://doi.org/10.3390/su12030986

Baeza EJ, Pérez-Parra JJ, Montero JI, Bailey BJ, López JC, Gázquez JC. 2009. Analysis of the role of sidewall vents on buoyancy-driven natural ventilation in parral-type greenhouses with and without insect screens using computational fluid dynamics. Biosystems Engineering 104 (1): 86–96. https://doi.org/10.1016/j.biosystemseng.2009.04.008

Bartzanas T, Boulard T, Kittas C. 2004. Effect of vent arrangement on windward ventilation of a tunnel greenhouse. Biosystems Engineering 88 (4): 479–490. https://doi.org/10.1016/j.biosystemseng.2003.10.006

Bournet PE, Rojano F. 2022. Advances of computational fluid dynamics (CFD) applications in agricultural building modelling: Research, applications and challenges. Computers and Electronics in Agriculture 201: 107277. https://doi.org/10.1016/j.compag.2022.107277

Carpentieri M, Robins AG. 2015. Influence of urban morphology on airflow over building arrays. Journal of Wind Engineering and Industrial Aerodynamics 145: 61–74. https://doi.org/10.1016/j.jweia.2015.06.001

Castro IP, Xie ZT, Fuka V, Robins AG, Carpentieri M, Hayden P, Hertwig D, Coceal O. 2017. Measurements and computations of flow in an urban street system. Boundary-Layer Meteorology 162 (2): 207–230. https://doi.org/10.1007/s10546-016-0200-7

Choab N, Allouhi A, El-Maakoul A, Kousksou T, Saadeddine S, Jamil A. 2019. Review on greenhouse microclimate and application: Design parameters, thermal modeling and simulation, climate controlling technologies. Solar Energy 191: 109–137. https://doi.org/10.1016/j.solener.2019.08.042

Chu CR, Lan TW. 2019. Effectiveness of ridge vent to wind-driven natural ventilation in monoslope multi-span greenhouses. Biosystems Engineering 186: 279–292. https://doi.org/10.1016/j.biosystemseng.2019.08.006

El-Alaoui M, Chahidi L, Rougui M, Mechaqrane A, Allal S. 2023. Evaluation of CFD and machine learning methods on predicting greenhouse microclimate parameters with the assessment of seasonality impact on machine learning performance. Scientific African 19: e01578. https://doi.org/10.1016/j.sciaf.2023.e01578

Espinoza K, López A, Valera DL, Molina-Aiz FD, Torres JA, Peña A. 2017. Effects of ventilator configuration on the flow pattern of a naturally-ventilated three-span Mediterranean greenhouse. Biosystems Engineering 164: 13–30. https://doi.org/10.1016/j.biosystemseng.2017.10.001

Fatnassi H, Boulard T, Benamara H, Roy JC, Suay R, Poncet C. 2017. Increasing the height and multiplying the number of spans of greenhouse: How far can we go? Acta Horticulturae 1170: 137–144. https://doi.org/10.17660/ActaHortic.2017.1170.15

Flores-Velázquez J, López-Cruz IL, Mejía-Sáenz E, Montero-Camacho JI. 2014. Evaluación del desempeño climático de un invernadero baticenital del centro de México mediante dinámica de fluidos computacional (CFD). Agrociencia 48 (2): 131–146.

Flores-Velázquez J, Ojeda-Bustamante W. 2015. Consideraciones agronómicas para el diseño de invernaderos típicos de México. Secretaría de Medio Ambiente y Recursos Naturales. Jiutepec, México. 179 p.

Ghoulem M, Moueddeb K, Nehdi E, Zhong F, Calautit J. 2020. Analysis of passive downdraught evaporative cooling windcatcher for greenhouses in hot climatic conditions: Parametric study and impact of neighboring structures. Biosystems Engineering 197: 105–121. https://doi.org/10.1016/j.biosystemseng.2020.06.016

Gómez-Mataix G, Montero JI, Raya V, Suay R. 2012. Benchmark study of the distance between greenhouses and its effect on wind driven ventilation. Acta Horticulturae 1008: 207–211 https://doi.org/10.17660/ActaHortic.2013.1008.27

He X, Wang J, Guo S, Zhang J, Wei B, Sun J, Shu S. 2018. Ventilation optimization of solar greenhouse with removable back walls based on CFD. Computers and Electronics in Agriculture 149: 16–25. https://doi.org/10.1016/j.compag.2017.10.001

Kacira M, Sase S, Okushima L. 2004. Effects on side vents and span numbers on wind-induced natural ventilation of a Gothic multi-span greenhouse. Japan Agricultural Research Quarterly 38 (4): 227–233. https://doi.org/10.6090/jarq.38.227

King MF, Gough HL, Halios C, Barlow JF, Robertson A, Hoxey R, Noakes CJ. 2017. Investigation of the influence of neighboring structures on the natural ventilation potential of a full-scale cubic building using time-dependent CFD. Journal of Wind Engineering and Industrial Aerodynamics 16: 265–279. https://doi.org/10.1016/j.jweia.2017.07.020

Li H, Li Y, Yue X, Liu X, Tian S, Li T. 2020. Evaluation of airflow pattern and thermal behavior of the arched greenhouses with designed roof ventilation scenarios using CFD simulation. PloS One 15 (9): e0239851. https://doi.org/10.1371/journal.pone.0239851

López A, Valera DL, Molina-Aiz FD, Peña A. 2011. Effects of surrounding buildings on air patterns and turbulence in two naturally ventilated Mediterranean greenhouses using tri-sonic anemometry. Transactions of the ASABE 54 (5): 1941–1950. https://doi.org/10.13031/2013.39835

Ortiz-Rocha GA, Pichimata MA, Villagrán E. 2021. Research on the microclimate of protected agriculture structures using numerical simulation tools: A technical and bibliometric analysis as a contribution to the sustainability of under-cover cropping in tropical and subtropical countries. Sustainability 13 (18): 10433. https://doi.org/10.3390/su131810433

Piscia D, Muñoz P, Panadés C, Montero JI. 2015. A method of coupling CFD and energy balance simulations to study humidity control in unheated greenhouses. Computers and Electronics in Agriculture 115: 129–141. https://doi.org/10.1016/j.compag.2015.05.005

Román-Roldán NI, López-Ortiz A, Ituna-Yudonago JF, García-Valladares O, Pilatowsky-Figueroa I. 2019. Computational fluid dynamics analysis of heat transfer in a greenhouse solar dryer "chapel-type" coupled to an air solar heating system. Energy Science and Engineering 7 (4): 1123–1139. https://doi.org/10.1002/ese3.333

Romero-Gómez P, Choi CY, Lopez-Cruz IL. 2010. Enhancement of the greenhouse air ventilation rate under climate conditions of central Mexico. Agrociencia 44 (1): 1–15.

Ruiz-García A, López-Cruz I, Arteaga-Ramírez R, Ramírez-Arias JA. 2015. Natural ventilation rates of a greenhouse at central Mexico estimated by energy balance. Agrociencia 49 (1): 87–100.

Si C, Qi F, Ding X, He F, Gao Z, Feng Q, Zheng L. 2023. CFD Analysis of solar greenhouse thermal and humidity environment considering soil-crop-back wall interactions. Energies 16 (5): 2305. https://doi.org/10.3390/en16052305

Villagrán E, León R, Rodríguez A, Jaramillo J. 2020a. 3D Numerical analysis of the natural ventilation behavior in a Colombian greenhouse established in warm climate conditions. Sustainability 12 (19): 8101. https://doi.org/10.3390/su12198101

Villagrán EA, Baeza-Romero EJ, Bojacá CR. 2019. Transient CFD analysis of the natural ventilation of three types of greenhouses used for agricultural production in a tropical mountain climate. Biosystems Engineering 188: 288–304. https://doi.org/10.1016/j.biosystemseng.2019.10.026

Villagrán EA, Bojacá CR. 2019. Effects of surrounding objects on the thermal performance of passively ventilated greenhouses. Journal of Agricultural Engineering 50 (1): 20–27. https://doi.org/10.4081/jae.2019.856

Villagrán EA, Jaramillo JE, León-Pacheco RI. 2020b. Ventilación natural en invernadero con mallas anti-insecto evaluadas con un modelo computacional de fluidos. Agronomía Mesoamericana 31 (3): 698–717. https://doi.org/10.15517/am.v31i3.40782

Agrociencia

BIOGAS PRODUCTION BY ANAEROBIC CO-DIGESTION OF AGRO-INDUSTRIAL WASTE AND CRUDE GLYCEROL

Sergio **Muñoz-Martínez**[1], Angélica María **Salmerón-**Alcocer[1,2], Felipe Neri **Rodríguez-Casasola**[1], Deifilia **Ahuatzi-Chacón**[1,2*]

[1]Instituto Politécnico Nacional. Escuela Nacional de Ciencias Biológicas, Departamento de Ingeniería en Sistemas Ambientales. Avenida Wilfrido Massieu s/n, Zacatenco, Gustavo A. Madero, Mexico City, Mexico. C. P. 07738.
[2]Instituto Politécnico Nacional. Escuela Nacional de Ciencias Biológicas, Departamento de Ingeniería Bioquímica. Avenida Wilfrido Massieu s/n, Zacatenco, Gustavo A. Madero, Mexico City, Mexico. C. P. 07738.
* Author for correspondence: dahuatzi@hotmail.com

Citation: Muñoz-Martínez S, Salmerón-Alcocer AM, Rodríguez-Casasola FN, Ahuatzi-Chacón D. 2025. Biogas production by anaerobic co-digestion of agro-industrial waste and crude glycerol. **Agrociencia** 59(4): 500-514. https://doi.org/ 10.47163/agrociencia.v59i4.3329

Editor in Chief:
Dr. Fernando C. Gómez Merino

Received: October 18, 2024.
Approved: May 07, 2025.
Published in Agrociencia: May 12, 2025.

ABSTRACT

The use of fossil fuels continues to represent a significant percentage of energy production in Mexico; this, together with the generation of considerable amounts and poor disposal of organic waste, has contributed greatly to the emission of greenhouse gases, exacerbating the problem of environmental pollution. In Mexico City's central supply center alone, more than 500 Mg of organic waste is produced daily, and its disposal is not the most appropriate. An alternative for the correct disposal of this waste is the anaerobic digestion process, which, in addition to being an environmentally friendly technology, offers benefits such as the possibility of obtaining value-added products such as biogas, which represents a viable alternative to the use of fossil fuels. In this study, waste generated in Mexico City's central supply center was collected for use in anaerobic co-digestion to produce biogas using crude glycerol obtained as a byproduct of the biodiesel plant located in the same center. Throughout the bioprocess lasting 12 weeks, with a hydraulic retention time of 33.3 ± 0.04 days and an organic matter removal efficiency of 77.6 %, it was possible to obtain perfectly flammable biogas with a methane composition between 60 and 70 %, with an average production of 0.576 ± 0.084 m^3 d^{-1}.

Key words: biodigestion, biomass, organic waste, gaseous biofuel.

INTRODUCTION

Agriculture is a very important economic sector in Mexico, with a share in gross domestic product (GDP) of 2.5 %; in addition, Mexico ranks first in vegetable production in Latin America and second in fruit cultivation (Statista Research Department, 2023). In 2023, the flow of foreign direct investment exceeded USD 109 million, and agri-food exports exceeded USD 50 billion for the first time. Avocado exports generated the highest income for the national economy, with a value of USD 3.153 million in 2023. As for vegetables, tomato exports generated the most revenue, with a value of USD 2.67 billion (Statista Research Department, 2023). This abundance of agricultural raw

materials leads to a great potential for agroindustrial development (Martínez-Prats *et al*., 2022).

Agricultural activities (sowing and harvesting) represent 5 to 18 % of Latin America's GDP; however, when agro-industrial activities (transformation of farm products) are considered, the percentage increases to 21 %, which shows the importance of agro-industry (Sarandón, 2020). In Mexico, fresh products such as fruits, vegetables, leaves, and pods are processed, as well as other already transformed products such as flours, oils, juices, wines, jams, and concentrates, which generates a large amount of waste throughout the entire process, from harvesting, concentration, distribution, industrialization, marketing, and consumption (Mejías-Brizuela *et al*., 2016).

According to Mejías-Brizuela *et al*. (2016), who consider the definition given by the General Law for the Prevention and Integral Management of Waste in Mexico, "Agro-industrial waste are solid, semi-solid, and liquid organic products generated from the direct use of primary products or their industrialization, not useful for the process that generated them, but susceptible to a use or transformation that generates another product with economic value, of commercial and/or social interest."

In 2020, Mexico's Ministry of the Environment and Natural Resources published the Basic Diagnosis for Integrated Waste Management, which addresses the state of the country's waste generation and management. Composting or biodigestion can treat an estimated 56 427 Mg of organic waste produced per day; however, the number of waste treatment or utilization plants is very limited, as there are only 47 plants distributed in 15 states, which separate, grind, and compact. Of the 47 plants, 19 perform composting and only five perform biodigestion (SEMARNAT, 2020).

This problem is also present worldwide, where around 500 million Mg of agro-industrial waste is generated each year (Singh *et al*., 2021). Its poor disposal has resulted in a significant contribution to environmental pollution, causing negative impacts on the health of animals and humans (Herrera-Uchalin *et al*., 2023). Hence the importance of adding value to agro-industrial wastes through so-called clean technologies, which help reduce their environmental impact and follow the current trend of the circular economy (Matiacevich *et al*., 2023).

The valorization of agro-industrial wastes has two aspects: biotechnological and energetic utilization. Biotechnological valorization is done by direct extraction or by chemical or microbial transformation to higher value-added commercial products such as pigments, polymers, antioxidants, polyphenols, antibiotics, and enzymes (Singh *et al*., 2021). Energy valorization includes the chemical or microbiological transformation of agro-industrial by-products and residues containing significant amounts of biomass rich in cellulose, hemicellulose, lignin, glycosides, and fatty acids into bioenergy such as bioethanol, biodiesel, and biogas (Mejías-Brizuela *et al*., 2016). *Saccharomyces* yeasts ferment saccharides contained in sugarcane or corn and produce bioethanol (Pérez-Contreras *et al*., 2023). Biodiesel is produced through the transesterification reaction of fatty acids found in animal or plant oils (Singh *et al*., 2021).

In the case of biogas, specialized microorganisms degrade, under anaerobic conditions, the organic matter and produce the gaseous fuel, whose main component is methane,

a high-quality energy source. Consequently, it can be used to generate electricity or steam in high-efficiency cogeneration systems (Jameel *et al*., 2024). The anaerobic digestion process can be improved by feeding more than one organic waste. Co-digestion is a process in which simultaneous anaerobic digestion of two or more wastes is carried out, improving the C/N ratio and increasing biogas production (Prasertsan *et al*., 2021). Several co-substrates have been used for biogas production, including sludge from wastewater treatment plants, municipal solid waste, cheese whey, grass (González *et al*., 2022), rice and banana husks (Olugbemide *et al*., 2023), and glycerol, among others (de Mello *et al*., 2024).

Biodiesel production generates crude glycerol as a byproduct; it is estimated that 10 kg of glycerol are obtained for every 100 kg of biodiesel produced (Chilakamarry *et al*., 2021). The purification process of this by-product is not economically viable, so its use in the food, pharmaceutical, and cosmetic industries is not recommended. Due to this, alternatives for its disposal have been sought, one of them being its use as a cosubstrate for biogas production, since its high carbon content increases the C/N ratio, avoiding inhibition by nitrogen and increasing biogas production from 50 to 200 % (Alves *et al*., 2020; Butkowska *et al*., 2022).

The objective of this work was to implement a bioprocess at the pilot plant level of anaerobic co-digestion, using agro-industrial waste and glycerol for biogas production, as a feasible solution to the serious pollution problem caused by the large amount of waste generated at Mexico City's Central de Abastos (CEDA) and, at the same time, the valorization of glycerol, a by-product of the biodiesel production plant of the same supply central.

MATERIALS AND METHODS

Biodigestor

The anaerobic digestion process was carried out in a 300 L pilot plant level biodigester with a programmable logic controller (PLC) (Figure 1).

The stainless steel biodigester with jacket-type exchanger was built at the Clean Technologies Laboratory, located in the Environmental Systems Engineering Department of the National School of Biological Sciences of the National Polytechnic Institute in Mexico City. The PLC controller receives information from connected sensors and input devices, processes the data, and issues outputs based on pre-programmed parameters (López *et al*., 2016). It has a home screen with a general menu where the user can monitor and record operating temperature information, as well as start and stop the heat exchanger operation automatically for temperature regulation. It also has programming for agitation control and dosing of the feed medium and acids or alkalis for pH control. The residues for anaerobic digestion were taken from fruit and vegetable waste from CEDA. Glycerol was provided by CEDA's biodiesel plant.

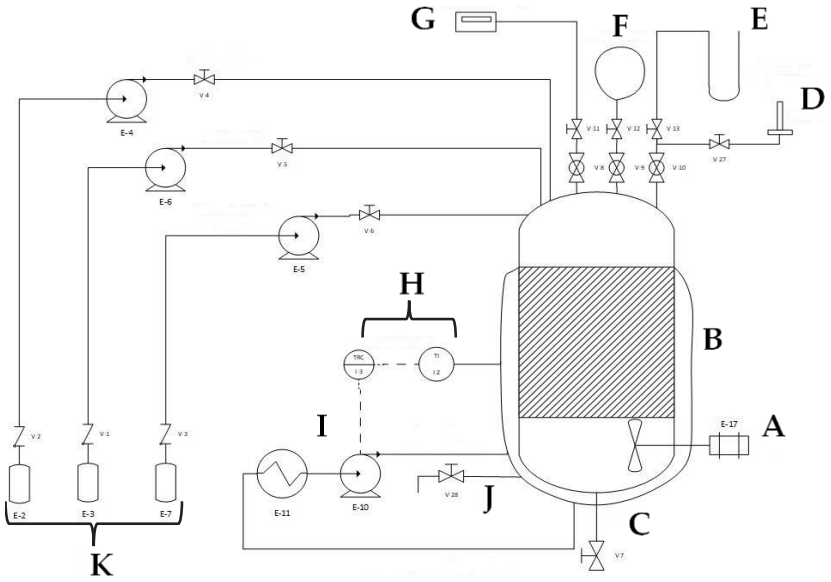

Figure 1. Diagram of the bioreactor used for biogas production. A: blade agitator; B: bioreactor body; C: drain; D: burner; E: differential pressure gauge; F: gasometer; G: gas detector; H: temperature control; I: heat exchanger with hot water recirculation; J: sampling; K: feed tanks.

Analytical methods

The analytical methods were performed according to the official Mexican standard corresponding to each determination: moisture, NMX-F-083-1986 (DOF, 1986); ash, NMX-F-066-S-1978 (DOF, 1978a); fat, NMX-F-615-NORMEX-2018 (DOF, 2018); total carbohydrates, NMX-F-312-1978 (DOF, 1978b); proteins, NMX-F-068-S-1980 (DOF, 1980); pH, NMX-F-317-S-1978 (DOF, 1978c); and total solids and volatile solids, NMX-AA-034-SCFI-2015 (DOF, 2015). Determinations of total nitrogen, total phosphorus, total organic carbon, and chemical oxygen demand were performed according to Hach (2024).

Volumetric consumption rate and chemical oxygen demand (COD) removal efficiency

The volumetric rate of COD consumption (VVC) was calculated through time (t) with the following relationship:

$$VVC = \frac{[COD]fed - [COD]soluble}{\Delta t}$$

The COD removal efficiency (η) was calculated with the following relationship:

$$\eta = \frac{[COD]fed - [COD]soluble}{[COD]fed} \times 100$$

Hydraulic retention time

The hydraulic retention time (HRT) was calculated with the ratio:

$$HRT = \frac{Operation\ volume}{Feeding\ load}$$

Biogas production measurement

Gas was purged from inside the biodigester through the tubing used for biogas measurement until a decrease in pressure was observed in both the gasometer and the U-shaped differential pressure gauge. After emptying the gasometer, the time it took to fill up to 2 L was registered. The pressure difference in the differential pressure gauge was calculated with the following expression (Tippens, 2011):

$$Differential\ pressure = \rho \times g \times h$$

where g is the acceleration of gravity, h is the height difference between the two levels of the "U" pipe, and ρ is the density of the glycerin contained in the tubing.

With pressure, the number of moles was calculated using the ideal gas equation (Tippens, 2011):

$$PV = nRT$$

where P is the pressure of the gas, V is the volume, n is the number of moles, R is the ideal gas constant, and T represents the temperature, with the values of T = 311.15 °K and R = 8.31 m^3 Pa mol^{-1} $°K^{-1}$.

Biogas composition measurement

Biogas is a mixture of different gases, mainly composed of methane and carbon dioxide, but it can also contain nitrogen, hydrogen sulfide, and traces of water vapor. Their total composition may depend on the type of material used as a substrate (Jameel *et al*., 2024). Biogas composition was determined using a NOVA Plus model MRU 947010US portable gas multidetector (MRU Instruments, TX, USA**).**

Culture medium for biodigester start-up and conditioning stage

Before starting the biodigestion process with the organic waste, the aim was to adapt and strengthen the microbial consortia present in the inoculum and generate an adequate anaerobic environment inside the biodigester. For this purpose, a minimal mineral medium with glucose and glycerol as carbon sources (MMMC) was formulated using the following stoichiometric balances:

$$For\ glucose: C_6H_{12}O_6 + 6\ O_2 \rightarrow 6\ CO_2 + 6\ H_2O$$

$$For\ glycerol: C_3H_8O_3 + 3.5\ O_2 \rightarrow 3\ CO_2 + 4\ H_2O$$

The concentration of the components for the MMMC formulation was determined, considering a glucose concentration of 10 g L^{-1} with 2.5 % glycerol. The percentage of glycerol was determined based on the maximum daily production of the CEDA biodiesel plant and considering that this production would work with 20 Mg of residue per day. Urea was used as a nitrogen source, considering a C/N ratio of 25:1, suitable for anaerobic digestion (Andlar *et al*., 2021), taking into account glucose and glycerol contained in the medium prepared for starting the bioreactor as a carbon source. Potassium phosphate was used as a phosphorus source, considering an N/P ratio of 6:1. Additionally, some nutrients were added at concentrations that stimulate methane production in anaerobic microorganisms (Jameel *et al*., 2024).

Taking all the above into account, the following composition of the culture medium was reached (in g L^{-1}): glucose 9.75, glycerol 0.22, urea 0.35, potassium phosphate 0.12, calcium 0.1, potassium 0.2, magnesium 0.075, iron 0.04, cobalt 0.004, molybdenum 0.0001, nickel 0.006, and one part of sodium bicarbonate was added for every 20 parts of glucose to regulate pH.

Microorganisms

Inoculum for the process was collected from swine manure from a pig farm located in the State of Mexico. Swine manure contains a wide variety of microorganisms, including bacteria, fungi, yeasts, and actinomycetes that coexist in a complex symbiosis where they perform a specific and complementary function (Ruvalcaba-Gómez *et al*., 2019). When performing the physicochemical characterization of the inoculum, the following results were obtained: moisture 85 %, ash 0.9 %, total solids 0.14 g per gram of sample, volatile solids 0.11 g per gram of sample, COD 31.4 g of O^2 per liter, total phosphorus 2.97 g L^{-1}, and total nitrogen 3.2 g L^{-1}.

Waste conditioning and characterization

Fruit and vegetable waste was collected from general containers at the CEDA. Three samples were taken in different months of the year and were physicochemically characterized; the percentages of moisture, ash, total solids, volatile solids, fats, proteins, and carbohydrates were determined for each sample. Likewise, COD, total phosphorus, total nitrogen, and total organic carbon were recorded (in g L^{-1}), as well as pH. Conditioning consisted of size reduction by liquefying waste using a professional Ninja blender (Mexico). The average solids content in each sample was 15 %, and 0.5 L of water was added to each kilogram of residue to obtain a fluid with a total solids content of 10 %.

Inoculum conditioning

For the anaerobic digestion process, swine manure was used as inoculum. Manure has a large number of microorganisms that require acclimatization (Zhang *et al*., 2022). For

this process, the biodigester was inoculated with 12 kg of pig manure (17 L in volume). Considering that solid excreta should enter the biodigester as a suspension in water with at least 3 % solids (Botero and Preston, 1987), 48 L of water and 15 L of MMMC were added, resulting in a proportion of 81 % inoculum and 19 % substrate in a total volume of 80 L.

Once the biodigester was inoculated, it was sealed, and anaerobic biodigestion began. To achieve a system as homogeneous as possible, the stirrer was activated, keeping it at a speed of 48 rpm to avoid the incorporation of air. The temperature was maintained in the mesophilic regime at 38 °C by means of the jacket-type heat exchanger, recirculating hot water. Samples of the digestate mixture were taken every 48 hours and analyzed for COD, total nitrogen, total phosphorus, total solids, and volatile solids. In addition, measurements of the biogas produced with the gas multidetector were performed.

Once COD levels decreased by 25 %, the first feeding was performed, adding 12 L of MMMC. Feedings were performed every 48 h until a greater than 80% decrease in COD was observed; at that time, the feeding load was increased to 15 L of MMMC every 48 h until the difference between soluble COD and fed COD remained constant.

Biodigestion with agro-industrial waste

Biodigestion of agro-industrial wastes started when the soluble COD remained approximately constant during the inoculum conditioning process. At that time, the substrate was changed with a 10 L load of a mixture of 50 % MMMC and 50 % of previously conditioned organic residues. This feeding was maintained until a decrease in soluble COD and an increase in methane production were observed again, at which time a new substrate change was made to only organic waste with 2.5 % glycerol.

RESULTS AND DISCUSSION

Waste conditioning and characterization

The values obtained in the characterization did not have a large variation among the three samples collected at different times of the year, so the values obtained were averaged to take into account the variation of the parameters according to the type of fruits and vegetables available in different seasons (Table 1).

Conditioning organic waste is recommended to break down the compact structures of cellulose, hemicellulose, and lignin found in fruits and vegetables. These structures form a complex network that is difficult for microorganisms to degrade directly, increasing fermentation time and decreasing the efficiency and speed of biogas production (Zhang *et al*., 2022). Cellulose, hemicellulose, and lignin must be hydrolyzed to simpler subunits by extracellular enzymes. Hydrolysis of cellulose to glucose units is carried out by enzymes called cellulases. Lignin is degraded by a complex of enzymes, including laccases, lignin peroxidase, Mn peroxidases, and tyrosinases, which act synergistically (González-Rentería *et al*., 2011).

Table 1. Characterization of agro-industrial organic wastes generated in the central supply center (Central de Abasto) of Mexico City, Mexico, used in biogas production.

Parameter	Value
Moisture (%)	85.00 ± 5.91
Ash (%)	0.54 ± 0.23
Total solids (%)	15.00 ± 2.23
Volatile solids (%)	13.00 ± 1.98
COD (g of O_2 L^{-1})	99.00 ± 8.77
Total phosphorus (g L^{-1})	2.50 ± 3.76
Total nitrogen (g L^{-1})	2.20 ± 1.15
Total organic carbon (g L^{-1})	21.00 ± 1.56
Fat (%)	0.38 ± 0.09
Proteins (%)	1.00 ± 0.11
Total carbohydrates (%)	7.60 ± 3.40
pH	4.80 ± 0.20

Organic waste can be treated in a variety of ways, including physical, chemical, biological, and combined. By using physical methods, the cell wall structure of the raw materials can be destroyed, increasing the accessibility of enzymes and anaerobic bacteria to the organic matter, which facilitates its digestion. In the case of chemical methods, the use of acids or alkalis that break cellulose, hemicellulose, and lignin structures increases enzyme accessibility; however, they can be toxic to microorganisms, affecting anaerobic digestion (Espinosa-Negrín *et al*., 2021). Biological methods use microorganisms that can degrade cellulose, hemicellulose, and lignin, but, in this case, the bioprocess can be prolonged for much longer, increasing the substrate consumption to produce the required conditions of the degrading microorganisms, affecting biogas production (Zhang *et al*., 2022).

In this work, the physical method used for the conditioning of organic waste allowed reducing the particle size and increasing the rate of the anaerobic digestion process and biogas production by increasing the contact surface and the substrate/inoculum mass transfer (Theuretzbacher *et al*., 2015).

Inoculum conditioning

Adaptation of microorganisms to a new substrate is essential for good results in biogas production (Zhang *et al*., 2022; Atelge *et al*., 2020). Once the COD level decreased by 25 % after one week of culture (Figure 2), the first feeding was performed, adding 12 L of MMMC. Immediately afterwards, a sample was taken and analyzed, obtaining the following values for the mixture in the biodigester: COD 13.4 g L^{-1}, total nitrogen 1.1 g L^{-1}, total phosphorus 0.21 g L^{-1}, total solids (TS) 7.7 g L^{-1}, and volatile solids (VS) 5.45 g L^{-1}, at a pH of 7.

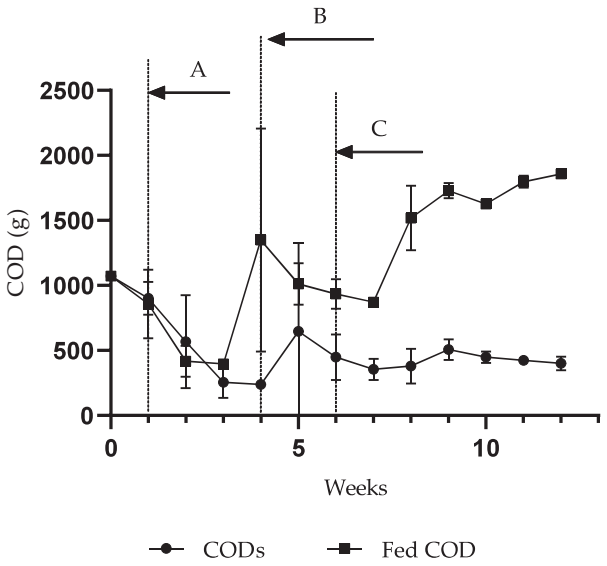

Figure 2. Chemical oxygen demand (COD) and its average consumption during anaerobic digestion. A: start of feeding with minimal mineral medium with glucose and glycerol as carbon sources (MMMC); B: change to MMMC mixture with residue; C: total substrate change to only organic residue in mixture with 2.5 % glycerol. CODs: soluble COD.

When COD decreased by about 80 %, the feed load was increased to 15 L of MMMC every 48 h until the difference between soluble COD and fed COD remained in a constant range. During that time, the composition of the biogas produced was measured (Figure 3), which initially could be increased by the addition of more organic matter

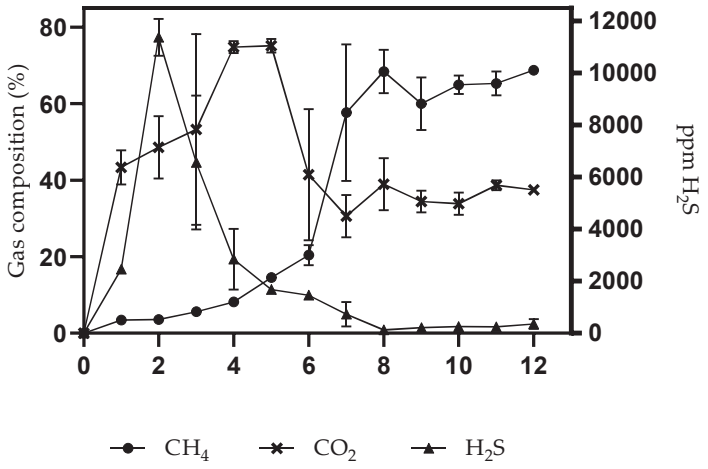

Figure 3. Average composition of biogas produced in the anaerobic digestion of agro-industrial organic waste generated in the central supply center (Central de Abasto) of Mexico City, Mexico.

(Jameel *et al*., 2024). After 30 days of processing, with 15 % of methane produced, the substrate was changed (Figure 2), initiating the anaerobic digestion stage of the agro-industrial waste.

Anaerobic digestion of agro-industrial waste

Anaerobic digestion of organic waste was initiated with a 10 L load of a mixture of 50 % MMMC and 50 % waste. After the substrate change, a volume of 217 L was reached in the biodigester. This volume was considered the final operating volume and was kept constant by draining 5 L of sludge before each 5 L waste feed with MMMC. The feeding with MMMC/waste mixture was maintained for two weeks, during which time the COD decreased by 30 % and the methane percentage increased from 10 to 25 % (Figure 3), which is why the total change of substrate to only waste in mixture with 2.5 % glycerol (R/G) was carried out (Figure 2).

A total of 5 L of the latter substrate (R/G) were added every 48 hours due to the rapid consumption of COD and the high percentage of methane produced. The feeding load was increased until a volume of 13 L of substrate (R/G) was reached every 48 hours. Methane production continued to increase until it reached a biogas composition with a methane percentage of 72 % (Figure 3). The CO_2 percentage peaked at week five and subsequently decreased to 30 %. Biogas production was maintained for more than 2 weeks with a methane percentage that ranged between 60 and 70 % and a CO_2 percentage between 40 and 30 % (Figure 3). At this point, the biogas produced was already fully flammable.

These results confirm that in order to increase the yield, speed, and efficiency of biogas production, simultaneous digestion of two or more substrates is necessary, since a better nutritional balance, adequate C/N ratio, buffering capacity, and stability in the biodigestion system are achieved (Andlar *et al*., 2021). Co-digestion of agro-industrial waste with glycerol increased biogas and methane production from 15 to 70 %, i.e., 4.6 times more than when only glycerol was fed. This increase is greater than that obtained in other glycerol co-digestion processes (Alves *et al*., 2020; Butkowska *et al*., 2022). In addition, stability was achieved in the bioprocess, maintaining biogas production with a high percentage of methane for more than 2 weeks (Figure 3).

Phosphorus, nitrogen, and solids concentrations during bioprocessing

At start-up, nitrogen and phosphorus concentrations were balanced at a 6:1 ratio. However, throughout the process, both residual concentrations had variations, equalizing at some times and at others increasing the phosphorus concentration. These variations did not affect methane production, since neither nutrient accumulated in excess nor was limited during the bioprocess.

During biodigestion, ammonia may be produced as a result of the anaerobic degradation of proteins or amino acids present in the feedstock. Although ammonia nitrogen is an important nutrient for bacterial growth, if found in excess, it can limit bacterial growth (Jameel *et al*., 2024). In this case, the total nitrogen concentration

remained in the range of 0.3 to 1.5 g L^{-1}, which was still lower than those reported as toxic. Concentrations higher than 3 g L^{-1} may be inhibitory (Jameel *et al*., 2024).
Phosphorus concentration also did not show large variations (between 0.21 and 1.7 g L^{-1}), which reflects that the microorganisms had an adequate proportion of these nutrients during the bioprocess. As for the concentration of total solids, it was maintained in a range of 8 to 12 g L^{-1}; this concentration was sufficient for the microorganisms to utilize the organic material and transform it to biogas (Jameel *et al*., 2024). Volatile solids represented more than 50 % of total solids.

Temperature and pH

A temperature of 38 °C was maintained from the beginning of the process. Temperature affects the reaction rate, and although anaerobic digestion can be performed at thermophilic temperatures (50 to 60 °C), many biodigesters are operated at mesophilic conditions (30 to 40 °C) because of the ease in system control and lower energy demand (Atelge *et al*., 2020). During the first three weeks, the pH was decreasing, indicating acidification of the medium to a value close to six due to the accumulation of volatile fatty acids. At this point it was necessary to add 5 L of a 5% sodium bicarbonate solution to avoid further acidification that could inhibit the activity of methanogenic bacteria (Jameel *et al*., 2024). After 4 weeks, when a new decrease in pH was observed, sodium bicarbonate was added again. Once the methane composition increased, a parallel increase in pH was observed, remaining between 7.1 and 7.5 during methane production. The high methane production implies a high consumption of organic acids produced, which explains the increase and stabilization of pH.

Volumetric rate of consumption and COD removal efficiency

During the first weeks of the process, the volumetric rate of COD consumption (VVC) increased. This can be explained by the fact that the first substrate is easily assimilated. Over the next 4 weeks, the VVC decreased and then increased as the feeding of the MMMC/residue mixture was initiated. At week 12, VVC took an average value of approximately 2.84 ± 0.2 g L^{-1} d^{-1}.
The COD removal efficiency (η) showed a similar behavior, reaching 60 % in the first weeks of the process. Subsequently, it decreased in the same week as VVC did, and at the same time, it increased to an average value of 77.6 ± 0.3 %.

Hydraulic retention time and biogas production

The hydraulic retention time (HRT) was 28 days at week four. When the substrate was changed to only glycerol residue with a constant volume of 217 L, the feed was reduced to 5 L due to the high concentration of COD in the residue. At week 6, the HRT was 87 days; to reduce it, the feeding volume was doubled, and at 8 weeks, an HRT of 43 days was reached. Feeding was again increased to 13 L, and finally an HRT of 33 days was reached. The average HRT for anaerobic digestion processes was between 20 and 30 days (Atelge *et al*., 2020), so the HRT obtained in this study is in line with the average.

On the other hand, biogas production was increasing, obtaining in the last week a volume of 0.576 ± 0.084 m^3 d^{-1} (Table 2). This value, which corresponds to 0.681 ± 0.098 m^3 of CH_4 kg^{-1} VS, is higher than that reported for fruit residues as substrate (Andlar *et al*., 2021), demonstrating that co-digestion of organic residues with glycerol increases the production and quality of biogas obtained during biodigestion.

Table 2. Biogas production at different bioprocessing stages.

Time (weeks)	Volume (m^3 d^{-1})	Pressure (Pa)	Feeding (L d^{-1})	Feeding (kg of waste d^{-1})	HRT (days)
4	0.048 ± 0.023	469.22 ± 2.51	7.5 ± 0.3	-	28.9 ± 0.5
6	0.144 ± 0.035	617.40 ± 1.92	2.5 ± 0.4	1.6 ± 0.1	86.8 ± 0.2
8	0.360 ± 0.103	1173.06 ± 3.28	5.0 ± 0.5	3.0 ± 0.3	43.4 ± 0.3
11	0.576 ± 0.084	1111.32 ± 2.84	6.5 ± 0.2	4.5 ± 0.2	33.3 ± 0.4

HRT: Hydraulic retention time.

Alves *et al*. (2020) demonstrated that the process of co-digestion of sludge from a wastewater treatment plant and glycerol for biogas production increases methane production by 5.7 % compared to digestion of only sewage treatment plant sludge, achieving 368.8 L of CH_4 kg^{-1} VS. Butkowska *et al*. (2022) were able to increase methane production 3.1 times by adding glycerol as a cosubstrate to the manure digestion process. The results obtained in this work confirm that biogas production using agro-industrial wastes improves methane production more than four times when glycerol is added as a cosubstrate, obtaining up to 681 ± 0.098 L of CH_4 kg^{-1} VS.

The co-digestion process stabilized in this research represents a good alternative for the disposal of organic waste generated at the CEDA, providing a solution to the social problem, with the option of regularizing scavengers and recyclers and, above all, mitigating the problem of environmental pollution caused by the disposal of waste in open-air deposits, producing large volumes of methane and carbon dioxide in the atmosphere.

CONCLUSIONS

An anaerobic digestion process was implemented at the pilot plant level, using organic waste generated at the central supply center of Mexico City as a substrate for biogas production. At the same time, value was given to the glycerol obtained as a by-product in the biodiesel plant of the same center, using it as a co-substrate to reduce the hydraulic retention time, increase the production volume, and improve the quality of the biogas. The organic matter removal efficiency obtained was 77.6 ± 0.3 %, achieving a biogas production of 0.576 ± 0.084 m_3 d^{-1}, with a methane

composition of between 60 and 70 %, corresponding to 681 ± 0.098 L of CH_4 kg^{-1} of volatile solids, with the prospect of its use in the generation of high-efficiency heating and electrical energy.

ACKNOWLEDGMENTS

This work was funded by SIP-IPN project support; COFAA-IPN grants for Deifilia Ahuatzi-Chacón, Angélica María Salmerón-Alcocer, EDI-IPN grant for Deifilia Ahuatzi-Chacón, EDD-IPN grant for Angélica María Salmerón-Alcocer, and SECIHTI grant for Sergio Muñoz-Martínez.

REFERENCES

Alves IRFS, Mahler CF, Oliveira LB, Reis M, Bassin JP. 2020. Assessing the use of crude glycerol from biodiesel production as an alternative to boost methane generation by anaerobic co-digestion of sewage sludge. Biomass and Bioenergy 143: 105831. https://doi.org/10.1016/j.biombioe.2020.105831

Andlar M, Belskaya H, Morzak G, Ivančić SM, Rezić T, Petravić TV, Šantek B. 2021. Biogas production systems and upgrading technologies: A review. Food Technology and Biotechnology 59 (4): 387–412. https://doi.org/10.17113/ftb.59.04.21.7300

Atelge MR, Krisa D, Kumar G, Eskicioglu C, Nguyen DD, Chang SW, Atabani AE, Al-Muhtaseb AH, Unalan S. 2020. Biogas production from organic waste: Recent progress and perspectives. Waste and Biomass Valorization 11 (3): 1019–1040. https://doi.org/10.1007/s12649-018-00546-0

Botero BR, Preston TR. 1987. Biodigestores de bajo costo para la producción de combustible y fertilizante a partir de la excreta. Manual para su instalación, operación y utilización. San José, Costa Rica. 20 p.

Butkowska K, Mikucka W, Pokój T. 2022. Enhancement of biogas production from cattle manure using glycerine phase as a co-substrate in anaerobic digestion. Fuel 317: 123456. https://doi.org/10.1016/j.fuel.2022.123456

Chilakamarry CR, Sakinah AMM, Zularisam AW, Pandey A. 2021. Glycerol waste to value added products and its potential applications. Systems Microbiology and Biomanufacturing 1 (4): 378–396. https://doi.org/10.1007/s43393-021-00036-w

de Mello BS, Pozzi A, Rodrigues BCG, Costa MAM, Sarti A. 2024. Anaerobic digestion of crude glycerol from biodiesel production for biogas generation: Process optimization and pilot scale operation. Environmental Research 244: 117938. https://doi.org/10.1016/j.envres.2023.117938

DOF (Diario Oficial de la Federación). 1978a. NORMA Mexicana NMX-F-066-S-1978. Determinación de cenizas en alimentos. Gobierno de México. Secretaría de Economía. Ciudad de México, México.

DOF (Diario Oficial de la Federación). 1978b. NORMA Mexicana NMX-F-312-1978. Determinación de reductores directos y totales en alimentos. Gobierno de México. Secretaría de Economía. Ciudad de México, México.

DOF (Diario Oficial de la Federación). 1978c. NORMA Mexicana NMX-F-317-S-1978. Determinación de pH en alimentos. Ciudad de México. Gobierno de México. Secretaría de Economía. Ciudad de México, México.

DOF (Diario Oficial de la Federación). 1980. NORMA Mexicana NMX-F-68-S-1980. Determinación de proteínas en alimentos. Gobierno de México. Secretaría de Economía. Ciudad de México, México.

DOF (Diario Oficial de la Federación). 1986. NORMA Mexicana NMX-F-083-1986. Determinación de humedad en productos alimenticios. Gobierno de México. Secretaría de Economía. Ciudad de México, México.

DOF (Diario Oficial de la Federación). 2015. NORMA Mexicana NMX-AA-034-SCFI-2015. Medición de sólidos y sales disueltas en aguas naturales, residuales y residuales tratadas. Gobierno de México. Secretaría de Economía. Ciudad de México, México.

Espinosa-Negrín AM, López-González LM, Casdelo-Gutiérrez NL. 2021. Pretratamiento de biomasas lignocelulósicas: breve revisión de los principales métodos utilizados. Revista Centro Azúcar 48 (3): 108–119.

González R, Peña DC, Gómez X. 2022. Anaerobic co-digestion of wastes: Reviewing current status and approaches for enhancing biogas production. Applied Science 12 (17): 8884. https://doi.org/10.3390/app12178884

González-Rentería SM, Soto-Cruz NO, Rutiaga-Quiñones OM, Medrano-Roldán H, Rutiaga-Quiñones JG, López-Miranda J. 2011. Optimización del proceso de hidrólisis enzimática de una mezcla de pajas de frijol cuatro variedades (Pinto villa, Pinto saltillo, Pinto mestizo y Flor de mayo). Revista Mexicana de Ingeniería Química 10 (1): 17–28.

Hach. 2024. Water analysis handbook. Loveland, CO, USA. https://www.hach.com/resources/water-analysis-handbook (Retrieved: March 2024).

Herrera-Uchalin MG, Valiente-Saldaña YM, Garibay-Castillo JV, Herrera-Cherres S. 2023. Manejo de residuos sólidos en la gestión municipal: revisión sistémica. Revista Arbitrada Interdisciplinaria Koinonía 8 (16): 150–170. https://doi.org/10.35381/r.k.v8i16.2540

Jameel MK, Mustafa MA, Ahmed HS, Mohammed AJ, Ghazy H, Shakir MN, Lawas AM, Mohammed SK, Idan AH, Mahmoud ZH, Sayadi H, Kianfar E. 2024. Biogas: Production, properties, applications, economic and challenges: A review. Results in Chemistry 7: 101549. https://doi.org/10.1016/j.rechem.2024.101549

López C, Martínez F, Paredes O. 2016. Automatización de un proceso de biodigestión anaeróbica. Revista Cubana de Ciencias Informáticas 10 (1): 1–16.

Martínez-Prats G, Chacón-Lozano LE, Silva-Hernández F. 2022. Análisis del sector agroindustrial de México 2020-2021. Revista de Investigaciones Universidad del Quindío 34 (S5): 133–138. https://doi.org/10.33975/riuq.vol34nS5.1089

Matiacevich S, Soto MD, Gutiérrez CM. 2023. Economía circular: obtención y encapsulación de compuestos polifenólicos provenientes de residuos agroindustriales. RIVAR 10 (28): 77–100. https://doi.org/10.35588/rivar.v10i28.5343

Mejías-Brizuela N, Orozco-Guillen E, Galáan-Hernández N. 2016. Aprovechamiento de los residuos agroindustriales y su contribución al desarrollo sostenible de México. Revista de Ciencias Ambientales y Recursos Naturales 2 (6): 27–41.

Olugbemide AD, Lajide L, Likozar B, Ighodaro A, Omunagbe OC, Ifijen IH. 2023. Biogas production through anaerobic co-digestion of rice husk and plantain peels: Investigation of substrate mixing ratios, digestate quality, and kinetic analysis. Brazilian Journal of Chemical Engineering 42 (1): 83–94. https://doi.org/10.1007/s43153-023-00415-x

Pérez-Contreras S, Hernández-Martínez R, Hernández-Rosas F, Herrera-Corredor JA, Varela-Santos EC. 2023. Enzymatic saccharification of pretreated sugarcane bagasse by hydrogen

peroxide for bioethanol production**.** Tropical and Subtropical Agroecosystems 26 (2). http://doi.org/10.56369/tsaes.4831

Prasertsan P, Leamdum C, Chantong S, Mamimin C, Kongjan P, O-Thong S. 2021. Enhanced biogas production by co-digestion of crude glycerol and ethanol with palm oil mill effluent and microbial community analysis. Biomass and Bioenergy 148: 106037. https://doi.org/10.1016/j.biombioe.2021.106037

Ruvalcaba-Gómez JM, Arteaga-Garibay RI, Domínguez-Araujo G, Galindo-Barboza AJ, Salazar-Gutiérrez G, Martínez-Peña MD, Delgado-Macuil RJ. 2019. Uso de bacterias ácido lácticas para descontaminación de estiércol porcino mediante ensilaje experimental. Revista Internacional de Contaminación Ambiental 35 (1): 247–257. https://doi.org/10.20937/rica.2019.35.01.18

Sarandón SJ. 2020. Biodiversidad, agroecología y agricultura sustentble. Editorial de la Universidad Nacional de la Plata: Buenos Aires, Argentina. 429 p.

SEMARNAT (Secretaría de Medio Ambiente y Recursos Naturales). 2020. Diagnóstico básico para la gestión integral de los residuos. Ciudad de México, México. 272 p.

Singh R, Das R, Sangwan S, Rohatgi B, Khanam R, Ghouse Peera SK, Das S, Lyngdoh YA, Langyan S, Shukla A, *et al.* 2021. Utilisation of agro-industrial waste for sustainable green production: A review. Environmental Sustainability 4 (4): 619–636. https://doi.org/10.1007/s42398-021-00200-x

Statista Research Department. 2023. El sector agrícola en México. Datos estadísticos. https://es.statista.com/temas/7029/el-sector-agricola-en-mexico/#topicOverview (Retrieved: March 2023).

Theuretzbacher F, Lizasoain J, Lefever C, Saylor MK, Enguidanos R, Weran N, Gronauer A, Bauer A. 2015. Steam explosion pretreatment of wheat straw to improve methane yields: Investigation of the degradation kinetics of structural compounds during anaerobic digestion. Bioresource Technology 179: 299–305. https://doi.org/10.1016/j.biortech.2014.12.008

Tippens PE. 2011. Física, conceptos y aplicaciones (Séptima edición). McGraw Hill: Lima, Perú. 828 p.

Zhang Y, Lin J, Song T, Su H. 2022. Anaerobic digestion of waste for biogas production. *In* Abomohra AEF, Wang Q, Huang J. (eds.), Waste-to-Energy. Springer: Cham, Switzerland. https://doi.org/10.1007/978-3-030-91570-4_6

Agrociencia

EFFECT OF DIFFERENT SOLVENTS AND DRYING CONDITIONS ON THE EXTRACTION OF PHYTOCHEMICAL BIOACTIVES FROM ORANGE PEEL

Almadalia **Velasco-Hernández**[1], Ángela **Suárez-Jacobo**[2], Efraín **Obregón-Solís**[1], Nohemí del Carmen **Reyes-Vázquez**[1], Jorge Alberto **García-Fajardo**[1]*

[1]Centro de Investigación y Asistencia en Tecnología y Diseño del Estado de Jalisco, Subsede Noreste. Vía de la Innovación 404, Parque de Investigación e Innovación Tecnológica. Autopista Monterrey-Aeropuerto km 10, Apodaca, Nuevo León, Mexico. C. P. 66628.
[2]Centro de Investigación y Asistencia en Tecnología y Diseño del Estado de Jalisco. Tecnología Alimentaria. Camino Arenero 1227, El Bajío, Zapopan, Jalisco, Mexico. C. P. 45019.
* Author for correspondence: jgarcia@ciatej.mx

Citation: Velasco-Hernández A, Suárez-Jacobo A, Obregón-Solís E, Reyes-Vázquez NC, García-Fajardo JA. 2025. Effect of different solvents and drying conditions on the extraction of phytochemical bioactives from orange peel. **Agrociencia** 59(4): 515-527. https://doi.org/ 10.47163/agrociencia.v59i4.3346

Editor in Chief:
Dr. Fernando C. Gómez Merino

Received: November 17, 2024.
Approved: April 23, 2025.
Published in Agrociencia: May 09, 2025.

ABSTRACT

Oranges (*Citrus sinensis* L.) are one of the most cultivated citrus fruits worldwide. Citrus peel is the main residue left after processing. The disposal of this agro-waste represents a problem for citrus industries, where the implementation of strategies for its valorization is essential. This study compared the effects of two different drying methods for leftover orange peel (*C. sinensis* var. Valencia) on extract yield, its chemical composition, and antioxidant capacity using two extraction solvents. The experimental design was completely randomized in a 3 × 2 factorial arrangement, including three types of peel: dehydrated peel at 60 °C pilot level (C60), dehydrated peel at 204 °C industrial level (CI), and fresh peel (CF), and two extraction solvents: 70 % ethanol and methanol. The extraction yield was higher ($p < 0.05$) using CF with 70 % ethanol. The content of total phenols (TPC), total flavonoids (TFC), and antioxidant capacity in orange peel was higher ($p < 0.05$) using CF with 70 % ethanol or methanol. The concentration of hesperidin was similar in all types of peel using methanol, and CF presented a higher amount of naringin than peels dehydrated using 70 % ethanol or methanol. The use of CF with 70 % ethanol or methanol as extraction solvents allowed a higher extraction yield (46 and 38 %), higher concentrations of TPC (12.31 and 14.03 mg GAE g^{-1} DW), TFC (9.5 and 8.74 mg QE g^{-1} DW), antioxidant capacity (273.9 and 272.69 μM TE g^{-1} DW), and naringin (13.6 mg g^{-1} DW) compared to dried orange peels.

Keywords: *Citrus sinensis* var. Valencia, flavonoids, antioxidant capacity, hesperidin, naringin.

INTRODUCTION

Orange (*Citrus sinensis* L.) is one of the most cultivated fruit species worldwide. Mexico ranked fourth in global orange production, after Brazil, India, and China, with an annual total of 4800 Gg (FAO, 2022). According to García-Salazar *et al*. (2021), of the total orange production in Mexico, 56 % is consumed fresh, 34 % is used for

industrial juice extraction, and 10 % is lost post-harvest. In the course of citrus fruit juice preparation, 30–34 % of peel is obtained as the main residue (Rafiq *et al*., 2018). Harnessing citrus peels for the revalorization of bioactive compounds can potentially improve the economic viability of citrus cultivation in a circular economy framework that promotes sustainable agriculture (Wang *et al*., 2022).

There is scientific evidence that citrus peel contains bioactive substances such as flavonoids (Afifi *et al*., 2023), pectins (Hosseini *et al*., 2016), carotenoids (Suri *et al*., 2021), essential oils (Boukroufa *et al*., 2015), and sugars (Choi *et al*., 2013) that are potential ingredients for food (antimicrobials, additives, prebiotics), pharmaceuticals (anti-inflammatory, anticancer), and cosmetics industries (Panwar *et al*., 2021; Suri *et al*., 2022). The main citrus flavonoids are flavones, flavanones, and their polymethoxy derivatives, distinguishing between glycosides and aglycones (Ammar *et al*., 2022). In them, naringenin and hesperitin occur under the aglycone forms, and naringin, neohesperidin, hesperidin, narirutin, and didimin are found under the glycoside forms (Kumar *et al*., 2022). Hesperidin has been shown to possess antioxidant, anti-inflammatory, hypoglycemic, anticancer, and antiviral capabilities (Zheng *et al*., 2021). Due to the polarity of flavonoids, organic solvents such as methanol are efficient for their extraction. Non-toxic and biodegradable alternatives such as ethanol are used in extraction methods to reduce the impact of organic solvents on the environment while providing similar performance (Fu *et al*., 2020). Flavonoid-enriched compounds obtained by solvent extraction frequently contain other soluble components, and are thus called crude extracts. The crude extract is suitable for flavonoid detection, but additional separation and purification are required to obtain citrus flavonoid monomers (Zhu *et al*., 2023).

In this study, the effects of two drying methods for *C. sinensis* var. Valencia peel were evaluated: a) dehydrated peel at 60 °C pilot level (C60), b) dehydrated peel at 204 °C industrial level (CI), and c) fresh peel (CF) on the extraction yield, chemical composition, and antioxidant capacity of the peel, using two extraction solvents, 70 % ethanol and methanol. The chemical composition analysis included the content of total phenols, total flavonoids, and two individual flavonoids, hesperidin and naringin. Two antioxidant assays, the free radical 2,2′-azino-bis(3-ethylbenzothiazoline-6-sulfonic acid)-diammonium salt (ABTS) and the free radical 2,2-diphenyl-1-picrylhydrazyl (DPPH), were used for antioxidant capacity tests.

MATERIALS AND METHODS

Reagents

Methanol and ethanol were purchased from Meyer Chemicals. Quercetin, hesperidin, and naringin grade high-performance liquid chromatography (HPLC, ≥ 95 %), 2,2-diphenyl-1-picryhydrazyl (DPPH, ≥ 97 %), 2,2′-azino-bis(3-ethylbenzothiazoline-6-sulfonic acid)-diammonium salt (ABTS, ≥ 98 %), 6-hydroxy-

2,5,7,8-tetramethylchromane-2-carboxylic acid (Trolox), potassium persulfate (≥ 99 %), aluminum chloride (99 %), gallic acid, and Folin-Ciocalteu's reagent (2 M) were purchased from Sigma-Aldrich.

Raw Material

Valencia orange peel was provided by an agroindustry located in Veracruz, Mexico. The peel was obtained after the juice and oil extraction process and consisted of the flavedo (exocarp), albedo, and endocarp membranes. To dehydrate the peel at 60 °C, a convection oven with six racks and 66.04 × 45.72 cm trays was used until the weight of the peel was constant. The industrially dehydrated peel was provided by an agroindustry and contained 6.16 ± 0.02 % moisture; this peel was dehydrated in a rotary industrial oven at an initial temperature of 204 °C. The dehydrated shells were then ground (Micron pulverizer mill, model K20A, Mexico) and sieved to obtain a flour (particle size < 250 μm).

The moisture percentage in fresh peel was calculated using NMX-F-083-1986 (DOF, 1986). The total ash content was determined according to the NMX-F-607-NORMEX-2020 guidelines (DOF, 2020). The fat content of the ethereal extract was determined using NOM-086-SSA1-1994 (normative appendix C, numeral 1) (DOF, 1994). The crude protein content (N × 6.25) was calculated using NMX-F-608-NORMEX-2011, and crude fiber with NMX-F-613-NORMEX-2017 (DOF, 2017). Total carbohydrates were calculated using the proximate analysis difference, while dietary fiber, soluble dietary fiber, and insoluble dietary fiber were determined using the NMX-F-622-NORMEX-2008 (DOF, 2008) method.

Experimental design

The experiment was completely randomized in a factorial arrangement (3 × 2), resulting in three types of peel: dehydrated peel at 60 °C pilot level (C60), dehydrated peel at 204 °C industrial level (CI), and fresh peel (CF), and two extraction solvents: 70 % ethanol and methanol. Each treatment was done in triplicate.

Polyphenol extraction

Polyphenol extraction was performed according to the methodology described by Perlatti *et al*. (2016) for both solvents. Samples (1 g) of dried peel (C60 and CI) and fresh peel were placed in 50 mL Falcon tubes (Corning, NY, USA) containing 20 mL of solvent. The samples were placed in an ultrasonic bath (Branson model 2800, Danbury, CT, USA) at 40 kHz for 30 min, pausing every 5 min for 3 min to avoid heating the samples. The temperature of the water bath was 30 ± 2 °C. The tubes were then centrifuged (Heraeus Megafuge model 16R, Germany) for 30 min at 4 °C and 20 800 ×g. The supernatant was recovered and the precipitate was re-extracted with 10 mL of solvent and ultra-sonication for 15 min. Both supernatants were combined for each sample and the solvent was removed in a rotary evaporator (Buchi model R-215, Flawil, Switzerland) at 40 °C. Finally, the extract was resuspended in 5 ml of HPLC-

grade methanol and stored at -20 °C until analysis. Experiments were performed in triplicate for each sample. The extraction yield was expressed as grams of extract per 100 grams of orange peel on a dry basis (g 100 g^{-1} DW).

Total phenol determination

The total phenol content (TPC) was determined according to the methodology described by Waterhouse (2002) with some modifications. The extracts were diluted (1:10), and 500 µL of diluted extract were mixed with 3 mL of deionized water, adding 250 µL of Folin-Ciocalteu 1 N reagent (1:1 (v/v). After 5 min, 750 µL of a 20 % (w/v) sodium carbonate solution and 950 µL of deionized water were added. The mixture was vortexed and kept in the dark for 30 min at room temperature. Then, the absorbance was measured at 765 nm using a spectrophotometer (Shimadzu UV-1800 Kyoto, Japan). Gallic acid with concentrations from 10 to 80 µg mL^{-1} was used as a standard for calibration ($y = 0.01024\ x + 0.0100942$; $R^2 = 0.9986$). Results were expressed as milligrams of gallic acid equivalents per gram of orange peel on a dry basis (mg GAE g^{-1} DW).

Total flavonoid determination

Total flavonoid content (TFC) was determined using the colorimetric method with aluminum chloride (Chang *et al*., 2002). Quercetin was used to calculate the calibration curve ($y = 0.00766959\ x - 0.0137669$; $R^2 = 0.99799$). Ten milligrams of quercetin were dissolved in 10 mL of 80 % methanol and diluted to 5, 10, 25, 50, 70, and 100 µg mL^{-1}. The diluted standard solutions (0.5 mL) were mixed separately with 1.5 mL of 80 % methanol, 0.1 mL of 10 % aluminum chloride, 0.1 mL of 1 M potassium acetate, and 2.8 mL of deionized water. After incubation at room temperature for 30 min, the absorbance of the reaction mixture was measured at 415 nm with a spectrophotometer (Shimadzu UV-1800, Kyoto, Japan). Similarly, for the diluted orange peel extracts, 0.5 mL were reacted with aluminum chloride to determine flavonoid content as described above. The results were expressed as milligrams of quercetin equivalents per gram of orange peel on a dry basis (mg QE g^{-1} DW).

HPLC analysis

High-performance liquid chromatography (HPLC) was used to determine the hesperidin and naringin content of orange peel extracts. The concentration of the extracts was 10 mg mL^{-1}. Each sample was filtered through a 0.45 µm syringe filter. The flavonoids in the extract were analyzed using an HPLC system and a diode array detector (PDA) at a 280 nm detection wavelength. The injection volume was 1 µL with a flow rate of 1 mL min^{-1}. Identification of hesperidin and naringin in the extract was achieved by comparing the retention time and UV absorption pattern with those of the standard compound. The calibration equation was used to quantify the amount of each flavonoid, the result being expressed as milligrams of flavonoid per gram of orange peel on a dry basis (mg g^{-1} DW). Each measurement was conducted in triplicate.

Determination of antioxidant capacity by means of spectrophotometric assays

DPPH method

Determination of DPPH antioxidant capacity was carried out according to Brand-Williams *et al*. (1995). Diluted extract samples (100 µL) were mixed with 3.9 mL of a 6 × 10^{-5} mol L^{-1} DPPH solution in HPLC-grade methanol. The reaction mixture was incubated in the dark for 60 min, and the absorbance was determined at 515 nm using a spectrophotometer (Shimadzu UV-1800, Kyoto, Japan). Trolox standard concentrations from 160 to 1200 µM were used for calibration (y = - 2.17922 x + 0.695740; R^2 = 0.9988). Results were expressed as equivalent micromoles of Trolox per gram of orange peel on a dry basis (µM TE g^{-1} DW). Each sample was analyzed in triplicate.

ABTS method

The ability of orange peel extracts to inhibit the ABTS radical was determined as described by Re *et al*. (1999). A stock solution was prepared with a 7 mM ABTS-+ solution containing 140 mM potassium persulfate; this solution was kept in the dark at room temperature for 12 to 16 h. The ABTS-+ working solution was prepared by diluting the ABTS-+ stock solution with 0.15 M phosphate buffer saline (PBS), pH = 7.4, so that the absorbance of the total mixture was 0.70 ± 0.02 at 734 nm. A 2970 µL of ABTS-+ working solution was added to 30 µL of the diluted shell extracts, and the mixture was shaken, allowed to stand in the dark for 30 min and the absorbance at 734 nm was read using a spectrophotometer (Shimadzu UV-1800, Kyoto, Japan).

A calibration curve (y = - 0.0002106 x + 0.674245; R^2 = 0.9951) was prepared using Trolox standard (125 to 3000 µM). Each sample was analyzed in triplicate. Results were expressed as equivalent micromoles of Trolox per gram of orange peel on a dry basis (µM TE g^{-1} DW).

Statistical analysis

All treatments were performed in triplicate, and the data obtained were expressed as the mean value ± standard deviation. The data obtained were subjected to analysis of variance and comparison of treatments using Tukey's test ($p < 0.05$) with SAS 9.00 statistical software (NC, USA).

RESULTS AND DISCUSSION

Proximal analysis

Residual orange peel had a high content of total carbohydrates and soluble and insoluble dietary fiber (Table 1), which was similar to the amounts reported by other authors (de Moraes *et al*., 2013; Batool *et al*., 2020). The dietary fiber of citrus fruits is of higher quality than that of alternative sources such as cereals because citrus has a higher proportion of soluble dietary fiber (de Moraes *et al*., 2013).

Table 1. Proximal analysis and fiber content in residual peel of Valencia orange (*Citrus sinensis* L.)

Determination	Percentage (%)
Moisture	74.25
Ash	0.62
Fats (ethereal extract)	0.56
Crude protein	1.37
Crude fiber	2.86
Total carbohydrates	23.20
Dietary fiber	18.00
Soluble dietary fiber	8.72
Insoluble dietary fiber	10.28

Extraction yield

The extraction yield was high ($p < 0.05$) using CF with 70 % ethanol or methanol. The lowest yield was obtained when CI was used, and an intermediate yield was obtained with C60, approximately 30 % (Figure 1). In this regard, Chakroun *et al.* (2023) reported that Thomson Navel orange peel, which had been dehydrated at 50 °C for 9 h and macerated with methanol for 72 h, obtained a 35 % extract yield, similar to the peel dehydrated at 60 °C. On the other hand, Lai *et al.* (2024) obtained an extraction yield of 33.36 ± 5.19 % using ground Newhall orange peel dehydrated at 50 °C for 12 h and subjected to ultrasound extraction for 30 min with a frequency of 45 kHz and a temperature of 35 °C.

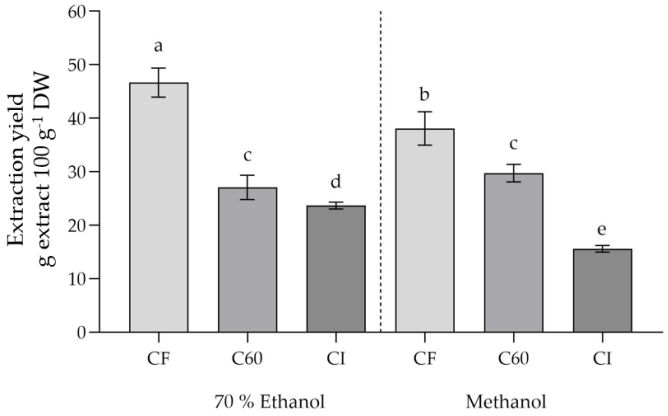

Figure 1. Extraction yield (grams of extract per 100 grams of orange (*Citrus sinensis* L.) peel on a dry basis, g 100 g^{-1} DW) using 70 % ethanol or methanol with ultrasonication. CF: fresh peel; C60: dehydrated peel at 60 °C, pilot level; CI: dehydrated peel at 204 °C, industrial level. Data are mean values ± standard deviation. Different letters indicate significant differences between orange peel samples (Tukey, $p < 0.05$).

Total phenol and flavonoid content

TPC was higher ($p < 0.05$) using fresh peel and 70 % ethanol or fresh peel and methanol compared to dry peels C60 and CI (Table 2). Covarrubias-Cárdenas *et al*. (2018) reported that dried sour orange peels presented the lowest phenolic content (22.7 ± 0.94 mg GAE g^{-1} DW), while the highest total phenol content was observed in fresh peels (40.9 ± 3.44 mg GAE g^{-1} DW); both peel samples were subjected to ultrasound-assisted extraction (20 kHz, 130 W) for 12.5 min at 80 % radiation, indicating that drying the peel could influence yield as cell membranes and organelles adhere, preventing the extraction of phenols. On the other hand, Barrales *et al*. (2018) measured the phenol content in orange peels that were dehydrated in an air circulation oven at 50 °C for 24 h, ground in a blade mill, and subjected to ultrasound-assisted extraction with 50 % (v/v) ethanol in an ultrasonic bath at 30 °C for 15 min. The value of total phenol content obtained by these authors was 5.5 ± 0.1 mg GAE g^{-1} DW, which is similar to that obtained in this study when dehydrated peels (C60 and CI) were used.

Table 2. Total phenols and flavonoids content in residual orange (*Citrus sinensis* L.) peel.

Solvent	Peel	TPC (mg GAE g^{-1} DW)*	TFC (mg QE g^{-1} DW)**
Ethanol (70 %)	CF	12.31 ± 1.39 a	9.50 ± 1.47 a
	C60	5.96 ± 0.27 b	3.07 ± 0.60 b
	CI	4.94 ± 0.32 b	2.67 ± 0.35 b
Methanol	CF	14.03 ± 0.76 a	8.74 ± 1.08 a
	C60	5.98 ± 0.87 b	2.61 ± 0.25 b
	CI	4.55 ± 0.17 b	2.01 ± 0.20 b

The data are mean values ± standard deviation. Different letters in the same column indicate significant difference between orange peels (Tukey, $p < 0.05$). TPC: Total phenol content; TFC: total flavonoid content; CF: fresh peel; C60: dehydrated peel at 60 °C, pilot level; CI: dehydrated peel at 204 °C, industrial level. *Milligrams of gallic acid equivalents per gram of orange peel on a dry basis; **milligrams of quercetin equivalents per gram of orange peel on a dry basis.

On the other hand, fresh orange peel presented higher TFC ($p < 0.05$) using 70 % ethanol or methanol, with 9.50 ± 1.47 and 8.74 ± 1.08 mg QE g^{-1} DW, respectively. Meanwhile, de Miera *et al*. (2023) mentioned that the content of total phenols and flavonoids was higher when using 80 % ethanol and orange peel dehydrated at 40 °C for 24 h, compared to water and ethyl acetate as solvents by means of an ultrasound-assisted extraction at 60 °C for 30 min.

Individual flavonoid content

Hesperidin and naringin content in orange peels was quantified by HPLC. There was no difference ($p \geq 0.05$) in the hesperidin content in fresh and dehydrated peels when methanol was used as an extraction solvent (Table 3). This coincides with the study by Lai *et al*. (2024), who obtained a higher amount of hesperidin in navel orange peel extracts obtained by ultrasound extraction with methanol (129.77 ± 19.65 mg g^{-1}) than in extracts obtained with 70 % ethanol (48.89 ± 7.36 mg g^{-1}). In addition, the solubility of hesperidin is limited in water (< 20 mg L^{-1}) (Londoño *et al*., 2007), which could have affected during extraction with 70 % ethanol. In turn, naringin was found in greater amounts in fresh peels than in dehydrated peels, regardless of the solvent used during extraction (Table 3). Unlike hesperidin, naringin is water soluble but is generally found in lower amounts than hesperidin in orange peel (Zuin *et al*., 2021; Baglioni *et al*., 2024).

Table 3. High-performance liquid chromatography (HPLC) quantification analysis of hesperidin and naringin in residual orange (*Citrus sinensis* L.) peel.

Solvent	Peel	Hesperidin (mg g^{-1} DW)*	Naringin (mg g^{-1} DW)*
Ethanol (70 %)	CF	14.75 ± 5.66 bc	13.37 ± 0.56 a
	C60	4.97 ± 0.43 c	7.67 ± 0.36 c
	CI	7.07 ± 1.81 c	7.09 ± 0.34 c
Methanol	CF	44.80 ± 9.26 a	13.62 ± 0.25 a
	C60	33.03 ± 14.13 ab	9.77 ± 0.82 b
	CI	34.53 ± 3.12 ab	5.77 ± 0.20 d

Data are mean values ± standard deviation. Different letters in the same column indicate significant differences between orange peel samples (Tukey, $p < 0.05$). CF: fresh peel; C60: dehydrated peel at 60 °C, pilot level; CI: dehydrated peel at 204 °C, industrial level. *Milligrams of flavonoid per gram of orange peel on a dry basis.

Antioxidant capacity

Antioxidant capacity was evaluated by DPPH and ABTS assays as mean values of three replicates. ABTS values were higher ($p < 0.05$) in extracts using fresh peel and 70 % ethanol or methanol compared to dehydrated C60 and CI peels (Table 4). In this regard, Mehmood *et al*. (2017) reported 9.16 ± 0.29 μmol TE g^{-1} of sample using methanolic extracts (50 % v/v) of orange waste (peel and bagasse) that were dehydrated at 60 °C for 6–8 hours. Furthermore, when the same authors used ethanolic extracts (50 % v/v), they quantified ABTS values of 8.94 ± 0.29 μmol TE g^{-1} of sample, suggesting that when using ethanol (50 % v/v) or methanol (50 % v/v), similar ABTS values were obtained.

DPPH values were higher ($p < 0.05$) when using dehydrated peels (C60 and CI) and 70 % ethanol and when fresh peels were used with methanol (Table 4). Covarrubias-

Table 4. Antioxidant capacity in residual orange (*Citrus sinensis* L.) peel extracts determined by 2,2-diphenyl-1-picryhydrazyl (DPPH) and 2,2′-azino-bis(3-ethylbenzothiazoline-6-sulfonic acid) (ABTS) methods.

Solvent	Peel	ABTS (μM TE g^{-1} DW)*	DPPH (μM TE g^{-1} DW)*
70 % Ethanol	CF	273.90 ± 24.05 a	6.31 ± 0.57 c
	C60	144.29 ± 14.14 b	15.57 ± 0.57 a
	CI	119.87 ± 9.05 b	15.80 ± 1.37 a
Methanol	CF	272.69 ± 37.67 a	16.04 ± 0.66 a
	C60	133.34 ± 15.59 b	11.96 ± 0.38 b
	CI	93.99 ± 4.66 b	6.67 ± 0.28 c

Data are mean values ± standard deviation. Different letters in the same column indicate significant difference between orange peel samples (Tukey $p < 0.05$). CF: fresh peel; C60: dehydrated peel at 60 °C, pilot level; CI: dehydrated peel at 204 °C, industrial level. *Micromoles of Trolox per gram of orange peel on a dry basis.

Cárdenas *et al.* (2018) reported higher antioxidant capacity (DPPH) in dried sour orange peels and lower antioxidant capacity for fresh orange peel extracts. This suggests that some phytochemical compounds react during the drying process, forming other antioxidant compounds by the formation of phenol complexes with proteins (Martín-Cabrejas *et al*., 2009).

Barrales *et al*. (2018) reported a similar DPPH value (17 μM TE g^{-1} dried peel) to that obtained in this work (16 μM TE g^{-1} DW) using the dried peels and ethanol as an extraction solvent. These authors measured the antioxidant capacity in orange peel dehydrated in an air circulation oven at 50 °C for 24 h, ground, and subjected to ultrasound-assisted extraction with 50 % (v/v) ethanol in an ultrasonic bath at 30 °C for 15 min. On the other hand, in this study, the ABTS radical scavenging capacity was higher than the DPPH radical scavenging capacity (Table 4), which is in agreement with the study by Kim and Lim (2020) on ethanol, methanol, and acetone extracts of immature Satsuma mandarin peel, in which ABTS radical scavenging capacity was four times higher than the DPPH radical scavenging capacity in an ethanol extract, indicating that its radical scavenging capacity works better in a hydrophilic system. The DPPH assays use radicals dissolved in organic solvents, which is applicable to the hydrophobic system, but the ABTS assay is applicable to both hydrophilic and lipophilic systems (Floegel *et al*., 2011).

CONCLUSIONS

The drying conditions affected the yields of orange peel phytochemical bioactives when using both extraction solvents. The highest extract yield was obtained in fresh residual peel, with 46 and 38 % using 70 % ethanol and pure methanol, respectively.

Similarly, the highest concentration for total phenol content (14.03 mg GAE g^{-1} DW), total flavonoid content (9.5 mg QE g^{-1} DW), antioxidant capacity (273.90 μM TE g^{-1} DW), and naringin (13.62 mg g^{-1} DW) was found in fresh residual peel. In the case of hesperidin content, methanol extraction obtained better yields (44.80 mg g^{-1} DW) and no differences were found in the content of both types of peels (fresh and dry). The use of fresh or dehydrated orange peel is an option for the orange fruit processing company within the revaluation alternatives as a source of flavonoids, particularly hesperidin and naringin.

ACKNOWLEDGEMENTS

We thank the Secretariat of Science, Humanities, Technology and Innovation (SECIHTI) for the postdoctoral grant awarded to Almadalia Velasco-Hernández. We also thank the citrus industry for providing the raw material (orange peels) necessary to carry out this study.

REFERENCES

Afifi SM, Kabbash EM, Berger RG, Krings U, Esatbeyoglu T. 2023. Comparative untargeted metabolic profiling of different parts of *Citrus sinensis* fruits via liquid chromatography-mass spectrometry coupled with multivariate data analyses to unravel authenticity. Foods 12 (3): 579. https://doi.org/10.3390/foods12030579

Ammar NM, Hassan HA, Abdallah HMI, Afifi SM, Elgamal AM, Farrag ARH, El-Gendy AENG, Farag MA, Elshamy AI. 2022. Protective effects of naringenin from *Citrus sinensis* (var. Valencia) peels against CCl4-induced hepatic and renal injuries in rats assessed by metabolomics, histological and biochemical analyses. Nutrients 14 (4): 841. https://doi.org/10.3390/nu14040841

Baglioni M, Fries A, Müller JM, Omarini A, Müller M, Breccia JD, Mazzaferro LS. 2024. *Acremonium* sp. diglycosidase-aid chemical diversification: Valorization of industry by-products. Applied Microbiology and Biotechnology 108 (1): 250. https://doi.org/10.1007/s00253-023-12957-8

Barrales FM, Silveira P, Barbosa PPM, Ruviaro AR, Paulino BN, Pastore GM, Macedo GA, Martinez J. 2018. Recovery of phenolic compounds from citrus by-products using pressurized liquids — An application to orange peel. Food and Bioproducts Processing 112: 9–21. https://doi.org/10.1016/J.FBP.2018.08.006

Batool A, Imran S, Tanweer A. 2020. Relative nutritional and phytochemical composition of citrus fruit compartments- A case against wasting citrus peels. Nurture 14 (1): 6–11. https://doi.org/10.55951/nurture.v14i1.8

Boukroufa M, Boutekedjiret C, Petigny L, Rakotomanomana N, Chemat F. 2015. Bio-refinery of orange peels waste: A new concept based on integrated green and solvent free extraction processes using ultrasound and microwave techniques to obtain essential oil, polyphenols and pectin. Ultrasonics Sonochemistry 24: 72–79. https://doi.org/10.1016/j.ultsonch.2014.11.015

Brand-Williams W, Cuvelier ME, Berset C. 1995. Use of a free radical method to evaluate antioxidant activity. LWT - Food Science and Technology 28 (1): 25–30. https://doi.org/10.1016/S0023-6438(95)80008-5

Chakroun I, Bouraoui Z, Ayachi T, Hosni K, Guerbèj H, Snoussi M, Jebali J, Gharred T. 2023. Phytochemical constituents and potential applications of Thomson Navel orange (*Citrus* × *aurantium* var. *sinensis* L.) peel extracts: Antioxidant, antimicrobial and antiproliferative properties. Industrial Crops and Products 206: 117597. https://doi.org/10.1016/j.indcrop.2023.117597

Chang CC, Yang MH, Wen HM, Chern JC. 2002. Estimation of total flavonoid content in propolis by two complementary colometric methods. Journal of Food and Drug Analysis 10 (3): 178–182. https://doi.org/10.38212/2224-6614.2748

Choi IS, Kim JH, Wi SG, Kim KH, Bae HJ. 2013. Bioethanol production from mandarin (*Citrus unshiu*) peel waste using popping pretreatment. Applied Energy 102: 204–210. https://doi.org/10.1016/j.apenergy.2012.03.066

Covarrubias-Cárdenas A, Patrón-Vázquez J, Espinosa-Andrews H, Ayora-Talavera T, García-Cruz U, Pacheco N. 2018. Antioxidant capacity and UPLC–PDA ESI–MS polyphenolic profile of *Citrus aurantium* extracts obtained by ultrasound assisted extraction. Journal of Food Science and Technology 55 (12): 5106–5114. https://doi.org/10.1007/s13197-018-3451-0

de Miera BS, Cañadas R, González-Miquel M, González EJ. 2023. Recovery of phenolic compounds from orange peel waste by conventional and assisted extraction techniques using sustainable solvents. Frontiers in Bioscience-Elite 15 (4): 30. https://doi.org/10.31083/j.fbe1504030

de Moraes CT, Jablonski A, de Oliveira RA, Rech R, Flôres SH. 2013. Dietary fiber from orange byproducts as a potential fat replacer. LWT - Food Science and Technology 53 (1): 9–14. https://doi.org/10.1016/J.LWT.2013.02.002

DOF (Diario Oficial de la Federación). 1986. NORMA Mexicana NMX-F-083-1986. Alimentos. Determinación de humedad en productos alimenticios. Gobierno de México. Secretaría de Agricultura y Recursos Hidráulicos. Ciudad de México, México.

DOF (Diario Oficial de la Federación). 1994. NORMA Oficial Mexicana NOM-086-SSA1-1994. Bienes y servicios. Alimentos y bebidas no alcohólicas con modificaciones en su composición. Especificaciones nutrimentales. Gobierno de México. Secretaría de Salud. Ciudad de México, México.

DOF (Diario Oficial de la Federación). 2008. NORMA Mexicana NMX-F-622-NORMEX-2008. Alimentos. Determinación de fibra dietética, fracción insoluble y fracción soluble (método gravimétrico enzimático) en alimentos. Método de prueba. Gobierno de México. Secretaría de Economía. Ciudad de México, México.

DOF (Diario Oficial de la Federación). 2017. NORMA Mexicana NMX-F-613-NORMEX-2017. Alimentos. Determinación de fibra cruda en alimentos. Método de prueba. Gobierno de México. Secretaría de Economía. Ciudad de México, México.

DOF (Diario Oficial de la Federación). 2020. NORMA Mexicana NMX-F-607-NORMEX-2020. Alimentos. Determinación de cenizas en alimentos. Método de prueba. Gobierno de México. Secretaría de Economía. Ciudad de México, México.

FAO (Food and Agriculture Organization). 2022. FAOSTAT. Crops and livestock products. United Nations Food and Agriculture Organization. Rome, Italy. https://www.fao.org/faostat/en/#data/QCL (Retrieved: February 2024).

Floegel A, Kim DO, Chung SJ, Koo SI, Chun OK. 2011. Comparison of ABTS/DPPH assays to measure antioxidant capacity in popular antioxidant-rich US foods. Journal of Food Composition and Analysis 24 (7): 1043–1048. https://doi.org/10.1016/j.jfca.2011.01.008

Fu X, Belwal T, Cravotto G, Luo Z. 2020. Sono-physical and sono-chemical effects of ultrasound: Primary applications in extraction and freezing operations and influence on food components. Ultrasonics Sonochemistry 60: 104726. https://doi.org/10.1016/j.ultsonch.2019.104726

García-Salazar JA, Bautista-Mayorga F, Borja-Bravo M, Guzmán-Soria E. 2021. Variation in the orange (*Citrus sinensis* L.) prices in Mexico. Agronomía Mesoamericana 32 (1): 209–223. https://doi.org/10.15517/am.v32i1.40679

Hosseini SS, Khodaiyan F, Yarmand MS. 2016. Optimization of microwave assisted extraction of pectin from sour orange peel and its physicochemical properties. Carbohydrate Polymers 140: 59–65. https://doi.org/10.1016/j.carbpol.2015.12.051

Kim DS, Lim SB. (2020). Extraction of flavanones from immature *Citrus unshiu* pomace: process optimization and antioxidant evaluation. Scientific Reports 10 (1): 19950. https://doi.org/10.1038/s41598-020-76965-8

Kumar D, Ladaniya MS, Gurjar M, Kumar S. 2022. Impact of drying methods on natural antioxidants, phenols and flavanones of immature dropped *Citrus sinensis* L. Osbeck fruits. Scientific Reports 12 (1): 6684. https://doi.org/10.1038/s41598-022-10661-7

Lai C, Huang M, Xiong Q, Liang Y, Jiang Y, Zhang J. 2024. Green and efficient approach to extract bioactive flavonoids with antioxidant, antibacterial, antiglycation, and enzyme inhibitory activities from navel orange peel. Sustainable Chemistry and Pharmacy 38: 101479. https://doi.org/10.1016/j.scp.2024.101479

Londoño J, Ramírez R, Sierra J. 2007. Efecto de la hesperidina sobre la captación de HDL en células hepáticas y evaluación de hesperidina liposomal sobre la oxidación de LDL. Scientia et Technica 1 (33): 63–66.

Martín-Cabrejas MA, Aguilera Y, Pedrosa MM, Cuadrado C, Hernández T, Díaz S, Esteban RM. 2009. The impact of dehydration process on antinutrients and protein digestibility of some legume flours. Food Chemistry 114 (3): 1063–1068. https://doi.org/10.1016/j.foodchem.2008.10.070

Mehmood T, Khan MR, Shabbir MA, Zia MA. 2017. Phytochemical profiling and HPLC quantification of citrus peel from different varieties. Progress in Nutrition 20 (1): 279–288. https://doi.org/10.23751/pn.v20i1-S.6357

Panwar D, Saini A, Panesar PS, Chopra HK. 2021. Unraveling the scientific perspectives of citrus by-products utilization: Progress towards circular economy. Trends in Food Science and Technology 111: 549–562. https://doi.org/10.1016/j.tifs.2021.03.018

Perlatti B, Fernandes JB, Silva MFGF, Ardila JA, Carneiro RL, Souza BHS, Costa EN, Eduardo WI, Boiça Junior AL, Forim MR. 2016. Application of a quantitative HPLC-ESI-MS/MS method for flavonoids in different vegetables matrices. Journal of the Brazilian Chemical Society 27 (3): 475–483. https://doi.org/10.5935/0103-5053.20150273

Rafiq S, Kaul R, Sofi SA, Bashir N, Nazir F, Ahmad Nayik G. 2018. Citrus peel as a source of functional ingredient: A review. Journal of the Saudi Society of Agricultural Sciences 17 (4): 351–358. https://doi.org/10.1016/J.JSSAS.2016.07.006

Re R, Pellegrini N, Proteggente A, Pannala A, Yang M, Rice-Evans C. 1999. Antioxidant activity applying an improved ABTS radical cation decolorization assay. Free Radical Biology and Medicine 26 (9–10): 1231–1237. https://doi.org/10.1016/S0891-5849(98)00315-3

Suri S, Singh A, Nema PK. 2021. Recent advances in valorization of citrus fruits processing waste: a way forward towards environmental sustainability. Food Science and Biotechnology 30 (13): 1601–1626. https://doi.org/10.1007/s10068-021-00984-y

Suri S, Singh A, Nema PK. 2022. Current applications of citrus fruit processing waste: A scientific outlook. Applied Food Research 2 (1): 100050. https://doi.org/10.1016/j.afres.2022.100050

Wang Z, Chen X, Guo Z, Feng X, Huang P, Du M, Zalán Z, Kan J. 2022. Distribution and natural variation of free, esterified, glycosylated, and insoluble-bound phenolic compounds in brocade orange (*Citrus sinensis* L. Osbeck) peel. Food Research International 153: 110958. https://doi.org/10.1016/j.foodres.2022.110958

Waterhouse AL. 2002. Determination of total phenolics. Current Protocols in Food Analytical Chemistry 6 (1). https://doi.org/10.1002/0471142913.fai0101s06

Zheng M, Lu S, Xing J. 2021. Enhanced antioxidant, anti-inflammatory and α-glucosidase inhibitory activities of citrus hesperidin by acid-catalyzed hydrolysis. Food Chemistry 336: 127539. https://doi.org/10.1016/j.foodchem.2020.127539

Zhu CQ, Chen JB, Zhao CN, Liu XJ, Chen YY, Liang JJ, Cao JP, Wang Y, Sun CD. 2023. Advances in extraction and purification of citrus flavonoids. Food Frontiers 4 (2): 750–781. https://doi.org/10.1002/fft2.236

Zuin VG, Ramin LZ, Segatto ML, Stahl AM, Zanotti K, Forim MR, da Silva MFGF, Fernandes JB. 2021. To separate or not to separate: What is necessary and enough for a green and sustainable extraction of bioactive compounds from Brazilian citrus waste. Pure and Applied Chemistry 93 (1): 13–27. https://doi.org/10.1515/pac-2020-0706

Agrociencia

ENHANCING ANTIOXIDANT ACTIVITY AND PHENOLIC CONTENT IN DATE PALM (*Phoenix dactylifera* L.) CALLUS CULTURES THROUGH TRACE ELEMENT SUPPLEMENTATION

Wael **Shehata**[1]

[1]King Faisal University. College of Agriculture and Food Sciences. Department of Agricultural Biotechnology. Al-Ahsa, Saudi Arabia. 31982.
* Author for correspondence: wshehata@kfu.edu.sa

Citation: Shehata W. 2025. Enhancing antioxidant activity and phenolic content in date palm (*phoenix dactylifera* l.) Callus cultures through trace element supplementation. **Agrociencia** 59(4): 528-545. https://doi.org/ 10.47163/ agrociencia.v59i4.3405

Editor in Chief:
Dr. Fernando C. Gómez Merino

Received: January 16, 2025.
Approved: May 02, 2025.
Published in Agrociencia: May 26, 2025.

ABSTRACT

This study investigates the impact of trace element supplementation on phenolic content, antioxidant activity, and callus initiation in Hassawi date palm (*Phoenix dactylifera* L.) cultivars (Khalas, Ruziz, and Shishi) grown on Murashige and Skoog (MS) medium. Varying concentrations of trace elements ($MgSO_4 \cdot 7H_2O$, $MnSO_4 \cdot 4H_2O$, $ZnSO_4 \cdot 7H_2O$, and $CuSO_4 \cdot 5H_2O$ at zero, half, full, and double Stock E) were tested to evaluate their effects on secondary metabolite production and oxidative stress management. Results demonstrated that double concentrations of Stock E significantly enhanced phenolic content (2.68 mg g^{-1} GAE) and antioxidant activity (96.28 % inhibition and 978.69 mg g^{-1} μM Trolox), with the Shishi cultivar showing the most pronounced response. The improved phenolic accumulation and antioxidant capacity were attributed to the activation of enzymatic pathways, including phenylalanine ammonia-lyase (PAL), and the regulation of reactive oxygen species (ROS) through enhanced antioxidant enzyme activity. Additionally, reduced browning in callus tissues indicated effective modulation of polyphenol oxidase (PPO) activity. The study underscores the potential for optimizing trace element concentrations to enhance bioactive compound production in date palms. These findings contribute to sustainable agricultural practices, offering practical applications in food, pharmaceutical, and nutraceutical industries. Future research should focus on molecular analyses to elucidate the precise pathways influenced by trace elements and explore large-scale production systems for commercial antioxidant extraction.

Keywords: Antioxidants, browning, callus initiation, date palm, total phenolic, trace element, μM Trolox.

INTRODUCTION

Al-Ahsa Oasis, the largest green oasis in Saudi Arabia and the world, is a critical source of food security for the kingdom. It hosts approximately 4.1 million date palm trees (*Phoenix dactylifera* L.). Hasawi cultivars constitute the main crop alongside other plants unique to the region (MEWA, 2023). The oasis's primary cultivars—Khalas, Ruziz, and Shishi—account for over 70 % of date palm tree production (Almadini *et*

al., 2021; Ismail *et al*., 2022). These cultivars are particularly notable for their resilience to drought and heat, contributing significantly to environmental sustainability in line with Saudi Arabia's Vision 2030.

Dates from these cultivars are rich in fiber, minerals, and beneficial sugars, enhancing immunity and preventing diseases (Al-Saikhan, 2006). Furthermore, dates are distinguished by their high antioxidant content, such as phenolic compounds and dactylifera acid (Al-Shwyeh, 2019). This positions date palms as a valuable source for enhancing human health and combating chronic diseases (Zhang and Sun, 2021). It also contributes to cell regeneration and repair (Qiu *et al*., 2022).

Despite their long growth cycle, the ability to harness antioxidants from date palms through advanced tissue culture techniques presents a sustainable solution. Plant tissue culture, particularly callus culture, offers a controlled platform for producing bioactive compounds, essential for food, pharmaceutical, and nutraceutical industries. The increasing demand for antioxidants has driven research into optimizing tissue culture systems to enhance phenolic compound production (Batista *et al*., 2018).

This study aims to optimize the concentrations of trace elements in Murashige and Skoog (MS) medium to enhance phenolic production and antioxidant activity in callus cultures of Khalas, Ruziz, and Shishi cultivars. Trace elements such as zinc, manganese, and copper serve as cofactors for enzymes in the phenylpropanoid pathway, crucial for phenolic biosynthesis (Vazquez-Marquez *et al*., 2024). Iron, a key trace element, supports the synthesis of enzymes related to respiration and photosynthesis, reducing oxidative stress by mitigating free radicals (Amente and Chimdessa, 2021). The experimental design incorporates controlled treatments and robust statistical analyses to validate the effects of trace elements on callus initiation, phenolic content, and antioxidant activity. By systematically assessing these variables, the study provides practical insights for enhancing tissue culture protocols and scaling antioxidant production (Zhang, 2023).

Aligning with global priorities for sustainable agriculture, this research explores the potential of date palm tissue culture to improve phenolic biosynthesis and antioxidant activity. The findings contribute to developing efficient, large-scale production systems, such as bioreactors, and assessing the economic feasibility of these protocols for commercial use (Liu *et al*., 2018; Muszyńska and Labudda, 2019; Dai *et al*., 2023). This approach underscores the broader relevance of optimizing trace element concentrations in tissue culture systems to support sustainable food systems and agricultural resource utilization.

MATERIALS AND METHODS

Callus initiation

The plant material for this study consisted of three primary date palm cultivars (Khalas, Ruziz, and Shishi) from Al-Ahsa Oasis, collected during the period from October 2021 to April 2022. Young offshoots (50–70 cm in height and weighing 5–7 kg) were separated from adult *Phoenix dactylifera L.* trees.

Under sterile conditions, explants underwent surface sterilization. First, they were rinsed three times with sterile distilled water, followed by a 20-min soak in a 3.2 % sodium hypochlorite solution (60 %; v/v commercial bleach with three drops of Tween, 20 per 100 mL), and then rinsed again three times with sterile distilled water (Alturki *et al*., 2013). The explants were then transferred to sterile Petri dishes and cut into 5 × 5 mm pieces. Subsequently, all explants were soaked in 70 % ethanol for 3 min, rinsed three times with sterile water, and immersed in a 1.5 g L^{-1} mercuric chloride ($HgCl_2$) solution for 3–5 minutes. Finally, explants were rinsed three times with sterile distilled water and cultured under laminar flow conditions (Shehata *et al*., 2014).

The explants were cultured on a basal Murashige and Skoog (MS) nutrient medium (Murashige and Skoog, 1962), formulated with specific concentrations of inorganic salts (Table 1). To prepare the final medium, 20 mL of stock solutions A and B and 5 mL of stock solutions C, D, E, F, and G were added to 1 L of distilled water and

Table 1. Minor mineral element concentrations (Stock E) and additional components used in Murashige and Skoog (MS) medium for date palm (*Phoenix dactylifera* L.) explant culture.

Stock solution	Constituents	Concentration in MS medium (g L^{-1})	To make up 1 L of MS medium (mL L^{-1})	Concentration difference	Code
A	NH_4NO_3	82.500	20	Full	---
B	KNO_3	95.000	20	Full	---
C	H_3BO_3	1.240	5	Full	---
	KH_2PO_4	34.000			
	KI	0.166			
	$Na_2MoO_4 \cdot 2H_2O$	0.050			
	$CoCl_2 \cdot 6H_2O$	0.005			
D	$CaCl_2 \cdot 2H_2O$	88.000	5	Full	---
E	$MgSO_4 \cdot 7H_2O$	74.000	5	Zero	E-1
	$MnSO_4 \cdot 4H_2O$	4.460		Half	E-2
	$ZnSO_4 \cdot 7H_2O$	1.720		Full	E-3
	$CuSO_4 \cdot 5H_2O$	0.005		Double	E-4
F*	$Na_2 \cdot EDTA$	7.450	5	Full	---
	$FeSO_4 \cdot 7H_2O$	5.570			
G	Thiamine·HCl	0.200	5	Full	---
	Nicotinic acid	0.100			
	Pyrodoxine·HCl	0.100			
	Glycine	0.400			

*This stock solution was prepared by dissolving each constituent in 200 mL-distilled water. The $Na_2 \cdot EDTA \cdot 2H_2O$ solution was heated, and the $FeSO_4 \cdot 7H_2O$ solution was added with continuous stirring. After cooling, it was diluted to 1000 mL with distilled water. All stocks were stored in amber colored bottles in refrigerator. Modified media used for cultures were supplemented with different concentrations of phytohormones, carbohydrates, vitamins, and other addenda (Murashige and Skoog, 1962).

stirred. The mix was supplemented as follows (in mg L^{-1}): 170 $NaH_2PO_4 \cdot 2H_2O$, 80 adenine sulfate, 100 myo-inositol, 2 biotin, 2.5 vitamin B_1 (thiamine-HCl), 100 2,4-dichlorophenoxyacetic acid, 5 6-benzylaminopurine, 30 000 sucrose, 7000 agar, and 2000 activated charcoal (Sigma Chemical Co., St. Louis, MO, USA). Before adding the agar and activated charcoal, the pH was adjusted to 5.7. The medium was autoclaved at 1.2 kg cm^{-2} at 121 °C for 20 min, then dispensed into small jars with 25 mL of media each (Shehata *et al*., 2014).

The explants were transferred to a modified MS medium with different stock E ($MgSO_4 \cdot 7H_2O$, $MnSO_4 \cdot 4H_2O$, $ZnSO_4 \cdot 7H_2O$, and $CuSO_4 \cdot 5H_2O$] concentrations, i.e., zero, half, full, and double (0, 2.5, 5, and 10 mL L^{-1}, respectively). Cultures were incubated at 25 ± 2 °C in a totally dark growth room for six months and maintained by transferring to fresh media every two months. Data was recorded for all cultivars at the end of each subculture. The visual scoring system by Pottino (1981) was used to read the callus data and brown discoloration on the explants of each cultivar under study, with five replicates per treatment. The surviving and browning explant jars were numbered, and cultivars with callus initiation were registered to determine the effects of microelements on callus initiation and phenolic compounds on browning.

Antioxidant analysis

The following chemicals and reagents were used: Folin-Ciocalteu's phenol reagent, gallic acid, sodium carbonate, ascorbic acid, trichloroacetic acid, catechin, sodium nitrite, sodium nitrate, aluminum chloride, and methanol (all from Merck, Darmstadt, Germany), along with 2,2′-azino-bis(3-ethylbenzothiazoline-6-sulfonic acid) (ABTS) diammonium salt, 2,4,6-tripyridyl-S-triazine (TPTZ), and 2,2′-azinobis (3-ethylbenzothiazoline-6-sulphonic acid) from Sigma-Aldrich (USA). Additionally, $FeCl_3 \cdot 3H_2O$, 6-hydroxy-2,5,7,8-tetramethylchroman-2-carboxylic acid (Trolox), sodium acetate, sodium carbonate, and potassium persulfate from Sigma-Aldrich were used as analytical-grade reagents for analyzing antioxidant compounds (Alturki *et al*., 2013).

For sample preparation, 3 g of callus tissue were crushed and dry-blended for 10 min, then extracted with 100 mL methanol using an orbital shaker (LSI-LabTECH, Korea) at 20 °C for 5 h. The extract was filtered and centrifuged at 4000 rpm for 10 min, then concentrated using a rotary evaporator (Heidolph-Laborota, Germany) under reduced pressure at 40 °C for 3 h. Extracts were stored in dark glass bottles at -20°C until further analysis (Shehata *et al*., 2014).

Antioxidant activity was measured using the ABTS method as described by Cai *et al*. (2004). ABTS radical cations were prepared by reacting 7 μM ABTS with 2.45 μM potassium persulfate in the dark at 23 °C for 16 h, then diluting with 80 % ethanol to an absorbance of 0.7 ± 0.005 at 734 nm. To each 0.1 mL test sample, 3.9 mL of ABTS were added, and absorbance was measured at 734 nm after 6 min at room temperature. A Trolox standard curve (0–15 μM in 80 % ethanol) was used for comparisons, and results were expressed in Trolox equivalents (Aldaej *et al*., 2014).

Total phenolics were determined using Folin-Ciocalteu reagent (Singleton and Rossi, 1965). Every 40 mL explant extract or gallic acid standard was mixed with 1.8 mL of 10-fold prediluted Folin-Ciocalteu reagent, incubated for 5 min at room temperature, and combined with 1.2 mL of 7.5 % sodium bicarbonate. Absorbance was measured at 765 nm after 60 min, and results were expressed as milligrams of gallic acid equivalents (GAE) per 100 g of sample (Shehata *et al*., 2014).

Statistical analysis

Data were analyzed using analysis of variance (ANOVA) for a completely randomized design as per (Gomez and Gomez, 1984). Treatment means were compared using the least significant difference (LSD) at a 5 % probability level. All computations and analyses were performed using SAS software (SAS Institute Inc., 2001). Multivariate analysis, including heat map analysis via the Orange Data Mining software (Demsar *et al*., 2013), was used to illustrate correlations between antioxidant activity and total phenolic content.

RESULTS AND DISCUSSION

Effect of microelements on callus initiation

The number of surviving explants (Figures 1 and 2) significantly varied among cultivars and Stock E (SE) concentrations ($p < 0.01$). The survival rate of explants increased with higher SE concentrations, with the highest survival observed at E-4 (mean = 3.89) and the lowest at E-1 (mean = 2.44). Among the cultivars, Khalas (Kh) exhibited the highest overall survival (mean = 4.5), followed by Ruziz (Ru) (mean =

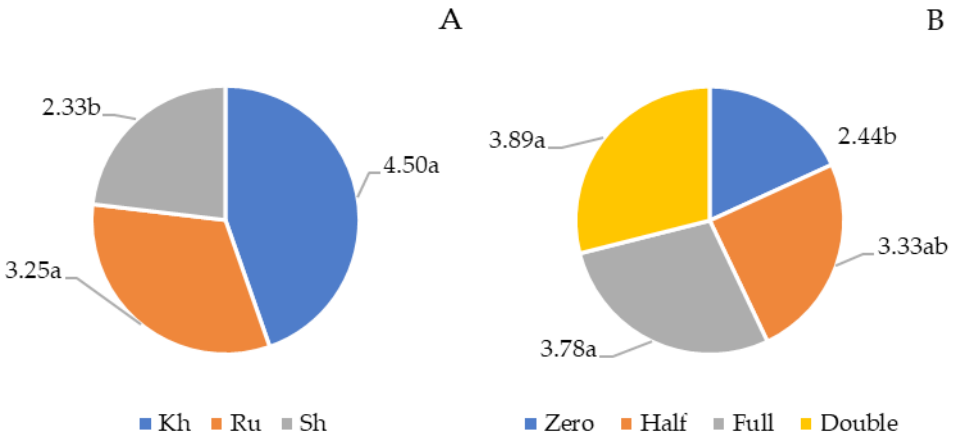

Figure 1. Specific effect of three date palm (*Phoenix dactylifera* L.) cultivars (A) and different Stock E concentrations (B) on the number of surviving explants during callus stage of *in vitro* culture. Cultivars (Kh: Khalas; Ru: Ruziz; Sh: Shishi); Stock E solution (Zero: E-1; half: E-2; full: E-3; double: E-4).

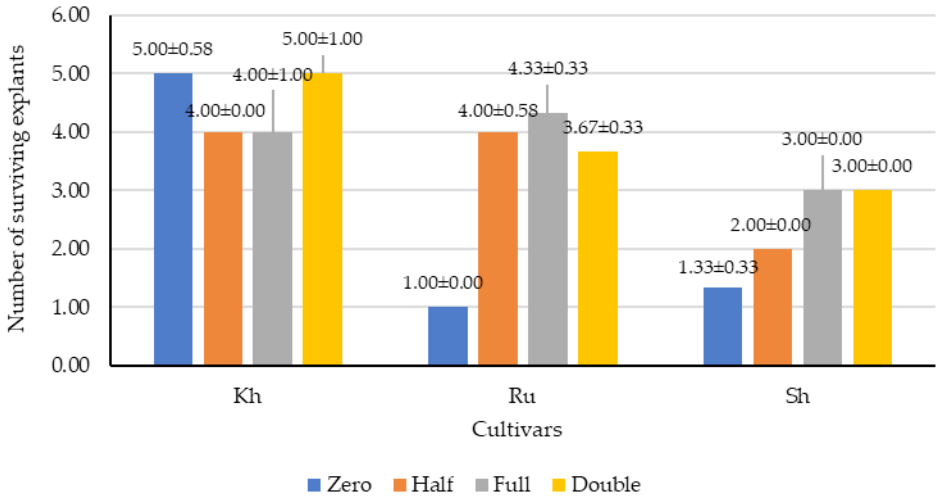

Figure 2. Interaction effect of different Stock E concentrations and three date palm (*Phoenix dactylifera* L.) cultivars on the number of surviving explants during the callus stage of *in vitro* culture. Cultivars (Kh: Khalas; Ru: Ruziz; Sh: Shishi); Stock E solution (Zero: E-1; half: E-2; full: E-3; double: E-4). Significance level (S = 0.006, T = 0.008, S * T = 0.005).

3.25), while Shishi (Sh) had the lowest survival (mean = 2.33), suggesting a cultivar-dependent response to microelement availability. The statistical analysis confirmed that SE concentration (S), Treatment (T), and their interaction (S*T) were all highly significant ($p < 0.01$), indicating that both nutrient composition and cultivar type play a crucial role in explant viability.

The positive correlation between SE levels and survival suggests that trace elements such as manganese, zinc, and iron play a crucial role in maintaining cellular integrity, enzymatic activity, and oxidative stress reduction, thereby promoting explant survival in plant tissue cultures (Vazquez-Marquez *et al*., 2024; Amente and Chimdessa, 2021). Studies on *Triticum aestivum* L. have shown similar trends, where microelement supplementation enhances survival by minimizing oxidative stress and supporting cellular metabolism (Amente and Chimdessa, 2021). However, Shishi consistently exhibited the lowest survival rate, which may indicate a cultivar-specific sensitivity to microelements due to metabolic differences or a heightened oxidative stress response (Zhang, 2023). This highlights the need for optimized nutrient supplementation strategies, particularly for sensitive cultivars like Shishi, to improve viability and enhance tissue culture performance.

The number of surviving explants varied significantly depending on both the cultivar and the concentration of SE. For instance, higher concentrations of stock E generally led to a higher number of surviving explants, but this effect was also influenced by the specific cultivar. This is consistent with findings that microelements such as SE can significantly impact tissue culture success rates (Al-Khayri *et al*., 2019).

The callus initiation response (Figures 3 and 4) was also significantly influenced by Stock E concentrations (p = 0.01), with the highest callus formation observed at E-3 (mean = 1.67), while the lowest occurred at E-1 and E-4 (1.0 and 1.11, respectively). Among cultivars, Sh exhibited the highest overall callus initiation (1.42), followed by Ru (1.25), while Kh had the lowest callus formation (1.08). Statistical analysis confirmed that SE concentration (S) had a significant effect (p = 0.01), whereas Treatment (T) and

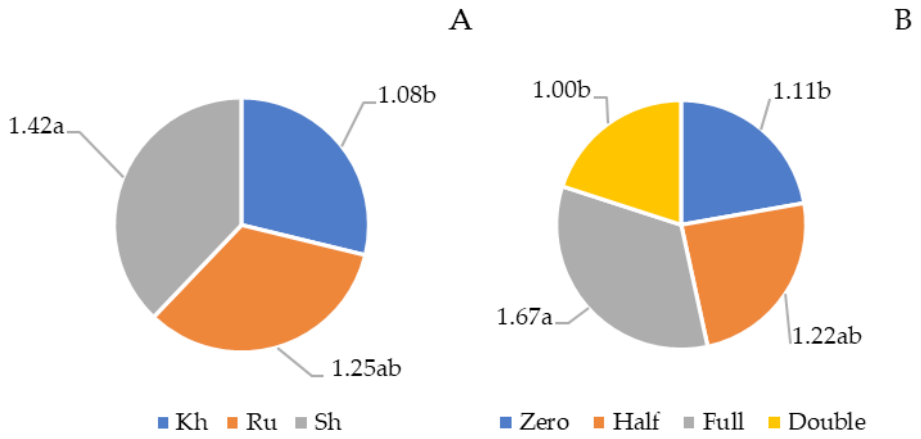

Figure 3. Specific effects of date palm (*Phoenix dactylifera* L.) cultivars (A) and different Stock E concentrations (B) on callus initiation during six months of *in vitro* culture. Cultivars (Kh: Khalas; Ru: Ruziz; Sh: Shishi); Stock E solution (Zero: E-1; half: E-2; full: E-3; double: E-4).

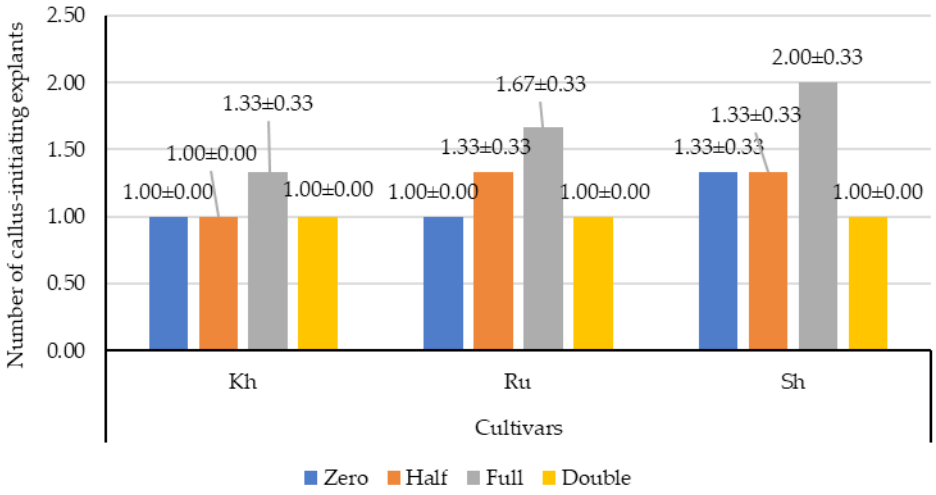

Figure 4. Combined influence of stock E concentrations and date palm (*Phoenix dactylifera* L.) cultivars on callus initiation during six months of *in vitro* culture. Cultivars (Kh: Khalas; Ru: Ruziz; Sh: Shishi); Stock E solution (Zero: E-1; half: E-2; full: E-3; double: E-4). Significance level (S = 0.01, T = not significant (NS), S * T = NS).

the interaction (S*T) were not significant, indicating that microelement availability played a more crucial role in callus induction than cultivar differences. However, the full SE concentration yielded the highest callus initiation rates, with Sh (2.00 ± 0.33), Ru (1.67 ± 0.33), and Kh (1.33 ± 0.33) outperforming other concentrations. With half SE, Sh, and Ru *cvs* exhibited similar initiation rates (1.33 ± 0.33), as did Shishi in the absence of microelements (1.33 ± 0.33). The lowest callus formation was observed with double E-4 concentration (1.0 ± 0.0).

Callus formation was optimal at E-3 but declined at E-4, likely due to excessive microelement accumulation disrupting cellular metabolism (Dai *et al*., 2023). Moderate trace element supplementation at E-3 appears to enhance phenolic metabolism and enzyme activation, promoting cell differentiation and division (Liu *et al*., 2018; Muszyńska and Labudda, 2019). Microelements such as zinc, copper, iron, and manganese serve as essential cofactors in enzymatic processes regulating tissue growth and oxidative stress balance (Zhang, 2023). Studies on *Capsicum annuum* L. demonstrated that copper supplementation enhances callus formation by stimulating peroxidase activity, which plays a key role in oxidative stress regulation and tissue development (Liu *et al*., 2018; Muszyńska and Labudda, 2019). However, at E-4, excessive copper or manganese may induce toxicity, disrupting oxidative balance and limiting callus growth (Amente and Chimdessa, 2021). These findings emphasize the importance of precisely controlling trace element concentrations to optimize callus initiation while preventing toxicity-related metabolic imbalances in plant tissue cultures. This is consistent with studies showing that genetic factors play a significant role in callus formation, alongside the influence of trace elements (Al-Khayri *et al*., 2019).

Browning (Figure 5) intensity varied significantly across SE concentrations, with the highest observed at E-4 (mean = 2.89) and E-2 (1.89), while the lowest occurred at E-3

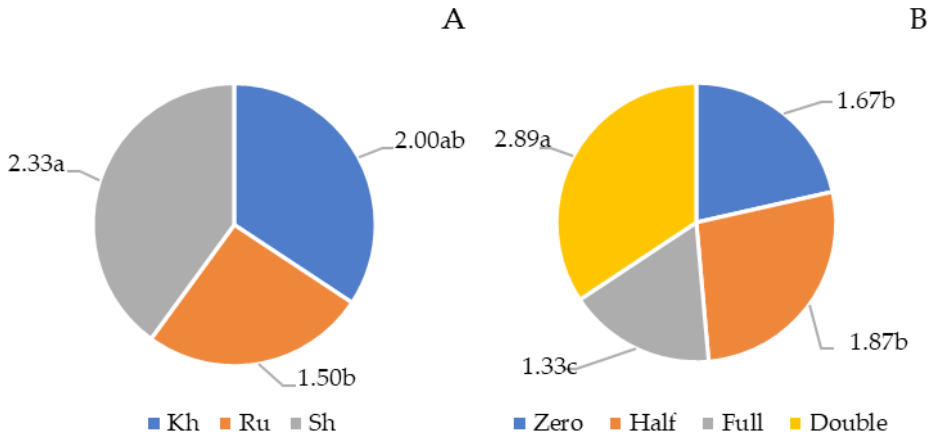

Figure 5. Specific effects of date palm (*Phoenix dactylifera* L.) cultivars (A) and different Stock E concentrations (B) on callus browning during six months of *in vitro* culture. Cultivars (Kh: Khalas; Ru: Ruziz; Sh: Shishi); Stock E solution (Zero: E-1; half: E-2; full: E-3; double: E-4).

(1.33). Among the cultivars, Sh exhibited the highest browning (2.33), followed by Kh (2.00) and Ru (1.50). Statistical analysis confirmed that the SE concentration (S) significantly affected browning (p = 0.007), whereas Treatment (T) and the interaction (S*T) were not significant, suggesting that browning was primarily influenced by nutrient levels rather than cultivar differences.

Cultivars Sh and Ru displayed the most intense browning at the double (E-4) concentration (3.00 ± 0.0), followed by Kh (2.67 ± 0.33) (Figure 6). At half concentration (E-2), Sh and Kh also showed pronounced browning (2.33 ± 0.33). Callus browning was

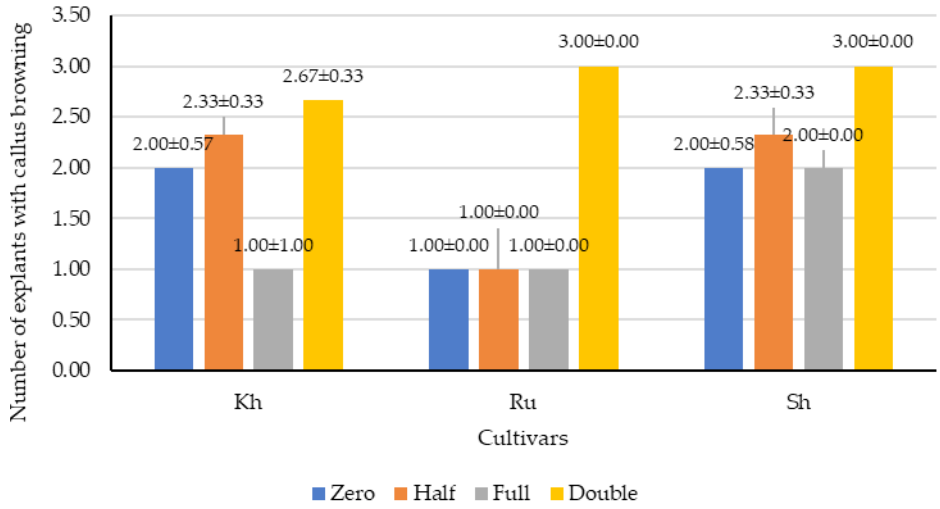

Figure 6. Interaction effect of stock E concentrations and date palm (*Phoenix dactylifera* L.) cultivars on callus browning during six months of *in vitro* culture. Cultivars (Kh: Khalas; Ru: Ruziz; Sh: Shishi); Stock E solution (Zero: E-1; half: E-2; full: E-3; double: E-4). Significance level (S = 0.007, T = not significant (NS), S * T = NS).

minimal at the full concentration (E-3), as recommended by Murashige and Skoog, which reduced discoloration across cultivars (Shehata *et al*., 2014). Overall, Shishi exhibited the greatest browning sensitivity to both high and low SE concentrations, suggesting it has a higher phenolic compound content. This indicates Shishi's potential for greater antioxidant, fiber, and mineral content compared to other cultivars, supporting findings on its distinct nutritional profile (Al-Saikhan, 2006).

Increased browning at high Stock E concentrations (E-4) can be attributed to polyphenol oxidation by polyphenol oxidase (PPO), a common challenge in plant tissue cultures caused by oxidative stress or imbalanced nutrient availability (Amente and Chimdessa, 2021). Excess iron and copper at E-4 may trigger PPO and peroxidase activity, accelerating phenolic oxidation and tissue discoloration (Zhang and Sun, 2021). In contrast, browning was minimized at E-3, suggesting that a balanced microelement supply helps regulate oxidative stress by enhancing antioxidant enzyme

activity, thereby improving tissue stability (Zhang, 2023). These findings align with research indicating that iron and manganese influence PPO activity, directly affecting browning intensity in plant tissue cultures (Zhang, 2023). Therefore, optimizing Stock E concentrations is essential for minimizing browning and maintaining tissue quality in plant micropropagation systems.

The findings suggest that E-3 (full-strength) is the most effective concentration for maximizing explant survival, enhancing callus initiation, and minimizing browning, whereas E-4 (double-strength) may induce oxidative stress and metabolic imbalances. Optimizing trace element concentrations is crucial for improving phenolic biosynthesis and antioxidant activity, with potential applications in commercial propagation and bioactive compound production (Dai *et al*., 2023). Similar trends have been observed in *Solanum lycopersicum* L., where balanced trace element supplementation reduced oxidative browning by stabilizing phenolic metabolism and regulating PPO activity (Vazquez-Marquez *et al*., 2024). Future research should focus on molecular pathways regulating oxidative stress and enzymatic activity in response to trace element variations to further enhance tissue culture performance.

Effect of microelements (Stock E) on total phenolic contents and antioxidant production

The antioxidant analysis results for the three Hassawi date palm cultivars highlight the role of varying micro-mineral (SE) concentrations on antioxidant production during *in vitro* callus formation (Table 2). The total phenolic content in date palm

Table 2. Effect of different stock E concentrations and date palm (*Phoenix dactylifera* L.) cultivars on total phenolic content and antioxidant production during six months of in vitro culture.

Cultivars	Stock E	Total phenolic content (mg GAE g^{-1})*	Antioxidant activity by ABTS Inhibition (%)	Antioxidant activity by ABTS µM Trolox
Kh	E-1	0.389 ± 0.004^{l}	14.579 ± 0.070^{l}	81.707 ± 2.147^{l}
	E-2	1.021 ± 0.070^{e}	42.853 ± 0.090^{e}	391.654 ± 1.458^{e}
	E-3	0.744 ± 0.003^{h}	36.061 ± 0.244^{h}	317.608 ± 3.435^{h}
	E-4	1.237 ± 0.007^{b}	54.467 ± 0.240^{c}	437.489 ± 1.391^{c}
Ru	E-1	$0.395 \pm 0.002^{k,l}$	14.756 ± 0.060^{k}	80.427 ± 1.466^{l}
	E-2	0.998 ± 0.02^{f}	42.194 ± 0.325^{f}	324.336 ± 3.965^{g}
	E-3	0.653 ± 0.002^{j}	28.945 ± 0.197^{j}	233.401 ± 3.001^{j}
	E-4	1.139 ± 0.003^{d}	47.195 ± 0.050^{d}	382.457 ± 2.236^{d}
Sh	E-1	0.711 ± 0.003^{i}	29.726 ± 0.280^{i}	243.270 ± 2.388^{i}
	E-2	$1.246 \pm 0.004^{b,c}$	55.305 ± 0.329^{b}	518.794 ± 4.301^{b}
	E-3	0.955 ± 0.010^{g}	39.324 ± 0.287^{g}	359.867 ± 5.173^{f}
	E-4	2.676 ± 0.005^{a}	96.283 ± 0.171^{a}	978.692 ± 3.122^{a}
Least significant difference ($p \leq 0.05$)		1.754	0.404	4.825

Cultivars (Kh: Khalas; Ru: Ruziz; Sh: Shishi). Stock E solution (Zero: E-1; half: E-2; full: E-3; double: E-4). *Expressed as milligrams of gallic acid equivalents (GAE) per 100 g of sample.

cultivars shows a clear trend of increasing with higher concentrations of Stock E. In Khalas, phenolic content rose from 0.389 mg g^{-1} at E-1 to 1.237 mg g^{-1} at E-4, indicating enhanced biosynthesis with more microelements. Ruziz followed a similar pattern, increasing from 0.395 mg g^{-1} at E-1 to 1.139 mg g^{-1} at E-4, suggesting a positive response to microelement supplementation. Shishi exhibited the highest phenolic content, peaking at 2.676 mg g^{-1} at E-4, highlighting its superior capacity for phenolic production in response to higher microelement concentrations, which is crucial for its antioxidant properties.

The antioxidant activity demonstrates a positive correlation with the concentration of Stock E. In Khalas, the inhibition percentage increased from 14.579 % at E-1 to 54.467 % at E-4, with μM Trolox values peaking at 437.489 mg g^{-1} under E-4. Ruziz followed a similar pattern, with inhibition percentages rising from 14.756 % at E-1 to 47.195 % at E-4, accompanied by an increase in μM Trolox values. Shishi exhibited the highest antioxidant activity, with inhibition reaching 96.283 % and μM Trolox values at 978.692 mg g^{-1} under E-4, highlighting its potential for significant antioxidant production and suitability for further research and agricultural development. Additionally, double SE concentration was found to be the most effective for phenolic production, though it caused callus discoloration from brown to black, while half SE concentration led to lighter browning. The callus cultured in full MS medium or without SE microelements retained a tan or yellowish-white color.

ABTS inhibitory activity in adventitious callus tissues decreased with increasing SE concentration from zero to half to full to double SE strength (Table 2). A strong positive correlation ($R^2 = 0.99$, $p < 0.05$) was observed between total phenolic content and ABTS radical scavenging in callus extracts with all SE concentrations in media, which is consistent with findings by other researchers (Shehata *et al*., 2014). Tawaha *et al*. (2007) also noted a positive correlation between total phenolic content and antioxidant activity in methanolic extracts of 51 plant species, including *P. dactylifera*.

The heat maps provide a detailed visualization of how the different microelement concentrations (E-1, E-2, E-3, and E-4) influenced total phenolic content, inhibition percentage, and μM Trolox (an antioxidant capacity measure) in the evaluated date palm cultivars. Shishi demonstrated the highest phenolic content (2.676 mg g^{-1}) and antioxidant capacity (μM Trolox value of 978.692 mg g^{-1}) under the E-4 treatment, highlighting its superior phenolic accumulation and antioxidant activity. Khalas and Ruziz showed moderate levels, with both reaching peak phenolic content under E-4. In terms of inhibition percentage, Shishi led at 96.283 %, followed by Khalas at 54.467 % and Ruziz at 47.195 % (Figure 7).

These results indicate that the E-4 microelement combination significantly boosts antioxidant properties, especially in Shishi. Phenolic compounds and antioxidants are essential for plant defense and human health, as they neutralize free radicals and mitigate oxidative stress (Amente and Chimdessa, 2021). Shishi's enhanced response to E-4 supports existing research on the positive effects of specific micronutrient formulations in promoting phenolic and antioxidant responses in date palms (Al-Shwyeh, 2019).

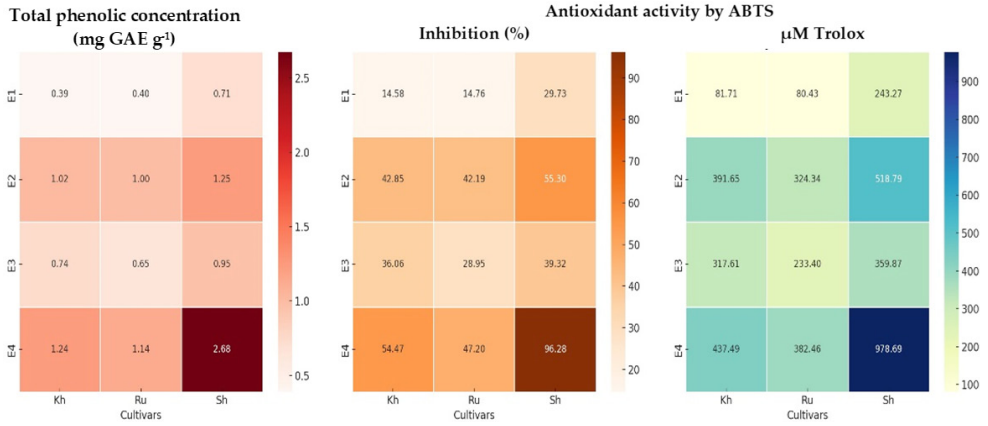

Figure 7. Heatmap visualization of the impact of microelements on phenolic content, antioxidant activity, and µM Trolox levels in date palm (*Phoenix dactylifera* L.) cultivars. Cultivars (Kh: Khalas; Ru: Ruziz; Sh: Shishi). Stock E solution (Zero: E-1; half: E-2; full: E-3; double: E-4).

These findings align with prior studies showing the impact of microelements like zinc, manganese, and copper in activating enzymatic pathways involved in phenolic biosynthesis, enhancing antioxidant capacity in plants (Vazquez-Marquez *et al*., 2024). Overall, E-4, enriched with essential microelements, significantly improved both phenolic content and antioxidant activity across cultivars, with Shishi demonstrating the most robust response. This makes Shishi a promising candidate for further research and agricultural initiatives focused on optimizing antioxidant production. Trace elements play a crucial role in enhancing phenolic biosynthesis and antioxidant activity. For instance, studies on *Glycine max* L. (soybean) and *Triticum aestivum* L. (wheat) have shown similar trends where trace element supplementation leads to increased secondary metabolite production and stress resistance (Zhang, 2023; Amente and Chimdessa, 2021).

The positive correlation between microelement concentration and phenolic content in callus tissues supports the hypothesis that trace elements act as essential cofactors in enzymatic pathways, particularly those involved in phenylpropanoid metabolism. Enhanced activity of enzymes such as PAL and PPO in response to higher microelement concentrations could explain the increased phenolic production and reduced browning in the callus tissues (Vazquez-Marquez *et al*., 2024).

Previous research examined the role of MS medium components in antioxidant formation (Alturki *et al*., 2013; Shehata *et al*., 2014; Aldaej *et al*., 2014). Findings suggest a relationship between medium nutrient strength and the accumulation of secondary metabolites in callus cultures, as full-strength nutrient media primarily promote primary metabolism and cellular growth, which can inhibit tissue differentiation at the morphological and biochemical levels (Hamza *et al*., 2016). Earlier studies have also explored related aspects, such as the effects of various growth regulators and

nutrient media on callus tissue regeneration (Al-Khayri *et al*., 2019), highlighting how nutrient and hormonal environments shape secondary metabolite production.

Mineral elements in the MS medium, such as those in Stock E, are often bound to sulfur compounds (SO_4), highlighting sulfur's essential role in antioxidant formation, cell division, growth, and tissue development in cultured plants (Narayan *et al*., 2022). Sulfur is crucial for plants, as it contributes to amino acids, vitamins, and coenzymes involved in synthesizing proteins, enzymes, and other organic molecules (Al-Mayahi, 2021). Sulfur-containing compounds, including glutathione, are key antioxidants that aid in reducing oxidative stress in plants (Cao *et al*., 2023).

In the MS medium, sulfur is supplemented as adenine sulfate ($AdSO_4$) at 40–80 mg L^{-1}, which, alongside cytokinin, promotes bud and branch formation and supports cell elongation (Rency *et al*., 2018). Trace elements like copper, zinc, and manganese are also introduced as sulfates in Stock E, while iron is provided separately in a chelated form (Stock F) to prevent precipitation, as free iron ions can become toxic to tissues (Xiao *et al*., 2021). Sulfate assimilation enhances sulfur-based antioxidant defenses in plants. Sulfate uptake influences antioxidant production, though its effects on date palm tissues may vary with factors such as physiological state, environmental conditions, and nutrient balance (Drira *et al*., 2022).

Antioxidants are vital in protecting plants from oxidative stress caused by pollutants, UV radiation, and pathogens by neutralizing reactive oxygen species (ROS) (Hasanuzzaman *et al*., 2020). Maintaining balanced micronutrient levels in the medium is essential for optimal antioxidant production in date palm callus tissues. Environmental factors, such as pH and organic matter, can also impact micronutrient availability (Xiao *et al*., 2021; Abd Elaziem *et al*., 2022). Stock E in the MS medium provides key micro-mineral elements, including $ZnSO_4{\cdot}7H_2O$, $CuSO_4{\cdot}5H_2O$, $MnSO_4{\cdot}4H_2O$, and $MgSO_4{\cdot}7H_2O$, each playing a specific role in callus growth, secondary metabolite production, and antioxidant formation.

Zinc is a crucial cofactor for enzymes that regulate oxidative stress and support antioxidant defenses. Zinc deficiency can compromise these defenses, underscoring its importance for plant health and antioxidant synthesis (Amiri *et al*., 2021; Abdellatif *et al*., 2022). Zinc is also fundamental in physiological processes like enzyme activation, photosynthesis, and the synthesis of phenolic compounds and flavonoids, which enhance antioxidant capacity (Lee, 2018). As a cofactor for key antioxidant enzymes, such as superoxide dismutase (SOD) and peroxidase, zinc aids in neutralizing reactive oxygen species (ROS) and reducing oxidative damage. Additionally, its role in chlorophyll structure and photosynthetic efficiency indirectly supports antioxidant production (Lee, 2018; Abdellatif *et al*., 2022). Adequate zinc levels enable the plant to better manage oxidative stress and activate antioxidant defenses as part of its stress response mechanisms.

Copper (Cu) in the form of copper sulfate pentahydrate ($CuSO_4{\cdot}5H_2O$) is an essential micronutrient present in Stock E of the MS medium. Copper is vital for antioxidant defense and various physiological processes in plants, including photosynthesis,

enzyme activation, and secondary metabolite synthesis. As a cofactor for antioxidant enzymes like SOD and ascorbate peroxidase, copper plays a key role in neutralizing ROS. However, copper levels must be balanced carefully, as excess can be toxic (Djamila *et al*., 2022). In the electron transport chain of photosynthesis, copper contributes to energy production. It also affects the synthesis of secondary metabolites, such as phenolic compounds, which can lead to browning in cultured tissues. Oxidation enzymes, such as polyphenol oxidase (PPO) and peroxidase, both of which contain copper, aid in the conversion of phenolics into quinones, causing tissue discoloration from yellow to brown or black.

Browning is caused by PPO-mediated oxidation and may impair explant viability by binding phenols to proteins, thus reducing enzyme effectiveness and ultimately leading to tissue death (Zein El-Din and Ibrahim, 2015). PPO, a copper-dependent enzyme localized in plastids, catalyzes the oxidation of phenolics to quinones, producing pigments in wounded tissue. This reaction, triggered by cellular disruption, is part of the plant's defense against insects and pathogens and plays roles in pigmentation, oxygen scavenging, and chloroplast function (Djamila *et al*., 2022).

Manganese (Mn), provided in the MS medium as manganese sulfate tetrahydrate ($MnSO_4 \cdot 4H_2O$), is essential for plant growth and plays a crucial role in activating enzymes related to antioxidant defense (Zein El-Din *et al*., 2022). Manganese acts as a cofactor for superoxide dismutase (SOD), an enzyme that neutralizes superoxide radicals and supports photosynthesis by participating in the water-splitting reaction, thereby aiding the conversion of light energy into chemical energy. Through these processes, manganese contributes indirectly to antioxidant production and the synthesis of phenolics and flavonoids, which enhance the plant's antioxidant capacity (Bagnoli *et al*., 2002). However, excessive manganese can be toxic, emphasizing the need for balanced levels.

The SE nutrient solution also contains magnesium sulfate heptahydrate ($MgSO_4 \cdot 7H_2O$), or Epsom salt, as a source of magnesium (Mg) and sulfur (S). Magnesium is central to chlorophyll structure and is essential for photosynthesis, as well as activating antioxidant enzymes like SOD, catalase (CAT), and peroxidase (POD), which help to scavenge ROS in plant cells (Al-Shamsi *et al*., 2021; Alkhoori *et al*., 2022). Sulfur supports the synthesis of amino acids, proteins, and antioxidants, contributing to overall plant health and resilience. Thus, $MgSO_4.7H_2O$ in the medium can positively impact antioxidant production in date palm cultures.

Other essential mineral elements in the MS medium, such as boron and molybdenum, are crucial for antioxidant formation in date palm callus cultures. Boron was supplied as boric acid (H_3BO_3) and molybdenum as sodium molybdate ($Na_2MoO_4.2H_2O$), both part of the medium's third group (Stock C) (Table 1). Boron (B) is essential for carbohydrate metabolism, cell wall maintenance, and the synthesis of phenolic compounds with antioxidant properties. Sufficient boron levels support antioxidant production and cell function, while boron deficiency can reduce antioxidant activity (Al-Mayahi, 2020; Gilani *et al*., 2021). Molybdenum (Mo) acts as a cofactor for enzymes involved

in nitrate reduction to ammonia, a key step in nitrogen metabolism that indirectly supports antioxidant production. Optimal molybdenum levels are important for plant health and may contribute to antioxidant synthesis (Schwarz *et al*., 2009).

CONCLUSIONS

Antioxidants can be efficiently produced from date palm explants through tissue culture, providing a year-round, scalable source without relying on fruit ripening or sacrificing cuttings. The Murashige and Skoog medium, enriched with minor mineral elements, supports optimal callus formation even in trace amounts; however, doubling these microelements enhances antioxidant production in cultured explants. Among the cultivars, Shishi, particularly with double Stock E concentration (E-4 treatment), showed strong potential for nutritional and pharmaceutical studies aimed at boosting antioxidant properties. This makes Shishi a promising candidate for future research and agricultural initiatives aimed at increasing antioxidant production.

ACKNOWLEDGEMENTS

I extend my thanks to the Deanship of Scientific Research, Vice Presidency for Graduate Studies and Scientific Research, King Faisal University, Saudi Arabia (Project No. KFU251251), for supporting this research work.

I also extend my sincere thanks to both Prof. Dr. Saleh Alturki and Prof. Dr. Mohammad Aldaej for participating in the previous work of this study. As well as Dr. Jamal Rayyan for his contribution in conducting the statistical analysis for this research.

FUNDING

This work was supported by the Deanship of Scientific Research, Vice Presidency for Graduate Studies and Scientific Research, King Faisal University, Saudi Arabia [Project No. KFU251251].

REFERENCES

Abd Elaziem TM, Ahmed ME, Abou El-Dis GR. 2022. *In vitro* propagation for conservation of the rare date palm (*Phoenix dactylifera* L.) 'Amri' using immature inflorescence. *In Vitro* Cellular and Developmental Biology - Plant 58 (6): 1048–1056. https://doi.org/10.1007/s11627-022-10296-3

Abdellatif YMR, Elsayed MS, Hassan MM, Ahmed IA, Ragab AH, Shams El-Din IM, Abdelaal WB, Abd El-Aal MS, Zein El Din AFM. 2022. Zinc oxide nanoparticles and Fe-modified activated carbon affecting the *in vitro* growth of date palm plantlets cv. Medjool. Horticulturae 8 (12): 1179. https://doi.org/10.3390/horticulturae8121179

Aldaej MI, Alturki SM, Shehata WF, Ghazzawy HS. 2014. Effect of potassium nitrate on antioxidants production of date palm (*Phoenix dactylifera* L.) *in vitro*. Pakistan Journal of Biological Sciences 17 (12): 1209–1218. https://doi.org/10.3923/pjbs.2014.1209.1218

Al-Khayri M J, Jain SM, Johnson DV. 2019. Date palm biotechnology protocols: Volume II: Germplasm conservation and molecular breeding. Humana: New York, NY, USA. 408 p. https://doi.org/10.1007/978-1-4939-7159-6

Alkhoori MA, Kong AS, Aljaafari MN, Abushelaibi A, Lim SE, Cheng WH, Chong CM, Lai KS. 2022. Biochemical composition and biological activities of date palm (*Phoenix dactylifera* L.) seeds: A review. Biomolecules 12 (11): 1626. https://doi.org/10.3390/biom12111626

Almadini AM, Ismail AH, Ameen FA. 2021. Assessment of farmers practices to date palm soil fertilization and its impact on productivity at Al-Hassa oasis of KSA. Saudi Journal of Biological Sciences 28 (2): 1451–1458. https://doi.org/10.1016/j.sjbs.2020.11.084

Al-Mayahi AW. 2020. Effect of calcium and boron on growth and development of callus and shoot regeneration of date palm 'Barhee'. Canadian Journal of Plant Science 100 (4): 357–364. https://doi.org/10.1139/cjps-2019-0084

Al-Mayahi AW. 2021. *In vitro* plant regeneration system for date palm (*Phoenix dactylifera* L.): Effect of chelated iron sources. Journal of Genetic Engineering and Biotechnology 19 (1): 83. https://doi.org/10.1186/s43141-021-00177-4

Al-Saikhan MS. 2006. Physical and chemical characteristics response of three date palm cultivars to source of pollen grains. Journal of Plant Production 31 (3): 1537–1546. https://doi.org/10.21608/jpp.2006.235752

Al-Shamsi SM, Rabert GA, Kurup SS, Alyafei MA, Jaleel A. 2021. Biochemical changes and antioxidant variations in date palm (*Phoenix dactylifera* L.) varieties during flower induction and development. Plants 10 (11): 2550. https://doi.org/10.3390/plants10112550

Al-Shwyeh HA. 2019. Date palm (*Phoenix dactylifera* L.) fruit as potential antioxidant and antimicrobial agents. Journal of Pharmacy and Bioallied Sciences 11 (1): 1–11. https://doi.org/10.4103/jpbs.jpbs_168_18

Alturki SM, Shehata WF, Aldaej MI. 2013. Influence of nutrient medium on antioxidants production of date palm (*Phoenix dactylifera* L.) cultivars *in vitro*. Asian Journal of Plant Sciences 12 (3): 119–127. https://doi.org/10.3923/ajps.2013.119.127

Amente G, Chimdessa E. 2021. Control of browning in plant tissue culture: A review. Journal of Scientific Agriculture 5: 67–71. https://doi.org/10.25081/jsa.2021.v5.7266

Amiri H, Mousavi M, Torahi A. 2021. Improving date palm (*Phoenix dactylifera* L. cv. Estamaran) calogenesis by the use of zinc oxide nanoparticles. Journal of Experimental Biology and Agricultural Sciences 4 (5): 557–563. https://doi.org/10.18006/2016.4(5).557.563

Bagnoli F, Giannin D, Caparrini S, Camussi A, Mariotti D, Racchi ML. 2002. Molecular cloning, characterization and expression of a manganese superoxide dismutase gene from peach (*Prunus persica* [L.] Batsch). Molecular Genetics and Genomics 267 (3): 321–328. https://doi.org/10.1007/s00438-002-0664-7

Batista DS, Felipe SHS, Silva TD, Castro KM, Mamedes- Rodrigues TC, Miranda NA, Ríos-Ríos AM, Faria DV, Fortini EA, Chagas K, Torres-Silva G, Xavier A, Arenciba AD, Otoni WC. 2018. Light quality in plant tissue culture: does it matter?. In Vitro Cellular and Developmental Biology - Plant 54: 195–215. https://doi.org/10.1007/s11627-018-9902-5

Cai Y, Luo Q, Sun M, Corke H. 2004. Antioxidant activity and phenolic compounds of 112 traditional Chinese medicinal plants associated with anticancer. Life Sciences 74 (17): 2157–2184. https://doi.org/10.1016/j.lfs.2003.09.047

Cao Y, Ma C, Yu H, Tan Q, Dhankher OP, White JC, Xing B. 2023. The role of sulfur nutrition in plant response to metal (loid) stress: Facilitating bio-fortification and phytoremediation. Journal of Hazardous Materials 443: 130283. https://doi.org/10.1016/j.jhazmat.2022.130283

Dai Q, Deng Z, Pan L, Nie L, Yang Y, Huang Y, Huang J. 2023. Effects of trace elements on traits and functional active compounds of *Camellia oleifera* in nutrient-poor forests. Forests 14 (4): 830. https://doi.org/10.3390/f14040830

Demsar J, Curk T, Erjavec A, Gorup C, Hocevar T, Milutinovic M, Mozina M, Polajnar M, Toplak M, Staric A, *et al*. 2013. Orange: Data mining toolbox in Pytho. Journal of Machine Learning Research 14: 2349−2353.

Djamila B, Eldine LS, Abderrhmane B, Nassiba A, Barhoum A. 2022. *In vitro* antioxidant activities of copper mixed oxide (CuO/Cu_2O) nanoparticles produced from the leaves of *Phoenix dactylifera* L. Biomass Conversion and Biorefinery 14 (5): 6567–6580. https://doi.org/10.1007/s13399-022-02743-3

Drira M, Elleuch J, Hadjkacem F, Hentati F, Drira R, Pierre G, Gardarin C, Delattre C, El Alaoui-Talibi Z, El Modafar C, *et al*. 2022. Influence of the sulfate content of the exopolysaccharides from *Porphyridium sordidum* on their elicitor activities on date palm vitroplants. Plant Physiology and Biochemistry 186: 99–106. https://doi.org/10.1016/j.plaphy.2022.06.012

Gilani SQ, Basit A, Sajid M, Shah ST, Ullah I, Mohamed HI. 2021. Gibberellic acid and boron enhance antioxidant activity, phenolic content, and yield quality in *Pyrus Communis* L. Gesunde Pflanzen 73 (4): 395–406. https://doi.org/10.1007/s10343-021-00555-5

Gomez KA, Gomez AA. 1984. Statistical procedures for agricultural research (Second edition). John Wiley and Sons: New York, NY, USA. 680 p.

Hamza H, Mrabet A, Jiménez-Araujo A. 2016. Date palm parthenocarpic fruits (*Phoenix dactylifera* L.) cv. Deglet Nour: Chemical characterization, functional properties and antioxidant capacity in comparison with seeded fruits. Scientia Horticulturae 211: 352-357, https://doi.org/10.1016/j.scienta.2016.09.031

Hasanuzzaman M, Bhuyan B, Zulfiqar F, Raza A, Mohsin SM, Al-Mahmud J, Fujita M, Fotopoulos V. 2020. Reactive oxygen species and antioxidant defense in plants under abiotic stress: Revisiting the crucial role of a universal defense regulator. Antioxidants 9 (8): 681. https://doi.org/10.3390/antiox9080681

Ismail AH, Hassaballa AA, Almadini AM, Daffalla S. 2022. Analyzing the spatial correspondence between different date fruit cultivars and farms' cultivated areas, case study: Al-Ahsa Oasis, Kingdom of Saudi Arabia. Applied Sciences 12 (11): 5728. https://doi.org/10.3390/app12115728

Lee SR. 2018. Critical role of zinc as either an antioxidant or a prooxidant in cellular systems. Oxidative Medicine and Cellular Longevity 2018 (1). https://doi.org/10.1155/2018/9156285

Liu J, Wang J, Lee S, Wen R. 2018. Copper-caused oxidative stress triggers the activation of antioxidant enzymes via ZmMPK3 in maize leaves. PLoS ONE 13 (9): e0203612. https://doi.org/10.1371/journal.pone.0203612

MEWA (Ministry of Environment, Water and Agriculture, Water and Agriculture). 2023. Saudi agriculture 2023. Department of General Information and Statistics. Deputyship of Economic and Investment Affairs. Ministry of Environment. Riyadh, Saudi Arabia. https://mewa.gov.sa/en/MediaCenter/Ads/Pages/Saudi-Agriculture-2023.aspx (Retrieved: February 2025).

Murashige T, Skoog FA. 1962. A revised medium for rapid growth and bioassays with tobacco tissue culture. Physiologia Plantarum 15 (3): 473–479. https://doi.org/10.1111/j.1399-3054.1962.tb08052.x

Muszyńska E, Labudda M. 2019. Dual role of metallic trace elements in stress biology—from negative to beneficial impact on plants. International Journal of Molecular Sciences 20 (13): 3117. https://doi.org/10.3390/ijms20133117

Narayan OP, Kumar P, Yadav B, Dua M, Johri AK. 2022. Sulfur nutrition and its role in plant growth and development. Plant Signaling and Behavior 18 (10). https://doi.org/10.1080/15592324.2022.2030082

Pottino BG. 1981. Methods in plant tissue culture. Kemtec Educational Corporation: College Park, MD, USA. 72 p.

Qiu M, Li B, Geng D, Xiang Q, Xin Y, Ding Q, Tang S. 2022. Aminated β-glucan with immunostimulating activities and collagen composite sponge for wound repair. International Journal of Biological Macromolecules 221: 193–203. https://doi.org/10.1016/j.ijbiomac.2022.08.202

Rency AS, Pandian S, Ramesh M. 2018. Influence of adenine sulphate on multiple shoot induction in *Clitoria ternatea* L. and analysis of phyto-compounds in *in vitro* grown plants. Biocatalysis and Agricultural Biotechnology 16: 181–191. https://doi.org/10.1016/j.bcab.2018.07.034

SAS Institute Inc. 2001. SAS for Windows, SAS user's guide: Statistics. Version 8.0 e. User's Guide. Cary, NC, USA.

Schwarz GR, Mendel R, Ribbe MW. 2009. Molybdenum cofactors, enzymes and pathways. Nature 460 (7257): 839–847. https://doi.org/10.1038/nature08302

Shehata WF, Aldaej MI, Alturki SM, Ghazzawy HS. 2014. Effect of ammonium nitrate on antioxidants production of date palm (*Phoenix dactylifera* L.) *in vitro*. Biotechnology 13 (3): 116–125. https://doi.org/10.3923/biotech.2014.116.125

Singleton V, Rossi J. 1965. Colorimetry of total phenolic compounds with phosphomolybdic-phosphotungstic acid reagents. American Journal of Enology and Viticulture 16 (3): 144–158. https://doi.org/10.5344/ajev.1965.16.3.144

Tawaha K, Alali FQ, Gharaibeh M, Mohammad M, El-Elimat T. 2007. Antioxidant activity and total phenolic content of selected Jordanian plant species. Food Chemistry 104 (4): 1372–1378. https://doi.org/10.1016/j.foodchem.2007.01.064

Vazquez-Marquez AM, Bernabé-Antonio A, Correa-Basurto J, Burrola-Aguilar C, Zepeda-Gómez C, Cruz-Sosa F, Nieto-Trujillo A, Estrada-Zúñiga ME. 2024. Changes in growth and heavy metal and phenolic compound accumulation in *Buddleja cordata* cell suspension culture under Cu, Fe, Mn, and Zn enrichment. Plants 13 (8): 1147. https://doi.org/10.3390/plants13081147

Xiao J, Park YG, Guo G, Jeong BR. 2021. Effect of iron source and medium pH on growth and development of *Sorbus commixta in vitro*. International Journal of Molecular Sciences 22 (1): 133. https://doi.org/10.3390/ijms22010133

Zein El-Din AM, Darwesh RSS, Ibrahim MM, Salama GY, Shams El-Din IM, Abdelaal WB, Ali GA, Elsayed MS, Ismail IA, Dessoky ES, Abdellatif YMR. 2022. Antioxidants application enhances regeneration and conversion of date palm (*Phoenix dactylifera* L.) somatic embryos. Plants 11 (15). https://doi.org/10.3390/plants11152023

Zein El-Din AM, Ibrahim HA. 2015. Some biochemical changes and activities of antioxidant enzymes in developing date palm somatic and zygotic embryos *in vitro*. Annals of Agricultural Sciences 60 (1): 121–130. https://doi.org/10.1016/j.aoas.2015.04.002

Zhang J, Sun X. 2021. Recent advances in polyphenol oxidase-mediated plant stress responses. Phytochemistry 181: 112588 https://doi.org/10.1016/j.phyto-chem.2020.112588

Zhang S. 2023. Recent advances of polyphenol oxidases in plants. Molecules 28 (5): 2158. https://doi.org/10.3390/molecules28052158

Agrociencia

IMPACT OF HUANGLONGBING ON THE MEXICAN LIME [*Citrus aurantifolia* (Christm.) Swingle] PHYSICOCHEMICAL QUALITY AND POSTHARVEST LIFE

Aideé **Hernández-Rivera**[1], María Alejandra **Gutiérrez-Espinosa**[2], Rigoberto **González-Mancillas**[3], Apolinar **González-Mancilla**[4], María de Jesús **Martínez-Hernández**[1*]

[1]Universidad Veracruzana. Facultad de Ciencias Agrícolas. Xalapa-Enríquez, Xalapa, Veracruz, Mexico. C. P. 91090.
[2]Colegio de Postgraduados Campus Montecillo. Carretera México-Texcoco km 36.5, Montecillo, Texcoco, State of Mexico, Mexico. C. P. 56264.
[3]Tecnológico Nacional de México. Instituto Tecnológico de la Cuenca del Papaloapan. Juan de la Barrera No. 2, San Bartolo, San Juan Bautista Tuxtepec, Oaxaca, Mexico. C. P. 68446.
[4]Universidad Juárez del Estado de Durango. Facultad de Agricultura y Zootecnia. Carretera Gómez Palacio-Tlahualilo km 32, Venecia Gómez Palacio, Durango, Mexico. C. P. 35170.
* Author for correspondence: mhernandezmj@gmail.com

Citation: Hernández-Rivera A, Gutiérrez-Espinosa MA, González-Mancillas R, González-Mancilla A, Martínez-Hernández MJ. 2025. Impact of huanglongbing on the Mexican lime [*Citrus aurantifolia* (Christm.) swingle] physicochemical quality and postharvest life. **Agrociencia** 59(4): 546-554. https://doi.org/ 10.47163/agrociencia.v59i4.3333

Editor in Chief:
Dr. Fernando C. Gómez Merino

Received: October 31, 2024.
Approved: June 10, 2025.
Published in Agrociencia: June 13, 2025.

ABSTRACT

Huanglongbing (HLB), the most devastating citrus disease, severely impacts the physicochemical quality and postharvest life of Mexican lime fruit [*Citrus aurantifolia* (Christm.) Swingle]. It increases susceptibility to cold-induced damage, accelerates weight loss and senescence, and reduces the content of key components, such as ascorbic acid, ultimately limiting storage time. This study aimed to evaluate the physicochemical quality and postharvest life of Mexican lime fruits, obtained from HLB asymptomatic and symptomatic trees, under ambient and refrigerated storage conditions. Lime fruits were harvested and classified based on the disease status of the source trees (symptomatic and asymptomatic). Two storage conditions were evaluated: room temperature (22 ± 2 °C) for 0, 4, and 8 d and refrigeration (9 ± 1 °C) for two weeks. During the storage period, titratable acidity, ascorbic acid content, weight loss, total soluble solids, and color index were analyzed. Results showed rapid weight loss in the fruits with HLB symptoms, suggesting sensitivity to cold-induced damage. Titratable acidity increased by 40 % in the fruits obtained from symptomatic trees. The color index was also affected in fruits from symptomatic trees after 4 and 8 d of storage at room and refrigeration temperatures, showing signs of senescence compared to asymptomatic fruits. A decrease in ascorbic acid content was also observed, affecting the fruit's nutritional quality and limiting its storage time. In conclusion, HLB significantly affects various quality parameters of the Mexican lime fruit, which increases its susceptibility to cold-induced damage and, consequently, limits its shelf life during storage.

Keywords: color index, weight loss, ascorbic acid, refrigeration, *Candidatus* Liberibacter, physiological disorders.

INTRODUCTION

Mexican lime [*Citrus aurantifolia* (Christm.) Swingle] belongs to the Rutaceae family, which comprises 150 genera and 900 species (Mohammed and Ayoub, 2016). This species is widely used as a raw material in food flavorings, beverage flavor enhancers, and as an ingredient in traditional medicine and cosmetics (Swandiny *et al*., 2021; Indriyani *et al*., 2023). Additionally, it is attributed with various biological activities, such as insecticidal, larvicidal, and repellent properties (Galovičová *et al*., 2022), as well as antioxidant, antineoplastic, and antimicrobial properties (Asmah *et al*., 2020; Julaeha *et al*., 2022). This species also exhibits antiseptic, antiviral, antifungal, astringent, anti-cholesterol, diuretic, appetite-stimulating, and laxative properties (Jeffrey *et al*., 2020). It is also notable for its anti-inflammatory and analgesic properties (Shchérazade *et al*., 2021). These properties are attributed to the content of secondary metabolites (Kazeem *et al*., 2020), making lime a phytogenetic resource with high commercial value.

Lime production faces several yield-impacting challenges, with huanglongbing (HLB) being one of the most devastating citrus diseases worldwide. This disease is associated with bacteria from the *Candidatus* Liberibacter genus, including *Ca*. L. asiaticus (*C*Las), present in Asia, Africa, and America; *Ca.* L. africanus (*C*Laf) in Africa (Jagoueix *et al*., 1994); *Ca.* L. americanus (*C*Lam), reported in Brazil and Asia (Teixeira *et al*., 2005; Antunes *et al*., 2010); and *Ca.* L. caribbeanus (*C*Lca) in Colombia (Folimonova and Achor, 2010; Vitor *et al*., 2013). These bacteria are mainly transmitted by insect vectors. The Asian citrus psyllid (*Diaphorina citri* Kuwayama) is responsible for transmitting *C*Las, *C*Lam, and CLca (da Graça and Kornsten, 2004; Antunes *et al*., 2010), while the African citrus triozid (*Trioza erytreae* Del Guercio) transmits *C*Laf (da Graça and Kornsten, 2004). These insects inoculate the bacteria while feeding on the sap of the leaves (Halbert and Manjunath, 2004; Belasque *et al*., 2010).

Candidatus Liberibacter spp. are Gram-negative bacteria (α-proteobacteria) that are restricted to the phloem of plants, interfering with the translocation of photosynthates and disrupting the movement of nutrients and sugars within the plant's internal tissues (Bendix and Lewis, 2018). This causes the yellowing of new shoots and leaf loss and alters fruit characteristics, such as deformities, changes in size, delayed ripening, modifications in flavor and texture, reduced yield, and decreased commercial quality. Finally, they cause premature fruit drop and tree death (Magomere *et al*., 2009; Bojórquez-Orozco *et al*., 2023). HLB symptoms can be confused with nutrient deficiency or the damage caused by pests and other diseases (Gottwald *et al*., 2007). Therefore, evaluating the physicochemical quality of fruits is fundamental to prevent changes in their properties during postharvest. Nutritional quality has become an essential component of overall quality, serving as a key factor in consumer preference. This study aimed to evaluate the physicochemical quality and postharvest life of Mexican lime fruits obtained from HLB asymptomatic and symptomatic trees under ambient and refrigerated storage conditions.

MATERIALS AND METHODS

Plant material

Mexican lime fruits (*Citrus aurantifolia*) were harvested in a plot located at km 35 of the Colima-Manzanillo highway in Tecomán, Colima, Mexico. A total of 300 asymptomatic fruits were collected from the greenhouse, and 300 HLB-symptomatic fruits were collected from an open field. The fruits were selected based on their uniform size, homogeneous green color, and absence of visible damage. Then, the fruits were washed with running water and commercial soap. Of the total collected, 150 asymptomatic and 150 symptomatic fruits were selected for storage at room temperature (20 ± 2 °C, 55 ± 5 % relative humidity (RH)) for 0, 4, and 8 d. The remaining were stored under refrigeration (9 ± 1 °C, 85 ± 5 % RH) for two weeks. Subsequently, the refrigerated fruits were transferred to room temperature conditions for 4 and 8 additional days to simulate the commercialization process.

Physical and chemical analyses

Changes in physical and chemical quality were evaluated by measuring total soluble solids (TSS) in degrees Brix (°Brix) using a digital refractometer (ATAGO PR-100, Bellevue, USA). Titratable acidity was expressed as grams of citric acid per 100 mL of juice (g 100 mL^{-1}). The ascorbic acid content (vitamin C) was quantified in milligrams of ascorbic acid per 100 ml of juice (mg 100 mL^{-1}) through extraction with oxalic acid and titration with 2,6-dichlorophenol-indophenol, following the AOAC (2023) method.

The external color was determined in the equatorial zone of all fruits using a reflection color meter (Hunter Lab D-25, Reston, VA, USA) based on the CIELab scale. The L*, a*, and b* parameters were used to calculate the color index (CI) using the equation proposed by Jiménez-Cuesta *et al*. (1981):

$$IC = \frac{1000 \times a^*}{b^* L}$$

where a^* defines the direction and degree of chromaticity on the red/green axis, b^* defines the direction and degree of chromaticity on the yellow/blue axis, and L represents luminosity or lightness of a color, from 0 (black) to 100 (white).

The fruit's weight loss (WL) was calculated with the following equation:

$$\%\, WL = \frac{Initial\ weight - Final\ weight}{Initial\ weight} \times 100$$

Statistical analysis

This study followed a completely randomized design. Each fruit was considered an experimental unit, and 50 fruits were used per treatment. All experiments were

carried out in triplicate. The experimental data were subjected to analysis of variance (ANOVA), followed by mean comparison by Tukey test ($p < 0.05$), using the SPSS 23 statistical software (IBM Corporation, Armonk, NY, USA). Normality and homogeneity of variance assumptions were verified using the Shapiro-Wilk and Bartlett tests, respectively. The percentage data were transformed using the following equation:

$$Y = arcsen\left(\sqrt{\frac{x}{100}}\right)$$

where X is the percentage value.

RESULTS AND DISCUSSION

Storage at room temperature

Significant differences in organoleptic quality and postharvest life of the fruits were observed between the evaluated treatments (Table 1). The greatest weight loss was recorded in HLB-symptomatic fruits after 8 d of storage, reaching 17.25 %. On the contrary, the lowest weight loss was observed in asymptomatic fruits after 4 d of storage, with 7.29 %. Regarding internal quality, an increase in titratable acidity was observed, with 9.24 % citric acid in HLB-symptomatic fruits at harvest. The lowest citric acid content (3.53 %) was observed in HLB-symptomatic fruits after 8 d of storage. As for total soluble solids, there were no significant differences between treatments. For the color index, the highest value (-22.06) was observed in asymptomatic fruits at harvest, showing a homogeneous green hue. The lowest color index (-8.46) was observed in HLB-symptomatic fruits after 8 d of storage. These fruits were characterized

Table 1. Organoleptic quality and postharvest life of huanglongbing (HLB) symptomatic and asymptomatic Mexican lime fruits [*Citrus aurantifolia* (Christm.) Swingle] stored under commercialization conditions (20 ± 2 °C, 55 ± 5 % relative humidity).

Treatment	Storage time (days)	Weight loss (%)	Citric acid (%)	Total soluble solids (%)	Color index (1000 *a*/b*L*)	Ascorbic acid (mg 100 mL^{-1})
Fruits with HLB symptoms	0	0.0 d	9.24 a	7.83 a	-18.19 b	41.24 b
	4	10.77 bc	6.40 b	7.46 a	-14.04 c	30.84 c
	8	17.25 a	3.53 d	6.83 a	-8.46 d	21.10 d
Fruits HLB asymptomatic	0	0.0 d	8.36 ab	7.60 a	-22.06 a	50.37 a
	4	7.29 c	7.44 b	7.40 a	-16.18 bc	44.85 b
	8	13.71 b	5.47 c	7.13 a	-12.75 d	33.15 c

Means with different letters within columns are statistically different (Tukey, $p < 0.05$).

by a yellowish hue that deteriorated their appearance, as their postharvest life was reduced due to the senescence process.

Regarding nutritional quality, the highest concentration of ascorbic acid was observed in asymptomatic fruits, with 50.37 mg 100 mL^{-1} of juice at harvest. The lowest concentration of ascorbic acid was recorded in HLB-symptomatic fruits, with 21.1 mg 100 mL^{-1} of juice after 8 d of storage, showing a more pronounced loss of ascorbic acid in the HLB-symptomatic fruits.

The effects of HLB on fruit weight loss were significant, which reduced shelf life. Robles-González *et al*. (2013) reported that Mexican lime fruits from trees with 50–80 % of their canopy damaged by HLB showed reduced size and weight. Muñoz-Lazcano *et al*. (2011) mentioned that Mexican lime fruits have a thinner peel and smaller size, making them more prone to water loss via transpiration, which leads to dehydration and weight loss. In this study, lime fruits started dehydrating over the course of the days, leading to weight loss.

The decrease in citric acid content in the fruits stored at room temperature was more pronounced in those with HLB symptoms. This is similar to that reported by Bassanezi *et al*. (2009) in sweet oranges, where the fruits harvested from trees with HLB symptoms had a greater acidity. As for total soluble solids, no significant differences were observed between groups, which coincides with Robles-González *et al*. (2013), who reported that HLB had no significant effect on the °Brix values of the Mexican lime. On the contrary, Bassanezi *et al*. (2009) observed an increase in °Brix in HLB-symptomatic oranges.

On the other hand, fruits with HLB symptoms showed a greater decrease in green color compared to asymptomatic fruits. Sagaram *et al*. (2009) and Hernández-Rivera *et al*. (2018) reported that HLB-symptomatic Mexican lime fruits had a significantly lower color index as storage time increased. Goldschmidt (1997) observed that the yellowish color in citrus fruits, including Mexican limes, is an adverse effect that leads to quality loss. This is due to the biosynthesis of ethylene (C_2H_4) during postharvest, which accelerates the senescence process, increases respiratory activity, and causes chlorophyll degradation.

Storage under refrigeration conditions

Significant differences were observed in the quality of the fruits stored under refrigeration temperatures (9 ± 1 °C, 85 ± 5 % RH) (Table 2). The greatest weight loss was observed in fruits with HLB symptoms, with a 19.3 % loss after 8 d of storage. Asymptomatic fruits showed a lower weight loss, with 9.6 % after 4 d of storage.

As for internal quality, no significant differences were observed in citric acid content between HLB-asymptomatic and symptomatic fruits, with values of 8.13 and 7.26 %, respectively, after refrigerated storage. The lowest citric acid content was observed in fruits with HLB symptoms, with 2.9 % of citric acid. As for total soluble solids, there were also no significant differences between groups. The color index was higher in asymptomatic fruits (-14.14), with a light green-yellow color, while a lower index was

Table 2. Organoleptic quality and postharvest life of huanglongbing (HLB) symptomatic and asymptomatic Mexican lime fruits [*Citrus aurantifolia* (Christm.) Swingle] stored under refrigeration (9 ± 1 °C, 85 ± 5 % relative humidity) for two weeks, followed by storage at room temperature (20 ± 2 °C, 55 ± 5 % relative humidity).

Treatment	Storage time (days)	Weight loss (%)	Citric acid (%)	Total soluble solids (%)	Color index (1000 *a*/b*L*)	Ascorbic acid (mg 100 mL^{-1})
Fruits with HLB symptoms	0	0.0 d	7.26 a	7.53 a	-12.85 ab	40.48 b
	4	11.8 bc	5.97 b	7.30 a	-8.70 c	31.17 c
	8	19.3 a	2.90 c	6.80 a	-4.50 d	23.67 d
HLB-asymptomatic fruits	0	0.0 d	8.13 a	7.73 a	-14.14 a	47.34 a
	4	9.6 c	6.86 ab	7.66 a	-10.96 b	41.26 b
	8	14.9 b	4.60 b	7.03 a	-7.79 c	31.82 c

Means with different letters within columns are statistically different (Tukey, $p < 0.05$).

observed in symptomatic fruits, with a value of -4.5 after 8 d of storage, showing a yellow hue.

Regarding ascorbic acid, the highest concentration was detected in fruits with HLB symptoms, with 40.48 mg 100 mL^{-1} of juice at harvest. This concentration decreased to 31.17 mg 100 mL^{-1} after 4 d of storage and to 37.67 mg 100 mL^{-1} after 8 d of storage, indicating a continuous loss of this compound. In asymptomatic fruits, the loss of ascorbic acid was lower, with a concentration of 47.34 mg 100 mL^{-1} at harvest, 46.26 mg 100 mL^{-1} at 4 d, and 24 mg 100 mL^{-1} after 8 d of storage, highlighting a greater loss in fruits with HLB symptoms. It is likely that storage at low temperatures reduces the incidence of diseases by inhibiting microbial growth, restricting enzymatic and respiratory activities, inhibiting water loss, delaying quality loss, and reducing ethylene production (da Silva *et al*., 2013).

Fruits with HLB symptoms exhibited faster softening and dehydration during refrigeration storage, along with increased senescence. As described by Cohen *et al*. (1994), Gaytán *et al*. (2012), and Hernández-Rivera *et al*. (2018), weight loss is an indicator of cold-induced damage, which reduces shelf life. Additionally, HLB-symptomatic fruits showed loss of green color and the appearance of brown spots, with some fruits showing signs of decay, further shortening their shelf life. According to Alferez *et al*. (2006), the loss of green color in citrus fruits is related to chlorophyll degradation and the progression of senescence, which explains the decrease in the color index observed during the storage periods. Muñoz-Lazcano *et al*. (2011) also reported a significant loss of green color in Mexican lime fruits without HLB and stored under refrigerated conditions for 2 or 4 weeks.

In this study, both groups of fruits showed a trend of acid content loss as storage days increased, which is consistent with the findings reported by Gaytán *et al*. (2012) in Mexican lime cultures. This group identified that the attack of microorganisms causing rot contributes to the loss of nutraceutical value due to the decrease in ascorbic acid and

the shortened shelf life. This decrease results from the oxidation of ascorbic acid due to senescence progression and hydric stress (Lee and Kader, 2000). According to Corzo-Martínez *et al*. (2012), ascorbic acid oxidation produces monodehydroascorbic acid, which reduces the biologic activity of vitamin C. The principal factors in this process are oxygen concentration, pH, and temperature. Despite the observed alterations, Mexican lime fruits with HLB symptoms could be used in agroindustry as they retain some organoleptic and nutraceutical characteristics.

CONCLUSION

The postharvest behavior of Mexican lime fruits was affected by the presence of huanglongbing symptoms in the source trees, altering their nutraceutical quality (ascorbic acid content), external quality (color index, weight loss), and internal quality (citric acid percentage), both under ambient and refrigerated storage conditions.

ACKNOWLEDGMENTS

Aideé Hernández Rivera thanks the Secretariat of Science, Humanities, Technology, and Innovation (SECIHTI) for the postgraduate scholarship awarded.

REFERENCES

Alferez F, Pozo L, Burns JK. 2006. Physiological changes associated with senescence and abscission in mature citrus fruit induced by 5-chloro-3-methyl-4-nitro-1H-pyrazole and ethephon application. Physiologia Plantarum 127 (1): 66–73. https://doi.org/10.1111/j.1399-3054.2006.00642.x

Antunes LCM, Ferreira RB, Buckner MM, Finlay BB. 2010. Quorum sensing in bacterial virulence. Microbiology 156 (8): 2271–2282. https://doi.org/10.1099/mic.0.038794-0

AOAC (Association of Official Analytical Chemists). 2023. Official methods of analysis (15th edition). Rockville, MD, USA. 1298 p.

Asmah N, Suniarti DF, Margono A, Mas'ud ZA, Bachtiar EW. 2020. Identification of active compounds in ethyl acetate, chloroform, and N-hexane extracts from peels of *Citrus aurantifolia* from Maribaya, West Java, Indonesia. Journal of Advanced Pharmaceutical Technology and Research 11 (3): 107–112. https://doi.org/10.4103/japtr.japtr_177_19

Bassanezi RB, Montesino LH, Stuchi ES. 2009. Effects of huanglongbing on fruit quality of sweet orange cultivars in Brazil. European Journal of Plant Pathology 125 (4): 565–572. https://doi.org/10.1007/s10658-009-9506-3

Belasque JJ, Bassanezi RB, Yamamoto PT, Ayres AJ, Tachibana A, Violante AR, Tank AJ, di Giorgi F, Tersi FEA, Menezes GM, *et al*. 2010. Lessons from huanglongbing management in Sao Paulo State, Brazil. Journal of Plant Pathology 92 (2): 285–302.

Bendix C, Lewis JD. 2018. The enemy within: Phloem-limited pathogens. Molecular Plant Pathology 19 (1): 238–254. https://doi.org/10.1111/mpp.12526

Bojórquez-Orozco AM, Arce-Leal ÁP, Montes RAC, Santos-Cervantes ME, Cruz-Mendívil, A, Méndez-Lozano J, Leyva-López NE. 2023. Differential expression of miRNAs involved in

response to *Candidatus* Liberibacter asiaticus infection in Mexican lime at early and late stages of huanglongbing disease. Plants 12 (5): 1039. https://doi.org/10.3390/plants12051039

Cohen E, Shapiro B, Shalom Y, Klein JD. 1994. Water loss: Nondestructive indicator of enhanced cell membrane permeability of chilling injured citrus fruit. Journal of the American Society Horticultural Science 119 (5): 983–986. https://doi.org/10.21273/jashs.119.5.983

Corzo-Martínez M, Corzo N, Villamiel M, del Castillo MD. 2012. Browning reactions. Food Biochemistry and Food Processing. *In* Simpson BK. (ed.), Food Biochemistry and Food Processing (Second Edition). John Wiley and Sons: Hoboken, NJ, USA, pp: 56–83. https://doi.org/10.1002/9781118308035.ch4

da Graça JV, Kornsten L. 2004. Citrus huanglongbing: Review, present status and future strategies. *In* Naqvi AMH. (ed.), Diseases of Fruits and Vegetables Volume I, Diagnosis and Management. Springer: Dordrecht, Netherlands, pp: 229–245. https://doi.org/10.1007/1-4020-2606-4_4

da Silva PG, Machado FL de C, da Costa JMC. 2013. Quality of 'Delta Valencia' orange grown in semiarid climate and stored under refrigeration after coating with wax. Food Science and Technology 33 (2): 276–281.

Folimonova SY, Achor DS. 2010. Early events of citrus greening (huanglongbing) disease development at the ultrastructural level. Phytopathology 100 (9): 949–958. https://doi.org/10.1094/phyto-100-9-0949

Galovičová L, Borotová P, Vukovic NL, Vukic M, Kunová S, Hanus P, Kowalczewski PŁ, Bakay L, Kačániová M. 2022. The potential use of *Citrus aurantifolia* L. essential oils for decay control, quality preservation of agricultural products, and anti-insect activity. Agronomy 12 (3): 735. https://doi.org/10.3390/agronomy12030735

Gaytán IF, Veloz CS, Franci SHC, León MTC, Espinoza JS. 2012. Efectividad del encerado y metil jasmonato en el control de daños por frío asociados al tratamiento de cuarentena por fríos en pomelos "Rio Red". Revista Iberoamericana de Tecnología Postcosecha 13 (2): 146–152.

Goldschmidt EE. 1997. Ripening of citrus and other non-climateric fruits: A role for ethylene. Acta Horticulturae 463: 333–340. https://doi.org/10.17660/actahortic.1998.463.42

Gottwald TR, Graca JVD, Bassanezi RB. 2007. Citrus huanglongbing: The pathogen and its impact. Plant Health Progress 8 (1): 31. https://doi.org/10.1094/php-2007-0906-01-rv

Halbert SE, Manjunath K. 2004. Asian citrus psyllids (Sternorrhyncha: Psyllidae) and greening disease of citrus: A literature review and assessment of risk in Florida. Florida Entomologist 87 (3): 330–353.

Hernández-Rivera A, Arellano-Ostoa G, Robles-Gonzáles MM, Jaén-Contreras D, Contreras-Oliva A, Saucedo-Veloz C. 2018. Calidad y vida postcosecha de frutos de limones mexicanos provenientes de árboles con síntomas de HLB y asintomáticos. Revista Mexicana de Ciencias Agrícolas 9 (8): 1801–1807. https://doi.org/10.29312/remexca.v9i8.1724

Indriyani NN, Anshori JA, Permadi N, Nurjanah S, Julaeha E. 2023. Bioactive components and their activities from different parts of *Citrus aurantifolia* (Christm.) Swingle for food development. Foods 12 (10): 2036. https://doi.org/10.3390/foods12102036

Jagoueix S, Bove JM, Garnier M. 1994. The phloem-limited bacterium of greening disease of citrus is a member of the α subdivision of the Proteobacteria. International Journal of Systematic and Evolutionary Microbiology 44 (3): 379–386. https://doi.org/10.1099/00207713-44-3-379

Jeffrey J, Sudigdoadi S, Kurnia D, Satari MH. 2020. A monoterpenoid isolated from *Citrus aurantifolia* peel and its potential as an antibacterial for the inhibition and eradication of *Streptococcus mutans* biofilm. Systematic Reviews in Pharmacy (11): 1205–1210. https://doi.org/10.31838/srp.2020.6.175

Jiménez-Cuesta M, Cuquerella J, Martínez-Jávega JM. 1981. Determination of color index for fruit degreening. Proceedings of the International Society of Citriculture 2 (3): 750–753.

Julaeha E, Nurzaman M, Wahyudi T, Nurjanah S, Permadi N, Anshori JA. 2022. The development of the antibacterial microcapsules of citrus essential oil for the cosmetotextile application: A review. Molecules 27 (22): 8090. https://doi.org/10.3390/molecules27228090

Kazeem MI, Bancole HA, Oladokun TI, Bello AO, Maliki, MA. 2020. *Citrus aurantifolia* (Christm.) Swingle (lime) fruit extract inhibits the activities of polyol pathway enzymes. Efood 1 (4): 310–315. https://doi.org/10.2991/efood.k.200824.001

Lee SK, Kader AA. 2000. Preharvest and postharvest factors influencing vitamin C content of horticultural crops. Postharvest Biology and Technology 20 (3): 207–220. https://doi.org/10.1016/S0925-5214(00)00133-2

Magomere TO, Obukosia SD, Mutitu E, Ngichabe C, Olubayo F, Shibairo S. 2009. Molecular characterization of '*Candidatus* Liberibacter' species/strains causing huanglongbing disease of citrus in Kenya. Electronic Journal of Biotechnology 12 (2): 5–6.

Mohammed RMO, Ayoub SMH. 2016. Study of phytochemical screening and antimicrobial activity of *Citrus aurantifolia* seed extracts. American Journal of Analytical Chemistry 7 (3): 254. https://doi.org/10.4236/ajac.2016.73022

Muñoz-Lazcano AC, Saucedo-Veloz C, García-Osorio, Robles-Gonzáles M. 2011. Evaluación de la calidad y tiempo de almacenamiento del fruto en tres variedades de limón mexicano. Revista Iberoamericana de Tecnología Postcosecha 12 (2): 156–163.

Robles-González MM, Velázquez-Monreal J, Manzanilla-Ramírez MÁ, Orozco-Santos M, Medina-Urrutia VM, López-Arroyo JI, Flores-Virgen R. 2013. Síntomas del huanglongbing (HLB) en árboles de limón mexicano [*Citrus aurantifolia* (Christm.) Swingle] y su dispersión en el estado de colima, México. Revista Chapingo Serie Horticultura 19 (1): 15–31. https://doi.org/10.5154/r.rchsh.2012.01.005

Sagaram US, de Angelis KM, Trivedi P, Andersen GL, Lu SE, Wang N. 2009. Bacterial diversity analysis of huanglongbing pathogen-infected citrus, using PhyloChip arrays and 16S rRNA gene clone library sequencing. Applied and Environmental Microbiology 75 (6): 1566–1574. https://doi.org/10.1128/aem.02404-08

Shchérazade OSF, Pétronille AZ, Joseph FKY, Georges A.2021. Study of the analgesic effect of the aqueous extract of the leaves of *Citrus aurantifolia* (Rutaceae) in mice. GSC Biological and Pharmaceutical Sciences 14 (3): 207–214. https://doi.org/10.30574/gscbps.2021.14.3.0072

Swandiny GF, Nafisa S, Gangga E, Fauzi M. 2021. Standardization of 70 % ethanol extract and 96 % lime leaves as antioxidants with DPPH and FRAP. Journal of Pharmacognosy and Phytochemistry 10 (4): 47–52.

Teixeira DC, Danet JL, Eveillard S, Martins EC, de Jesus WCJR, Yamamoto PT, Bové JM. 2005. Citrus huanglongbing in Sao Paulo State, Brazil: PCR detection of the *Candidatus* Liberibacter species associated with the disease. Molecular and Cellular Probes 19 (3): 173–179. https://doi.org/10.1016/j.mcp.2004.11.002

Vitor HB, Gabriel RR, Marcos RF, Alexandre DCU, Luiz FG, Wesley ACG, Pedro TY. 2013. Population Dynamics of *Diaphorina citri* Kuwayama (Hemiptera: Liviidae) in orchards of Valencia orange, Ponkan mandarin and Murcott tangor trees. Florida Entomologist 96 (1): 173–179. https://doi.org/10.1653/024.096.0123

Agrociencia

PREVENTION AND CONTROL OF *Fusarium oxysporum* Schltdl. USING BENEFICIAL ORGANISMS IN *Pinus oocarpa* Schiede ex Schltdl.

Diana Laura **Rodríguez-Castañeda**[1], Arnulfo **Aldrete**[1]*, Javier **López-Upton**[1], Víctor M. **Cetina-Alcalá**[1], Silvia E. **García-Díaz**[2]

[1]Colegio de Postgraduados Campus Montecillo. Postgrado en Ciencias Forestales. Carretera México-Texcoco km 36.5, Montecillo, Texcoco, State of Mexico, Mexico. C. P. 56264.
[2]Universidad Autónoma Chapingo. División de Ciencias Forestales. Carretera México-Texcoco km 38.5, Chapingo, Texcoco, State of Mexico, Mexico. C. P. 56230.
* Author for correspondence: aaldrete@colpos.mx

Citation: Rodríguez-Castañeda DL, Aldrete A, López-Upton J, Cetina-Alcalá VM, García-Díaz SE. 2025. Prevention and control of *Fusarium oxysporum* Schltdl. using beneficial organisms in *Pinus oocarpa* Schiede ex Schltdl. **Agrociencia** 59(4): 555-567. https://doi.org/ 10.47163/agrociencia.v59i4.3270

Editor in Chief:
Dr. Fernando C. Gómez Merino

Received: July 12, 2024.
Approved: June 13, 2025.
Published in Agrociencia: June 16, 2025.

ABSTRACT

The most common disease in forest nurseries is damping-off, commonly caused by the fungus *Fusarium oxysporum* Schltdl. The objective of this study was to evaluate the effect of a commercial product based on microorganisms (Bactiva®) and a strain of *Trichoderma paratroviride* Jaklitsch and Voglmayr on the incidence of damping-off and the morphology of *Pinus oocarpa* Schiede ex Schltdl. plants inoculated with *F. oxysporum*. A completely randomized design was used, with treatments in an increased factorial arrangement, to evaluate two biological products (a commercial product and *T. paratroviride*) and three application forms (to the seed, to the substrate, and through irrigation) were evaluated, with an additional control inoculated only with *F. oxysporum*. The factors revealed that using the commercial product and applying it to the seed reduced the incidence rate to 25 and 23%, respectively. In terms of interactions, the application of the commercial product to the seed, to the substrate, and by irrigation, and with *T. paratroviride* to the seed and by irrigation, showed the lowest percentage of incidence (<30 %). At 195 days after sowing, *T. paratroviride* and substrate application improved plant morphology. The interactions showed that the highest root collar diameter (6.5 mm), plant height (23.2 cm), aerial dry weight (3.15 g), total dry weight (4.15 g), and Dickson quality index (0.61) were obtained with substrate-applied *T. paratroviride*. However, the lowest sturdiness quotient was obtained with the control (3.27), while for root dry weight and aerial dry weight over root dry weight, there were no differences among the treatments evaluated.

Keywords: Pinaceae, biological control, damping-off, *Trichoderma paratroviride.*

INTRODUCTION

In Mexico, forest nurseries produce approximately 180 million plants per year, which are used in reforestation and ecosystem restoration to reduce soil degradation and mitigate the negative effects of climate change (Andivia *et al*., 2021). The significance of nursery management practices lies in their impact on plant quality, specifically their

morphological and physiological characteristics, which directly influence their ability to adapt to the conditions of the transplanting site (Rueda-Sánchez *et al*., 2014; Aldrete *et al*., 2023). On the other hand, according to Cibrián-Tovar *et al*. (2008), the decrease in forest mass is caused by land use change, overgrazing, and the presence of pests and diseases; the latter also cause the death of reforested trees and nursery plants, resulting in a significant economic loss for nurserymen.

Damping-off is a disease characterized by rotting at the base of the plant stem, resulting in wilting and death (Larios-Larios *et al*., 2019). According to Mojica-Marín *et al.* (2009), it is caused by the genera *Fusarium*, *Rhizoctonia*, *Pythium*, and *Phytophthora*. In the Mexican state of Durango, Prieto *et al*. (2009) found this disease in all nurseries evaluated. *Fusarium* fungi, for example, are filamentous, cosmopolitan ascomycetes with well-developed, septate mycelium and distinctive conidiophores (Sumalan *et al*., 2013). Their damage triggers a series of irreversible conditions in the host, which start in the roots or the above-ground parts of the plant (Ma *et al*., 2013). To avoid the proliferation of this pathogen, appropriate management is required in the nursery. Among the management actions used, the application of chemicals stands out, which frequently endangers human health and may cause pathogen resistance (García-Díaz *et al*., 2017). To prevent this disease, it is recommended to use certified and sanitized seeds and control irrigation after planting to avoid excess soil moisture (Gordon *et al*., 2015).

Okorski *et al*. (2014) indicate that in the control of *Fusarium oxysporum*, natural enemies of the pathogen can be used as biological control agents, which contributes to environmental conservation and prevents the pathogen from developing resistance. Additionally, natural enemies feed on organic matter and have the ability to compete for the nutrients required by pathogens. Generally, they present several mechanisms of competition and inhibition in the presence of pathogens such as *F. oxysporum*, so they are an effective and direct alternative against these types of diseases (Okorski *et al*., 2014).

Fungi of the genus *Trichoderma* are used as biological control agents against phytopathogenic fungi due to their mechanisms of action, which include antibiosis, mycoparasitism, production of secondary metabolites, and competition for space and nutrients (Hernández-Melchor *et al*., 2019). Sánchez-Rangel *et al*. (2016) obtained similar incidence percentages when applying Captan, copper sulfate pentahydrate, and two *Trichoderma* strains (SP6 and SP12) on plants of *Carica papaya* L. Meanwhile, García-Díaz *et al*. (2019) demonstrated that *T. harzianum* decreased the incidence of *Fusarium circinatum* on seedlings of *Pinus greggii* Engelm. ex Parl. when using sawdust as substrate. Larios-Larios *et al.* (2019) reduced the incidence of damping-off in *Capsicum chinense* Jacq. seedlings by applying *Trichoderma* spp. to the foliage. Rodríguez-Pinto *et al.* (2021) reduced wilt caused by *Fusarium* spp. on *Solanum melongena* L. plants *in vitro* and in the field by using native *Trichoderma* strains isolated and used as biocontrol. Ortega-Cerón *et al*. (2024) reported that applying *T. harzianum* to the substrate on *Pinus devoniana* Lindl. plants decreased the pathogenicity of *F. circinatum.*

Among the species produced in forest nurseries, *Pinus oocarpa* Schiede ex Schltdl. has the potential to be used in reforestation programs, since it is capable of growing in both fertile and marginal soils; in addition, it presents adequate production characteristics due to its growth speed and the conservation status of its populations (Fabián-Plesníková *et al*., 2020; CONAFOR, 2022). Considering the above, the objective of this research was to evaluate the effect of a commercial product based on microorganisms and a strain of *T. paratroviride*, using different forms of application, on the incidence of damping-off and the morphology of *P. oocarpa* plants inoculated with *F. oxysporum*, under the hypothesis that these products reduce the incidence of the pathogen and modify the morphology of the plants.

MATERIALS AND METHODS

Trial set-up

The experiment was established in a greenhouse of the Forestry Sciences Division of the Autonomous University of Chapingo in the municipality of Texcoco, State of Mexico, Mexico (19° 29′ 34″ N and 98° 53′ 38″ W, at an altitude of 2240 m). Seeds of *Pinus oocarpa* Schiede ex Schltdl. were collected from a natural population of the species in the municipality of San Simón de Guerrero, State of Mexico, by the National Institute of Forestry, Agriculture, and Livestock Research. Two *P. oocarpa* seeds, previously soaked in water (24 h) and disinfested in commercial chlorine (5 %), were sown in containers with a substrate of peat, perlite, and vermiculite 3:1:1 v/v, combined with a controlled-release fertilizer (7 g L^{-1}). Since they are artificial substrates, they were considered to be innocuous to a certain extent, so no sterilization process was applied. At 35 days after sowing (dds), a thinning was carried out, where one plant per container was left. Irrigation was applied every third day with tap water without causing splashing between the trays.

Experimental design and study factors

Two biological products were evaluated using a completely randomized design with treatments in an increased factorial arrangement. One of the products was a commercial product (Bactiva® TNI, Germany) based on fungi from the *Trichoderma* and *Gliocladium* genera, bacteria from the *Bacillus* and *Pseudomonas* genera, and a marine alga (*Ascophyllum nodosum*). The other was a strain of *Trichoderma paratroviride* that was collected from a plantation of *Eucalyptus* spp. in the state of Tabasco, Mexico. Both products were evaluated in three different application ways (to the seed, to the substrate, and through irrigation). Additionally, there was a control in which only *Fusarium oxysporum* was inoculated to the substrate at the base of the plant. Four replicates per treatment were carried out, which generated 28 experimental units, each one consisting of a tray with 42 plants in individual containers of 170 mL capacity.

Pathogen inoculation

At 49 dds, 20 mL of distilled water with two drops of polysorbate 20 and a concentration of 1×10^7 conidia per milliliter of *F. oxysporum* were applied to the substrate at the base of the plant. The inoculum was obtained from purified Petri dishes identified with the pathogen. At 90 dds, a pathogenicity test was performed by evaluating four plants with wilt symptoms per treatment (Soria *et al*., 2012). In this understanding, where only the pathogen (control) was inoculated, only *F. oxysporum* was found, and in those where the commercial product and the *T. paratroviride* strain were applied, the presence of the pathogen and *Trichoderma* was confirmed.

Application of the commercial product and *Trichoderma paratroviride*

The concentration used of the commercial product and *T. paratroviride* was 1 g L^{-1} and 1×10^7 conidia mL^{-1} water, respectively. When applied to the seed, it was allowed to stand for 5 min in 200 mL of sterile distilled water with the corresponding treatment before sowing. The application to the substrate took place while the substrate was being prepared, and the established concentration was diluted in 200 mL of sterile distilled water. At 49 dds, the treatments were applied through irrigation, where the established concentration was combined in sterile distilled water (200 mL), and all the trays belonging to each treatment were uniformly irrigated.

Response variables

Incidence of *Fusarium oxysporum*

The incidence of this pathogen was evaluated weekly by recording the number of plants per experimental unit with typical symptoms of the disease (Soria *et al*., 2012), i.e., color changes in needles and terminal bud wilting. In this sense, the accumulated percentage of dead plants in relation to the initial number of plants was obtained over 17 weeks from 49 dds. These values were transformed with the arcsine function prior to analysis.

Morphological indices in *Pinus oocarpa* plants

At the end of the experiment (195 dds), 12 plants per experimental unit were taken and removed from the container to eliminate all the root substrate. Root collar diameter was measured with a digital vernier in millimeters. Plant height was measured with a ruler graduated in centimeters, from the base of the stem to the apical bud. To measure root dry weight, aerial dry weight, and total dry weight, the root and aerial part of the plant were divided, placed separately in paper bags labeled with their experimental unit, and dried in an oven for 72 h at 70 °C. The ratio of aerial and root dry weight, sturdiness quotient, and Dickson's quality index were calculated according to Aldrete *et al*. (2023).

Statistical analysis

Data were analyzed for normality (Shapiro-Wilk) ($p \geq 0.05$), variance homogeneity (Bartlett) ($p \geq 0.05$), and residue independence tests; likewise, an analysis of variance was performed by as proposed by Federer (1955), corresponding to a randomized design with treatments in an increased factorial arrangement, and a multiple comparison of means with Tukey's honest minimum significant difference test ($p \leq 0.05$) using the R statistical program version 4.3.2.

RESULTS AND DISCUSSION

Incidence of *Fusarium oxysporum*

In both factors, the percentage of incidence increased similarly up to week eight between both biological products and the three forms of application (Figure 1).

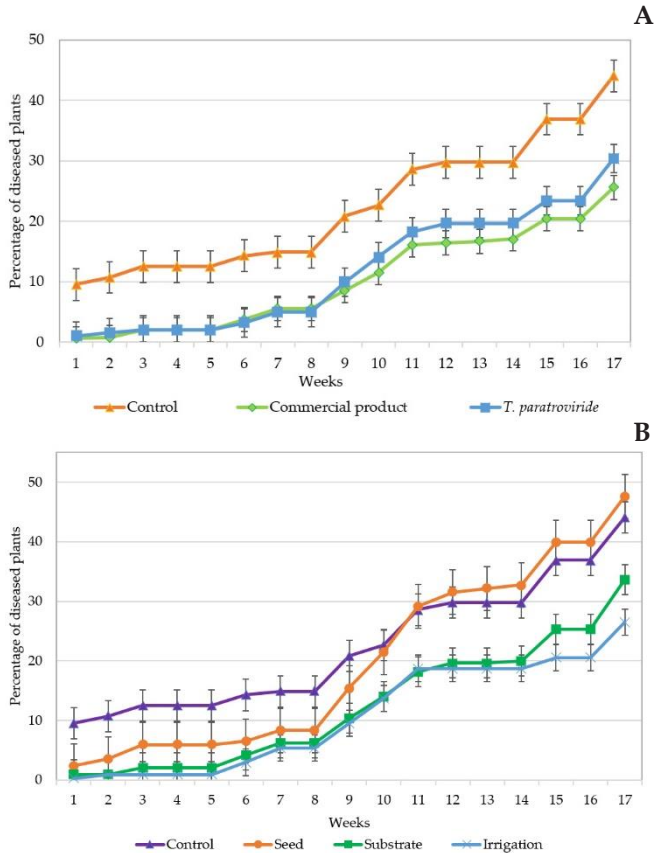

Figure 1. Percentage of cumulative incidence from inoculation of *Fusarium oxysporum* on *Pinus oocarpa* Schiede ex Schltdl. plants during 17 weeks of evaluation by the effect of the interaction of the product applied and the mode of application, and an additional control. A: biological product factor (Bactiva® and *Trichoderma paratroviride*); B: application form factor (seed, substrate, and irrigation). The standard deviation is indicated.

However, after this week, the percentages began to show different increases. In the biological product factor, *T. paratroviride* increased in relation to the commercial product until week 17, where the lowest percentage corresponded to the commercial product (25 %), followed by *T. paratroviride* (30 %) and the additional control (44 %) (Figure 1A). On the other hand, in the application method factor, application to the seed reported the lowest incidence percentages up to week 17 (23 %), in contrast to application through irrigation (26 %), to the substrate (33 %), and the control (44 %) (Figure 1B).

Regarding the interaction of factors and the additional control, the manifestation of disease symptoms in *P. oocarpa* plants started in the first week after inoculation (sdi) in the control (T_1), in some plants of treatments T_3, T_5, and T_7, and none of T_2, T_4, and T_6 (Figure 2). From the eighth sdi, there was a considerable increase in the percentage of incidence, where the application of *T. paratroviride* to the substrate and through irrigation presented a percentage close to the control. However, at 17 sdi, the control reported a 44 % incidence, a value close to that of *T. paratroviride* applied to the substrate (39 %) and higher than the rest of the treatments, which were found to be below 30 %.

The time in which symptoms appeared was similar to that reported by García-Díaz *et al.* (2019), who inoculated the substrate with *F. circinatum* on *P. greggii* plants and

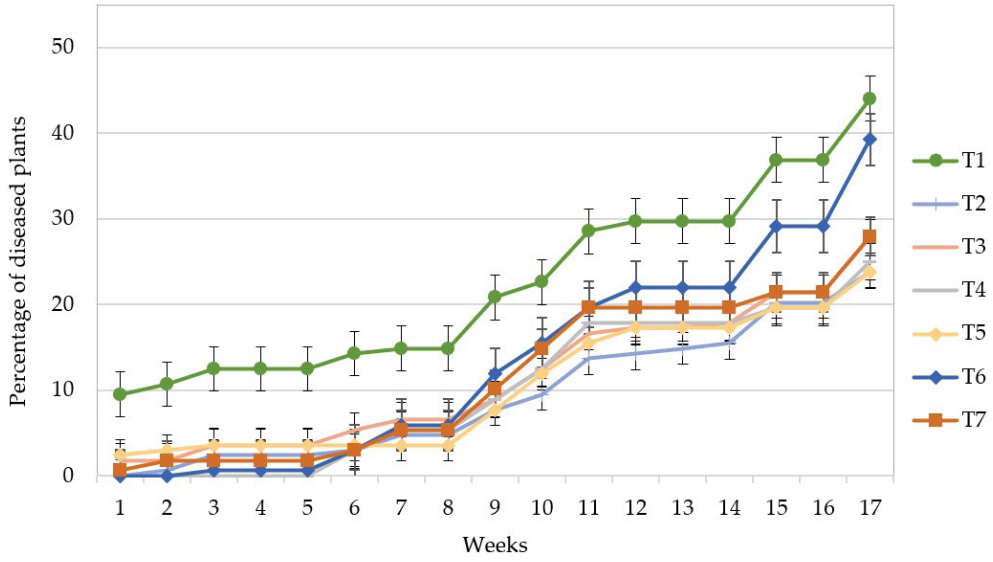

Figure 2. Percentage of cumulative incidence from inoculation of *Fusarium oxysporum* in *Pinus oocarpa* Schiede ex Schltdl. plants during 17 weeks of evaluation by the effect of the interaction of the product applied and the mode of application for the control of the pathogen, and an additional control. T_1: control; T_2: commercial product (Bactiva®) applied to the seed; T_3: commercial product applied to the substrate; T_4: commercial product applied by irrigation; T_5: *Trichoderma paratroviride* applied to the seed; T_6: *T. paratroviride* applied to the substrate; T_7: *T. paratroviride* applied by irrigation. The standard deviation is indicated.

found that the manifestation of the first symptoms occurred 20 days after inoculation. These findings were different from those of Robles-Carrión *et al.* (2014), where inoculating *F. oxysporum* to the substrate in plants of *Vasconcellea* × *heilbornii* (V.M. Badillo) V.M. Badillo, reported that symptomatology began 30 days after inoculation. Contrary to Soria *et al*. (2012), who suggest that a plant must have a wound in order for the pathogen to enter the tissue, the effects demonstrated in this study concur with García-Díaz *et al*. (2019), who assert that *Fusarium* spp. can directly infect the tissue even in the absence of a wound.

On the other hand, the commercial product and the application to the seed attenuated the incidence of the pathogen. Likewise, *T. paratroviride* applied to the seed and by irrigation reduced the incidence in a similar way to that of the commercial product in all forms of application. Bactiva® has a mixture of *T. harzianum, T. reesei, T. viride, Gliocladium virens, Bacillus subtilis, B. megaterium, B. polymyxa, Pseudomonas fluorescens,* and *Ascophyllum nodosum.* The findings demonstrated a better efficacy of the commercial product against the *T. paratroviride* strain, attributed to the mixture of strains present in the product, of which several authors have demonstrated the positive effects of the *Trichoderma* (Amaral *et al*., 2019; Rodríguez-Pinto *et al*., 2021; Ortega-Cerón *et al*., 2024) and *Bacillus* genus (Mejía-Bautista *et al*., 2016) in the control of *Fusarium*.

Similarly, when biological products were applied to the seed, a lower percentage of incidence was observed. Kthiri *et al*. (2020) indicate that when applying *Trichoderma* spp. to the seed there is an early relationship between the fungus and the roots of the seedling, which allows a better colonization in the rhizosphere and presents a positive effect on the development of the plant by having a greater tolerance to stress and a better absorption of nutrients.

The incidence reduction caused by *Trichoderma* application coincides with García-Díaz *et al*. (2019), Rodríguez-Pinto *et al*. (2021), and Ortega-Cerón *et al*. (2024), who were able to reduce the incidence of *Fusarium* spp. by applying *Trichoderma* spp. on *P. greggii*, *Solanum melongena*, and *P. devoniana*, respectively. According to Navaneetha *et al*. (2015), the positive effect of *Trichoderma* as a biocontrol agent against different pathogens is due to its ability to synthesize proteins, enzymes, antibiotics (antagonistic compounds), and substances that promote plant growth, such as vitamins and hormones. Joo and Hussein (2022) reported that the volatile organic compounds produced by *Trichoderma* spp. are a key factor in suppressing harmful rhizosphere microorganisms and enhancing defense. Amaral *et al*. (2019) found that *T. viride* shows good root colonization and has a prominent impact on defense mechanisms in pine plants.

Morphological indexes of plants

According to the analysis of variance, for the biological product factor, there were only significant differences in plant height (PLH), aerial dry weight (ADW), and total dry weight (TDW); the highest values were obtained with the *T. paratroviride* strain, with 19.81 cm and 2.43 and 3.31 g, respectively (Table 1). Regarding the application method,

significant differences only occurred in root collar diameter (RCD), ADW, TDW, and sturdiness quotient (SQ). Substrate application produced higher values in RCD, ADW, and TDW, but lower values in SQ, whereas seed application produced intermediate values (Tables 1 and 2).

On the other hand, for the interactions and the additional control, the analysis of variance only found significant differences in the RCD, PLH, ADW, TDW, SQ, and Dickson quality index (DQI) (Tables 1 and 2), where the application of *T. paratroviride* to the substrate had the highest RCD (6.5 mm), PLH (23.2 cm), ADW (3.15 g), TDW (4.15 g), and DQI (0.61). However, the best SQ was obtained with the control (3.27). As this variable shows the balance between the aerial and root parts, the lower the index, the better the balance in the plant. In this sense, sturdiness allows estimating the physical resistance of the plants during planting operations and their resistance to the mechanical effect of the wind (Gomes *et al*., 2002).

Table 1. Multiple comparison of means of the variables root collar diameter, plant height, and dry weight by the effect of the factors, their interaction, and the additional control in *Pinus oocarpa* Schiede ex Schltdl. plants inoculated with *Fusarium oxysporum* at 195 days after planting.

T	Biological product	Application form	RCD (mm)	PLH (cm)	PSR	ADW	TDW
					(g)		
	PC		4.61 a	17.45 b	0.76 a	1.94 b	2.71 b
	TP		5.02 a	19.81 a	0.87 a	2.43 a	3.31 a
		Seed	4.71 ab	18.5 a	0.78 a	2.10 ab	2.88 ab
		Substrate	5.65 a	20.00 a	0.85 a	2.56 a	3.42 a
		Irrigation	4.08 b	17.3 a	0.82 a	1.90 b	2.72 b
T_1	Control		4.61 ab	15.04 b	0.71 a	1.76 b	2.47 b
T_2	PC	Seed	5.04 ab	18.37 b	0.81 a	2.08 b	2.90 b
T_3	PC	Substrate	4.80 ab	16.80 b	0.71 a	1.97 b	2.69 b
T_4	PC	Irrigation	3.98 b	17.18 b	0.76 a	1.77 b	2.54 b
T_5	TP	Seed	4.37 b	18.75 ab	0.74 a	2.13 b	2.87 b
T_6	TP	Substrate	6.50 a	23.20 a	0.99 a	3.15 a	4.15 a
T_7	TP	Irrigation	4.17 b	17.76 b	0.87 a	2.02 b	2.90 b
General mean factors			4.81	18.63	0.81	2.19	3.01
General mean treatments			4.75	17.94	0.80	2.10	2.91
CV (%)			17.39	10.62	20.85	18.27	16.37
$MSD_{0.05}$ biological product			0.78	1.79	0.14	0.36	0.44
$MSD_{0.05}$ form of application			1.17	2.67	0.21	0.54	0.65
$MSD_{0.05}$ treatments			1.93	4.46	0.37	0.90	1.11

T: treatment; RCD: root collar diameter; PLH: plant height; PSR: root dry weight; ADW: aerial dry weight; TDW: total dry weight; PC: commercial product (Bactiva®); TP: *Trichoderma paratroviride*; CV: coefficient of variation; $MSD_{0.05}$: minimum significant difference with a significance of 0.05. Values with the same letter are statistically equal according to Tukey's honest minimum significant difference test ($p \leq 0.05$).

Table 2. Multiple comparison of means of the variables evaluated for the effect of the factors, their interaction, and additional control in *Pinus oocarpa* Schiede ex Schltdl. plants inoculated with *Fusarium oxysporum* 195 days after sowing.

T	Biological product	Application form	ADWR	SQ	DQI
	PC		2.55 a	3.83 a	0.42 a
	TP		2.84 a	4.10 a	0.48 a
		Seed	2.72 a	3.97 ab	0.43 a
		Substrate	2.96 a	3.62 b	0.52 a
		Irrigation	2.41 a	4.32 a	0.40 a
T_1	Control		2.47 a	3.27 b	0.43 ab
T_2	PC	Seed	2.57 a	3.66 a	0.46 ab
T_3	PC	Substrate	2.78 a	3.52 a	0.42 ab
T_4	PC	Irrigation	2.32 a	4.32 a	0.38 b
T_5	TP	Seed	2.88 a	4.29 a	0.40 b
T_6	TP	Substrate	3.14 a	3.71 a	0.61 a
T_7	TP	Irrigation	2.50 a	4.32 a	0.43 ab
	General mean factors		2.70	3.97	0.45
	General mean treatments		2.64	3.84	0.45
	CV (%)		16.90	10.87	19.10
	$MSD_{0.05}$ biological product		0.41	0.39	0.07
	$MSD_{0.05}$ form of application		0.61	0.59	0.11
	$MSD_{0.05}$ treatments		1.04	0.97	0.20

T: treatment; ADWR: aerial dry weight over root dry weight; SQ: sturdiness quotient; DQI: Dickson quality index; PC: commercial product (Bactiva®); TP: *Trichoderma paratroviride*; CV: coefficient of variation; $MSD_{0.05}$: minimum significant difference with a significance of 0.05. Values with the same letter are statistically equal according to Tukey's honest minimum significant difference test ($p \leq 0.05$).

Among the biological products, the *T. paratroviride* strain showed a positive effect on plant morphology; likewise, among the application methods, higher morphology values were observed when the products were applied to the substrate and to the seed. Ferreira *et al.* (2024) mention that the use of *Trichoderma* strains in the production of forest seedlings promotes the solubilization and availability of nutrients for these, with numerous benefits for their development. Specifically, Gutiérrez-Flores *et al.* (2022) indicate that the increase in plant growth caused by *Trichoderma atroviride* is due to a process called anastomosis, where thin hyphae combine with other hyphae to form a network, which facilitates the exchange of liquids and nutrients.

In the same way, the *Trichoderma* symbiosis, when applied to the substrate and the seed, increases the ability to uptake a greater amount of nutrients in plants and, in turn, provides a balance between the aerial and root parts, which favors greater tolerance to water stress (Navarro *et al*., 2006; Kthiri *et al*., 2020). It should be noted that the biological products were applied to the substrate and seed prior to *Fusarium* inoculation so that the strains of the two biological products were already established

at the time of pathogen inoculation, as opposed to irrigation, which was applied at the same time as the pathogen.

Most of the diameter values obtained in this research were within the range proposed by Prieto and Sáenz (2011), who indicate that they should be greater than 4 mm to be considered high-quality plants. The results obtained are similar to those of García-Díaz *et al.* (2019), who applied *T. harzianum* and obtained diameters up to 3.11 mm in *P. greggii* inoculated with *F. circinatum*. For their part, Regliński *et al*. (2012) reported better diameter, height, and total dry weight in *Pinus radiata* D. Don plants when using *T. atroviride*. On the other hand, other studies reported an increase in plant height when applying *Trichoderma* spp. on forest plants (Nunes *et al*., 2021) and *T. harzianum* on *Pinus sylvestris* L. (Saleh *et al*., 2023). In terms of DQI, Prieto and Sáenz (2011) establish that plants with values higher than 0.5 present a high quality, with only *T. paratroviride* applied to the substrate having an index higher than indicated. This agrees with Romero *et al.* (2008), who indicate that inoculating *Trichoderma* to the substrate promotes the growth and development of the seedling, as there is better contact and colonization between the substrate and the root.

CONCLUSIONS

The commercial product and *Trichoderma paratroviride* reduced the incidence of damping-off and modified the morphology of *Pinus oocarpa* plants inoculated with *Fusarium oxysporum*. The lowest percentage of incidence was obtained with the commercial product and the form of application to the seed; similarly, the interactions revealed that applying the commercial microorganism-based product to the seed, substrate, and irrigation, as well as *T. paratroviride* to the seed and through irrigation, resulted in the lowest percentage of incidence. Better results in plant morphology were obtained when *T. paratroviride* was applied to the substrate. The interactions revealed that applying *T. paratroviride* to the substrate resulted in better growth; however, this treatment did not reduce the percentage of incidence, so it is recommended to use *T. paratroviride* on the seed, as it demonstrated good growth and lower pathogen incidence.

ACKNOWLEDGMENTS

To the Secretariat of Science, Humanities, Technology and Innovation (SECIHTI) and the National Forestry Commission (CONAFOR) sectoral fund project entitled "Monitoring, evaluation, damage prevention and control of *Fusarium circinatum* and *Bradysia* and *Lycoriella* fungus flies" for funding for field work.

REFERENCES

Aldrete A, Sánchez-Velázquez JR, Aguilera-Rodríguez M, Cibrián-Tovar D, García-Díaz SE. 2023. Manual de buenas prácticas para el manejo de la salud de planta en viveros forestales. Universidad Autónoma Chapingo: Texcoco, México. 291 p.

Amaral J, Pinto G, Flores-Pacheco JA, Díez-Casero JJ, Cerqueira A, Monteiro P, Gómez-Cadenas A, Alves A, Martín-García J. 2019. Effect of *Trichoderma viride* pre-inoculation in pine species with different levels of susceptibility to *Fusarium circinatum*: Physiological and hormonal responses. Plant Pathology 68 (9): 1645–1653. https://doi.org/10.1111/ppa.13080

Andivia E, Villar-Salvador P, Oliet JA, Puértolas J, Dumroese RK, Ivetić V, Molina-Venegas R, Arellano EC, Ovalle JF. 2021. Climate and species stress resistance modulate the higher survival of large seedlings in forest restorations worldwide. Ecological Applications 31 (6): 11. https://doi.org/10.1002/eap.2394

Cibrián-Tovar D, García-Diaz S, Don Juan-Macías B. 2008. Manual de identificación y manejo de plagas y enfermedades en germoplasma y planta producida en viveros. Comisión Nacional Forestal. Ciudad de México, México. 144 p.

CONAFOR (Comisión Nacional Forestal). 2022. Estado que guarda el sector forestal en México. Ciudad de México, México. 459 p.

Fabián-Plesníková I, Sáenz-Romero C, Cruz-de León J, Martínez-Trujillo M, Sánchez-Vargas NM. 2020. Parámetros genéticos de caracteres de crecimiento en un ensayo de progenies de *Pinus oocarpa*. Madera y Bosques 26 (3): e2632014. https://doi.org/10.21829/myb.2020.2632014

Federer WT. 1955. Experimental design: Theory and application. Macmillan Publishers: New York, NY, USA. 591 p.

Ferreira NCF, Ramos MLG, Gatto A. 2024. Uso de *Trichoderma* en la producción de plántulas forestales. Microorganisms 12 (2): 237. https://doi.org/10.3390/microorganisms12020237

García-Díaz SE, Aldrete A, Alvarado-Rosales D, Cibrián-Tovar D, Méndez-Montiel JT, Valdovinos-Ponce G, Equihua-Martínez A. 2017. Efecto de *Fusarium circinatum* en la germinación y crecimiento de plántulas de *Pinus greggii* en tres sustratos. Agrociencia 51 (8): 895–908.

García-Díaz SE, Aldrete A, Alvarado-Rosales D, Cibrián-Tovar D, Méndez-Montiel JT. 2019. Biocontrol de *Trichoderma harzianum* Rifai sobre *Fusarium circinatum* Nirenberg & O´Donnell en plántulas de *Pinus greggii* Engelm. ex Parl. en tres sustratos. Revista Chapingo Serie Ciencias Forestales y del Ambiente 25 (3): 353–367. https://doi.org/10.5154/r.rchscfa.2018.12.088

Gomes JM, Couto L, Leite HG, Xavier A, Garcia SLR. 2002. Parâmetros morfológicos na avaliação de qualidade de mudas *Eucalyptus grandis*. Revista Árvore 26 (6): 655–664.

Gordon TR, Swett CL, Wingfield MJ. 2015. Manejo de las enfermedades por *Fusarium* que afectan a las coníferas. Protección de Cultivos 73 (3): 28–39. https://doi.org/10.1016/j.cropro.2015.02.018

Gutiérrez-Flores LM, López-Reyes L, Hipólito-Romero E, Torres-Ramírez E, Castañeda-Roldán EI, Mauricio-Gutiérrez A. 2022. Perspectivas del control biológico en el pinar (*Pinus* spp.), una alternativa respetuosa con el medio ambiente al uso de pesticidas. Revista Mexicana de Fitopatología 40 (3): 401–424. https://doi.org/10.18781/r.mex.fit.2205-5

Hernández-Melchor DJ, Ferrera-Cerrato R, Alarcón A. 2019. *Trichoderma*: importancia agrícola, biotecnológica, y sistemas de fermentación para producir biomasa y enzimas de interés industrial. Chilean Journal of Agricultural and Animal Sciences 35 (1): 98–112. https://doi.org/10.4067/s0719-38902019005000205

Joo JH, Hussein KA. 2022. Biological control and plant growth promotion properties of volatile organic compound-producing antagonistic *Trichoderma* spp. Frontiers in Plant Science 13. https://doi.or/10.3389/fpls.2022.897668

Kthiri Z, Jabeur MB, Machraoui M, Gargouri S, Hiba K, Hamada W. 2020. Coating seeds with *Trichoderma* strains promotes plant growth and enhance the systemic resistance against

Fusarium crown rot in durum wheat. Egyptian Journal of Biological Pest Control 30 (1): 139. https://doi.org/10.1186/s41938-020-00338-6

Larios-Larios EJ, Valdovinos-Nava JJW, Chan-Cupul W, García-López FA, Manzo-Sánchez G, Buenrostro-Nava MT. 2019. Biocontrol de *damping off* y promoción del crecimiento vegetativo en plantas de *Capsicum chinense* (Jacq.) con *Trichoderma* spp. Revista Mexicana de Ciencias Agrícolas 10 (3): 471–483. https://doi.org/10.29312/remexca.v10i3.332

Ma LJ, Geiser DM, Proctor RH, Rooney AP, O'Donnell K, Trail F, Kazan K. 2013. *Fusarium* pathogenomics. Annual Review of Microbiology 67: 399–416. https://doi.org/10.1146/annurev-micro-092412-155650

Mejía-Bautista MA, Reyes-Ramírez A, Cristóbal-Alejo J, Tun-Suárez JM, Borges-Gómez, LC, Pacheco-Aguilar JR. 2016. *Bacillus* spp. en el control de la marchitez causada por *Fusarium* spp. en *Capsicum chinense*. Revista Mexicana de Fitopatología 34 (3): 208–222. https://doi.org/10.18781/r.mex.fit.1603-1

Mojica-Marín V, Luna-Olvera HA, Sandoval-Coronado CF, Pereyra-Alférez B, Morales-Ramos LH, González-Aguilar NA, Hernández-Luna CE, Alvarado-Gomez OG. 2009. Control biológico de la marchitez del chile (*Capsicum annuum* L.) por *Bacillus thuringiensis*. Phyton 78 (2): 105–110.

Navaneetha T, Prasad RD, Venkateswara RL. 2015. Liquid formulation of *Trichoderma* species for management of gray mold in castor *(Ricinus communis* L.) and *Alternaria* leaf blight in sunflower *(Helianthus annuus* L.). Journal of Biofertilizers and Biopesticides 6 (1): 149–160. https://doi.org/10.4172/2155-6202.1000149

Navarro L, Dunoyer P, Jay F, Arnold B, Dharmasiri N, Estelle M, Voinnet O, Jones JDG. 2006. A plant miRNA contributes to antibacterial resistance by repressing auxin signaling. Science 312 (5772): 436–439. https://doi.org/10.1126/science.1126088

Nunes ACP, dos Santos AP, Piotto D, Niella GR, Medeiros JCG, Silva GLB. 2021. *Trichoderma* spp. reveals potential as growth bio-promoter in forest seedlings. Agrotrópica 33 (1): 17–28.

Okorski A, Oszako T, Nowakowska JA, Pszczółkowska A. 2014. The possibilities of biologically protecting plants against diseases in nurseries, with special consideration of oomycetes and *Fusarium* fungi. Instytut Badawczy Leśnictwa 75 (3): 301–321. https://doi.org/10.2478/frp-2014-0029

Ortega-Cerón MA, Hernández-Acosta E, García-Díaz SE, Villanueva-Morales A. 2024. Control biológico de *Fusarium circinatum* Nirenberg & O´Donnell 1998 con *Trichoderma harzianum* Rifai 1969 en *Pinus devoniana* Lindl. Revista Mexicana de Ciencias Forestales 15 (83): 107–130. https://doi.org/10.29298/rmcf.v15i83.1446

Prieto RJA, Sáenz JT. 2011. Indicadores de calidad de planta en viveros forestales de la Sierra Madre Occidental. Instituto Nacional de Investigaciones Forestales, Agrícolas y Pecuarias: Durango, México. 212 p.

Prieto RJA, Sigala RJA, Pinedo LS, Garcia RJL, Madrid ARE, García PJL, Mejía BJM. 2009. Calidad de planta en los viveros forestales del estado de Durango. Instituto Nacional de Investigaciones Forestales, Agrícolas y Pecuarias: Durango, México. 81 p.

Regliński T, Rodenburg N, Taylor JT, Northcott GL, Ah Chee A, Spiers TM, Hill RA. 2012. *Trichoderma atroviride* promotes growth and enhances systemic resistance to *Diplodia pinea* in radiata pine (*Pinus radiata)* seedlings. Forest Pathology 42 (1): 75–78. https://doi.org/10.1111/j.1439-0329.2010.00710.x

Robles-Carrión A, Salinas-Serrano D, Armijos-Armijos W, Sánchez-Rodríguez, A, Torres-Gutiérrez R. 2014. Estudio de la variabilidad morfológica de aislados fúngicos asociados con

la enfermedad de la marchitez vascular del babaco (*Vasconcellea heilbornii* var. *pentagona*) en Loja, Ecuador. Centro de Biotecnología 2 (2): 33–44.

Rodríguez-Pinto MV, Campo-Arana RO, Cardona-Ayala CE, Manjarres-Cogollo EE, Rossi-Tordecilla BJ. 2021. *Trichoderma* spp. biocontrolador de marchitez vascular (*Fusarium* spp.) de la berenjena en el Caribe colombiano. Biotecnología en el Sector Agropecuario y Agroindustrial 19 (2): 158–169. https://doi.org/10.18684/bsaa.v19.n2.2021.1847

Romero G, Baraibar-Lucas A, Crosara A. 2008. *Trichoderma harzianum*, un biocontrol y biopromotor en vivero de especies forestales. Ciencia e Investigación Forestal 14 (2): 335–345. https://doi.org/10.52904/0718-4646.2008.294

Rueda-Sánchez A, Benavides-Solorio JD, Saenz-Reyez JT, Muñoz-Flores HJ, Prieto-Ruiz JA, Orozco-Gutiérrez G. 2014. Calidad de planta producida en los viveros forestales de Nayarit. Revista Mexicana de Ciencias Forestales 5 (22): 58–73. https://doi.org/10.29298/rmcf.v5i22.350

Saleh A, Kalashnikova E, Kirakosyan R, Kozlov A. 2023. Evaluating the effect of culture filtrate of *Trichoderma harzianum* on the seed germination and seedling growth of *Pinus sylvestris*. E3S Web of Conferences 7 (420): 01017. https://doi.org/10.1051/e3sconf/202342001017

Sánchez-Rangel JC, Jurado-Gómez C, Manzo-Sánchez G, Barreto-Torres MA, Molina-Ochoa, J, Chan-Cupul W. 2016. Biocontrol of damping-off diseases in *Carica papaya* (Linnaeus) seedlings under greenhouse conditions using *Trichoderma* spp. Biotechnology Summit 3: 127–132.

Soria S, Alonso R, Bettucci L. 2012. Endophytic bacteria from *Pinus taeda* L. as biocontrol agents of *Fusarium circinatum* Nirenberg & O´Donnell. Chilean Journal of Agricultural Research 72 (2): 281–284.

Sumalan RM, Alexa E, Poiana MA. 2013. Assessment of inhibitory potential of essential oils on natural mycoflora and *Fusarium* mycotoxins production in wheat. Chemistry Central Journal 7 (1). https://doi.org/10.1186/1752-153x-7-32

Agrociencia

IN VITRO EFFECTIVENESS OF A COMMERCIAL PINE ESSENTIAL OIL ON FOOD BACTERIA AND PHYTOPATHOGENIC FUNGI

Silvia **Bautista-Baños**[1], Zormy Nacary **Correa-Pacheco**[1], Laura Leticia **Barrera-Necha**[1], Rosa Isela **Ventura-Aguilar**[2], Mónica **Hernández-López**[1]*

[1]Centro de Desarrollo de Productos Bióticos (CEPROBI). Instituto Politécnico Nacional. Carretera Yautepec-Jojutla km 6, Calle CEPROBI No. 8, San Isidro, Yautepec, Morelos, Mexico. C. P. 62731.
[2]Universidad Autónoma Metropolitana. Departamento de Biotecnología. Avenida Ferrocarril San Rafael Atlixco No. 186, Colonia Leyes de Reforma 1A Sección, Iztapalapa, Mexico City, Mexico. C. P. 09310.
* Author for correspondence: mohernandezl@ipn.mx

Citation: Bautista-Baños S, Correa-Pacheco ZN, Barrera-Necha LL, Ventura-Aguilar RI, Hernández-López M. 2025. *In vitro* effectiveness of a commercial pine essential oil on food bacteria and phytopathogenic fungi. **Agrociencia** 59(4): 568-579. https://doi.org/ 10.47163/agrociencia.v59i4.3258

Editor in Chief:
Dr. Fernando C. Gómez Merino

Received: July 03, 2024.
Approved: May 12, 2025.
Published in Agrociencia: May 28, 2025.

ABSTRACT

Pathogenic microorganisms in foods are harmful to human health and generate important economic losses. This investigation identified the main compounds in a pine essential oil (PEO), and its antimicrobial effect was evaluated in four food bacteria species and two phytopathogenic fungal species. Twenty major compounds were found in the PEO: α-terpinolene (47.1 %), eucalyptol (22 %), p-menthane (16.7 %), and p-cymene (8.43 %). The greatest antibacterial action was found on *Escherichia coli* and *Staphylococcus aureus*, with an inhibition halo measuring 2.3 and 2 cm, respectively, at a minimum inhibiting concentration of 90 %. Using the inverted box or well technique, the PEO had an effect on *Colletotrichum gloeosporioides* and *Rhizopus stolonifer* at all concentrations evaluated, with inhibition values ranging from 40 to 60 %. For *R. stolonifer*, the 45 % PEO concentration inhibited germination completely.

Keywords: *Staphylococcus aureus*, *Listeria monocytogenes*, *Escherichia coli*, *Salmonella* spp., *Colletotrichum gloeosporioides*, *Rhizopus stolonifer*.

INTRODUCTION

Diseases transmitted to humans through the consumption of fresh fruits and vegetables due to the presence of pathogenic bacteria and the deterioration caused by fungi in pre- and post-harvest are becoming an increasingly important issue in agricultural product conservation on a national and international scale. Consumption of agricultural products contaminated with bacteria such as *Staphylococcus aureus*, *Listeria monocytogenes*, *Escherichia coli*, and *Salmonella* spp. causes severe economic losses, including compensation to consumers for bacterial toxicity and total loss of the product (Cortés-Higareda et al., 2021), and in the international market, the closure of borders to the trade of these products. Occasionally, the consumption of

contaminated agricultural products with different serovars of *Salmonella* spp. causes severe symptoms in human beings, which can lead to the death of the consumer.

Phytopathogenic fungi of diverse genera and species cause losses of up to 40 % of the total harvest (Ramos-García *et al*., 2010). In the particular case of *Colletotrichum gloeosporioides* and *Rhizopus stolonifer*, their development causes severe rotting in a large diversity of agricultural products such as avocado (*Persea americana* Mill.), mango (*Mangifera indica* L.), soursop (*Annona muricata* L.), berries (*Rubus* spp., *Vaccinium* spp.), tomato (*Solanum lycopersicum* L.), and others (Bautista-Baños *et al*., 2014; Quintero-Mercado *et al*., 2019; Herrera-González *et al*., 2020).

The main and most common option to reduce the presence of these microorganisms is the use of synthetic compounds (sanitizers and fungicides). However, its use is currently questioned due to environmental contamination, harm to human health, and the generation of microbial resistance. Due to this, other alternatives have been evaluated, such as the use of essential oils from plants (Ramos-García *et al*., 2010; Bautista-Baños *et al*., 2020).

Pine (*Pinus* spp., Pinaceae) essential oils extracted from seeds, leaves, and flowers have made a great contribution to the pharmaceutical, cosmetics, and construction industries. Krauze-Baranowska *et al*. (2002) documented that the general composition of essential oils across the *Pinus* genus varies according to the species, although its composition lies within the group of monoterpenes (α-β pinene, germacrene, myrcene) and oxygenated monoterpenes (borneol, bornyl acetate, Δ-3-carene).

Regarding its bactericidal and fungicidal effect, there are *in vitro* investigations that verify this activity, mainly using *Pinus sylvestris* L. The essential oil, extracted from the needles of this species, presented bactericidal activity against *Bacillus cereus*, *Micrococcus luteus,* and *Alcaligenes faecalis*, although no fungicidal effect was observed (Chao *et al*., 2000). Fungicidal activity was displayed in *P. sylvestris* against *Aspergillus niger*, *Penicillium funiculosum,* and *Trichoderma viride*. The mycelia of *Penicillium funiculosum* were controlled by *P. sylvestris* extracts (Motiejūnaite and Peciulyte, 2004). Volatiles and extracts of the essential oil from *P. sylvestris* displayed a notable control in the germination of *Mucor* spp., *R. stolonifera*, and *Fusarium oxysporum* spores (Tullio *et al*., 2007). Control has also been reported on *Candida albicans* with the application of this essential oil (Salamon *et al*., 2019). The commercial product Resin Adher CE (MS Agros S.A. de C.V., Mexico City, Mexico), made with *P. sylvestris* essential oil, affects the germination of *Aspergillus flavus* (Segura-Palacios *et al*., 2021).

Based on the above, the goals of this investigation were to know the chemical composition of the commercial essential oil from *P. sylvestris* and evaluate its *in vitro* effect on four food bacteria and four phytopathogenic fungi of agricultural importance.

MATERIALS AND METHODS

Chemical profile of the *Pinus sylvestris* essential oil

The pine essential oil (PEO) was obtained from Xipe Naturals (Mexico City, Mexico). To determine its composition, the methodology by Black-Solís *et al*. (2017) was followed. A gas chromatograph-mass spectrometry (GS-MS SCION 456-GC, Bruker Daltonics Inc., Billerica, MA, USA) was used with the headspace technique. This system was operated using the software MS Workstation version 8.2 (Bruker Daltonics Inc., Billerica, MA, USA). The GC-MS detector was operated on exploration mode, between 50 and 500 mass/load. The GC oven was equipped with a BR-1MS capillary column with a film thickness of 0.25 mm, 30 m in length, and an internal diameter of 0.25 mm. The analysis was performed by direct injection, diluting the oil in chloroform, with a time of analysis of 29 min per sample, using helium (1 mL min^{-1}) as a carrier gas, at 220 °C for the injector and 250 °C for the transfer line. In 1 mL of chloroform, 5 µL of the sample were dissolved, and 1 µL of this solution was injected. The initial oven temperature was 55 °C and maintained for 1 min. Subsequently, it was raised to 155 °C at a heating speed of 5 °C min^{-1} and maintained for 2 min. Finally, a temperature of 255 °C was reached at a heating speed of 20 °C min^{-1} and maintained for 1 min.

Fungi and bacteria acquisition

Two Gram-positive strains (*Staphylococcus aureus* and *Listeria monocytogenes*) and two Gram-negative strains (*Salmonella typhi* and *Escherichia coli*) were used as trial bacteria, which were obtained from the Professional Interdisciplinary Biotechnology Unit of the National Polytechnic Institute (UPIBI-IPN, Mexico). Phytopathogenic fungi *Colletotrichum gloeosporioides* and *Rhizopus stolonifer* were obtained from the strain bank of the Postharvest Technology Laboratory of the Biotic Products Development Center (CEPROBI-IPN, Mexico).

The bacteria were activated in agar soybean tripcasein (AST) nutrient medium at 37 °C for 24 h. A bacterial concentration of 1–2 × 10^8 colony-forming units (CFU) per milliliter was determined in a spectrophotometer (GENESYS 10S UV-Vis, Thermo Scientific, USA) at an absorbance of 0.08–0.098 with a wavelength of 650 nm. The activation of fungi was carried out in potato dextrose agar (PDA) nutrient medium at 25 °C for 10 and 4 days for *C. gloeosporioides* and *R. stolonifer*, respectively.

Minimum inhibiting concentration (MIC)

The MIC of the PEO in the bacteria was determined with the agar diffusion technique as indicated by Lara-Cortés *et al*. (2016). For this purpose, 10 mL of 0.8 % AST previously inoculated with 20 µL of the bacteria studied and 5 mL of semisolid 1 % AST were emptied into Petri dishes (60 × 15 mm in diameter) and left to dry for 1 h. Using a hole puncher, 10 mm-diameter holes were made. Subsequently, 20 µL of the PEO were placed serially in each hole, in concentrations of 90, 45, 22.5, 11.2, and 5.6 %. The boxes were sealed and incubated for 48 h at 37 °C. After this time, the inhibition halo was

measured (clearer areas around the hole). The evaluation was carried out in six Petri dishes (repetitions) per concentration (treatment).

Growth and germination kinetics of the pathogenic fungi

To evaluate these variables, the reverse box and the well techniques were used. For the former, the methodology by Ramos-García *et al*. (2012) was followed. Sterile filter paper (Wattman No. 1), 15 mm in diameter, was placed on the lid of the Petri dish (100 × 15 mm in diameter), previously treated with 20 µL for each treatment with the different concentrations of the PEO (100, 90, 45, 22.5, 11.2, and 5.6 %). On the other hand, a 10 mm-diameter disk with fungus was placed in the center of the Petri dish. The dishes were sealed and incubated at 25 ± 2 °C and kept in an inverted position. Six repetitions were carried out per treatment.

For the well technique, the methodology by Moreno-Limón *et al*. (2012) was followed. To this end, every Petri dish (60 × 15 mm) with PDA culture medium under sterile conditions had 0.5 mL of spore suspension (10^5 spores mL^{-1}), which was spread throughout the Petri dish using a sterile metal spreader. The fungal solution was left to dry, and later, using a 10 mm-diameter borer, a well was made in the center of the dish, where 20 µL of each concentration was added (100, 90, 45, 22.5, 11.2, and 5.6 % of PEO). The dishes were sealed and incubated at 25 ± 2 °C. Six repetitions were carried out per treatment.

Mycelial growth

For the reverse box technique, culture diameter measurements were taken every day for 13 days for *C. gloeosporioides* and for 7 days for *R. stolonifer* (in centimeters) using two perpendicular directions traced in the center of the box as a reference point. The average value of the repetitions per treatment was taken.

Germination of spores

The germination of spores was determined in both techniques, according to the method described by Black-Solis *et al*. (2017). To this end, two Petri dishes with mycelial growth of the fungus from each treatment were used. Twenty milliliters of sterile distilled water were added, and the mycelium was scraped with a sterile bacteriological loop. The spore suspension was filtered and adjusted to 10^5 spores mL^{-1}. Subsequently, three disks (repetitions) of PDA culture medium with a diameter of 15 mm were placed along a slide inside a Petri dish. Twenty milliliters of the spore solution (10^5) were placed on each disk.

The Petri dishes were sealed and incubated for 2, 4, 6, 8, and 10 h for both fungal species. After incubation, one drop of lactophenol blue was added to each disk, and 100 conidia were evaluated per disk under an optic microscope at 40x (Nikon Alphaphot-2 YS2-H, Japan). The percentage of germination ($G_{(\%)}$) was determined using the following equation:

$$G_{(\%)} = \frac{E_C}{T_E}\ x\ 100$$

where E_G represents the number of germinated conidia and T_E the total of conidia. A conidium was considered germinated when a germinative tube was observed, regardless of its length. Three repetitions were carried out per treatment.

Statistical analysis

For the variables of mycelial growth and spore germination, a totally randomized design was used. The difference in the antifungal activity was established using an analysis of variance (ANOVA) and Tukey's test ($p \leq 0.05$). The data in percentages were transformed with the arcsine function. The InfoStat statistical package, version 2020 (di Rienzo *et al*., 2020), was used.

RESULTS AND DISCUSSION

Chemical profile of the essential oil

In regard to the composition of the *P. sylvestris* essential oil, 20 major compounds were obtained (Table 1). The main components identified were α-terpinolene (47.1 %),

Table 1. Chemical composition of the pine (*Pinus sylvestris* L.) essential oil used (Xipe Naturals, Mexico City, Mexico).

No.	Compound	Retention time	Total percentage
1	4-octene, 2,6-dimethyl-, [S-(E)]	5.90	0.358
2	α-tricyclene	6.09	0.421
3	camphene	6.63	6.339
4	β-myrcene	7.61	0.629
5	Terpinolene	7.86	1.618
6	α-phellandrene	7.93	0.282
7	p-mentane	8.14	16.722
8	p-cymene	8.33	8.431
9	Eucalyptol	8.53	22.022
10	Terpinene	9.30	3.279
11	α-terpinolene	10.10	47.195
12	Fenchol	10.60	1.347
13	Isoborneol	11.73	0.770
14	Iso-β-terpineol	11.85	0.252
15	Endo-borneol	11.96	0.966
16	Terpinen-4-ol	12.30	6.213
17	Terpineol	12.60	3.564
18	Isoterpinolene	12.79	1.071
19	Diphenyl ether	17.78	0.415
20	Longifolene	18.55	0.687

eucalyptol (22 %), p-menthane (16.7 %), and p-cymene (8.43 %) within a retention time of 8 to 10 min. These values mostly coincide with the chemical identification reported by Mitić *et al*. (2018) and Ibáñez and Blázquez (2019), who identified between 30 and 41 major compounds in fresh *P. sylvestris* needles within the group of oxygenated monoterpenes, sesquiterpene hydrocarbons, and oxygenated sesquiterpenes. The differences in the content of compounds can be explained mainly by the differences in the geographic locations of the tree (Maciag *et al*., 2007).

Antibacterial activity

In general terms, the greatest antibacterial action corresponded to the highest concentration of 90 % (Table 2). On the other hand, *P. sylvestris* exerted the highest inhibiting effect on *E. coli* and *S. aureus*. Regarding *L. monocytogenes*, only the 90 and 45 % concentrations inhibited it, and no effect was observed on *S. typhy* (Table 2).

Table 2. Effect of the minimum inhibiting concentration of the pine (*Pinus sylvestris* L.) essential oil on the growth of bacteria in foods.

	Minimum inhibiting concentration (%)				
Bacteria	90	45	22.5	11.2	5.6
	Inhibition halo (cm)[†]				
Escherichia coli	2.3 ± 0.23 b	2.1 ± 0.2 b	2.0 ± 0.1 b	2.0 ± 0.1 b	1.7 ± 0.3 b
Listeria monocytogenes	1.8 ± 0.29 b	1.6 ± 0.2 b	0 ± 0 a	0 ± 0 a	0 ± 0 a
Salmonella typhy	0 ± 0 a	0 ± 0 a	0 ± 0 a	0 ± 0 a	0 ± 0 a
Staphylococcus aureus	2.0 ± 0.12 b	1.9 ± 0.1 b	1.8 ± 0.1 b	1.6 ± 0.2 b	1.5 ± 0.2 b

[†]Means (± = mean standard error) with different letters in the same column are significantly different ($p < 0.05$).

Unlike other investigations, the inhibition area due to the effect of the *P. sylvestris* oil was not as large. Czerwińska and Szparaga (2015) found that applying this oil using the diffusion method (1 μg mL^{-1}) gave the largest inhibition halo in *S. aureus* (12 mm), followed by *L. monocytogenes* (10 mm) and *E. coli* (8.2 mm). In that study, other bacteria sensitive to the extract were *Micrococcus leuteus* (12 mm) and *Bacillus subtilis* (8.2 mm). Likewise, Oyewole *et al.* (2021) confirmed the bactericidal effect of the *P. sylvestris* needles using the same technique. In this case, the area of inhibition measured approximately 20 mm, whereas the CMI starting at 0.39 mg mL^{-1} significantly inhibited *E. coli* and *S. aureus*, with these two bacteria as the most affected by PEO.

Canillac and Mourey (2001) mentioned that among the factors associated with the bactericidal effect are the main components of the oil, the concentration used, and the bacteria under study. Likewise, Kim *et al.* (2013) pointed out that the antimicrobial activity against three Gram-positive bacteria (*B. subtilis*, *B. natto*, and *S. aureus*) and

four Gram-negative ones (*E. coli*, *Salmonella enteritidis*, *S. typhosa*, and *Pseudomonas aeruginosa*) may be due to the changes in chemical components, with monoterpenes and sesquiterpenes the major compounds in the essential oil of the *Pinus* genus. Zhang *et al*. (2023) documented the growing interest in natural products with antioxidant and antimicrobial effects and their mechanisms of action with extracts of *Pinus densiflora* needles as a natural and efficient antimicrobial agent, aimed at the food industry with safer, fresher, and healthier components, which generates a large demand for natural and safe conservation technologies.

Regarding the fungicidal effect, the dynamics of the mycelial growth in the different *C. gloeosporioides* treatments during the 13-day incubation period (Figure 1A) and *R.*

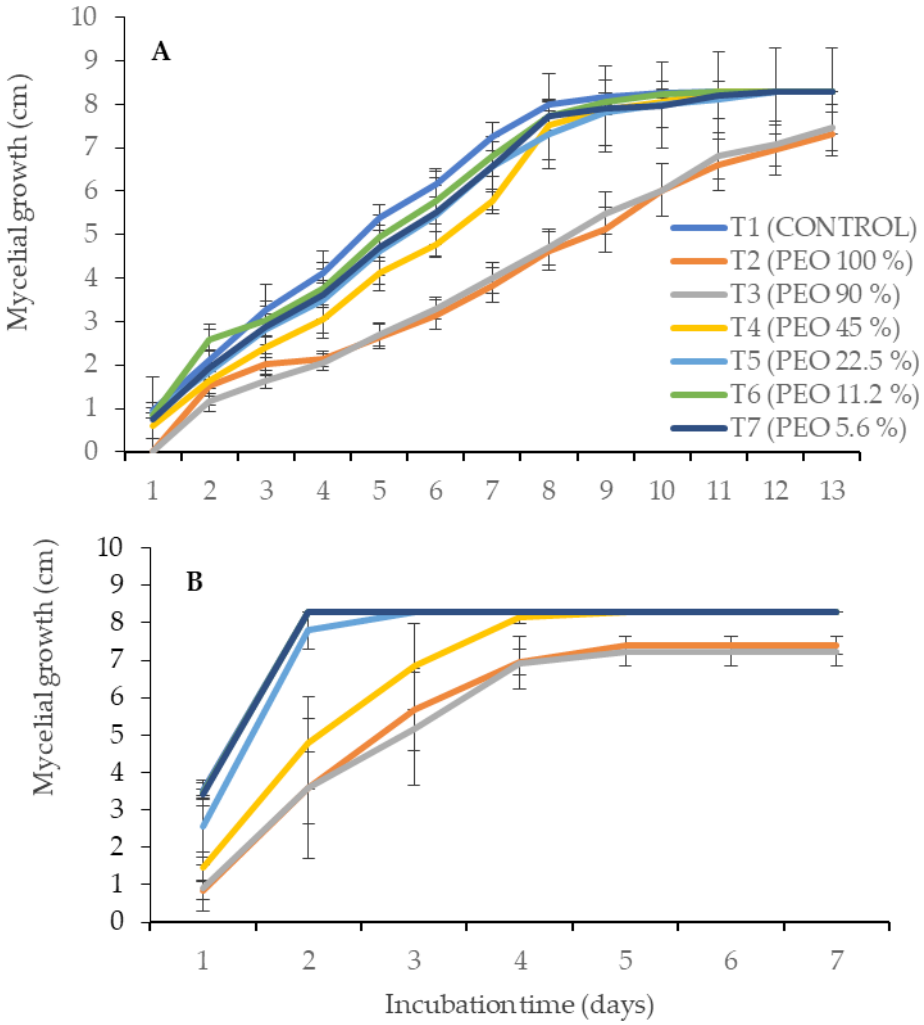

Figure 1. Mycelial growth kinetics of the fungi evaluated in the presence of different concentrations of pine (*Pinus sylvestris* L.) essential oil. A: *Colletotrichum gloeosporioides* in a 13-day incubation period; B: *Rhizopus stolonifer* in a 7-day incubation period. Vertical bars indicate the mean standard error.

stolonifer during the 7-day incubation period (Figure 1B) showed that *C. gloeosporioides* growth, in all treatments, increased gradually along the days of incubation, whereas in *R. stolonifer*, only in concentrations of 45, 90, and 100 % was gradual growth observed. In both fungi, the greatest fungicidal effect was with the application of PEO at concentrations of 90 and 100 %, with values at the end of incubation of around 6 to 7 cm.

Regarding germination, in the reverse box (Figure 2) and well (Figure 3) techniques, a rate increase was observed with incubation time. In both techniques, there was a

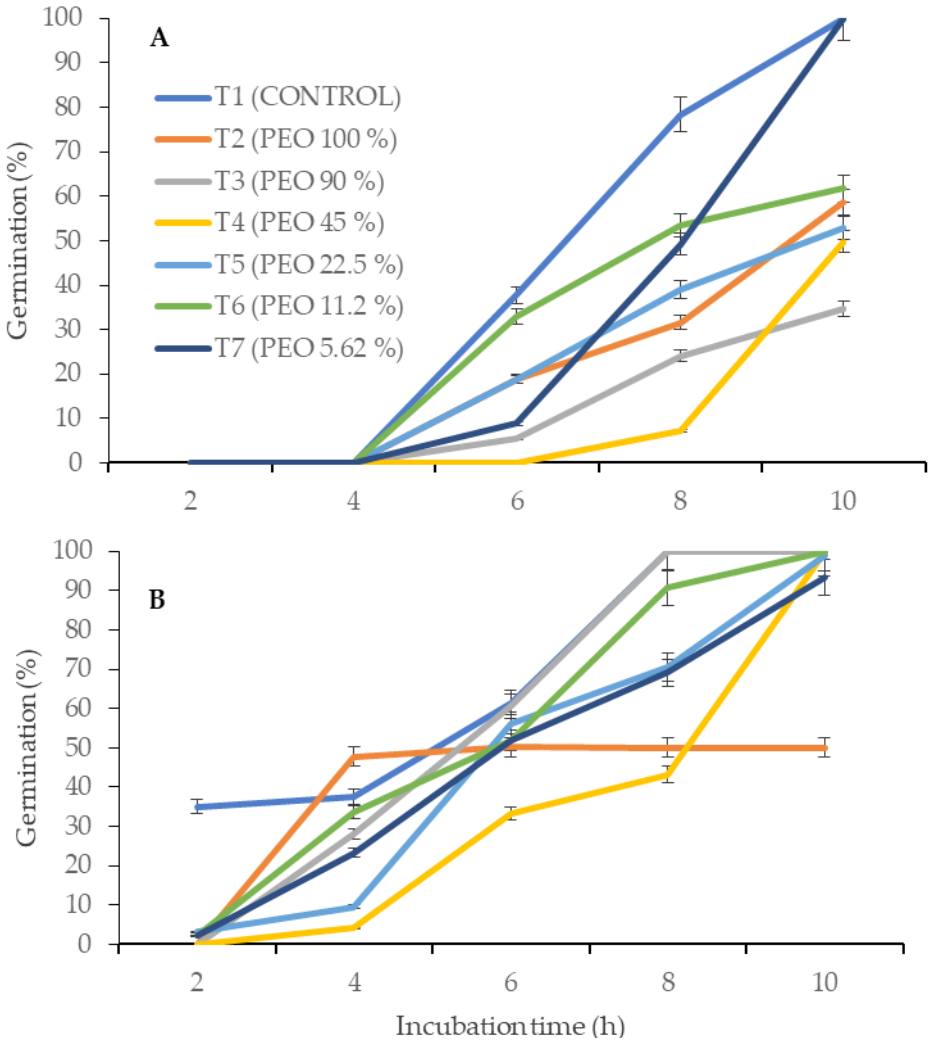

Figure 2. Germination kinetics of the fungi evaluated in the presence of different concentrations of pine (*Pinus sylvestris* L.) essential oil using the reverse box method during a 10-hour incubation period. A: *Colletotrichum gloeosporioides;* B: *Rhizopus stolonifer*. Vertical bars indicate the mean standard error. The data in percentages was transformed with the arcsine function. Kruskal-Wallis test A: (H = 0, 0, 36.79, 34.94, 32.56; p = 0.0001); B: (H = 32.63, 14.04, 9.91, 19.77, 6.94; p = 0.0001, 0.0290, 0.1282, 0.0026, 0.0526).

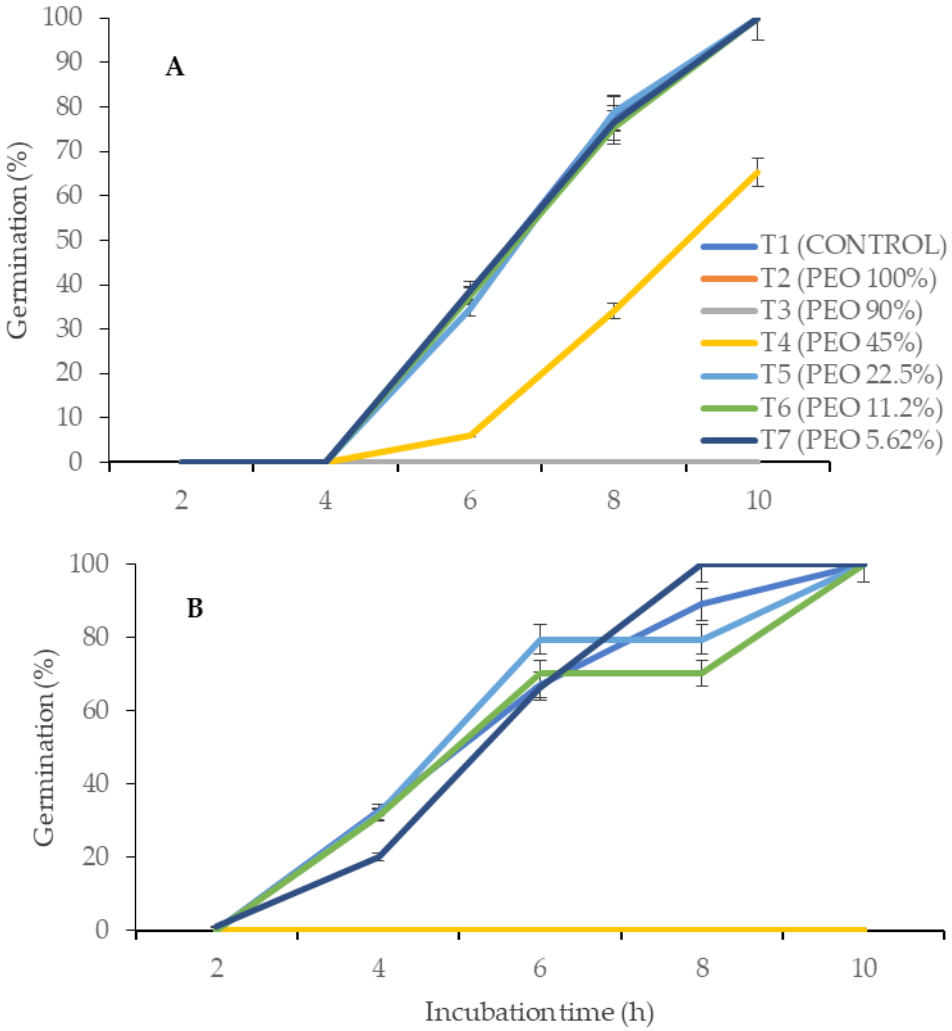

Figure 3. Germination kinetics of the fungi evaluated during a 10-hour incubation period in the presence of pine (*Pinus sylvestris* L.) essential oil using the well technique. A: *Colletotrichum gloeosporioides;* B: *Rhizopus stolonifer*. Vertical bars indicate the mean standard error. The data in percentages were transformed with the arcsine function. Kruskal-Wallis test A: (H = 0, 0, 32.38, 32.78, 32.29; p = 0.0001); B: (H = 10.47, 34.28, 32.03, 35.40, 30.14; p = 0.0001).

greater fungicidal effect of the PEO on *C. gloeosporioides*, since in both most of the concentrations applied, its germination was inhibited. The PEO concentrations from 11.2 % onwards inhibited germination between 40 and 60 %, whereas in *R. stolonifer*, only the concentrations of 45 and 100 % had an inhibiting effect. However, the inhibition with the 45 % concentration was total (Figure 3B).

In general, spores were more susceptible than the mycelia. In regard to the application technique, the PEO volatiles had a stronger inhibiting effect for both fungal species in

comparison with the direct application on the medium. Coinciding with these results, Tullio *et al*. (2006) documented a much lower inhibiting CMI in the development of *Fusarium oxysporum* (0.03 %), *Rhizopus* spp. (0.05 %), and *Cladosporium cladosporioides* (0.2 %) after 3 and 7 days of incubation when applying volatiles of the *P. sylvestris* essential oil, in comparison with the integration of the essential oil in the medium, since, in this case, the concentration needed to trigger inhibition was greater than 1 %. Other *Pinus* species with a notorious fungicidal activity on phytopathogenic fungi of the *Fusarium* genus were the essential oils from the needles of *P. ponderosa*, *P. resinosa*, and *P. strobus*, in concentrations of 2 and 5 % (Krauze-Baranowska *et al*., 2002). Likewise, Motiejūnaite and Peciulyte (2004) verified, in various species of the genus *Aspergillus*, the effectiveness of *P. sylvestris* with a concentration of 2.5 % when applied in the nutrient medium (1–1.5 % v/v). Additionally, in later studies, Amri *et al.* (2013) pointed out percentages of inhibition of more than 50 % in *Giberella avenaceae* and *Rhizoctonia solani* with the concentration of *P. sylvestris* of 4 μL mL^{-1}. Coinciding with Oyewole *et al.* (2021), this study also identified the following chemicals in the PEO under study with antimicrobial activity: terpineol, isoborneol, and fenchol.

CONCLUSIONS

According to the goals presented, 20 major compounds were identified in the commercial pine essential oil, all belonging to the terpene chemical group. Regarding the antimicrobial activity of the essential oil, the most affected bacteria were *Escherichia coli* and *Staphylococcus aureus* starting at a concentration of 90 %. For the fungi *Colletotrichum gloeosporioides* and *Rhizopus stolonifer*, spore germination was the most affected developmental stage during the incubation period. In *C. gloeosporioides*, inhibition occurred at all concentrations, whereas in *R. stolonifer*, it was only observed at a concentration of 45 %.

ACKNOWLEDGEMENTS

To project IPN-SIP 20211083 'Biodegradation of PLA/PBAT-based biocomposite meshes with pine essential oil under composting conditions for the packaging of avocado'. To Juan Raúl Orozco Avala for his support in the design of the figures.

REFERENCES

Amri I, Hanana M, Gargouri S, Jamoussi B, Hamrouni L. 2013. Comparative study of two coniferous species (*Pinus pinaster* Aiton and *Cupressus sempervirens* L. var. *dupreziana* [A. Camus] Silba) essential oils: Chemical composition and biological activity. Chilean Journal of Agricultural Research 73 (3): 259–266. https://doi.org/10.4067/s0718-58392013000300008

Bautista-Baños S, Bosquez-Molina E, Barrera-Necha LL. 2014. *Rhizopus stolonifer* (soft rot). *In* Bautista-Baños S. (ed.), Postharvest Decay Control Strategies. Academic Press: San Diego, CA, USA, pp: 1–44. https://doi.org/10.1016/B978-0-12-411552-1.00001-6

Bautista-Baños S, Correa-Pacheco ZN, Black-Solis JD. 2020. Current status of the effectiveness of essential oils for controlling phytopathogenic fungi, a review. Acta Agrícola y Pecuaria 1 (6): E0061008. https://doi.org/10.30973/aap/2020.6.0061008

Black-Solis J, Ventura-Aguilar RI, Barrera-Necha LL, Bautista-Baños S. 2017. Chemical characterization, compositional variability, and mathematical modelling of the effect of essential oils in *Alternaria alternata*. Revista Mexicana de Fitopatología 35 (2): 204–226. https://doi.org/10.18781/r.mex.fit.1612-5

Canillac N, Mourey A. 2001. Antibacterial activity of the essential oil of *Picea excelsa* on *Listeria*, *Staphylococcus aureus* and coliform bacteria. Food Microbiology 18 (3): 261–268. https://doi.org/10.1006/fmic.2000.0397

Chao SC, Young DG, Oberg CJ. 2000. Screening for inhibitory activity of essential oils on selected bacteria, fungi and viruses. Journal of Essential Oil Research 12 (5): 639–649. https://doi.org/10.1080/10412905.2000.9712177

Cortés-Higareda M, Bautista-Baños S, Ventura-Aguilar RI, Landa-Salgado P, Hernández-López M. 2021. Bacterias patógenas de los alimentos agrícolas frescos y mínimamente procesados. Estado actual en el control del género *Salmonella*. Revista Iberoamericana de Tecnología Postcosecha 22 (1): 12–28.

Czerwińska E, Szparaga A. 2015. Antibacterial and antifungal activity of plant extracts. Rocznik Ochrona Środowiska 17 (1): 209–229.

di Rienzo JA, Casanoves F, Balzarini MG, Gonzalez L, Tablada M, Robledo CW. InfoStat versión 2020. Centro de Transferencia InfoStat, FCA, Universidad Nacional de Córdoba, Argentina.

Herrera-González JA, Bautista-Baños S, Salazar-García S, Gutiérrez-Martínez P. 2020. Current situation of postharvest handling and fungal diseases of avocado 'Hass' for export in Michoacán, Mexico. Revista Mexicana de Ciencias Agrícolas 11 (7): 1647–1660. https://doi.org/10.29312/remexca.v11i7.2402

Ibáñez MD, Blázquez MA. 2019. Phytotoxic effects of commercial *Eucalyptus citriodora*, *Lavandula angustifolia*, and *Pinus sylvestris* essential oils on weeds, crops, and invasive species. Molecules 24 (15): 2847. https://doi.org/10.3390/molecules24152847

Kim H, Lee B, Yun KW. 2013. Comparison of chemical composition and antimicrobial activity of essential oils from three *Pinus* species. Industrial Crop and Research 44: 323–329. https://doi.org/10.1016/j.indcrop.2012.10.026

Krauze-Baranowska M, Mardarowicz M, Wiwart M, Pobłocka L, Dynowska M. 2002. Antifungal activity of the essential oils from some species of the genus *Pinus*. Zeitschrift für Naturforschung C 57 (5–6): 478–82. https://doi.org/10.1515/znc-2002-5-613

Lara-Cortés E, Troncoso-Rojas R, Hernández-López M, Bautista-Baños S. 2016. Evaluation of the antimicrobial activity of cinnamaldehyde in the preservation of edible dahlia flowers, under different storage conditions. Revista Chapingo Serie Horticultura 22 (3): 177–189. https://doi.org/10.5154/r.rchsh.2016.02.002

Maciag A, Milakovi D, Christensen HH, Antolovi V, Kalemba D. 2007. Essential oil composition and plant-insect relations in Scots pine (*Pinus sylvestris* L.). Food Chemistry and Biotechnology 71: 71–94.

Mitić ZS, Jovanović B, Jovanović SČ, Mihajilov-Krstev T, Stojanović-Radić ZZ, Cvetković VJ, Mitrović TLj, Marin PD, Zlatković BK, Stojanović GS. 2018. Comparative study of the essential oils of four *Pinus* species: Chemical composition, antimicrobial and insect larvicidal activity. Industrial Crops and Production 111: 55–62. https://doi.org/10.1016/j.indcrop.2017.10.004

Moreno-Limón S, Salcedo-Martínez SM, Cárdenas-Ávila ML, Hernández-Piñero JL, Núñez-González MA. 2012. Efecto antifúngico de capsaicina y extractos de chile piquín (*Capsicum annuum* L. var *aviculare*) sobre el crecimiento *in vitro* de *Aspergillus flavus*. Polibotánica 34: 191–204.

Motiejūnaite O, Peciulyte D. 2004. Fungicidal properties of *Pinus sylvestris* L. for improvement of air quality. Medicina (Kaunas) 40 (8): 787–794.

Oyewole KA, Oyedara OO, Awojide SH, Olawade MO, Adetunji CO. 2021. Chemical constituents and antibacterial activity of essential oils of needles of *Pinus sylvestris* (scots pine) from South West Nigeria. Research Square 1: 1–15. https://doi.org/10.21203/rs.3.rs-635195/v1

Quintero-Mercado A, Dangon-Bernier F, Páez-Redondo A. 2019. Aislamientos endofíticos de *Colletotrichum* spp. a partir de hojas y ramas de mango (*Mangifera indica* L.) cultivar Azúcar en el municipio de Ciénaga, Magdalena, Colombia. Revista de la Academia Colombiana de Ciencias Exactas, Físicas y Naturales 43 (166): 65–77. https://doi.org/10.18257/raccefyn.788

Ramos-García ML, Bautista-Baños S, Barrera-Necha LL, Bosquez-Molina E, Alia-Tejacal I, Estrada-Carrillo M. 2010. Compuestos antimicrobianos adicionados en recubrimientos comestibles para uso en productos hortofrutícolas. Revista Mexicana de Fitopatología 28 (1): 44–57.

Ramos-García ML, Hernández-López M, Barrera-Necha LL, Bautista-Baños S, Troncoso-Rojas R, Bosquez-Molina E. 2012. *In vitro* response of *Fusarium oxysporum* isolates to isothiocyanates application. Revista Mexicana de Fitopatología 30 (1): 1–10.

Salamon I, Kryvtsova M, Bucko D, Tarawneh AH. 2019. Chemical characterization and antimicrobial activity of some essential oils after their industrial large-scale distillation. Journal of Microbiology Biotechnology and Food Sciences 8 (4): 984–988. https://doi.org/10.15414/jmbfs.2019.8.4.984-988

Segura-Palacios MA, Correa-Pacheco ZN, Corona-Rangel ML, Martinez-Ramirez OC, Salazar-Piña DA, Ramos-García ML, Bautista-Baños S. 2021. Use of natural products on the control of *Aspergillus flavus* and production of aflatoxins *in vitro* and on tomato fruit. Plants 10 (12): 2553. https://doi.org/10.3390/plants10122553

Tullio V, Nostro A, Mandras N, Duo P, Banche G, Cannatelli MA, Cuffini AM, Alonzo V, Carlone NA. 2007. Antifungal activity of essential oils against filamentous fungi determined by broth microdilution and vapour contact methods. Journal of Applied Microbiology 102 (6): 1544–1550. https://doi.org/10.1111/j.1365-2672.2006.03191.x

Zhang Y, Chung WK, Moon SH, Lee JG, Om AS. 2023. Comparison of antibacterial activities of Korean pine (*Pinus densiflora*) needle steam distillation extract on *Escherichia coli* and *Staphylococcus aureus* focusing on membrane fluidity and genes involved in membrane lipids and stress. Molecules 29 (1): 165. https://doi.org/10.3390/molecules29010165

Agrociencia

FUTURE-PROOF COFFEE PLANT DISEASE DETECTION BASED ON COUNTER-FACTUAL RECOMMENDATION WITH A HYBRID VISION TRANSFORMER AND CONVOLUTIONAL NEURAL NETWORK MODEL

Karthik **Selvaraj**[1*], Raveena **Selvanarayanan**[2], Sam Kumar **Gopalsamy Venkatesan**[3], Surendran **Rajendran**[4*]

[1]Muthayammal Engineering College (Autonomous). Department of Computer Science and Business Systems. Rasipuram 637408, Tamil Nadu, India.
[2]Panimalar Engineering College, Department of Computer Science and Business Systems, Chennai 600123, Tamil Nadu, India.
[3]Koneru Lakshmaiah Education Foundation. Department of Computer Science and Engineering, Vaddeswaram 522302, Andhra Pradesh, India.
[4]Saveetha School of Engineering, Saveetha Institute of Medical and Technical Sciences. Department of Computer Science and Engineering. Chennai 602117, Tamil Nadu, India.
* Author for correspondence: surendran.phd.it@gmail.com

Citation: Selvaraj K, Selvanarayanan R, Gopalsamy Venkatesan SK, Rajendran S. 2025. Future-proof coffee plant disease detection based on counter-factual recommendation with a hybrid vision transformer and convolutional neural network model.
Agrociencia 59(4): 580-603. https://doi.org/ 10.47163/agrociencia.v59i4.3385

Editor in Chief:
Dr. Fernando C. Gómez Merino

Received: December 16, 2024.
Approved: May 30, 2025.
Published in Agrociencia: June 06, 2025.

ABSTRACT

Coffee plantations are vulnerable to several diseases that harm roots, leaves, and cherries, jeopardizing crop productivity and farmer livelihoods. Small-scale farmers lack access to precise and accessible technologies for diagnosing and controlling these diseases. Traditional machine learning methodologies are restricted to single-disease classification and lack the intricacies of multi-disease contexts. In this work, the proposed model has a unique hybrid model that integrates vision transformer (ViT) and convolutional neural network (CNN) architectures for the identification and early detection of several coffee plant diseases. The ViT module identifies global associations in plant images, while the CNN extracts intricate local characteristics, facilitating thorough disease diagnosis. Furthermore, the counterfactual recommendation system models the impacts of several treatments and preventative strategies on the original images, offering practical insights. Our model attains an accuracy of 0.9881 % on a dataset of 1056 images, surpassing current methodologies. The suggested solution is included in the Affogato app, enabling farmers to make educated, customized choices about disease control. This method not only improves disease detection but also promotes sustainable coffee-growing techniques, enhancing crop production and farmer livelihoods.

Keywords: *Colletotrichum kahawae, Hemilieia vastatrix, Mycosphaerella coffeicola*, hybrid vision transformer, convolutional neural network, counter factual recommendation.

INTRODUCTION

Coffee is one of the most widely consumed beverages worldwide and plays a vital role in global agriculture and economies. However, coffee plants are highly susceptible to

various diseases that, if not promptly identified and managed, can lead to significant yield losses and reduced coffee quality. Coffee plant diseases pose a major threat to global coffee production, with leaf rust, root rot, and berry infections collectively contributing to over 30 % yield losses worldwide. These impacts are particularly severe for small-scale farmers who lack access to advanced diagnostic tools. Rapid detection and classification of infections are essential for mitigating economic losses and ensuring sustainable coffee production.

Several fungal, bacterial, and viral infections threaten coffee plants at various growth stages. coffee berry disease, caused by *Colletotrichum kahawae*, primarily affects *Coffea arabica* berries, leading to black, sunken lesions that spread rapidly, causing fruit decay and substantial economic losses. Similarly, brown eye spot disease (*Mycosphaerella coffeicola*) manifests as circular brown lesions with yellow halos on leaves and brown spots with fungal spore-containing gray cores in berries, leading to premature leaf abscission and reduced productivity. Leaf rust disease (*Hemileia vastatrix*) presents as yellow, greasy patches on the upper leaf surface, which progress into powdery orange pustules on the underside, ultimately causing defoliation and decreased coffee yield. Other severe infections, such as coffee wilt disease (*Fusarium xylarioides*) and coffee bark disease (*Fusarium stilboides*), disrupt plant vascular functions, leading to withering and mortality. Soilborne pathogens like *Pythium* and *Phytophthora* contribute to damping-off and root rot, resulting in significant seedling losses.

The sustainability of coffee production is highly dependent on soil conditions. Ensuring optimal soil quality is essential for maintaining consistent crop yields, as different coffee varieties require specific soil compositions. Effective soil management, particularly through fertilization techniques, plays a critical role in maximizing soil fertility and supporting long-term productivity. Organic fertilizers enhance soil fertility and nutrient retention while minimizing environmental impacts (Abdulsahib *et al*., 2025). Leguminous plants contribute to soil improvement by fixing atmospheric nitrogen, whereas biochar enhances soil structure and overall fertility. Although synthetic fertilizers supply concentrated nutrients that accelerate plant growth, their excessive use can negatively affect soil health. Bio-fertilizers, comprising beneficial microorganisms such as *Rhizobium* spp. and mycorrhizal fungi, represent a sustainable alternative. These agents improve nutrient uptake and positively influence the composition of soil microbiota (Dias *et al*., 2025). Furthermore, the integration of soil sensors with artificial intelligence (AI) systems enables real-time and accurate monitoring of key soil parameters, including pH, moisture, temperature, and nutrient levels, thereby supporting optimized irrigation and fertilization practices.

Emerging methods for crop analysis and forecasting have the potential to significantly enhance agricultural productivity. These approaches assist farmers in selecting crop varieties that are best suited to their specific climatic and soil conditions. In particular, machine learning techniques enable the automated identification of suitable crops as well as the detection of pests and diseases, thereby supporting farmers in maximizing yields while maintaining soil fertility and nutrient balance. In this study, seven

distinct machine learning algorithms were used for crop selection and yield estimation (Chaudhari *et al*., 2025). The recommended approach integrates soil composition and climate data to accurately predict the optimal crops for a given location. This form of crop recommendation holds promise for improving yield, sustainability, and profitability across a wide range of agricultural contexts. Through a comprehensive analysis of a large historical dataset and rigorous training and evaluation of multiple machine learning models, this study achieved a classification accuracy of 99.54 %, which represents the highest reported to date.

Advancements in artificial intelligence and imaging technologies have led to innovative approaches in disease detection and management. Conventional disease detection methods rely on expert knowledge and manual assessment, making them time-consuming and subjective. To overcome these limitations, machine learning and image processing techniques have been increasingly explored for automated and efficient disease classification (Signo *et al*., 2024). Early studies have demonstrated the effectiveness of machine learning-based models in classifying coffee leaf diseases. For instance, Coffee-Net, a deep learning approach, has achieved high precision in disease identification under controlled conditions. However, existing models primarily focus on single-disease classification, failing to account for multi-disease interactions. Additionally, environmental factors such as lighting variability, camera quality, and background noise significantly affect the accuracy and robustness of these models.

Contemporary machine learning architectures aim to enhance disease classification by integrating both global and local feature extraction methodologies. Using global context and local feature analysis helps to understand both the big picture and the small details of lesions, which greatly improves the ability to identify disease spots (Alharbi *et al*., 2023). Furthermore, the inclusion of environmental variables in disease prediction models is crucial for the development of effective management strategies. Advanced forecasting models that utilize climatic data and disease progression trends can support outbreak prediction and optimize resource allocation for coffee producers (Anand *et al*., 2024).

Beyond disease detection, machine learning has also been applied in broader domains related to coffee quality assessment. For example, coffee sample adulteration has been detected using an electronic nose (E-Nose) system equipped with volatile organic compound (VOC) sensors. In this context, the density-based spatial clustering of applications with noise (DBSCAN) algorithm has demonstrated efficacy in distinguishing between pure and adulterated coffee blends. Additionally, machine learning techniques have been explored in various agricultural and energy-related applications, such as wind power forecasting through observer-controller-based frameworks incorporating a modified flower pollination algorithm (M-FPA).

Despite recent advances, machine learning methods for coffee disease diagnosis continue to face challenges in real-world applications. The limitations of single-disease classification models, coupled with environmental constraints, underscore the need for more robust and comprehensive diagnostic frameworks (Duhan *et al*., 2025). To address

these shortcomings, this study proposes a hybrid vision transformer-convolutional neural network (ViT-CNN) model for the detection of coffee plant diseases. The model integrates global and local features to enhance disease classification performance under diverse field conditions. Additionally, a counterfactual recommendation system is incorporated to support personalized management strategies for coffee farmers, thereby enabling earlier diagnosis and more effective responses. The Affogato mobile application delivers real-time diagnostic insights to farmers, ultimately aiming to increase crop yields and promote sustainable coffee cultivation.

MATERIALS AND METHODS

A substantial methodological groundwork was used to create the hybrid ViT-CNN model for thorough coffee plant health monitoring. Multi-angle images of leaves, cherries, and flowers were taken utilizing unmanned aerial vehicles (UAVs), plantation-fixed cameras, and high-resolution sensors. To increase model generalization, preprocessing procedures included augmentation, contrast enhancement, and noise reduction. CNN for localized spatial feature learning and ViT for global feature extraction were combined in the hybrid architecture.

A large annotated dataset was used to train the model, including data-driven hyperparameter tweaking, batch normalization, and adaptive learning rates. Accuracy, precision, recall, F1-score, and area under the curve of the receiver operating characteristic (AUC-ROC) were used to assess performance, and benchmark deep learning models, including ResNet, DenseNet, and Inception were compared. By effectively addressing the shortcomings of traditional methods and improving early disease detection for optimal coffee yield management, the results displayed through statistical analyses, confusion matrices, and visual segmentation maps showed superior disease classification accuracy and predictive reliability.

Image segmentation, object detection, and classification

Images of coffee berries, cherries, leaves, flowers, roots, and stems from public websites and captured directly at coffee plantations served as the basis for the study (Shafik *et al*., 2025). Real-time monitoring of coffee plantations using IoT sensors was conducted to gather data on soil and fertilizer use. The dataset included 640 photos of symptomatic coffee cherries, 180 leaves exhibiting damping-off symptoms, 250 occurrences of root rot, and 1840 soil monitoring images at a resolution of 256 × 256.

Images were preprocessed using Python libraries for computer vision, augmented using normalization, augmentation, and noise reduction approaches to optimize input for deep learning models. The YOLOv8 model was used for object identification, enabling rapid and precise training for the investigation of coffee plant diseases. Comparisons were conducted using the Efficient-Det, SSD, and R-CNN models. The result comprises bounding boxes labeled as “Leaf” or “Coffee Cherry.” For image classification, ResNet101 functioned as the principal pre-trained model, exhibiting

enhanced performance in complexity and accuracy relative to VGG-Net, InceptionV3, InceptionV4, and Mobile-Net (Chinnasamy *et al*., 2023). This phase classified photos using designations such as "Healthy" or "Diseased."

Image segmentation was used to identify distinct regions within images based on color, texture, spatial data, and object boundaries. The objects of interest encompassed "leaves," "buds," "secondary stems," and "primary branches" of coffee plants. DeepLabV3+ was chosen for segmentation tasks, exhibiting enhanced performance on intricate datasets relative to U-Net, R-CNN, and Mask R-CNN models. The segmentation procedure was executed utilizing open-source PyTorch libraries for model development and training (Essa and Murshid, 2023).

A three-stage deep learning pipeline was developed for coffee plant disease detection (Rehman *et al*., 2025): 1): object detection to locate diseased areas within images; 2): segmentation of detected areas to differentiate healthy and unhealthy portions of leaves; and 3): classification of segmented regions to confirm the presence or absence of disease (Figure 1).

Coffee plant disease analysis using hybrid ViT-CNN

Vision transformers (ViTs) and convolutional neural networks (CNNs) were effectively integrated to enhance performance (Isinkaye and Erute, 2022). C CNNs extract local

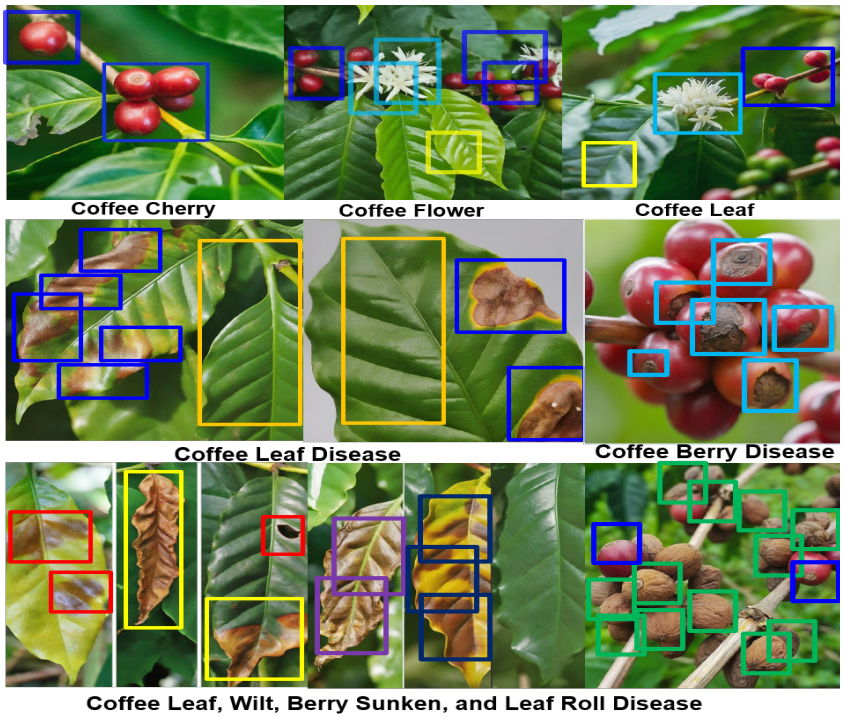

Figure 1. Object detection and instance segmentation demonstration on collected coffee plant images using YOLOv8. Bounding boxes (colored rectangles) indicate detected objected such as healthy coffee cherry, diseased leaves, and flowers.

features, while ViTs learn global dependencies, which have the potential to improve interpretability. The classified image dataset is split into rectangular patches. These patches are flattened into 1D vectors (height *H*, width *W*, and channel *C*) (Equation 1). A linear projection is applied to these vectors, transforming them into a fixed-size representation (Equation 2) where W_e is the embedding weight matrix and b_e is the embedding bias vector. Both W_e and b_e are learned during training. Linear projection consists of two main steps: first, flattening a vector, and second, transforming it into a fixed-size representation. This operation is performed twice in the original text and is thus reiterated here for completeness. Furthermore, the function *pow* increases exponentially with the index *i*, using a base of 10 000. These exponentially increasing values are used to generate different frequencies for the sine and cosine functions used in positional encodings.

$$flattened_{patch} = reshape(patch, [1, H * W * C]) \tag{1}$$

$$embedding = W_e * flattened_{patch} + b_e \tag{2}$$

$$PE(pos, i) = \sin\left(\frac{pos}{pow\left(10\,000, 2 * \frac{i}{d_{model}}\right)}\right) if\ i\ is\ even \tag{3}$$

$$PE(pos, i) = cos\left(\frac{pos}{pow\left(10\,000, \frac{2 * i + 1}{d_{model}}\right)}\right) if\ i\ is\ odd \tag{4}$$

$$encoded_{patch} = embedding + PE(pos) \tag{5}$$

Each image patch is effectively compressed into a lower-dimensional space through this method. To retain spatial information, positional encoding is incorporated into the embedding, thereby enabling the model to capture the relative position of each patch within the original image. Common approaches for positional encoding use sine and cosine functions (Equations 3 and 4), which define the positional encoding (PE) for a given position pos and embedding dimension *i*. The model dimension corresponds to the size of the output embedding vector. By utilizing sine and cosine functions at different frequencies across each dimension, this method generates a position-specific encoding with values ranging from -1 to 1. Consequently, for each component of the embedding vector, a position-specific encoding is established (Equation 5).

Multi-Head Self-Attention (MHA)

The interrelationships among various components within an image prompt the model to generate multiple "heads," each functioning as an autonomous attention mechanism that analyzes the image from a distinct perspective. Through linear projections, each head is transformed into three separate vectors: the Query (*Q*), the Key (*K*), and the Value (*V*) (Jiang *et al*., 2025). The Query vector is responsible for locating the portion of the image that potentially contains the disease. The Key vector encodes the salient features of the disease, such as the color, shape, and texture of lesions on the leaf. Meanwhile, the Value vector stores supplementary information relevant to the disease, including its name, its impact on the plant, associated soil conditions, required fertilizers, and possible treatment options:

$$Q = WQ * X + bQ \tag{6}$$

$$K = WK * X + bK \tag{7}$$

$$\mathrm{V} = \mathrm{WV} * \mathrm{X} + \mathrm{bV} \tag{8}$$

where *X* is a flattened image patch (d-dimensional vector); *WQ*, *WK*, and *WV* are weight matrices for Query (Equation 6), Key (Equation 7), and Value (Equation 8) projections; and *bQ*, *bK*, and *bV* are bias vectors for Query, Key, and Value projections. Attention scores assign a score to each pair of patches, indicating how relevant one patch (Value) is to the query of another. This score is calculated by taking the dot product of the Query and Key vectors for each pair (Jung *et al*., 2023). The compute inner product function calculates the inner product of a specific patch's query vector (*Q*) and the key vector (*K*) of all patches in the image. This operation indicates how close the current patch is to other areas of the image (Equation 9):

$$A_{ij} = Q_i * K_j \tag{9}$$

where *i* refers to the current patch and *j* iterates over all patches. The SoftMax function is applied to the inner products to normalize the attention scores and ensure they total to one. This function transforms them into weights that reflect the relative significance of each patch, depending on its resemblance to the current patch (Equation 10).

$$Attention(Q_i, K) = Softmax(A_i) \tag{10}$$

Attention scores are computed using weighted values, whereby the model produces a weighted sum of the Value (*V*) vectors corresponding to each patch. Patches assigned higher attention scores exert a greater influence on the final output (Lee and Rianto, 2024). Specifically, these scores are obtained by multiplying the attention weights, derived from the SoftMax function with the respective Value vectors across all patches.

This mechanism serves to emphasize the contributions of the most relevant patches, as dictated by their attention scores (Equation 11).

$$Weighted_{Value_i} = Attention(Q_i, K) * V \quad (11)$$

The context vector that includes information from relevant parts of the image based on their similarity to the current patch (Equation 12).

$$Z_i = \Sigma\left(Weighted_{Value_i}\right) \quad (12)$$

Every head generates concatenated outputs to gather data from many angles. Applying a last linear projection helps to alter the result overall.

Feed-forward network with convolutional layers

Convolutional neural networks (CNNs) layers use image processing techniques to identify features such as edges, textures, and color patterns in the input image (coffee plant leaf, coffee berry, and flower) (Wang *et al*., 2025). By layering many convolutional layers, the network progressively enhances its comprehension of complex features that may be used for illness identification.

A feed-forward network (FFN) is a class of neural networks composed of multiple perceptrons, each of which uses a nonlinear activation function, specifically the Gaussian error linear unit (GELU). In the context of multiclass classification tasks, the primary loss function utilized is cross-entropy loss, which is widely used for predicting multiple disease categories, such as coffee leaf rust and berry disease. For the convolutional neural network (CNN) component within the hybrid model framework, stochastic gradient descent (SGD) with momentum is applied. This optimization strategy enhances convergence by promoting a more stable and directed trajectory throughout training iterations, thereby reducing oscillations.

These functions allow the network to learn about non-linear connections between the retrieved characteristics, which is necessary for distinguishing between healthy and diseased leaves with minor differences, as shown in the following algorithm:

```
def create_model(img_shape): # Define model architecture
    model = models.Sequential()
    model.add(layers.Conv2D(32, (3, 3), activation=" relu", input_shape=img_shape))
    model.add(layers.MaxPooling2D((2, 2)))
    model.add(layers.Conv2D(64, (3, 3), activation="relu"))
    model.add(layers.MaxPooling2D((2, 2)))
    model.add(layers.Flatten())
    model.add(layers.Dense(128, activation="relu"))
    model.add(layers.Dropout(0.2)) # Optional for regularization
```

```
    model.add(layers.Dense(3, activation="softmax")) # Multi-class for healthy/
    diseased/other
    model.compile(loss="categorical_crossentropy", optimizer="adam",
    metrics=["accuracy"])
    return model
train_data, train_labels, test_data, test_labels = load_data() # Load preprocessed data
(replace with your data loading logic)
img_shape = train_data.shape[1:] # Define image shape based on your data
    model = create_model(img_shape) # Create and train the model
    model.fit(train_data, train_labels, epochs=10, validation_data=(test_data, test_
    labels))
loss, accuracy = model.evaluate(test_data, test_labels) # Evaluate the model on
unseen data
print ("Test Accuracy:", accuracy)
new_image = load_new_image() # Use the model for prediction on a new image
(replace with your image loading logic)
prediction = model.predict(np.expand_dims(new_image, axis=0))
predicted_class = np.argmax(prediction) # Get class with highest probability
```

The network incorporates a ViT module that emphasizes local features. ViT excels at capturing long-distance connections throughout the image (Shafik *et al*., 2025). This is especially useful for detecting diseases in coffee plants, as disease symptoms can be found throughout the leaf rather than just one area. The convolutional layers, along with feed-forward networks (FFNs), act as feature extractors, identifying patterns and textures in the coffee leaf image. The ViT module then examines the interrelations of the extracted characteristics over the whole leaf. Combining these functionalities allows the model to efficiently acquire the complex visual cues associated with various coffee plant diseases.

Batch normalization

Batch normalization layers can be positioned after every convolutional layer and fully connected FFN layer in the hybrid ViT-CNN architecture (Mamba Kabala *et al*., 2023). During the training process, batch normalization would adjust the activations of these layers by normalizing them according to the statistics calculated from each mini-batch. Batch normalization is an approach that standardizes the following algorithm.

```
def create_model(img_shape): # Define the model
inputs = layers.Input(shape=img_shape)
    x = layers.Conv2D(32, 3, activation="relu")(inputs) # Convolutional block with
    Batch Norm
```

```
    x = layers.BatchNormalization()(x)
    x = layers.MaxPooling2D(pool_size=(2, 2))(x)
    x = layers.Conv2D(64, 3, activation="relu")(x)
    x = layers.BatchNormalization()(x)
    x = layers.MaxPooling2D(pool_size=(2, 2))(x)
    x = layers.Flatten()(x) # Flatten layer
    x = layers.Dense(128, activation="relu")(x) # Fully connected layers
    x = layers.Dropout(0.5)(x)
outputs = layers.Dense(3, activation="softmax")(x) # Multi-class for healthy/diseased/
other
model = models.Model(inputs=inputs, outputs=outputs)
return model
model = create_model((224, 224, 3)) # Replace with your image size # Compile the
model
model.compile(optimizer="adam", loss="categorical_crossentropy",
metrics=["accuracy"])
# Train the model (Coffee Wilt disease and Coffee berry disease)
X_train, X_test, y_train, y_test = ... # Load your training and testing data
model.fit(X_train, y_train, epochs=10, validation_data=(X_test, y_test))
loss, accuracy = model.evaluate(X_test, y_test) # Evaluate the model
print("Test accuracy:", accuracy)
# Use the model for prediction
new_image = ... # Load a new image
prediction = model.predict(np.expand_dims(new_image, axis=0))
predicted_class = np.argmax(prediction) # Get the class with highest probability
```

In neural networks, the activations of each layer, excluding the input layer, are typically normalized across each mini-batch of training data to have a mean of zero and a standard deviation of one. This normalization enhances both the reliability and accuracy of the model during training. Batch normalization, as described by Chai Abel *et al*. (2025), is a technique that stabilizes the learning process, thereby accelerating training and improving convergence of the network. This approach mitigates the issue of internal covariate shift, a phenomenon that contributes to the vanishing or exploding gradient problem, which can hinder the effective training of deep neural networks.

Feature fusion and classification head

Feature fusion refers to the integration of data from multiple locations within the network. In the hybrid ViT-CNN architecture, the primary feature streams comprise convolutional feature maps generated by convolutional layers, which effectively capture local features such as edges and textures (Palanisamy *et al*., 2023). In parallel, the ViT module produces embeddings that represent global relationships across the entire leaf image. While convolutional features provide fine-grained, localized

information about specific regions of the leaf, the ViT embeddings capture broader disease patterns and their spatial context.

The final component of the disease prediction network is the classification head, which receives the fused features from preceding stages. This classification head typically consists of fully connected layers equipped with SoftMax or other non-linear activation functions. The number of neurons in the final layer corresponds to the number of target classes to be identified (i.e., healthy, rust disease, leaf spot disease). During training, the classification head learns to map the fused features to the corresponding disease probabilities (Balasundaram *et al*., 2025).

Counterfactual recommendation using hybrid ViT-CNN

The recommendations are hypothetical by comparing the actual generated data to historical data (Figure 2). There are three methods used to compare the suggestion. The dataset is divided into three types: historical data, current data, and a combination of current and historical data.

A coffee farmer utilizes a smartphone application integrated with a coffee plant health monitoring system to detect anomalies in plant components, including leaves, blossoms, and cherries. Upon observing irregularities, the farmer captures an image of the affected leaves and uploads it via the mobile application (Ratanoo *et al*., 2024). The image is transmitted to a server, where it is analyzed by the Affogato system, which utilizes a hybrid ViT-CNN model that leverages both global and local image features to identify the most probable disease.

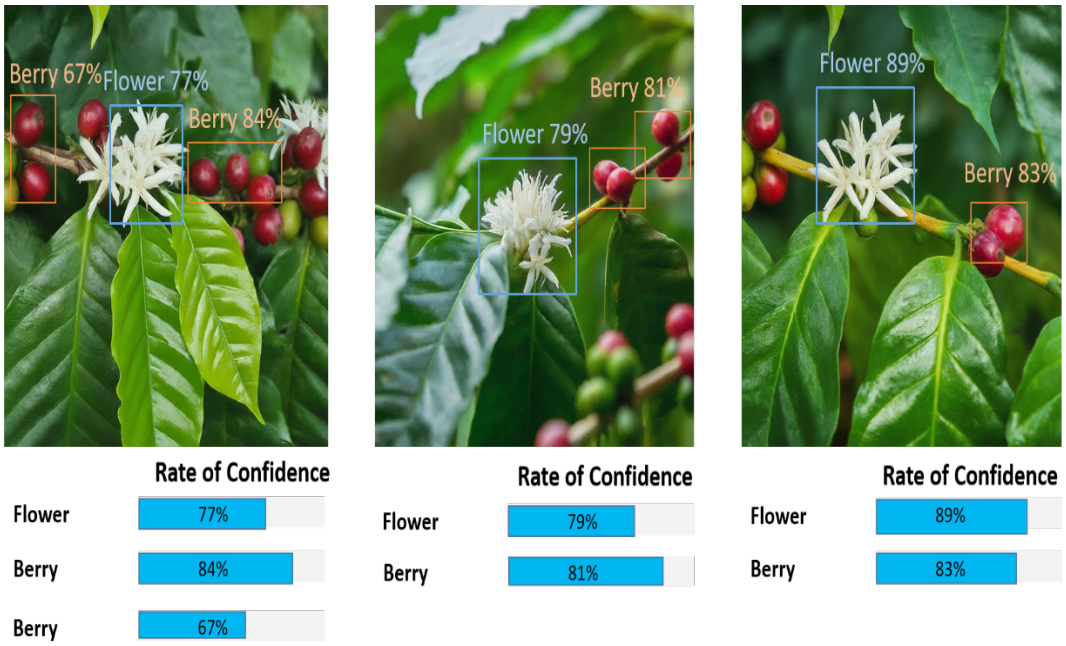

Figure 2. Virtual observation of the object detection results. Coffee flower and berry localization with confidence scores.

Subsequently, the system queries its database to retrieve detailed information regarding the diagnosed condition. The coffee producer is then presented with a comprehensive explanation of the disease and its associated symptoms, as well as treatment options. These treatment recommendations include assessments of therapeutic effectiveness and potential adverse effects. The application displays the identified disease and suggests the most appropriate counterfactual treatment, derived from the model's prediction and database insights (Selvanarayanan *et al*., 2024).

In the image analysis process, local binary patterns (LBPs) are used to examine localized texture features. LBPs function by detecting spatial variations in pixel intensity between a central pixel and its neighboring pixels. These intensity patterns are encoded into binary sequences, which represent the local texture characteristics (Equation 13).

$$LBP = \sum \left(2^n * S(p_i - p_c)\right) \tag{13}$$

where p_i is the intensity value of the i-th neighbor in the circular neighborhood, p_c is the intensity value of the central pixel, $S(x)$ is a Thresholding function, $S(x) = 1$ if $x \geq 0$, otherwise $S(x) = 0$, and n is the position of the bit in the binary string (0 for top-left neighbor, increasing clockwise). Round neighborhoods surround a central pixel in the image. This neighborhood contains 8 or 16 circular pixels. The intensity of the core pixel is compared to its neighbors in the defined neighborhood (Selvanarayanan *et al*., 2023). The binary code generation for each neighbor's intensity is designated as one if it exceeds the center pixel, and zero otherwise. Starting with the top-left neighbor, these binary values rotate clockwise. This binary string surrounds the central pixel and reflects the local texture pattern. During the conversion, each bit is assigned a weight of 2^n, where n represents the bit position in the binary string, starting from zero. The decimal value is calculated by summing the set bit weights.

RESULTS AND DISCUSSION

The proposed technique was tested using a dataset of coffee blossoming, coffee berry, and diseased leaf images. The hybrid ViT-CNN algorithm, combined with Vision, was used to detect coffee plant diseases at an early stage. Evaluation metrics such as accuracy, precision, and recall were used. The ViT-CNN model outperformed other current models, demonstrating higher levels of accuracy.

Evaluation setup and datasets

A total of 1056 images were collected using unmanned aerial vehicles (UAVs), fixed plantation cameras, and high-resolution agricultural imaging sensors. These images captured various stages of disease affecting the leaves, cherries, and roots of coffee plants. To ensure the generation of high-quality labeled data, expert agronomists

annotated the images during the selection process. Subsequently, data augmentation techniques were employed to enhance model generalization.

The proposed model was developed using the Keras Python framework (Version 2.7) and implemented in Python 3.6.5. It was executed on a workstation equipped with an Intel Core i5-8600k processor, a GeForce 1050Ti graphics card (4 GB memory), 16 GB of RAM, a 250 GB solid-state drive (SSD), and a 1 TB hard disk drive (HDD). The model was trained with the following hyperparameters: batch size of 5, learning rate of 0.01, dropout rate of 0.5, and 55 training epochs (Serrato-Diaz *et al*., 2024).

The input image sizes used in testing ranged from 32 × 32 × 3 to 256 × 256 × 3. Notably, the proposed method outperformed alternative approaches when applied to images with dimensions of 224 × 224 × 3. Model evaluation was conducted using standard classification metrics, including true positives, true negatives, false positives, and false negatives. A high-resolution digital camera was utilized to detect color variations during berry development stages, capture detailed images of coffee flowers at various blooming phases, identify sunken berries, and diagnose specific foliar diseases through changes in leaf pigmentation (Figure 3).

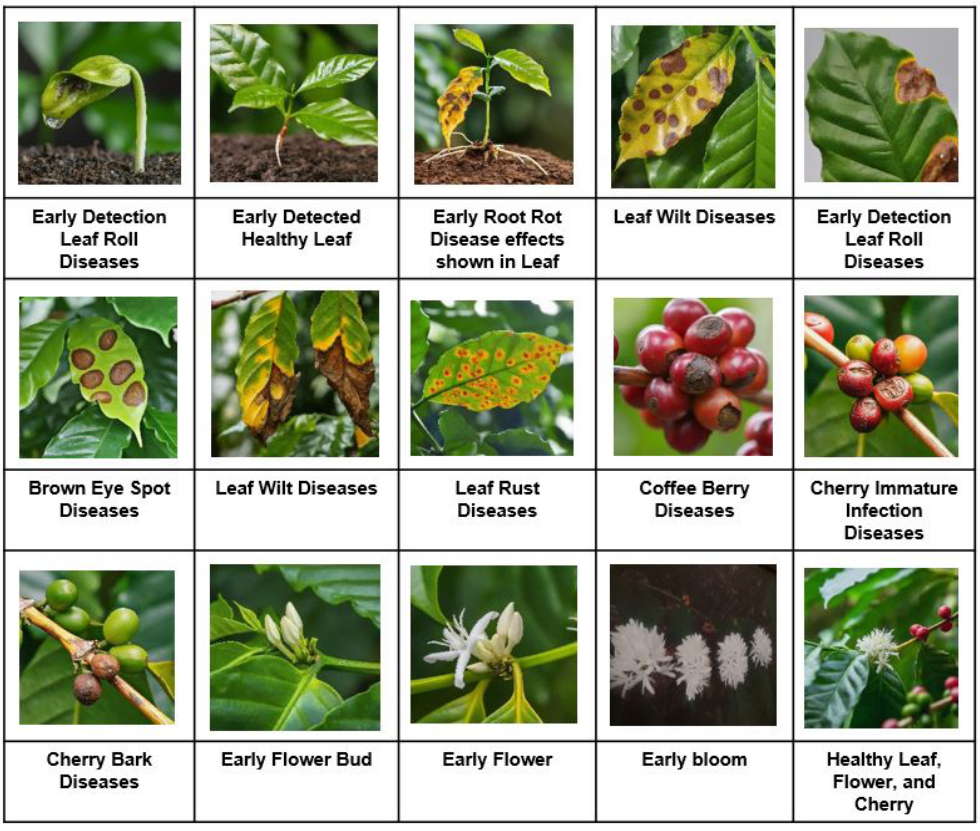

Figure 3. Visual representation of the 15-class coffee plant image dataset, showing representative samples from each class, encompassing various growth stages and disease manifestations used for training the convolutional neural network for automated classification.

The enlargement features for taking close-up pictures of a cherry, a berry, and a sickly leaf, data analysis, algorithm execution, and image processing were all handled by cloud computing, offering a large amount of storage space for pictures, annotations, and results (Sharma *et al*., 2024). The image processing software used Fiji and OpenCV. Custom algorithms for the early identification and surface segmentation of plant diseases were devised and executed using TensorFlow and PyTorch.

Field setup for observing coffee plant disease

A high-resolution digital camera with interchangeable lenses capable of capturing detailed photographs of coffee plant leaves, coffee berries, root rot, damping off disease, flowers at various stages of flowering, and close-up shots of flowers. Macro lenses help take close-up photos of individual cherries, damping disease, blossoms, and basic roots. The monitoring of coffee plant disease can be accomplished by using cloud storage systems to store collected photos (Figure 4). A virtual environment simulates real-world scenarios. The findings stemmed from the implemented system following the training and execution of a smartphone application designed to detect coffee plant diseases. A 2.4 GHz TM i5-9300H CPU, Google Collab, and Python 3.0.6 were used to train and execute a smartphone application for identifying coffee plant diseases (Signo *et al*., 2024).

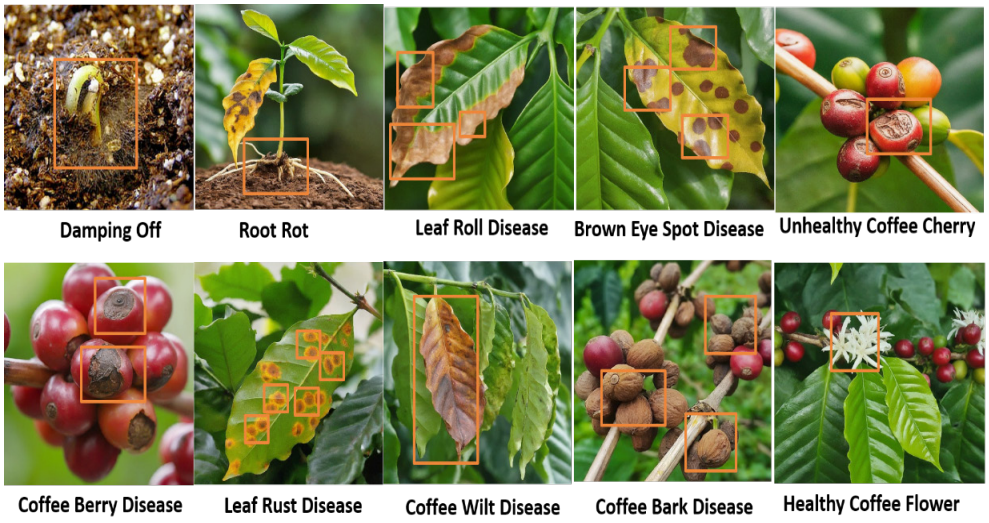

Figure 4. Real-time coffee plant disease monitoring via object detection.

Performance evaluation using hybrid ViT-CNN

Classification accuracy (Equation 14) is a metric that represents the percentage of samples correctly classified as healthy or sick. True Positives (TP) indicate several accurately diagnosed diseased samples. True Negatives (TN) show several correctly categorized healthy samples. Total Samples is a list of all the samples in the dataset.

The precision (Equation 15) statistic calculates the proportion of correctly identified unhealthy cases while minimizing false positives, indicating the accuracy of positive predictions (Taha and Hussein, 2022).

$$Accuracy = \frac{True\ Positives\ +\ True\ Negatives}{Total\ Samples} \tag{14}$$

$$Precision = \frac{TP}{TP\ +\ False\ Positives\ (FP)} \tag{15}$$

False positives (FP) are the number of healthy samples that are incorrectly classified as sick. The percentage of actual disease instances that are successfully recognized with no false negatives is known as recall (sensitivity) (Equation 16). False Negatives (FN) are samples of sick material that are mistaken for healthy. The F1-Score (Equation 17) effectively balances precision and recall, making it especially useful when both metrics are required. The intersection over union (IoU) segmentation metric (Equation 18) assesses the degree of overlap between actual and projected disease zones on coffee plant leaves, cherries, flowers, or fruits.

$$Recall = \frac{TP}{TP\ +\ False\ Negatives\ (FN)} \tag{16}$$

$$F1 - Score = 2 * \frac{Precision * Recall}{Precision + Recall} \tag{17}$$

$$IoU = \frac{Intersection\ Area}{Union\ Area} \tag{18}$$

The area under the curve (AUC) measures the model's ability to differentiate between healthy and diseased groups using two metrics: true positive rate (TPR) (Equation 19) and false positive rate (FPR) (Equation 20). These metrics can be used for multi-class tasks, such as understanding various types of sickness, by assessing each class separately. Crossing the line where the masks of the expected and ground reality overlap. The entire union area is covered by either the expected or actual mask, whichever is larger.

$$TPR = \frac{TP}{TP\ +\ FN} \tag{19}$$

$$FPR = \frac{FP}{FP\ +\ TN} \tag{20}$$

True positive (TP) represents the number of correctly classified positive cases where indicated. False negative (FN) refers to several cases that were misclassified as negative (missed positive). False positive (FP) count of cases misclassified as negative but actually positive. True negative (TN) refers to several accurately identified undesirable events (Tamilvizhi *et al*., 2022). The experimental parameters were set to 16 batches with a learning rate of 0.01, and the performance was compared to other deep-learning models for detecting coffee plant diseases (Table 1).

Table 1. Comparative performance analysis of hybrid vision transformer-convolutional neural network (ViT-CNN) model and existing models, showing accuracy and loss metrics for the proposed model across training, validation, and testing phases, benchmarked against state-of-the-art deep learning models.

Model	Training accuracy	Validation accuracy	Testing accuracy	Training loss	Validation loss	Testing loss
Hybrid ViT-CNN	1.000	0.9867	0.9879	0.0047	0.0124	0.0578
MVGG16	0.9976	0.9802	0.9711	0.0720	0.0777	0.0701
Inception V3	0.9941	0.9791	0.9766	0.0752	0.0711	0.0714
Xception	0.9921	0.9716	0.9657	0.0272	0.0930	0.0817
DenseNet-121	0.9711	0.9651	0.9611	0.0547	0.0577	0.0991
MobileNet-V2	0.9418	0.9374	0.9457	0.0478	0.0321	0.0840
Visual transformer (ViT)	0.9089	0.8947	0.9055	0.0145	0.0477	0.0944
ResNet50	0.8776	0.8624	0.8518	0.0594	0.0749	0.0741

Pre-trained models utilized in this study include MVGG16, Inception V3, Xception, DenseNet-121, MobileNet-V2, ViT, and ResNet50. Among these, the hybrid ViT-CNN model demonstrated the most favorable overall performance across key evaluation metrics. Specifically, it achieved a high training-validation accuracy balance (0.9867), along with superior classification outcomes, including accuracy (0.9881), precision (0.9893), recall (0.9895), and area under the curve (AUC) (0.9896). These results indicate the model's strong capability in both the accurate classification of coffee plant diseases and the effective differentiation between healthy and diseased specimens.

The intersection over union (IoU) value of 0.9833 indicates a high degree of agreement between the predicted and actual disease regions (Table 2). The proposed model (blue line) achieves a higher training accuracy, approaching 1.0, and does so more rapidly than the previous model (green line), demonstrating superior learning efficiency (Figure 5). Furthermore, the validation accuracy (dashed blue line) closely follows the training accuracy, exhibiting a narrower gap in comparison to the existing model (dashed green line) (Figure 6). This suggests improved generalization performance of the new model. Finally, the classification-based confidence score for specific disease detection (Figure 7) is defined as the predicted probability of belonging to the corresponding disease class (Equation 21).

Table 2. Comprehensive performance metrics of the hybrid vision transformer-convolutional neural network (ViT-CNN) comparing accuracy, precision, F1-score, recall, area under the curve (AUC), and intersection over union (IoU) against other deep learning models, demonstrating superior performance across multiple evaluation metrics.

Model	Accuracy	Precision	F1-score	Recall	AUC	IoU
Hybrid ViT-CNN	**0.9881**	0.9893	0.9849	0.9895	0.9896	0.9833
MVGG16	0.9679	0.9643	0.9604	0.9691	0.9616	0.9619
Inception V3	0.9517	0.9515	0.9521	0.9536	0.9604	0.9607
Xception	0.9257	0.9280	0.9251	0.9232	0.9225	0.9257
DenseNet-121	0.8871	0.8793	0.8814	0.8890	0.8891	0.8879
MobileNet-V2	0.8557	0.8505	0.8561	0.8536	0.8644	0.8657
Visual Transformer (ViT)	0.8152	0.8182	0.8106	0.8132	0.8125	0.8157
ResNet50	0.7857	0.7882	0.7856	0.7832	0.7820	0.7807

$$Confidence_{score}(Disease_i) = Predicted_{probability}(Class_i) \quad (21)$$

where $Disease_i$ represents a specific coffee plant disease class, and $Predicted_{probability}(Class_i)$ is the probability value predicted by the model for the image region belonging to class.

The model demonstrated exceptional accuracy for detecting critical objects (Figure 7), such as "Bud" (99.99 %), "Plant" (98.67 %), and "Tree" (97.23 %), indicating strong reliability in identifying plant structures. The horizontal bar chart efficiently displays the confidence scores, making it easy to compare detection accuracy across different objects.

The bubble-enhanced line graph adds an interesting visual layer by displaying confidence variations in a structured manner (Figure 8). High confidence indicates that the model is well-trained and capable of distinguishing between various plant components with minimal error.

Mobile application

Farmers can utilize the user-friendly Affogato mobile application to upload images of their coffee plants, including diseased flowers, cherries, and leaves (Figure 9). Upon upload, each image undergoes a series of preprocessing steps, such as resizing, normalization, and, if necessary, color space adjustments, to ensure compatibility with the subsequent analytical model. The preprocessed image is then input into the hybrid ViT-CNN model, which has been trained on an extensive dataset comprising coffee plant images under various conditions, including healthy and diseased specimens of flowers, cherries, and leaves.

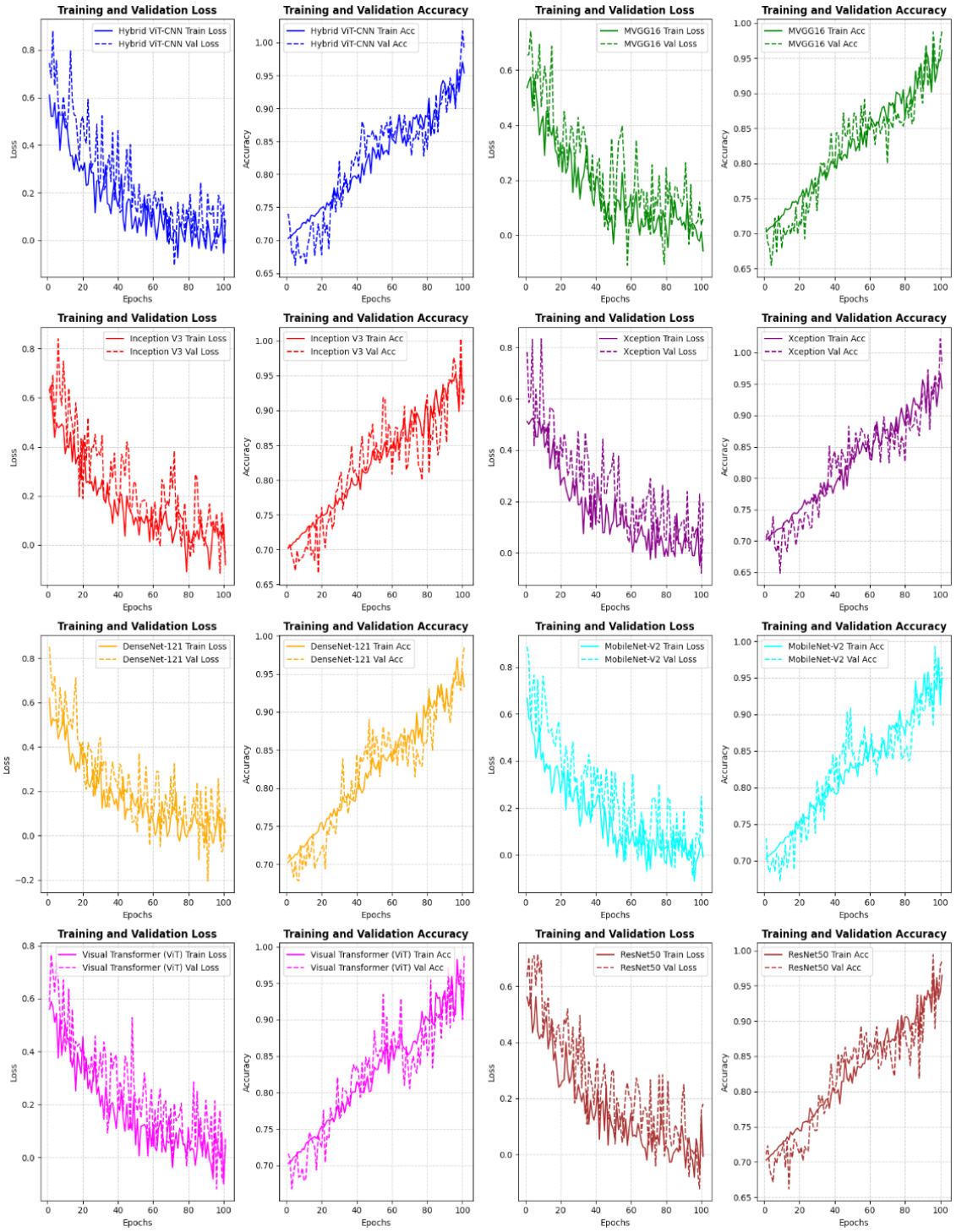

Figure 5. Comparison of training and validation loss and accuracy for different deep learning models over 100 epochs.

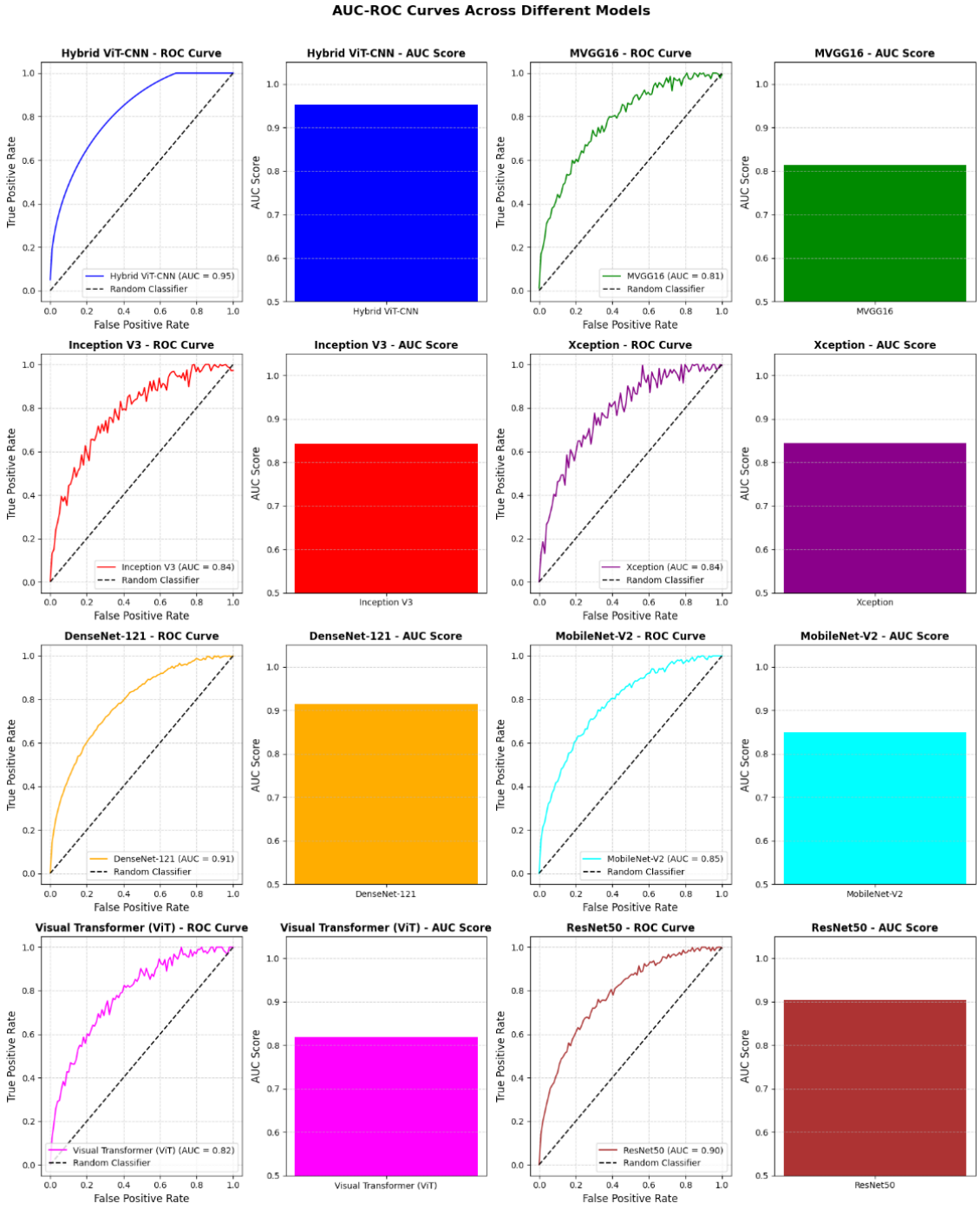

Figure 6. Performance comparison of the area under the curve of the receiver operating characteristic (AUC-ROC) scores for each model.

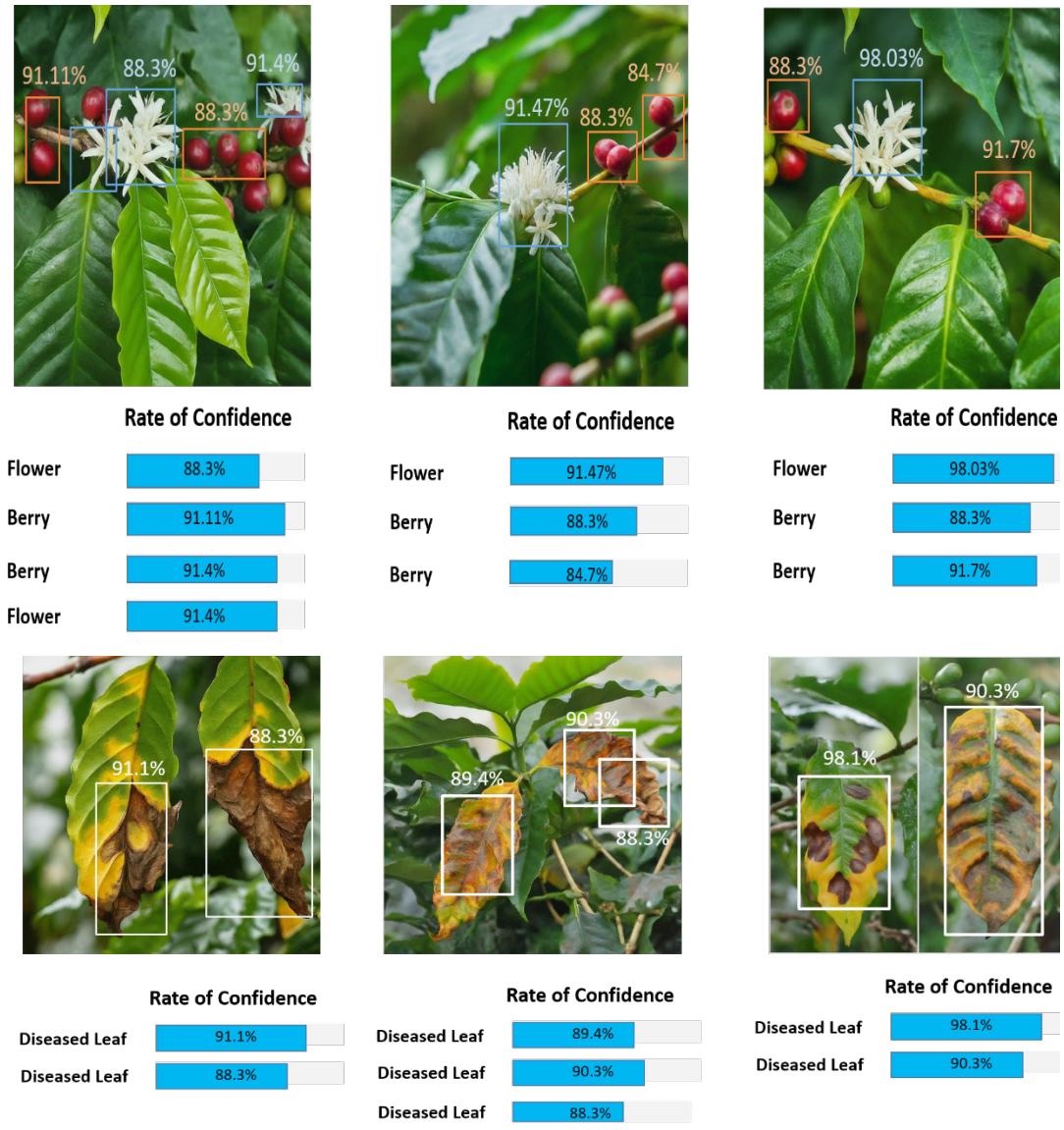

Figure 7. Coffee plant disease detection using confidence rates.

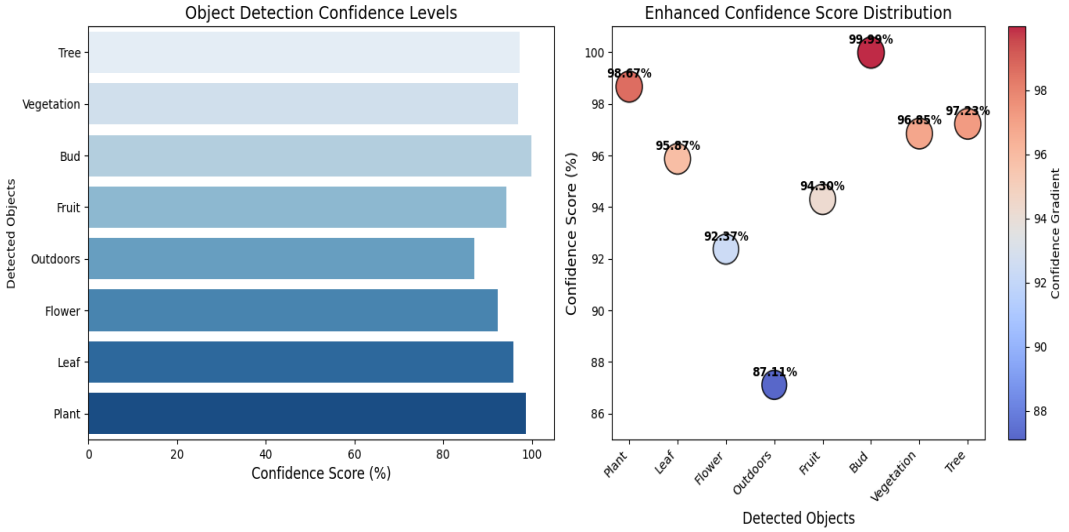

Figure 8. Visualization of object detection confidence levels. A comparative analysis is presented using two graphical formats: a bar chart (left) and a bubble chart (right). The bar chart illustrates the confidence scores associated with detected objects, while the enhanced bubble chart displays the distribution of these scores using variations in both size and color gradients to convey magnitude and intensity.

Figure 9. Affogato: an AI-powered system for the diagnosis and prevention of coffee plant diseases. This platform provides a step-by-step framework that guides farmers from the initial detection of plant diseases to the implementation of preventive strategies, utilizing counterfactual analysis and farm-centric advisory approaches.

The model performs real-time analysis to identify the specific plant part depicted (i.e., flower, cherry, or leaf) and to predict the most probable condition based on visual characteristics. Subsequently, the system generates personalized recommendations informed by the predicted condition and supplemented by additional contextual data provided by the farmer. This contextual data may include historical and current observations, such as geographical location, soil type, and climatic conditions.

CONCLUSIONS

A smartphone-based system for the detection of plant diseases and the recommendation of treatments was developed using machine learning techniques. The proposed hybrid model, integrating Vision Transformers and Convolutional Neural Networks (ViT-CNN), combines the global contextual awareness of Vision Transformers with the localized feature extraction capabilities of Convolutional Neural Networks. This synergistic architecture enables accurate diagnosis of various coffee plant diseases. A key advancement in the system is the implementation of counterfactual suggestion processes, which extend beyond mere disease identification. These processes simulate the health status of the plant under multiple hypothetical treatment scenarios, thereby allowing farmers to explore "what-if" analyses and make more informed decisions regarding disease management. Future research should focus on enhancing the model's generalizability across diverse coffee plant varieties, environmental conditions, and disease phenotypes.

ACKNOWLEDGEMENTS

Data related to the study are publicly available and can be accessed at Selvanarayanan R. 2024. Coffee plant leaf disease. Zenodo. https://zenodo.org/records/13674477

The source code used for leaf disease classification is available at Selvanarayanan R. 2024. Leaf disease classification code. Zenodo. https://zenodo.org/records/11107971

REFERENCES

Abdulsahib GM, Hassan HJ, Khalaf OI. 2024. A modified bandwidth prediction algorithm for wireless sensor networks. Journal of Information Science and Engineering 40 (1): 177–188. https://doi.org/10.6688/JISE.202401_40(1).0011

Alharbi M, Rajagopal SK, Rajendran S, Alshahrani M. 2023. Plant disease classification based on ConvLSTM U-net with fully connected convolutional layers. Traitement du Signal 40 (1): 157. https://doi.org/10.18280/ts.400114

Anand D, Khalaf OI, Abdulsahib GM, Chandra GR. 2024. Original research article identification of meningioma tumor using recurrent neural networks. Journal of Autonomous Intelligence 7 (2): 1–27. https://doi.org/10.32629/jai.v7i2.653

Balasundaram A, Sundaresan P, Bhavsar A, Mattu M, Kavitha MS, Shaik A. 2025. Tea leaf disease detection using segment anything model and deep convolutional neural networks. Results in Engineering 25: 103784. https://doi.org/10.1016/j.rineng.2024.103784

Chai AYH, Lee SH, Tay FS, Goëau H, Bonnet P, Joly A. 2025. PlantAIM: A new baseline model integrating global attention and local features for enhanced plant disease identification. Smart Agricultural Technology 10: 100813. https://doi.org/10.1016/j.atech.2025.100813

Chaudhari RR, Jain S, Gupta S. 2025. Agricultural machine learning platform: Enhancing crop suggestion and crop yield estimates. Journal of Integrated Science and Technology 13 (1): 1017. https://doi.org/10.62110/sciencein.jist.2025.v13.1017

Chinnasamy P, Wong WK, Raja AA, Khalaf OI, Kiran A, Babu JC. 2023. Health recommendation system using deep learning-based collaborative filtering. Heliyon 9 (12): 1–27. https://doi.org/10.1016/j.heliyon.2023.e22844

Dias JS, Boa Sorte LX, Fambrini F, Saito JH. 2025. Coffee plant disease detection using JSEG segmentation and near sets clustering. Fifth Symposium on Pattern Recognition and Applications (SPRA 2024) 13540: 40–52. https://doi.org/10.1117/12.3056434

Duhan S, Gulia P, Gill NS, Narwal E. 2025. RTR_Lite_MobileNetV2: A lightweight and efficient model for plant disease detection and classification. Current Plant Biology 42: 100459. https://doi.org/10.1016/j.cpb.2025.100459

Essa HM, Murshid AM. 2023. Optimizing image processing with CNNs through transfer learning: Survey. Al-Kitab Journal for Pure Sciences 7 (1): 57–68. https://doi.org/10.32441/kjps.07.01.p6

Isinkaye FO, Erute ED. 2022. A smartphone-based plant disease detection and treatment recommendation system using machine learning techniques. Trees 10 (1): 1–18. https://doi.org/10.14738/tmlai.101.11313

Jiang J, Ji H, Zhou G, Pan R, Zhao L, Duan Z, Liu X, Yin J, Duan Y, Ma Y, *et al*. 2025. Non-destructive monitoring of tea plant growth through UAV spectral imagery and meteorological data using machine learning and parameter optimization algorithms. Computers and Electronics in Agriculture 229: 109795. https://doi.org/10.1016/j.compag.2024.109795

Jung M, Song JS, Shin AY, Choi B, Go S, Kwon SY, Park J, Park SG, Kim YM. 2023. Construction of deep learning-based disease detection model in plants. Scientific Reports 13 (1): 7331. https://doi.org/10.1038/s41598-023-34549-2

Lee CH, Rianto B. 2024. An AI-powered e-nose system using a density-based clustering method for identifying adulteration in specialty coffees. Microchemical Journal 197: 109844. https://doi.org/10.1016/j.microc.2023.109844

Mamba Kabala D, Hafiane A, Bobelin L, Canals R. 2023. Image-based crop disease detection with federated learning. Scientific Reports 13 (1): 19220. https://doi.org/10.1038/s41598-023-46218-5

Palanisamy S, Abdulsahib GM, Khalaf OI, SS A Wong WK, Pan SH. 2023. Design of artificial magnetic conductor based stepped V-shaped printed multiband antenna for wireless applications. International Journal of Advances in Soft Computing and its Applications 15 (3): 1–25.

Ratanoo R, Walia SS, Saini KS, Dheri GS. 2024. Residual effects of chemical fertilizers, organic manure, and biofertilizers applied to preceding Gobhi Sarson crop on summer mung bean (*Vigna radiata* L.). Legume Research 47 (1): 64–68. https://doi.org/10.18805/lr-4767

Rehman M, Petrillo A, Baffo I, Iovine G, de Felice F. 2025. Optimizing coffee supply chain transparency and traceability through mobile application. Procedia Computer Science 253: 2116–2126. https://doi.org/10.1016/j.procs.2025.01.272

Selvanarayanan R, Rajandran S, Alotaibi Y. 2023. Using hierarchical agglomerative clustering in e-nose for coffee aroma profiling: Identification, quantification, and disease detection. Instrumentation Mesure Métrologie 22 (4): 127–140. https://doi.org/10.18280/i2m.220401

Selvanarayanan R, Rajendran S, Alotaibi Y. 2024. Early detection of disease in coffee cherry based on computer vision techniques. Computer Modeling in Engineering and Sciences 139 (1): 759–782. https://doi.org/10.32604/cmes.2023.044084

Serrato-Diaz LM, Mariño YA, de Jesús-González J, Goenaga R, Bayman P. 2024. Coffee fruit rot: The previously unrecognized role of *Fusarium* and its interactions with the coffee berry borer (*Hypothenemus hampei*). Phytopathology 22 (1): 1–18. https://doi.org/10.1094/phyto-02-24-0046-r

Shafik W, Tufail A, de Silva LC, Apong RAAHM. 2025. A novel hybrid inception-xception convolutional neural network for efficient plant disease classification and detection. Scientific Reports 15 (1): 3936. https://doi.org/10.1038/s41598-024-82857-y

Shafik W, Tufail A, de Silva LC, Apong RAAHM. 2025. An enhanced deep convolutional neural network for plant disease detection and classification: Elevating sustainable agriculture. Artificial Intelligence and Data Science for Sustainability 12: 297–322. https://doi.org/10.4018/979-8-3693-6829-9.ch010

Sharma V, Tripathi AK, Mittal H, Nkenyereye L. 2025. SoyaTrans: A novel transformer model for fine-grained visual classification of soybean leaf disease diagnosis. Expert Systems with Applications 260: 125385. https://doi.org/10.1016/j.eswa.2024.125385

Signo SDR, Tuquero CLG, Arboleda ER. 2024. Coffee disease detection and classification using image processing: A literature review. International Journal of Science and Research Archive 11 (1): 1614–1621. https://doi.org/10.30574/ijsra.2024.11.1.0212

Taha MD, Hussein KA. 2022. Generation S-box, and P-layer for PRESENT algorithm based in 6D hyper chaotic system. Al-Kitab Journal for Pure Sciences 7 (1): 48–56. https://doi.org/10.32441/kjps.07.01.p5

Tamilvizhi T, Surendran R, Anbazhagan K, Rajkumar, K. 2022. Quantum behaved particle swarm optimization-based deep transfer learning model for sugarcane leaf disease detection and classification. Mathematical Problems in Engineering 2022 (1): 3452413. https://doi.org/10.1155/2022/3452413

Wang Y, Wang Y, Mu J, Raza Mustafa G, Wu Q, Wang Y, Zhao B, Zhao S. 2025. Enhanced multiscale plant disease detection with the PYOLO model innovations. Scientific Reports 15 (1): 5179. https://doi.org/10.1038/s41598-025-89034-9

Agrociencia

FARMER WILLINGNESS TO PAY FOR IMPROVED IRRIGATION WATER QUALITY AND PRODUCE INNOCUOUS FOODS IN IRRIGATION DISTRICT 003 TULA, HIDALGO

Jonathan **Hernández-Pérez**[1], Oscar Antonio **Arana-Coronado**[2], Ramón **Valdivia-Alcalá**[1], Fermín **Sandoval-Romero**[1], Juan **Hernández-Ortiz**[1*]

[1]Universidad Autónoma Chapingo. División de Ciencias Económico-Administrativas. Carretera México-Texcoco km 38.5, Chapingo, Texcoco, State of Mexico, Mexico. C. P. 56230.
[2]Colegio de Postgraduados Campus Montecillo. Posgrado en Socioeconomía, Estadística e Informática-Economía. Carretera México-Texcoco km 36.5, Montecillo, Texcoco, State of Mexico, Mexico. C. P. 56264.
* Author for correspondence: jhdzo@yahoo.com.mx

Citation: Hernández-Pérez J, Arana-Coronado OA, Valdivia-Alcalá A, Sandoval Romero F, Hernández-Ortiz J. 2025. Farmer willingness to pay for improved irrigation water quality and produce innocuous foods in irrigation district 003 Tula, Hidalgo. **Agrociencia** 59(4): 604-613. https://doi.org/ 10.47163/agrociencia.v59i4.3297

Editor in Chief:
Dr. Fernando C. Gómez Merino

Received: September 05, 2024.
Approved: April 30, 2025.
Published in Agrociencia: May 26, 2025.

ABSTRACT

Irrigation district 003 Tula, Hidalgo, is an example of wastewater irrigation in Mexico; however, it results in greater pollution for the environment, farmers, and consumers. The aim of this work was to determine farmers' willingness to pay (WTP) for treated, better-quality water, thus producing innocuous products. A sample of 104 farmers was obtained through simple randomized sampling. The contingent valuation method was used, with two econometric limited dependent variable models, where the interest is primarily in the probability of a response to a binary indicator. The non-linear adjusted binary response models were logit and probit. The best model, according to the log pseudolikelihood, Akaike information criterion, pseudo-R-squared criteria, and the number of correctly predicted cases, was the logit model. The results indicate that education (22.6 %) and income levels (20.3 %) have positive effects on WTP, whereas the opposite occurred with the fee (-0.026 %), the number of economic dependents (-11 %), and the number of hectares planted (-4.2 %). If the farmer considers that there are risks to the health of consumers of foods produced with untreated residual waters, the WTP increases by 11 %. The logit and probit models produced an average WTP of MXN 1649.18 and 1685.08, respectively. The reuse of wastewater requires compliance with acceptable and required quality standards for crops to produce healthy foods that protect the health of farmers and consumers.

Keywords: contingent valuation, logit, probit, residual water, Mezquital Valley.

INTRODUCTION

Economic growth, population growth, and urbanization are catalysts of water pollution. Reusing wastewater for agriculture is common around the globe. However, its treatment is rare in many countries (Contreras *et al*., 2017). Worldwide, two-thirds of the wastewater applied is not treated (Trinh *et al*., 2013). Its agricultural use ranges from 1.5 to 6.6 %, with 4.5 to 20 million ha irrigated globally, with China, Mexico,

Egypt, India, Indonesia, Iran, and Pakistan standing out. In Mexico, it is estimated that 70 000 and 190 000 ha are irrigated with treated and untreated wastewater, respectively (Sato *et al*., 2013).

It is estimated that high-income countries treat approximately 70 % of all wastewater produced; medium-high-income countries, 38 %; medium-low-income countries, 28 %; and low-income countries treat only 8 % (WWAP, 2017). The countries with the highest amount of wastewater use are China, Mexico, and the USA, with 14.8, 4.4, and 7.6 million m^3 of water a day, respectively, but in the first two cases, the wastewater is untreated. The most important countries in terms of reusing treated wastewater are the USA, Saudi Arabia, and Egypt, with 7.6, 1.8, and 1.7 million m^3 of water a day, respectively (Jiménez and Asano, 2008).

In developing countries, the highest proportion of recycled water is used in agriculture, whereas in developed nations, it is used for urban activities (Brissaud, 2009). In Israel, 75 % of recycled water is used for irrigation agriculture in 19 000 ha. In Kuwait, agricultural irrigation with recycled water accounts for 25 % of the total irrigated surface. In India, Egypt, and Vietnam, approximately 73 000, 42 000, and 9000 ha are irrigated with wastewater, respectively (Chen *et al*., 2013). In France and Italy, wastewater treated for agricultural irrigation covers over 3000 and 4000 ha, respectively (Angelakis *et al*., 2003). In Spain, 79.2 % of the volume of treated wastewater is reused in agriculture (Iglesias-Esteban and Ortega-de Miguel, 2008).

Mexico is second in the world in terms of wastewater used in agriculture with 4.4 million m^3 of water a day, followed by Egypt and Syria with 1.9 and 1.1 million m^3 of water a day, respectively (Jiménez and Asano, 2008). The water system of the Mezquital Valley in Hidalgo, Mexico, is the world's largest and oldest example in terms of untreated wastewater use for agricultural irrigation (Lesser *et al*., 2018). More than 90 000 ha of plantations are irrigated with untreated wastewater from Mexico City, which are distributed in the agricultural irrigation districts of Tula, Ajacuba, and Alfajayucan. The high availability of wastewater has placed farmers in a comfort zone where the treatment of this water is viewed as a threat (Durán-Álvarez *et al*., 2021).

Irrigation plays an important part in the Mezquital Valley due to the scarcity of fresh water, weather conditions, low rainfalls, a higher demand for water by tourism and other sectors, and the increase in the availability of wastewater from Mexico City (Contreras-Román, 2018; García-Salazar, 2019). Wastewater use in irrigation district (ID) 003 Tula dates back more than 100 years ago, with an annual volume of reuse of 1780 million m^3 (56.6 $m^3 s^{-1}$) (Jiménez *et al*., 2005). Its use has led to a physical and chemical degradation of the soil, which influences agricultural productivity. The presence of toxic metals in the region is a risk to human health and the environment (Cornejo-Oviedo *et al*., 2012). Wastewater contains a high pollutant load composed of organic material, metals, bacteria, and detergents, which can lead to public health issues (García-Salazar, 2019), as well as an increase in diarrheal diseases in children (Contreras *et al*., 2017).

Masterplan DR 003 mentions that the chemical composition of wastewater reduces the lifespan of hydro-agricultural infrastructure (floodgates, dams, farm intakes), which must be replaced at least every three years. The gases produced by wastewaters cause the corrosion of structures like culverts and tunnels (CONAGUA, 2005). Farmers, communities, and consumers are at risk due to the harmful components of untreated wastewater. The use of wastewater for irrigation can cause considerable damage to public health and the environment. Its use in agriculture causes externalities for both public health (through the consumption of agricultural products irrigated with wastewater) and the environment (since it constantly pollutes underground water and soil and causes an unpleasant odor) (Wichelns and Qadir, 2015).

The crops sprayed with wastewater can be contaminated with heavy metals, including arsenic, cadmium, lead, and mercury, causing serious health problems, such as osteoporosis. These metals enter the human and animal bodies not only through the intake of vegetables but also by the inhalation of polluted soils (Kesari *et al*., 2021; Qadir *et al*., 2010). Consequently, farmers, agricultural workers, their families, and the consumers of crops irrigated with wastewater are more prone to suffer parasitic diseases (Weldesilassie *et al*., 2009).

Some studies have been carried out on the willingness to pay (WTP) for the improvement of the drinking water service in Mexico (Valdivia-Alcalá *et al*., 2022; Briseño and Macedo, 2021), but there are no studies on WTP for the implementation of irrigation with treated wastewater in an ID or an aquifer. Therefore, the aim of this investigation was to estimate the WTP of farmers in ID 003 Tula, Hidalgo, for better-quality water to understand the factors that impact their will to improve the water they already use and produce innocuous and better-quality crops. The hypothesis is that farmers in ID 003 Tula Hidalgo are willing to pay for better-quality water to irrigate their crops and thus avoid worrying about the health of consumers.

MATERIALS AND METHODS

The contingent valuation method was used, which implies directly asking people how much they would pay in case a hypothetical change was to take place in the future state. A question was asked regarding the WTP, and socioeconomic data was requested in order to describe the interviewee (socioeconomic characteristics such as age, education, income, and gender). Likewise, matters regarding attitudes and beliefs were incorporated, such as stances regarding environmental policies (Young and Loomi, 2014).

The interviews were conducted on the farmers of ID 003 Tula, Hidalgo, between July 5 and 25, 2024. The sample was obtained with the simple randomized sampling method (Anderson *et al*., 2008; Lind *et al*., 2012), using the following formula:

$$n = \pi(1-\pi)\left(\frac{Z}{E}\right)^2$$

where n is the sample size, Z is the standard normal value corresponding to the desired level of trust of 95 % (z = 1.96), π is the proportion of the population (0.5), and E is the maximum tolerable error (9.6 %). The number of users of the ID was 37 267, out of which 57.6 % are commonly owned (ejido) and 42.4 % are small-scale properties. The final sample was of 104 farmers interviewed.

In this study, the dependent variable is dichotomic (binary), where one indicates farmers are willing to pay (a "yes" response) and zero means they are not (a "no" response). Two models were formulated: one logit and another probit (Zegeye *et al*., 2023), in which the probability of paying for better water quality is estimated as follows:

$$P_i = \frac{1}{1 + e^{-(\beta_0+\beta_1X_1+\beta_2X_2+\beta_3X_3+\beta_4X_4+\beta_5X_5+\beta_6X_6)}} = \frac{e^{(\beta_0+\beta_1X_1+\beta_2X_2+\beta_3X_3+\beta_4X_4+\beta_5X_5+\beta_6X_6)}}{1 + e^{(\beta_0+\beta_1X_1+\beta_2X_2+\beta_3X_3+\beta_4X_4+\beta_5X_5+\beta_6X_6)}}$$

where X_1 is the variable fee, X_2 is the education level, X_3 is income, X_4 is the number of economic dependents, X_5 is the number of hectares planted by the farmer, and X_6 is a dichotomic variable of the response to the question "Do you consider there is a health risk in consumers for eating produce irrigated with wastewater?" where a value of one is assigned to an answer "yes" and zero to the answer "no."

The probability of not paying for better quality of water was calculated as follows:

$$1 - P_i = \frac{1}{1 + e^{(\beta_0+\beta_1X_1+\beta_2X_2+\beta_3X_3+\beta_4X_4+\beta_5X_5+\beta_6X_6)}}$$

The odds ratio of paying relative to the probability of not paying is expressed as follows:

$$\frac{P_i}{1 - P_i} = \frac{1 + e^{(\beta_0+\beta_1X_1+\beta_2X_2+\beta_3X_3+\beta_4X_4+\beta_5X_5+\beta_6X_6)}}{1 + e^{-(\beta_0+\beta_1X_1+\beta_2X_2+\beta_3X_3+\beta_4X_4+\beta_5X_5+\beta_6X_6)}} = e^{(\beta_0+\beta_1X_1+\beta_2X_2+\beta_3X_3+\beta_4X_4+\beta_5X_5+\beta_6X_6)} \quad (1)$$

Applying a natural logarithm, L_i is obtained to linearize the parameters:

$$L_i = ln\left(\frac{P_i}{1 - P_i}\right) = \beta_0 + \beta_1X_1 + \beta_2X_2 + \beta_3X_3 + \beta_4X_4 + \beta_5X_5 + \beta_6X_6$$

To estimate the parameters of the model, the maximum likelihood method was used with the statistical software Stata 16:

$$L_i = ln\left(\frac{P_i}{1 - P_i}\right) = \beta_0 + \beta_1X_1 + \beta_2X_2 + \beta_3X_3 + \beta_4X_4 + \beta_5X_5 + \beta_6X_6 + u_i$$

where u_i corresponds to the error term; that is, factors that affect the WTP but are not explicitly included in the model.

To obtain the farmers' mean WTP for better-quality water to produce innocuous and higher-quality foods, the following formula was used:

$$DAP_{media} = \frac{\sum_{i=1}^{n} \frac{\beta_0 + \beta_2 X_{2i} + \beta_3 X_{3i} + \beta_4 X_{4i} + \beta_5 X_{5i} + \beta_6 X_{6i}}{\beta_1}}{n} \quad (2)$$

RESULTS AND DISCUSSION

All the farmers surveyed were men, with an average age of 57, out of whom 91.3 % are married and the rest, single. In terms of land ownership, 50 % owned small-scale lands, while the rest was commonly owned (ejidos). Maize was planted by 61.5 % of farmers, followed by alfalfa (24 %), beans (11.5 %), and chili peppers (2.9 %). Regarding education levels, 16.3 % of farmers have not completed elementary school, 36.5 % have completed elementary school, 37.5 % have middle school, 7.7 % have high school, and 1.9 % have a university degree. Farmers with an income of MXN 5000 made up 1 % of those surveyed, 72.1 % have incomes of MXN 5000 to 10 000, 24 % make between MXN 10 000 and 15 000, and 2.9 % make between MXN 15 000 and 20 000.

Out of the 104 farmers surveyed, 69.23 % expressed a positive stance regarding their WTP for better-quality recycled water, which represents fewer environmental impacts on the crops and on the health of farmers and consumers. The education level had a positive effect, with 54.2 and 20.8 % of those who completed elementary school and high school having a positive stance, respectively. Meanwhile, 61.1 % of those with an income between MXN 5000 and 10 000, and 33.3 % of those between MXN 10 000 and 15 000 had a positive attitude (Table 1). The farmers surveyed that are willing to pay

Table 1. Frequency of the variables of the willingness to pay (WTP), education level, and income of the farmers interviewed in irrigation district 003 Tula, Hidalgo, Mexico.

WTP	Education level	Frequency	%	Income level	Frequency	%
Yes	Elementary, incomplete	9	12.5	< 5000	1	1.4
	Elementary, complete	15	20.8	5000–10000	44	61.1
	High school	39	54.2	10 000–15 000	24	33.3
	Media superior	7	9.7	15 000–20 000	3	4.2
	Professional	2	2.8			
No	Elementary, incomplete	8	25.0	< 5000	0	0
	Elementary, complete	23	71.9	5000–10000	31	96.9
	High school	0	0	10 000–15 000	1	3.1
	Media superior	1	3.1	15 000–20 000	0	0
	Professional	0	0			

for an improvement in irrigation water quality have 1–6 economic dependents, out of which 15.3 % have one dependent, 26.4 % have two, 27.8 % have three, and 20.8 % have four.

In terms of the hectares planted, farmers with a positive attitude towards their WTP have 1–8 ha planted. Those with three (28.8 %), four (26.4 %), five (15.3 %), and two hectares (11.1 %) stand out. Out of the total of farmers, 59.7 % consider that irrigating with wastewater has effects on the health of consumers and had a positive response to the WTP.

In the logit and probit models, all parameters were statistically significant according to the statistic *z*. The global statistical significance of the Wald chi-squared model was lower than 1 % for both models. However, the best, according to the log pseudolikelihood, Akaike Information Criterion (AIK), pseudo-R-squared, and the number of correctly predicted cases, was the logit model (Table 2).

Table 2. Results of the coefficient estimations of the models evaluating the willingness to pay (WTP) of farmers in irrigation district 003 Tula, Hidalgo, Mexico.

WTP	Logit	Probit
Fee	-0.004***(0.001)	-0.002***(0.001)
Education level	3.300***(1.022)	1.717***(0.422)
Income level	2.969***(1.062)	1.772***(0.559)
Dependents	-1.606***(0.365)	-0.902***(0.167)
Hectares planted	-0.607**(0.300)	-0.324**(0.154)
Consumer health	1.371*(0.847)	0.710*(0.433)
Constant	-2.184(2.422)	-1-475(1.223)
Log pseudolikelihood	-29.730	-30.299
Wald $chi^2(6)$	26.56***	38.28***
Akaike information criterion	73.461	74.598
Pseudo R^2	0.537	0.528
Correctly predicted	88.46%	86.54%
Observations	104	104

*** $p < 0.01$; ** $p < 0.05$; * $p < 0.1$. Standard error in parentheses.

To interpret the models, the odds ratios (Equation 1) and the marginal effects (dy/dx) of each variable were calculated. The variable fee had a marginal effect of -0.026, which means that for every MXN increase, the WTP decreased by 0.026 %. The marginal effect for the education level showed that, for every additional level of education, WTP increased by 22.598 %. The marginal effect of income showed that when the incomes of farmers increased, WTP rose by 20.333 %. When the number of economic dependents increased by one, the WTO decreased by 10.999 %. If the farmer's planted surface increased by 1 ha, the WTP decreased by 4.156 %. Finally, if the farmer considered

that there are risks for the health of the consumer of products irrigated with untreated wastewater, the WTP increased by 11.042 % (Table 3).

Table 3. Marginal effects and odds ratio of the variables used in the evaluation of the willingness to pay (WTP) of farmers in irrigation district 003 Tula, Hidalgo, Mexico.

	Logit			Probit		
Variable	*dy/dx*	%	Odds ratio	*dy/dx*	%	Odds ratio
Fee	-0.000	-0.026	0.996	0.000	-0.032	0.998
Education level	0.226	22.598	27.118	0.280	28.032	5.567
Income level	0.203	20.333	19.480	0.289	28.939	5.885
Dependents	-0.110	-10.999	0.201	-0.147	-14.723	0.406
Hectares planted	-0.042	-4.156	0.545	-0.053	-5.295	0.723
Consumer health	0.110	11.042	3.940	0.129	12.941	2.035

In order to obtain the mean WTO, equation (2) was used and values of MXN 1649.18 and 1685.08 were obtained using the logit and probit model, respectively. On average, the producer would be willing to pay those amounts per hectare irrigated with better quality water in DR 003 Tula.

The variable with the greatest effect on the WTP of farmers for the use of treated wastewater was education. Farmers with higher education levels are considered as having access to information sources on the treatment of wastewater, such as the internet, journals, and news (Deh-Haghi *et al*., 2020; Lazaridou *et al*., 2019). The income level of farmers had a positive relation with WTP, in which the higher the income (regardless of whether the farmer has other income sources), the higher the probability of paying more for better-quality water to irrigate their fields. However, the opposite is true with the number of economic dependents, since more economic dependents means a smaller budget available to buy other goods and services not related to the family, such as paying more than what they already pay for the irrigation service.

Out of the total of farmers surveyed, 60.6 % considered that there is a risk involved in consuming products irrigated with wastewater, and 77.9 % considered there are environmental risks involved in irrigating with untreated wastewater. The perception of health risks has impacts on the willingness to use treated wastewater (Deh-Haghi *et al*., 2020; Khanpae *et al*., 2020). The use of untreated or partially treated wastewater for irrigation involves the risk of contracting diseases, both for farmers and their families, as well as consumers. The diseases prevalent among farmers include hookworm infection, ascariasis, and giardiasis. Diseases related to the consumption of raw vegetables include shigellosis, cholera, typhoid fever, and diarrhea (Leonel and Tonetti, 2021).

CONCLUSIONS

The willingness to pay (WTP) for improved irrigation water quality revealed that education level, income level, and consumer perception of health had positive effects, whereas the fee, the number of the farmer's economic dependents, and the number of hectares planted had negative effects. Therefore, the most appropriate mechanism is to raise awareness and educate farmers about health risks for both themselves and consumers so they increase their WTP for higher-quality irrigation water and consequently manage proper wastewater treatment for agricultural use.

The farmers of the irrigation district are worried about risks and therefore are willing to pay for better quality water. The treatment and reuse of wastewater is an option to face water scarcity problems, as well as contributing to its sustainable use. Reusing requires that these waters have the required quality for crops to produce healthy foods that guarantee the health of farmers and consumers.

ACKNOWLEDGEMENTS

To the Autonomous University of Chapingo for the partial funding of this investigation, particularly in the field stage.

REFERENCES

Anderson DR, Sweeney DJ, Williams TA. 2008. Estadística para administración y economía (10a edición). Cengage Learning Editores: Ciudad de México, México. 1056 p.

Angelakis AN, Bontoux L, Lazarova V. 2003. Challenges and prospectives for water recycling and reuse in EU countries. Water Supply 3 (4): 59–68. https://doi.org/10.2166/ws.2003.0046

Briseño H, Macedo E. 2021. Disposición a pagar para mejorar la calidad del agua en Zapopan. Tecnología y Ciencias del Agua 12 (1): 402–434. https://doi.org/10.24850/J-TYCA-2021-01-10

Brissaud F. 2009. Technologies for water regeneration and integrated management of water resources. *In* Sabater S, Barceló D. (eds.), The Handbook of Environmental Chemistry. Springer: Berlin, Germany, pp: 95–105. https://doi.org/10.1007/698_2009_30

Chen Z, Ngo HH, Guo W. 2013. A critical review on the end uses of recycled water. Critical Reviews in Environmental Science and Technology 43 (14): 1446–1516. https://doi.org/10.1080/10643389.2011.647788

CONAGUA (Comisión Nacional del Agua). 2005. Plan director para la modernización integral del riego del Distrito de Riego 003 Tula, Estado de Hidalgo. Gobierno de México. Comisión Nacional del Agua. Subdirección de Infraestructura Hidroagrícola. Ciudad de México, México. 329 p.

Contreras JD, Meza R, Siebe C, Rodríguez-Dozal S, López-Vidal YA, Castillo-Rojas G, Amieva RI, Solano-Gálvez SG, Mazari-Hiriart M, Silva-Magaña MA, *et al*. 2017. Health risks from exposure to untreated wastewater used for irrigation in the Mezquital Valley, Mexico: A 25-year update. Water Research 123: 834–850. https://doi.org/10.1016/j.watres.2017.06.058

Contreras-Román RH. 2018. Volver a la tierra: retorno migratorio y recampesinización forzada en el Valle del Mezquital, México. Perspectivas Rurales Nueva Época 16 (32): 16–32. https://doi.org/10.15359/prne.16-32.3

Cornejo-Oviedo F, López-Herrera M, Beltrán-Hernández R, Acevedo-Sandoval O, Lucho-Constantino C, Reyes-Santamaría M. 2012. Degradación del suelo en el Distrito de Riego 003 Tula, Valle del Mezquital, Hidalgo, México. UDO Agrícola 12 (4): 873–880.

Deh-Haghi Z, Bagheri A, Fotourehchi Z, Damalas CA. 2020. Farmers' acceptance and willingness to pay for using treated wastewater in crop irrigation: A survey in western Iran. Agricultural Water Management 239: 106262. https://doi.org/10.1016/j.agwat.2020.106262

Durán-Álvarez JC, Jiménez B, Rodríguez-Varela M, Prado B. 2021. The Mezquital Valley from the perspective of the new Dryland Development Paradigm (DDP): Present and future challenges to achieve sustainable development. Current Opinion in Environmental Sustainability 48: 139–150. https://doi.org/10.1016/j.cosust.2021.01.005

García-Salazar EM. 2019. El agua residual como generadora del espacio de la actividad agrícola en el Valle del Mezquital, Hidalgo, México. Estudios Sociales 29 (54): 2–34. https://doi.org/10.24836/es.v29i54.741

Iglesias-Esteban R, Ortega-de Miguel E. 2008. Present and future of wastewater reuse in Spain. Desalination 218 (1–3): 105–119. https://doi.org/10.1016/j.desal.2006.09.031

Jiménez B, Asano T. 2008. Water reclamation and reuse around the world. *In* Blanca J, Asano T. (eds.), Water Reuse - An International Survey of Current Practice, Issues and Needs. IWA Publishing: London, UK, pp: 3–26. https://doi.org/10.2166/9781780401881

Jiménez B, Siebe GC, Cifuentes GE. 2005. El reúso intencional y no intencional del agua en el valle de Tula. *In* Jiménez B, Marín L. (eds.), El Agua en México Vista desde la Academia. Academia Mexicana de Ciencias: Ciudad de México, México, pp: 33–56.

Kesari KK, Soni R, Jamal QMS, Tripathi P, Lal JA, Jha NK, Siddiqui MH, Kumar P, Tripathi V, Ruokolainen J. 2021. Wastewater treatment and reuse: A review of its applications and health implications. Water, Air, and Soil Pollution 232 (5): 1–28. https://doi.org/10.1007/s11270-021-05154-8

Khanpae M, Karami E, Maleksaeidi H, Keshavarz M. 2020. Farmers' attitude towards using treated wastewater for irrigation: The question of sustainability. Journal of Cleaner Production 243: 118541. https://doi.org/10.1016/j.jclepro.2019.118541

Lazaridou D, Michailidis A, Mattas K. 2019. Evaluating the willingness to pay for using recycled water for irrigation. Sustainability 11 (19): 5220. https://doi.org/10.3390/su11195220

Leonel LP, Tonetti AL. 2021. Wastewater reuse for crop irrigation: Crop yield, soil and human health implications based on giardiasis epidemiology. Science of the Total Environment 775: 145833. https://doi.org/10.1016/j.scitotenv.2021.145833

Lesser LE, Mora A, Moreau C, Mahlknecht J, Hernández-Antonio A, Ramírez AI, Barrios-Piña H. 2018. Survey of 218 organic contaminants in groundwater derived from the world's largest untreated wastewater irrigation system: Mezquital Valley, Mexico. Chemosphere 198: 510–521. https://doi.org/10.1016/j.chemosphere.2018.01.154

Lind DA, Marchal WG, Wathen SA. 2012. Estadística aplicada a los negocios y la economía (15a edición). McGraw-Hill: Ciudad de México, México. 856 p.

Qadir M, Wichelns D, Raschid-Sally L, McCornick PG, Drechsel P, Bahri A, Minhas PS. 2010. The challenges of wastewater irrigation in developing countries. Agricultural Water Management 97 (4): 561–568. https://doi.org/10.1016/j.agwat.2008.11.004

Sato T, Qadir M, Yamamoto S, Endo T, Zahoor A. 2013. Global, regional, and country level need for data on wastewater generation, treatment, and use. Agricultural Water Management 130: 1–13. https://doi.org/10.1016/j.agwat.2013.08.007

Trinh LT, Duong CC, van der Steen P, Lens PNL. 2013. Exploring the potential for wastewater reuse in agriculture as a climate change adaptation measure for Can Tho City, Vietnam. Agricultural Water Management 128: 43–54. https://doi.org/10.1016/j.agwat.2013.06.003

Valdivia-Alcalá R, Delgadillo-Vázquez MA, Sangerman-Jarquín, DM, Hernández-Ortíz J, Sandoval-Romero F, Garay-Jácome ÁS. 2022. Valoración económica de la calidad del agua potable en León, Guanajuato. Revista Mexicana de Ciencias Agrícolas 13 (3): 527–538. https://doi.org/10.29312/remexca.v13i3.3168

Weldesilassie AB, Frör O, Boelee E, Dabbert S. 2009. The economic value of improved wastewater irrigation: A contingent valuation study in Addis Ababa, Ethiopia. Journal of Agricultural and Resource Economics 34 (3): 428–449.

Wichelns D, Qadir M. 2015. Policy and institutional determinants of wastewater use in agriculture. *In* Drechsel P, Qadir M, Wichelns D. (eds.), Wastewater: Economic Asset in an Urbanizing World. Springer: Dordrecht, Netherlands, pp: 93–112 https://doi.org/10.1007/978-94-017-9545-6

WWAP (Programa Mundial de Evaluación de los Recursos Hídricos de las Naciones Unidas). 2017. Informe mundial de las Naciones Unidas sobre el desarrollo de los recursos hídricos 2017. Aguas residuales: el recurso desaprovechado. Organización de las Naciones Unidas para la Educación, la Ciencia y la Cultura: Paris, Francia. 202 p.

Young RA, Loomi JB. 2014. Determining the economic value of water (Second edition). RFF Press: New York, NY, USA. 358 p. https://doi.org/10.4324/9780203784112

Zegeye G, Erifo S, Addis G, Gebre GG. 2023. Economic valuation of urban forest using contingent valuation method: The case of Hawassa city, Ethiopia. Trees, Forests and People 12: 100398. https://doi.org/10.1016/j.tfp.2023.100398

VOLUME 59, NUMBER 4 | May 16 - June 30, 2025 | MEXICO